The Chemistry of Pentabenzoazacorannulene

ペンタベンゾアザコラニュレンの化学

Hiroki YOKOI

横井　寛生

Department of Applied Chemistry, Graduate School of Engineering
Nagoya University

2018

Preface

The studies in this thesis were carried out under the guidance of Prof. Dr. Hiroshi Shinokubo and Assistant Prof. Dr. Satoru Hiroto at Department of Molecular and Macromolecular Chemistry, Graduate School of Engineering, Nagoya University during the period from April 2013 to February 2018.

These studies mainly focus on the syntheses and properties of a nitrogen-embedded bowl-shaped molecule, that is, penta-*peri*-pentabenzoazacorannulene. To date, various kinds of polycyclic aromatic hydrocarbons have been synthesized, most of which consist of planar π-surfaces. Recently, many scientists have attempted the synthesis of bowl-shaped π-conjugated molecules. Among these studies, the introduction of heteroatoms to the nonplanar molecular skeleton has remained challenging. The aim of the research described in this thesis is to synthesize a bowl-shaped molecule with a nitrogen atom in its center and to discover its specific chemical and physical properties as well as functionalities derived from the heteroatom and the nonplanar π-system.

Table of Contents

List of Abbreviations

Å	ångström unit
Abs	absorbance
Ac	acetyl
APCI	atmospheric pressure chemical ionization
aq	aqueous or water solution
Ar	aryl or heteroaryl
BAHA	tris(4-bromophenyl)aminium hexachloroantimonate
BODIPY	4,4-difluoro-4-bora-3*a*,4*a*-diaza-*s*-indacene
Bu	butyl
calcd	calculated
cod	1,5-cyclooctadiene
COSY	correlation spectroscopy
CT	charge transfer
Cy	cyclohexyl
δ	chemical shift (NMR)
D	diffusion coefficient
dba	dibenzylideneaceton
DBU	1,8-diazabicyclo[5.4.0]undec-7-ene
DDQ	2,3-dichloro-5,6-dicyano-1,4-benzoquinone
DFT	density functional theory
DMA	*N*,*N*-dimethylacetamide
DMF	*N*,*N*-dimethylformamide
DOSY	diffusion-ordered two-dimensional NMR spectroscopy
dppf	1,1'-bis(diphenylphosphino)ferrocene
DPV	differential pulse voltammetry
equiv	equivalent(s)
ESI	electrospray ionization
ESR	electron spin resonance
Et	ethyl
EXSY	exchange spectroscopy
FE	field emission
FP-TRM	flash-photolysis
C	time-resolved microwave conductivity
FVP	flash vacuum pyrolysis
h	hour(s)
hv	irradiation with light
HOMO	highest occupied molecular orbital
HR	high-resolution(MS)
Int	intensity
i-Pr	1-methylethyl
J	coupling constant (NMR)
K_a	association constant
LUMO	lowest unoccupied molecular orbital
M	molar
MALDI	matrix assisted laser desorption ionization
Me	methyl
Mes	mesityl
min	minute(s)
MO	molecular orbital(s)
MS	mass spectrum
NBS	*N*-bromosuccinimide
NIR	near infra-red
NMR	nuclear magnetic resonance

NOESY	nuclear overhauser effect spectroscopy
ox	oxidation
Φ_f	fluorescence quantum yield
Ph	phenyl
PIFA	bis(trifluoroacetoxy)iodobenzene
POAV	π-orbital axis vector
ppm	parts per million
R	an organic group
r.t.	room temperature
SEM	scanning electron microscopy
t-Bu	1,1-dimethyl-1-ethyl
TD	time dependent
TFA	trifluoroacetic acid
THF	tetrahydrofuran
TMEDA	*N*,*N*,*N*',*N*'-Tetramethylethylenediamine
TOF	time-of-flight
UV	ultraviolet
v	volume
Vis	visible
VT	variable temperature
Xantphos	4,5-bis(diphenylphosphino)-9,9-dimethylxanthene
XRD	X-ray diffraction
ZPE	zero point energy

Chapter 1

General Introduction

Contents

1-1. Buckybowls

Buckybowls are bowl-shaped π-conjugated molecules such as corannulene and sumanene, which have a partial structure of fullerenes.[1,2] These curved π-conjugated molecules have attracted many scientists not only for their fascinating chemical and physical properties derived from their non-planar structures, but also as key starting materials for the bottom-up synthesis of fullerenes and carbon nanotubes. In 1966, Barth and Lawton have succeeded in the first chemical synthesis of corannulene in seventeen steps from acenaphthene (Scheme 1-1a).[2b] Corannulene corresponds to [5]circulene, where five benzene rings are fused with each other so as to construct the cyclic structure. Due to the bowl structure, the internal carbon atoms of corannulene adopt distorted sp^2 configuration. A few decades later, Hirao, Sakurai, and co-worker have reported the beautiful chemical synthesis of sumanene in three steps from norbornadiene (Scheme 1-1b).[2c] After the successful synthesis of these representative buckybowls, various kinds of bowl-shaped molecules have been reported so far.

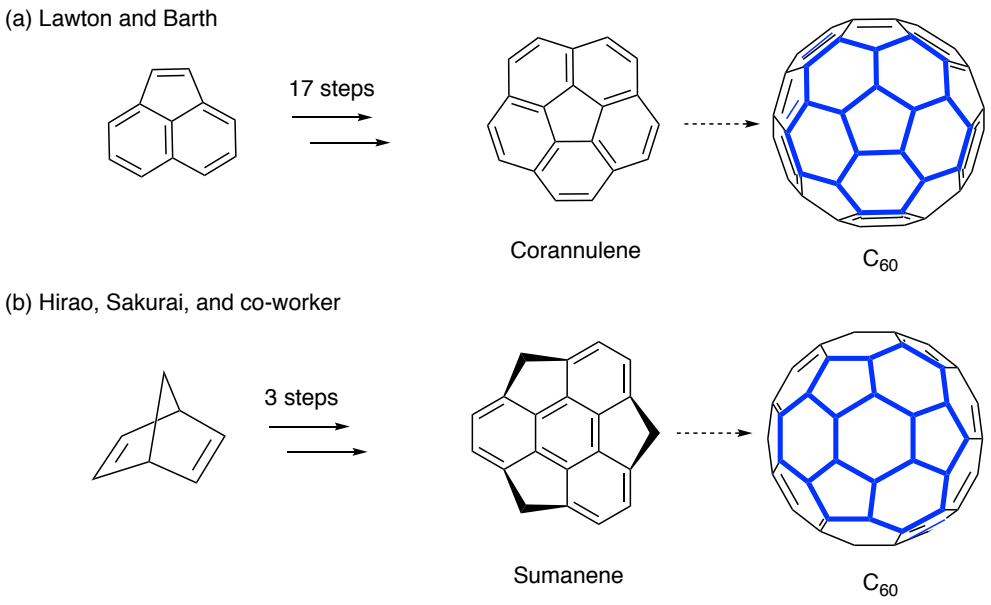

Scheme 1-1. The first syntheses of (a) corannulene and (b) sumanene.

A curved π-surface of buckybowls is suitable for the recognition of fullerenes because the concave surface of buckybowls can efficiently overlap with the convex surface of fullerenes.[3,4] For example, corannulene forms a 1:1 inclusion complex with C_{60} through the intermolecular concave–convex π-π interaction in the crystalline state (Figure 1-1).[4a] The introduction of electron-donating groups to buckybowls can enhance the binding ability toward C_{60} due to an attractive intermolecular donor-acceptor interaction (Chart 1-1).[4c,d] In the case of planar aromatic molecules such as porphyrins, a dimeric structure is required to achieve a strong association with C_{60}.[5]

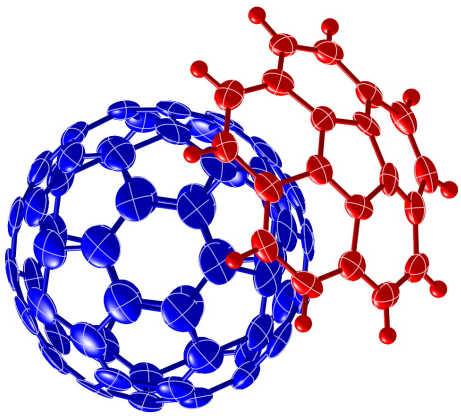

Figure 1-1. The X-ray crystal structure of 1:1 complex between corannulene and C_{60}.

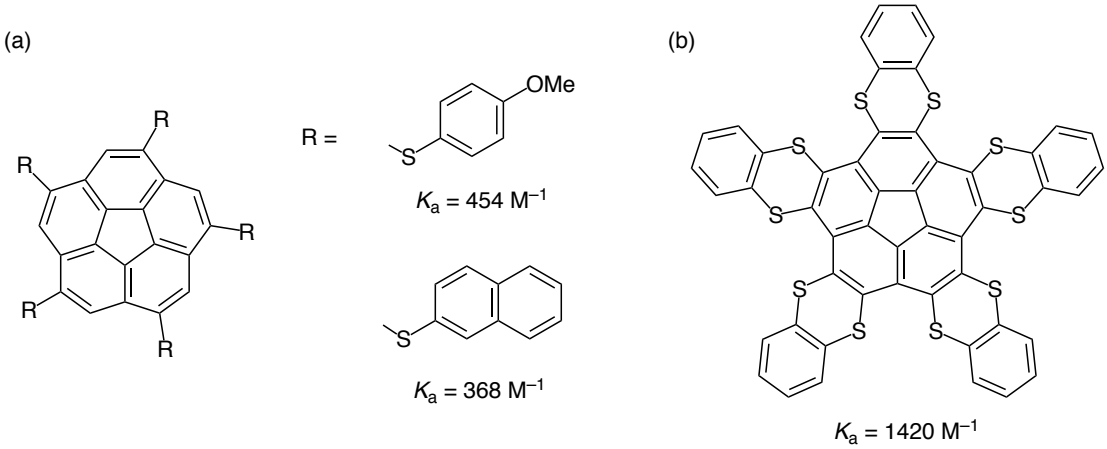

Chart 1-1. Corannulene derivatives functionalized with electron-donating groups and their binding constants in (a) toluene and (b) CS_2.

Non-planar bowl-shaped molecules are also known for exhibiting a bowl-to-bowl inversion behavior (Figure 1-2).[6] For example, the π-surface of corannulene inverts rapidly in the solution state around room temperature.[6a] The bowl-to-bowl inversion properties are extensively studied using a variety of functionalized corannulene derivatives. These dynamic characteristics are expected for the application to molecular machines as well as switching and memory materials.[7]

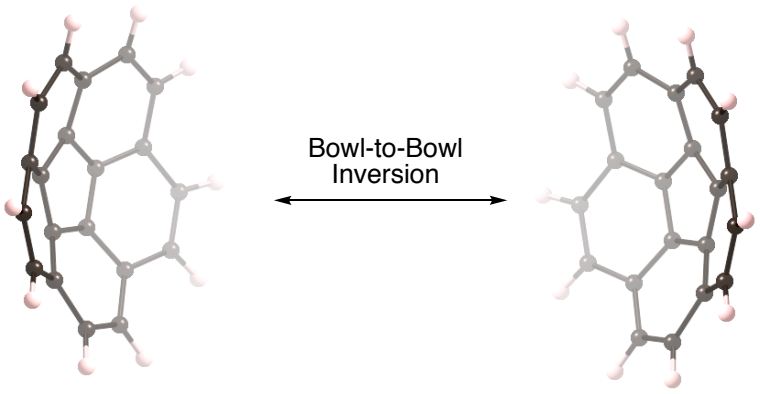

Figure 1-2. Bowl-to-bowl inversion behavior of buckybowls.

The reactivities of bowl-shaped molecules are also another interesting topic. While the chemical reactions of buckybowls usually occur at peripheral positions as in the case of planar π-systems, there are a few examples in which the reactions proceed at internal positions.[8] For example, some of electrophilic addition reactions of corannulene proceed at internal sp^2 carbon atoms (Scheme 1-2a). The similar reactivities were also observed in other bowl-shaped π-systems (Scheme 1-2b and Scheme 1-2c).

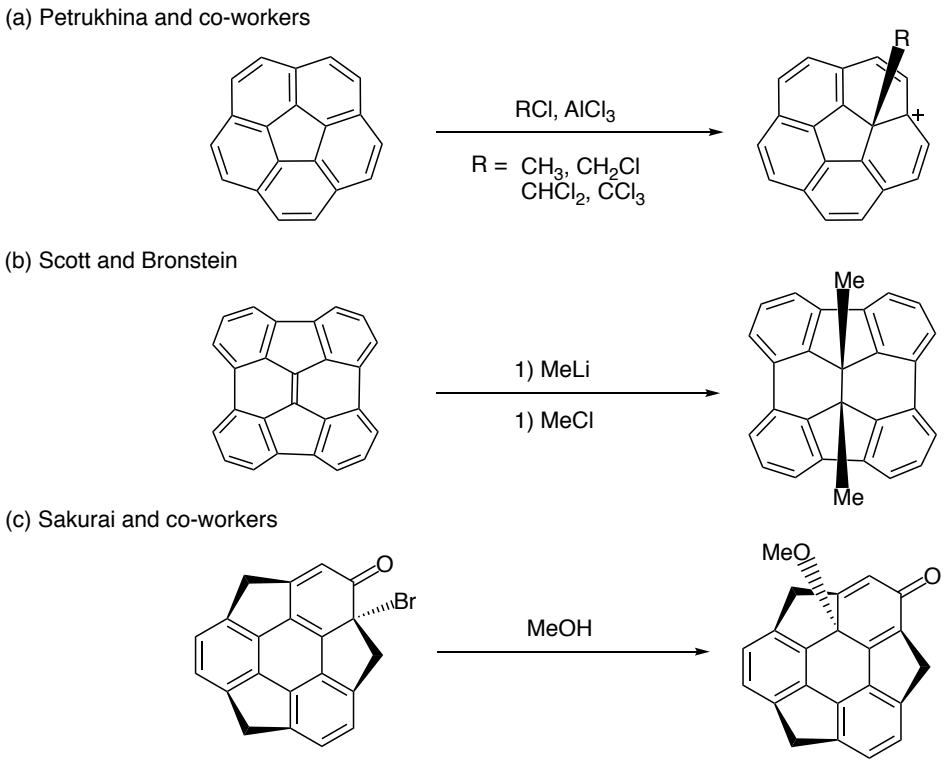

Scheme 1-2. The addition reactions to bowl-shaped molecules at internal positions.

1-2. The Synthesis of Bowl-Shaped Molecules

The synthesis of bowl-shaped molecules is usually difficult because the construction of their highly curved π-surface is energetically unfavorable, for which conventional oxidative fusion reaction does not work well. On the other hand, Scott and co-workers have found that flash vacuum pyrolysis (FVP) was effective for the synthesis of bowl-shaped molecules. FVP is a technique where a precursor is intensely heated for a short time under dynamic vacuum. The cleavage and recombination of chemical bonds in a substrate continuously occur under such harsh reaction conditions, finally producing a target product. FVP enables easy access to various bowl-shaped molecules.[9] For example, the number of steps for the synthesis of corannulene was shortened to six steps from commercially available acenaphthenequinone (Scheme 1-3).[9a] The synthesis of highly strained π-extended buckybowls, which have never been achieved by the conventional solution phase methods, were also prepared by employing this

technique (Scheme 1-4).[9g–i] However, there exist some problems in this method. (1) The product yield tends to be relatively low because of many side reactions and byproducts. (2) Special techniques and equipment are required. (3) A functional group cannot tolerate under such very harsh reaction conditions. For these reasons, a mild but facile another synthetic method was strongly needed.

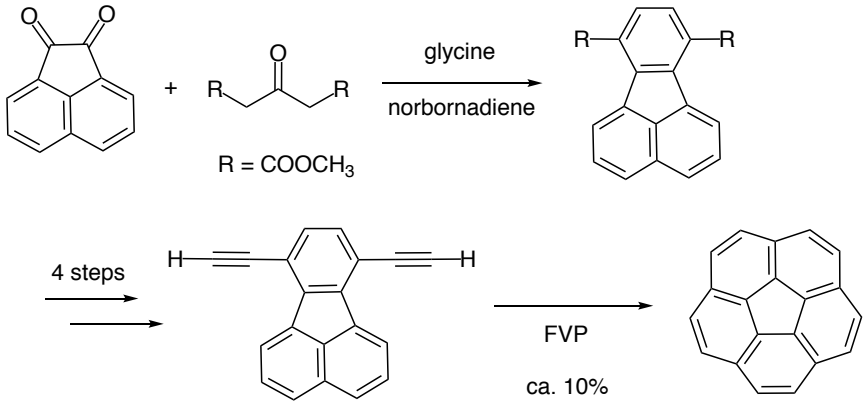

Scheme 1-3. The synthesis of corannulene from acenaphthenequinone.

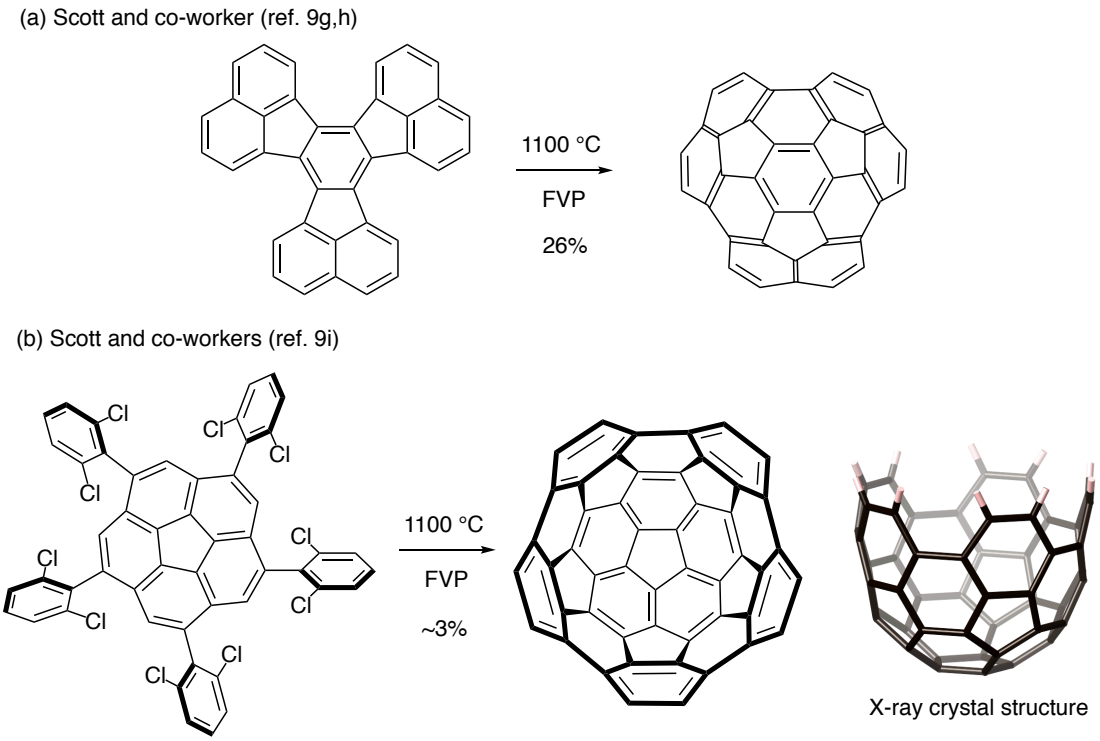

Scheme 1-4. The synthesis of π-extended buckybowls.

In 1996, Siegel and co-workers have reported a solution-phase synthesis of 2,5-dimethylcorannulene (Scheme 1-5).[10] This methodology utilized 3,8-dimethylacenaphthylene-1,2-dione as the starting material. The reductive coupling reaction with $TiCl_3/LiAlH_4$ (or $VCl_3/LiAlH_4$) followed by the oxidative aromatization with DDQ afforded the target bowl-shaped product in moderate yield. A variety of functionalized corannulene derivatives have been synthesized in similar strategies (Scheme 1-6).[11] Different from FVP, this strategy is also applicable to the large-scale synthesis.[12]

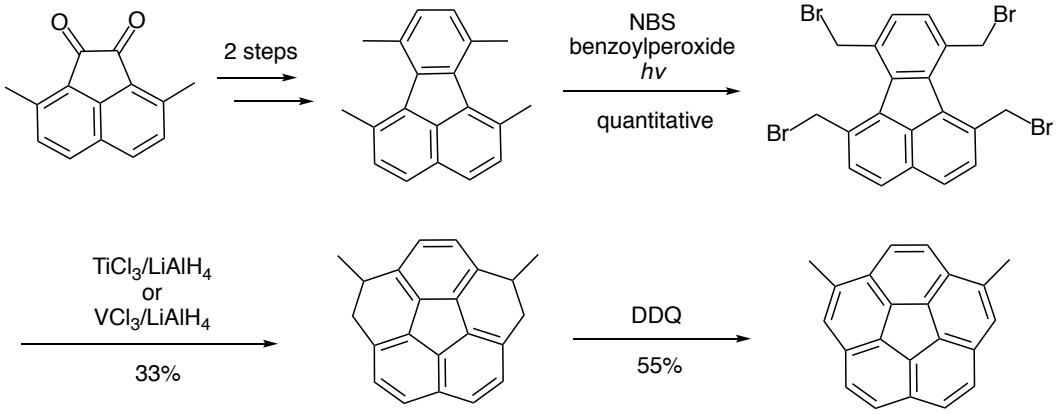

Scheme 1-5. The synthesis of 2,5-dimethylcorannulene.

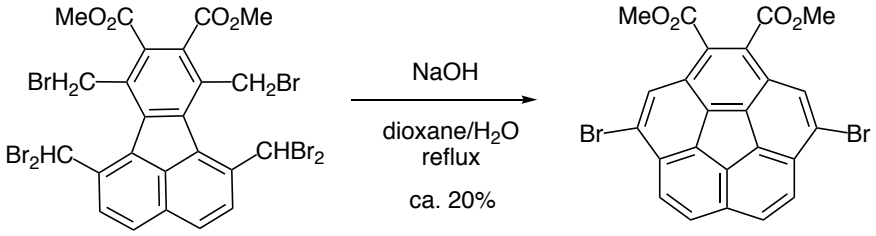

Scheme 1-6. The synthesis of highly functionalized corannulene (ref 11c).

Several research groups have developed other intramolecular C–X/C–H (X = F, Cl, Br) coupling reactions for the synthesis of bowl-shaped molecules.[13] Scott and co-workers have achieved the synthesis of dibenzo[*a*,*g*]corannulene in good yield through an intramolecular double C–H/C–Br coupling reaction using a palladium(II)

catalyst (Scheme 1-7a).[13c] Wu and co-workers have also succeeded in obtaining a π-extended bowl-shaped molecule with another palladium catalyst (Scheme 1-7b).[13d] Amsharov and co-workers reported the synthesis of buckybowls through elimination of HF using activated aluminum oxide (Scheme 1-8).[13f,g]

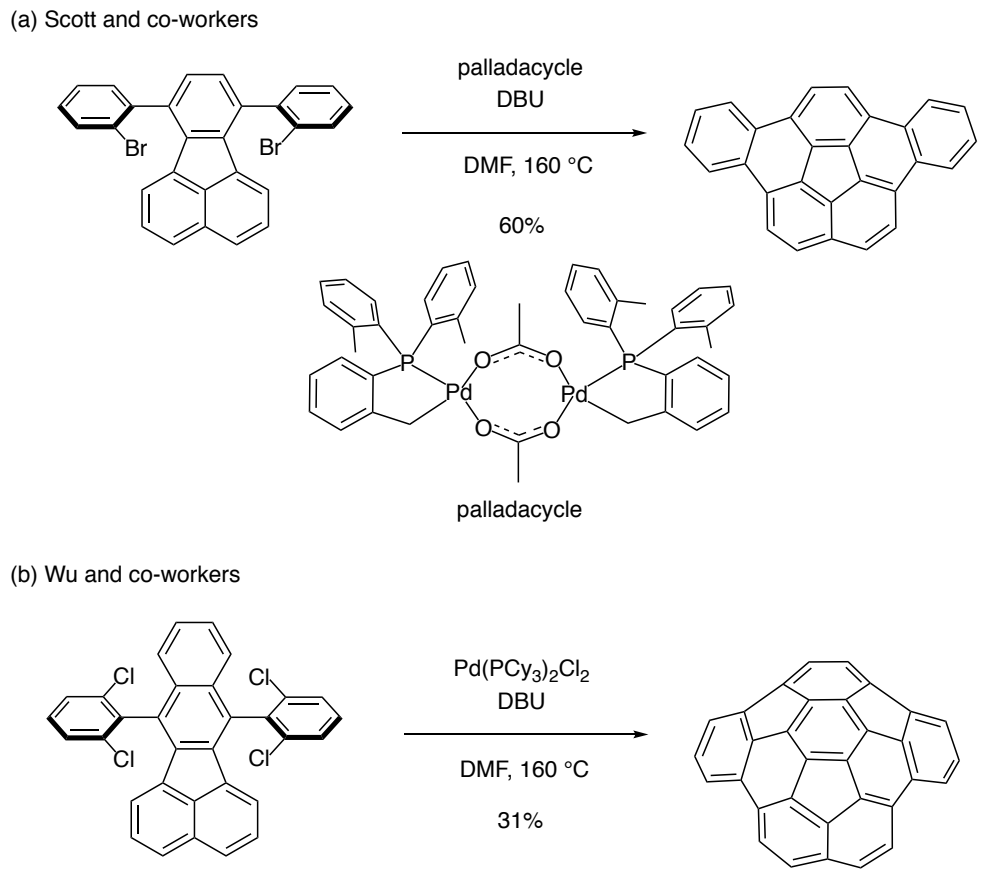

Scheme 1-7. The synthesis of bowl-shaped molecules through palladium-catalyzed intramolecular coupling reaction.

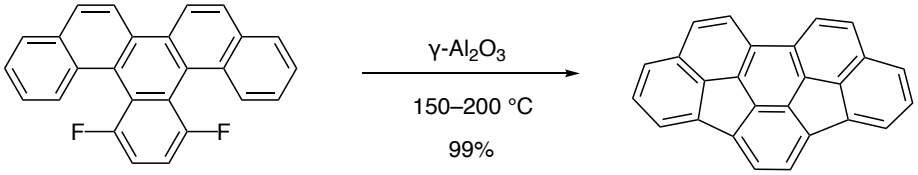

Scheme 1-8. The synthesis of bowl-shaped molecule using activated aluminum oxide.

1-3. Heterobuckybowls

Heterobuckybowl is a buckybowl that contains heteroatoms in its molecular framework, which is expected as a model compound to investigate the properties of heterofullerenes and heterocarbon nanotubes.[14] However, the synthesis of heteroatom-containing bowl-shaped molecules has remained challenging and only a few examples of heterobuckybowls have been reported to date. Among these studies, many scientists have challenged the synthesis of azacorannulenes. The author explains the history of an azacorannulene in this section.

According to the paper reported by Scott and co-workers,[15] the synthesis of azacorannulene was first attempted by Bratcher, where FVP reaction was applied to a fluoranthene derivative substituted with two nitrile groups on the basis of the reaction in Scheme 1-9b[16] (Scheme 1-9a). However, the intramolecular double cyclization reaction did not proceed, probably due to the endothermic character of this reaction. Rabideau also attempted the synthesis of another type of azacorannulene that contains one imine-type nitrogen atom in its skeleton (Scheme 1-10a). Rabideau utilized an azafluoranthene derivative with two α-chlorovinyl groups as the precursor. In the synthesis of corannulene, the introduction of the α-chlorovinyl groups to the precursor drastically improved the product yield.[9d] On the other hand, the C–N bond cleavage as well as the following rearrangement reaction unfortunately occurred in this case. Bodwell, Scott and co-workers have also tried the synthesis of diazadibenzocorannulene with one N=N unit (Scheme 1-10b).[17] However, the FVP reaction of the precursor afforded a undesired product without nitrogen atom in its skeleton. In this case, the palladium-catalyzed intramolecular coupling reaction with the same precursor also failed, resulting in the recovery of the starting material.

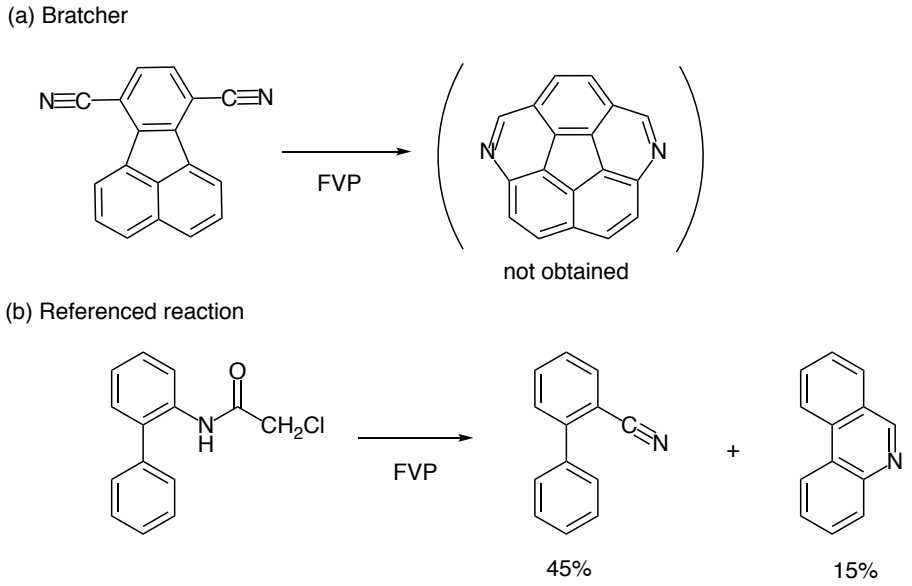

Scheme 1-9. (a) The first attempt to the synthesis of an azacorannulene. (b) Referenced reaction.

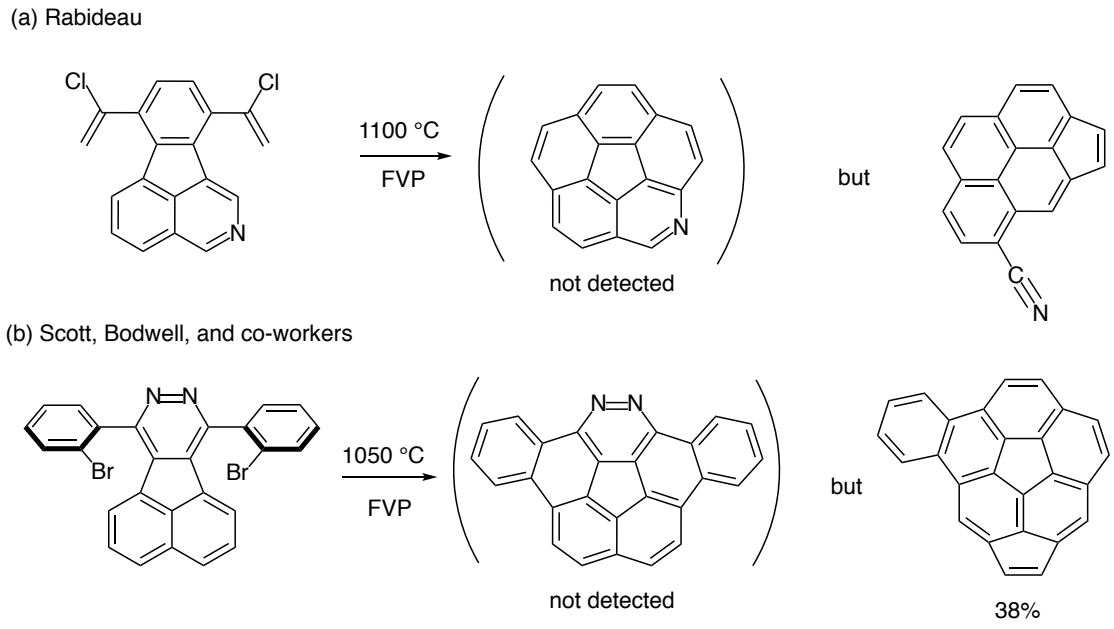

Scheme 1-10. The attempts to the synthesis of azacorannulenes.

Many scientists have also challenged the synthesis of heterosumanenes. Klemm and co-workers attempted the synthesis of trithiasumanene, where three benzylic carbon atoms of sumanene were replaced with three sulfur atoms (Scheme 1-11).[18]

The mixture of triphenylene and hydrogen sulfide was heated at 550 °C. While mono- and di-bridged species were obtained in low yields, tri-bridged species, that is trithiasumanene, was not detected.

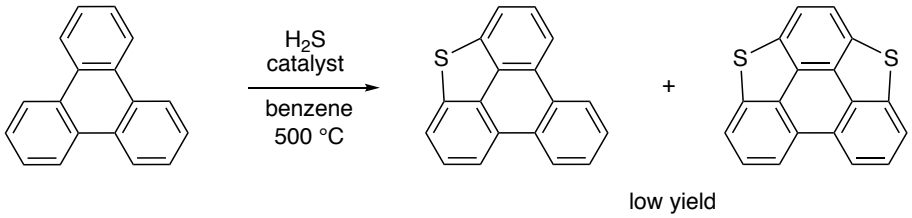

Scheme 1-11. The attempt to the synthesis of trithiasumanene.

Otsubo and co-workers have reported the first successful synthesis of heteroatom-containing bowl-shaped π-conjugated molecule, a trithiasumanene in 1999 (Scheme 1-12).[19] They employed benzo[1,2-*b*:3,4-*b*':5,6-*b*'']trithiophene as the precursor instead of triphenylene which was used in previous Klemm's work. They introduced three α-chlorovinyl groups to benzotrithiophene over three steps. The FVP reaction of the two regioisomers at 1000 °C provided the target product in 35% yield. The detailed structure of the trithiasumanene was elucidated by X-ray crystal diffraction analysis. As expected, the trithiasumanene has a bowl-shaped structure as in the case of parent sumanene. In addition, the bowl depth of the trithiasumanene (0.65 Å) is shallower than that of sumanene (1.11 Å).[20] The structural change is most probably due to the difference in bond lengths between carbon–carbon and carbon–sulfur bonds. Another group also achieved the synthesis of a triselenasumanene, in which three benzylic carbon atoms of sumanene were replaced with three selenium atoms (Scheme 1-13).[21] The bowl depth of the triselenasumanene is calculated to be 0.47 Å.

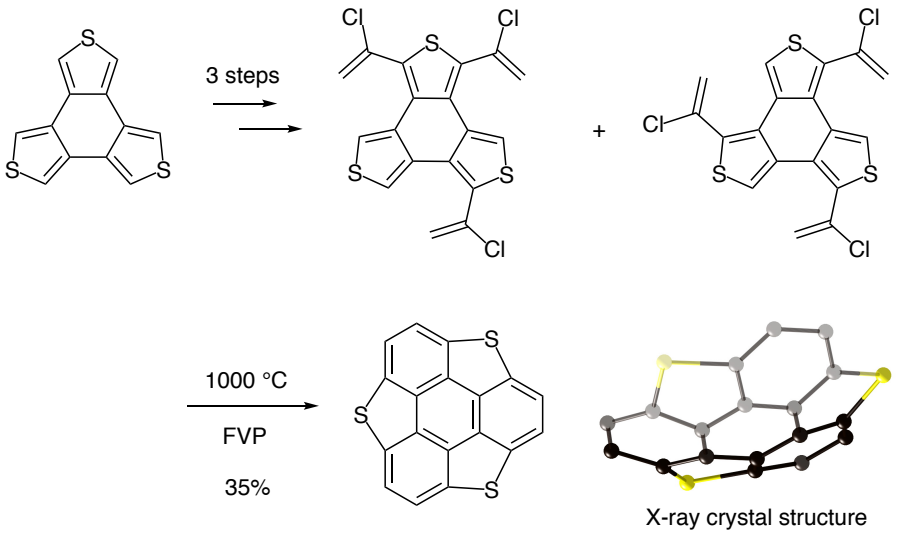

Scheme 1-12. The first chemical synthesis of a trithiasumanene.

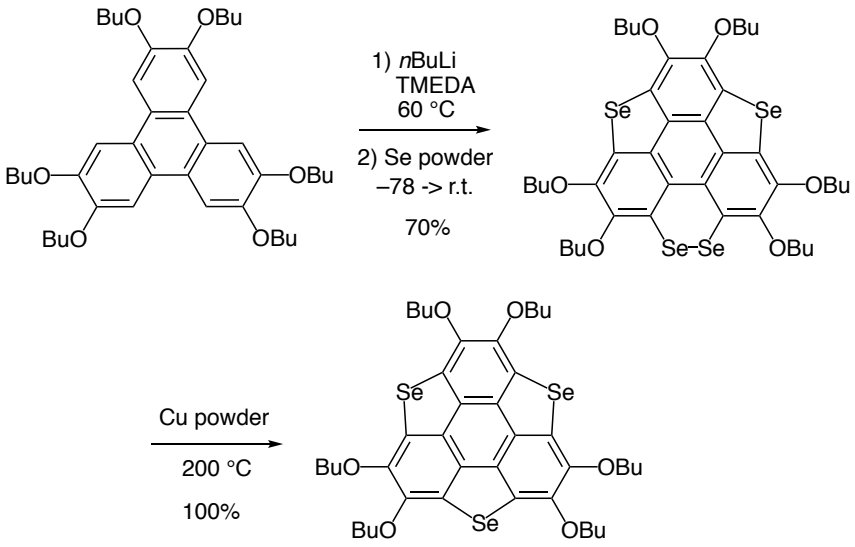

Scheme 1-13. The synthesis of a triselenasumanene.

Higashibayashi and Sakurai and co-workers have also succeeded in the synthesis of a nitrogen-doped azabuckybowl, that is, triazasumanene (Scheme 1-14).[22] In triazasumanene, three sp^2 carbon atoms of sumanene were replaced with three imine-type nitrogen atoms. They utilized a bowl-shaped intermediate with sp^3 carbon atoms in its skeleton, at which the pyramidalization strain is effectively relieved. The

following oxidative aromatization reaction successfully resulted in the construction of three pyridine rings. The triazasumanene has bowl chirality. From X-ray crystal diffraction analysis, the bowl depth of triazasumanene was measured to be 1.30 Å, while the value of parent sumanene is 1.11 Å. The bowl inversion energy was estimated to be ΔE = 39.9 kcal mol^{-1} by DFT calculations, which is much larger than that of sumanene (ΔE = 19.7–20.4 kcal mol^{-1} in various solvents).[23] The difference of these properties reflects the effect of the replacement of carbon atoms with nitrogen atoms.

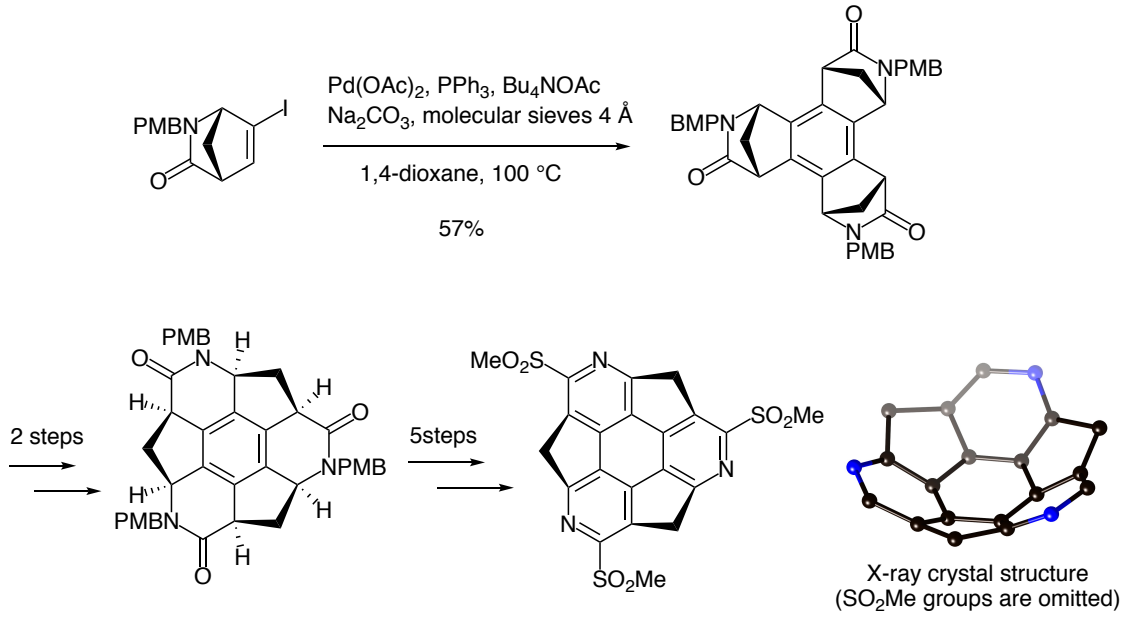

Scheme 1-14. The enantioselective synthesis of a triazasumanene.

After the author had reported the synthesis of nitrogen-embedded bowl-shaped molecules, several research groups succeeded in obtaining other kinds of heterobuckybowls. These examples are also summarized below.

In 2017, Scott and co-workers achieved the synthesis of a π-extended azacorannulene, that is, 5-azadibenzo[*a*,*g*]corannulene (Scheme 1-15).[15] The azacorannulene contains one nitrogen atom at the peripheral position. Because of the basicity of the imine-type nitrogen atom, the protonation reaction proceeded at this site reversibly. The azacorannulene was decomposed during silica gel chromatography due to the hydrolysis

of the C=N bond.

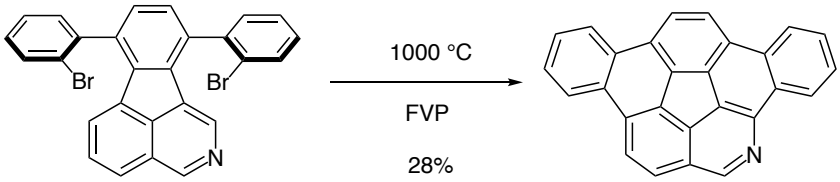

Scheme 1-15. The synthesis of 5-azadibenzo[*a*,*g*]corannulene.

In 2016, Higashibayashi and co-workers have synthesized a hydrazinobuckybowl, in which internal two sp^2 carbon atoms of diindenochrysene were replaced with an N–N unit (Scheme 1-16).[24] The hydrazinobuckybowl has twisted structure, while the corresponding one-electron oxidized species has bowl-shaped geometry. Further oxidation afforded the corresponding dicationic species, which has planar π-structure.

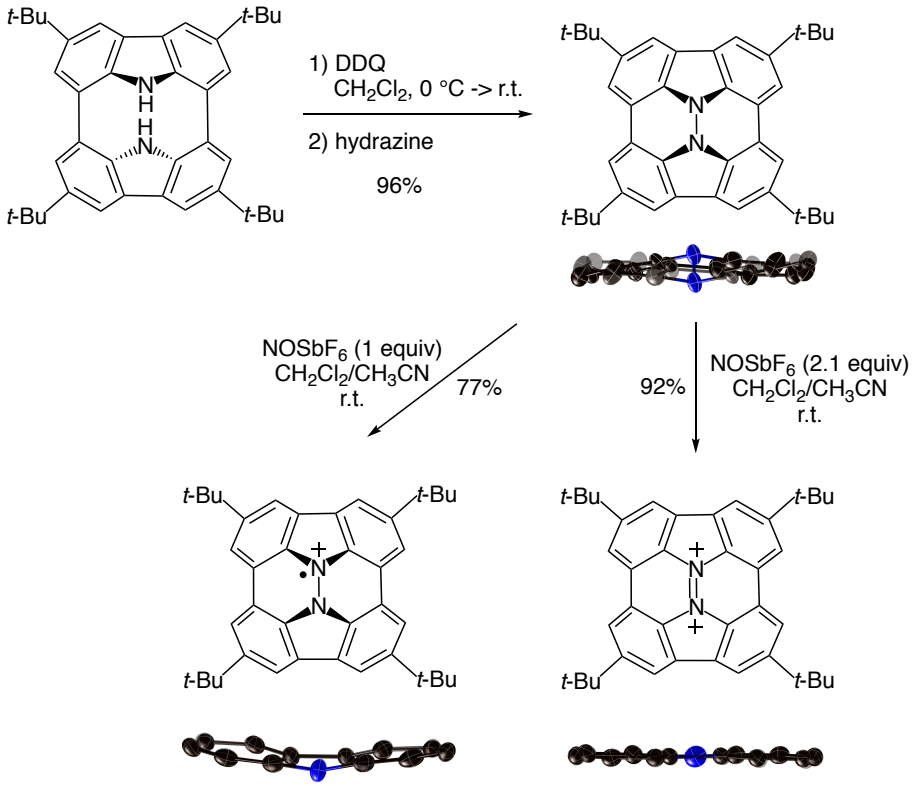

Scheme 1-16. The synthesis of a hydrazinobuckybowl.

Very recently, Saito, Furukawa, and co-workers have succeeded in the synthesis of triphosphasumanene trisulfide, in which three benzylic carbon atoms of sumanene were replaced with three phosphorus substituents (Scheme 1-17).[25] In this case, two isomers, that is *syn*- and *trans*-isomer, were formed. The three sulfur atoms face in the same direction in the *syn*-isomer, while one of the three sulfur atoms faces in the opposite direction in the *trans*-isomer. The *syn*-isomer has bowl-shaped structure. The bowl depth was determined to be 0.46 Å. On the other hand, *trans*-isomer has a planar π-surface. The *cis*-isomer exhibits high out-of-plane anisotropy. Furthermore, the π-surface of the *syn*-isomer, in which the three sulfur atoms are located, exhibits the electron-rich character. Consequently, the strong interaction between the electron-rich π-surface and a gold surface was observed.

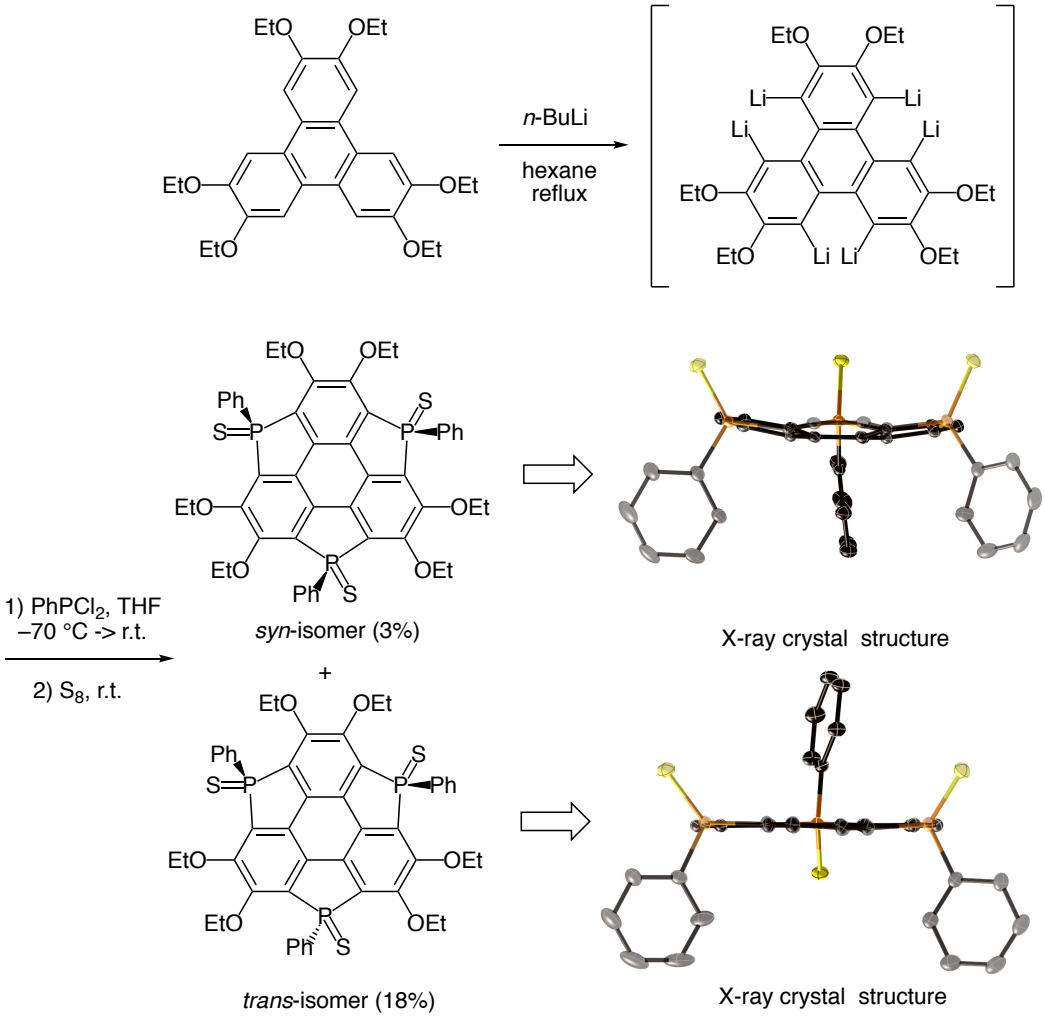

Scheme 1-17. The synthesis of triphosphasumanene trisulfide.

1-4. Overview of This Thesis

In this thesis, the author describes the synthesis of nitrogen-embedded bowl-shaped molecules, that is, penta-*peri*-pentabenzoazacorannulenes. Previous examples of heteroatom-containing bowl-shaped molecules have heteroatoms in their peripheral positions. On the other hand, a penta-*peri*-pentabenzoazacorannulene has a nitrogen atom in its central position. The introduction of electron-rich pyrrole skeleton to the bowl-shaped molecule drastically enhanced its electron-donating ability, which provided various functionalities to this molecule. Nozaki, Ito, and co-worker also reported the synthesis of a penta-*peri*-pentabenzoazacorannulene at around the same time (Chart

1-2).[26] They employed a π-extended azomethine ylide as the precursor.

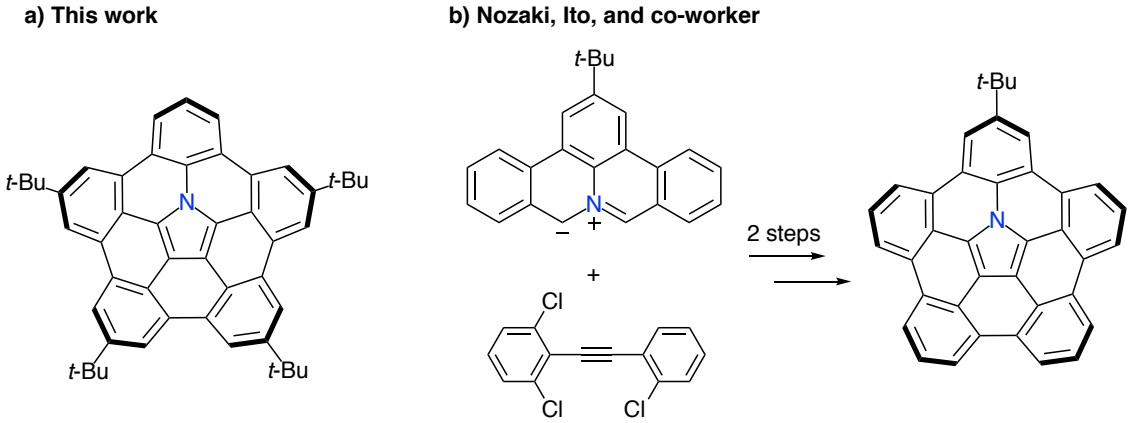

Chart 1-2. The structure of penta-*peri*-pentabenzoazacorannulenes.

The synthesis of penta-*peri*-pentabenzoazacorannulene is discussed in Chapter 2. The oxidative dimerization reaction followed by transition metal-catalyzed coupling reactions successfully afforded the target bowl-shaped compound. The penta-*peri*-pentabenzoazacorannulene exhibits electron-donating nature, which enables the strong association with C_{60} both in solution and solid state. In addition, the formation of the radical cation species was confirmed in the presence of acid.

Chapter 3 described the application of a penta-*peri*-pentabenzoazacorannulene to the generation of supramolecular assemblies. A directly connected penta-*peri*-pentabenzoazacorannulene dimer was synthesized via a palladium-catalyzed C–H/C–Br coupling. The dimer formed 1:1 complex with C_{60} in diluted solution, while 1D chain supramolecular assemblies were detected upon increasing the concentration of C_{60}.

In Chapter 4, the author investigated the reactivities of a bowl-shaped radical cation. The radical cation species of penta-*peri*-pentabenzoazacorannulene formed σ-dimer in the crystal state as well as in the solution state at low temperatures. Comparison experiment with analogous planar molecule revealed the importance of bowl-shaped structure for the bond formation at its internal carbon atom.

In the course of examining the scope and limitation of the oxidation reaction of aromatic amines, the author also found the oxidation of 2-amino-substituted BODIPY resulted in the formation of pyrazine-fused BODIPY trimers or diazo-bridged BODIPY dimer depending on the structure of the precursors. These results are also summarized in APPENDIX.

References

1. *Fragments of Fullerenes and Carbon Nanotubes: Designed Synthesis, Unusual Reactions, and Coordination Chemistry*, ed. M. A. Petrukhina and L. T. Scott, Wiley, Hoboken, 2012.

2. (a) Y. -T. Wu, J. S. Siegel, *Chem. Rev.* **2006**, *106*, 4843. (b) W. E. Barth, R. G. Lawton, *J. Am. Chem. Soc.* **1966**, *88*, 380. (c) H. Sakurai, T. Daiko, T. Hirao, *Science* **2003**, *301*, 1878.

3. T. Kawase, H. Kurata, *Chem. Rev.* **2006**, *106*, 5250.

4. (a) L. N. Dawe, T. A. AlHujran, H. -A. Tran, J. I. Mercer, E. A. Jackson, L. T. Scott, P. E. Georghiou, *Chem. Commun.* **2012**, *48*, 5563. (b) A. S. Filatov, M. V. Ferguson, S. N. Spisak, B. Li, C. F. Campana, M. A. Petrukhina, *Cryst. Growth Des.* **2014**, *14*, 756. (c) S. Mizyed, P. E. Georghiou, M. Bancu, B. Cuadra, A. K. Rai, P. Cheng, L. T. Scott, *J. Am. Chem. Soc.* **2001**, *123*, 12770. (d) P. E. Georghiou, A. H. Tran, S. Mizyed, M. Bancu, L. T. Scott, *J. Org. Chem.* **2005**, *70*, 6158. (e) A. Sygula, F. R. Fronczek, R. Sygula, P. W. Rabideau, M. M. Olmstead, *J. Am. Chem. Soc.* **2007**, *129*, 3842. (f) M. Yanney, F. R. Fronczek, A. Sygula, *Angew. Chem. Int. Ed.* **2015**, *54*, 11153. (g) C. M. Álvarez, L. A. García-Escudero, R. García-Rodríguez, J. M. Martíın-Álvarez, D. Miguel, V. M. Rayón, *Dalton Trans.* **2014**, *43*, 15693. (h) P. L. A. Kuragama, F. R. Fronczek, A. Sygula, *Org. Lett.* **2015**, *17*, 5292.

5. (a) D. Sun, F. S. Tham, C. A. Reed, L. Chaker, P. D. W. Boyd, *J. Am. Chem. Soc.* **2002**, *124*, 6604.

6. (a) L. T. Scott, M. M. Hashemi, M. S. Bratcher, *J. Am. Chem. Soc.* **1992**, *114*, 1920. (b) T. Amaya, H. Sakane, T. Muneishi, T. Hirao, *Chem. Commun.* **2008**, 765.

7. S. Fujii, M. Ziatdinov, S. Higashibayashi, H. Sakurai, M. Kiguchi, *J. Am. Chem. Soc.* **2016**, *138*, 12142.

8. (a) D. V. Preda, L. T. Scott, *Tetrahedron Lett.* **2000**, *41*, 9633. (b) A. V. Zabula, S. N. Spisak, A. S. Filatov, A. Yu. Rogachev, M. A. Petrukhina, *Angew. Chem. Int. Ed.* **2011**, *50*, 2971. (c) N. Ngamsomprasert, J. -S. Dang, S. Higashibayashi, Y. Yakiyama, H. Sa-

kurai, *Chem. Commun.* **2017**, *53*, 697. (d) L. T. Scott, *Chem. Soc. Rev.* **2015**, *44*, 6464. (e) C. Dubceac, A. V. Zabula, A. S. Filatov, F. Rossi, P. Zanello, M. A. Petrukhina, *J. Phys. Org. Chem.* **2012**, *25*, 553. (f) C. Dubceac, A. S. Filatov, A. V. Zabula, M. A. Petrukhina, *Cryst. Growth Des.* **2015**, *15*, 778. (g) M. Yanney, F. R. Fronczek, A. Sygula, *Org. Lett.* **2012**, *14*, 4942. (h) H. E. Bronstein, L. T. Scott, *J. Org. Chem.* **2008**, *73*, 88. (i) H. Y. Cho, R. B. M. Ansems, L. T. Scott, *Beilstein J. Org. Chem.* **2014**, *10*, 956.

9. (a) L. T. Scott, M. M. Hashemi, D. T. Meyer, H. B. Warren, *J. Am. Chem. Soc.* **1991**, *113*, 7082. (b) H. -J. Knölker, A. Braier, D. J. Bröcher, P. G. Jones, H. Piotrowski, *Tetrahedron Lett.* **1999**, *40*, 8075. (c) C. Z. Liu, P. W. Rabideau, *Tetrahedron Lett.* **1996**, *37*, 3437. (d) L. T. Scott, P. -C. Cheng, M. M. Hashemi, M. S. Bratcher, D. T. Meyer, H. B. Warren, *J. Am. Chem. Soc.* **1997**, *119*, 10963. (e) A. Borchardt, A. Fuchicello, K. V. Kilway, K. K. Baldridge, J. S. Siegel, *J. Am. Chem. Soc.* **1992**, *114*, 1921. (f) G. Mehta, G. Panda, *Tetrahedron Lett.* **1997**, *38*, 2145. (g) L. T. Scott, M. S. Bratcher, S. Hagen, *J. Am. Chem. Soc.* **1996**, *118*, 8743. (h) R. B. M. Ansems, L. T. Scott, *J. Am. Chem. Soc.* **2000**, *122*, 2719. (i) L. T. Scott, E. A. Jackson, Q. Zhang, B. D. Steinberg, M. Bancu, B. Li, *J. Am. Chem. Soc.* **2012**, *134*, 107. (j) L. T. Scott, M. S. Bratcher, S. Hagen, *J. Am. Chem. Soc.* **1996**, *118*, 8743. (k) H. E. Bronstein, N. Choi, L. T. Scott, *J. Am. Chem. Soc.* **2002**, *124*, 8870. (l) S. Hagen, M. S. Bratcher, M. S. Erickson, G. Zimmermann, L. T. Scott, *Angew. Chem. Int. Ed. Engl.* **1997**, *36*, 406.

10. T. J. Seiders, K. K. Baldridge, J. S. Siegel, *J. Am. Chem. Soc.* **1996**, *118*, 2754.

11. (a) T. J. Seiders, E. L. Elliott, G. H. Grube, J. S. Siegel, *J. Am. Chem. Soc.* **1999**, *121*, 7804. (b) Z. Marcinow, D. I. Grove, P. W. Rabideau, *J. Org. Chem.* **2002**, 67, 3537. (c) A. Sygula, S. D. Karlen, R. Sygula, P. W. Rabideau, *Org. Lett.* **2002**, *4*, 3135. (d) A. Sygula, P. W. Rabideau, *J. Am. Chem. Soc.* **1998**, *120*, 12666.

12. (a) A. Sygula, P. W. Rabideau, *J. Am. Chem. Soc.* **2000**, *122*, 6323. (b) A. M. Butterfield, B. Gilomen, J. S. Siegel, *Org. Process Res. Dev.* **2012**, *16*, 664.

13. (a) H. -I. Chang, H. -T. Huang, C. -H. Huang, M. -Y. Kuo, Y. -T. Wu, *Chem. Commun.* **2010**, *46*, 7241. (b) D. Kim, J. L. Petersen, K. K. Wang, *Org. Lett.* **2006**, *8*,

2313. (c) H. A. Reisch, M. S. Bratcher, L. T. Scott, *Org. Lett.* **2000**, *2*, 1427. (d) T. -C. Wu, H. -J. Hsin, M. -Y. Kuo, C. -H. Li, Y. -T. Wu, *J. Am. Chem. Soc.* **2011**, *133*, 16319. (e) J. Liu, S. Osella, J. Ma, R. Berger, D. Beljonne, D. Schollmeyer, X. Feng, K. Müllen, *J. Am. Chem. Soc.* **2016**, *138*, 8364. (f) K. Y. Amsharov, M. A. Kabdulov, Martin Jansen, *Angew. Chem. Int. Ed.* **2012**, *51*, 4594. (g) O. Papaianina, V. A. Akhmetov, A. A. Goryunkov, F. Hampel, F. W. Heinemann, K. Y. Amsharov, *Angew. Chem. Int. Ed.* **2017**, *56*, 4834.

14. (a) O. Vostrowsky, A. Hirsch, *Chem. Rev.* **2006**, *106*, 5191. (b) J. W. Jang, C. E. Lee, S. C. Lyu, T. J. Lee, C. J. Lee, *Appl. Phys. Lett.* **2004**, *84*, 2877. (c) K. Gong, F. Du, Z. Xia, M. Durstock, L. Dai, *Science* **2009**, *323*, 760.

15. V. M. Tsefrikas, A. K. Greene, L. T. Scott, *Org. Chem. Front.* **2017**, *4*, 688.

16. R. F. C. Brown, M. Butcher, R. A. Fergie, *Aust. J. Chem.* **1973**, *26*, 1319

17. V. M. Tsefrikas, S. Arns, P. M. Merner, C. C. Warford, B. L. Merner, L. T. Scott, G. J. Bodwell, *Org. Lett.* **2006**, *8*, 5195.

18. L. H. Klemm, E. Hall, L. Cousins, C. E. Klopfenstein, *J. Heterocycl. Chem.* **1989**, *26*, 345.

19. K. Imamura, K. Takimiya, Y. Asob, T. Otsubo, *Chem. Commun.* **1999**, 1859.

20. H. Sakurai, T. Daiko, H. Sakane, T. Amaya, T. Hirao, *J. Am. Chem. Soc.* **2005**, *127*, 11580.

21. X. Li, Y. Zhu, J. Shao, B. Wang, S. Zhang, Y. Shao, X. Jin, X. Yao, R. Fang, X. Shao, *Angew. Chem. Int. Ed.* **2014**, *53*, 535.

22. (a) Q. Tan, S. Higashibayashi, S. Karanjit, H. Sakurai, *Nat. Commun.* **2012**, *3*, 891. (b) P. Kaewmati, Q. Tan, S. Higashibayashi, Y. Yakiyama, H. Sakurai, *Chem. Lett.* **2017**, *46*, 146.

23. T. Amaya, H. Sakane, T. Muneishi, T. Hirao, *Chem. Commun.* **2008**, 765.

24. S. Higashibayashi, P. Pandit, R. Haruki, S. Adachi, R. Kumai, *Angew. Chem. Int. Ed.* **2016**, *55*, 10830.

25. S. Furukawa, Y. Suda, J. Kobayashi, T. Kawashima, T. Tada, S. Fujii, M. Kiguchi,

M. Saito, *J. Am. Chem. Soc.* **2017**, *139*, 5787.

26. S. Ito, Y. Tokimaru, K. Nozaki, *Angew. Chem. Int. Ed.* **2015**, *54*, 7256.

Chapter 2

Synthesis and Properties of Penta-*peri*-Pentabenzoazacorannulene

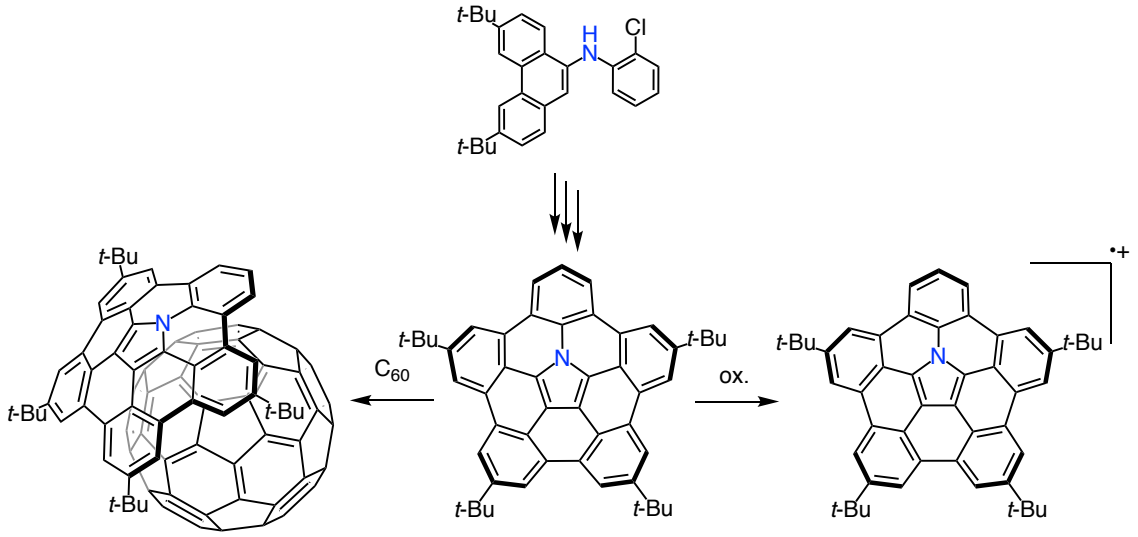

ABSTRACT: Curved π-conjugated molecules have attracted considerable interest because of the unique properties originating from their curved π surface. However, the synthesis of such distorted molecules requires harsh reaction conditions, which hamper easy access to heteroatom-containing curved π systems. In this chapter, the author reports the synthesis of a π-extended azacorannulene, which has a nitrogen atom in its center. The oxidation of 9-aminophenanthrene provides tetrabenzocarbazole, which is converted to the penta-*peri*-pentabenzoazacorannulene through palladium-catalyzed intramolecular cross-coupling reactions. The author also revealed its electron-donating nature and curved π-surface enable the efficient association with C_{60} both in solution and solid states. High charge-carrier mobility is observed for the penta-*peri*-pentabenzoazacorannulene/C_{60} assembly. This compound should be of broad interest in the fields of curved π-systems as fullerene hosts, anisotropic π-donors and precursors to nitrogen-containing nanocarbon materials.

Contents

2-1. Introduction

Bowl-shaped π-conjugated molecules such as corannulenes and sumanenes have attracted much attention as precursors for the bottom-up synthesis of fullerenes and nanotubes.[1,2] In 1966, Barth and Lawton reported the first chemical synthesis of corannulene.[2a] Since Scott and Siegel's groups developed their straightforward synthesis of corannulene, numerous bowl-shaped hydrocarbons have been synthesized.[3] To enhance these characteristics, the introduction of heteroatoms is an effective strategy. However, the synthesis of heteroatom-containing bowl-shaped π-conjugated molecules remains a challenge.[4] The preparation of such distorted π systems requires harsh reaction conditions that do not tolerate heterocyclic molecules.[4d,5]

Aniline, the representative example of aromatic amines, affords "aniline black" by oxidation.[6] This black pigment is a mixture of oligomeric products. Thus, in the oxidation reaction of a simple aromatic amine such as aniline, the control of the reaction is quite difficult. Recently, Shinokubo and co-workers have reported the efficient oxidative dimerization of aminoarenes to π-extended fused products in a one-step operation.[7] In the oxidation reactions of 2-aminoanthracenes with 2,3-dichloro-5,6-dicyano-1,4-benzoquinone (DDQ), the pyrazine-fused dimer formed in the presence of trifluoroacetic acid (TFA), while the pyrrole-fused dimer was predominantly obtained upon the addition of ethanol (Scheme 2-1).[7b] In the course of examining the scope and limitation of these oxidative dimerization reactions, the author discovered that the oxidation of *N*-aryl-9-aminophenanthrenes afforded *N*-aryl-tetrabenzocarbazole in good yields (Scheme 2-2). This tetrabenzocarbazole has a partial structure of π-extended azacorannulene with nitrogen atom in its center.[8] As a result, the consecutive fusion reactions of tetrabenzocarbazole through palladium-catalyzed C–H/C–Cl and C–H/C–Br coupling achieved the synthesis of nitrogen-embedded bowl-shaped molecule, that is, penta-*peri*-pentabenzoazacorannulene under mild conditions.[9]

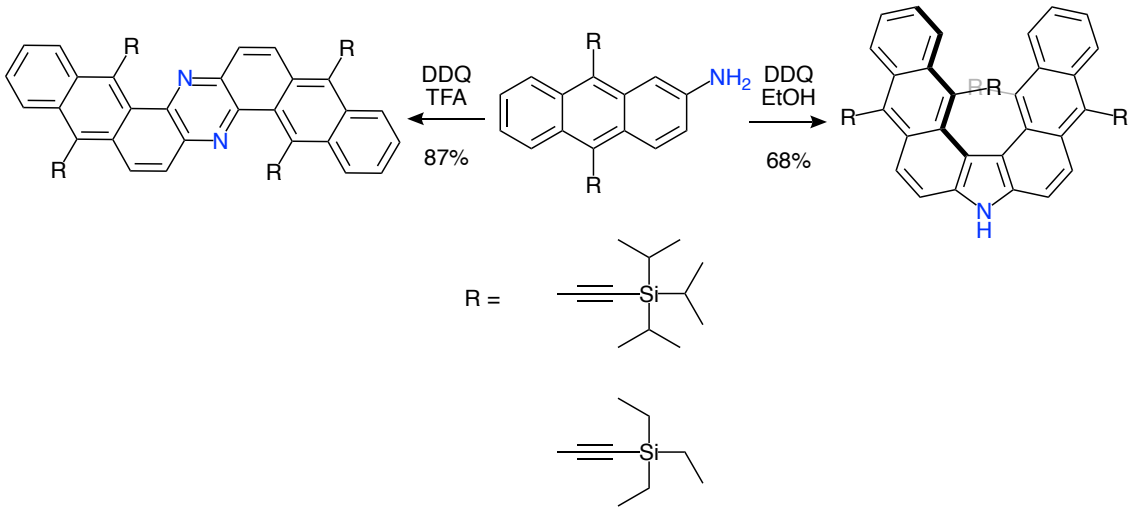

Scheme 2-1. Oxidation of 2-aminoanthracenes.

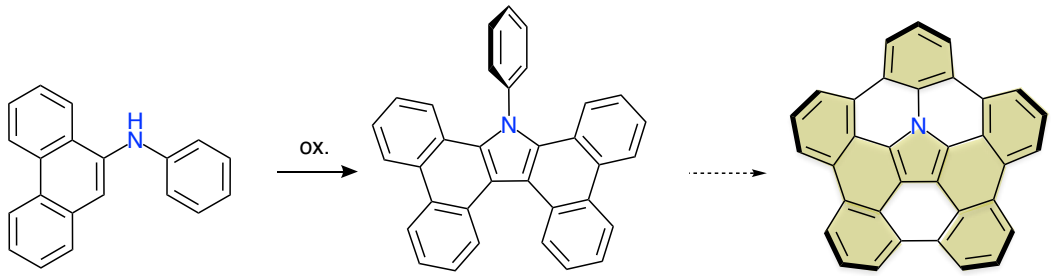

Scheme 2-2. Synthetic strategy for the synthesis of penta-*peri*-pentabenzoazacorannulene.

2-2. Synthesis and Characterization

The synthesis of nitrogen-embedded bowl-shaped molecule **6** started with the bromination of 3,6-di-*tert*-butylphenanthrene, which resulted in the formation of 9-bromophenanthrene **1** (Scheme 2-3). The Buchwald-Hartwig cross coupling reaction of **1** with 2-chloroaniline afforded 9-aminophenanthrene **2**. **2** was successfully converted into tetrabenzocarbazole **3** by oxidation with DDQ and TFA. Reaction of **3** with palladium(II) acetate and tricyclohexylphosphonium tetrafluoroborate successfully provided singly fused product **4** in 63% yield.[10] However, the oxidative fusion reaction of **4** with strong oxidant did not proceed well.[11] Thus, the author adopted transition met-

al-catalyzed cross-coupling reaction for the synthesis of penta-*peri*-pentabenzoazacorannulene. The bromination of **4** with bromine afforded tribrominated product **5** in 56% yield. The twisted conformations of **4** and **5** were unambiguously elucidated by X-ray diffraction analysis (Figure 2-1 and 2-2). Finally, the palladium-catalyzed double C–H/C–Br coupling reaction of **5** furnished penta-*peri*-pentabenzoazacorannulene **6** in 37% yield. In this time, doubly fused product **7** was also obtained in 5% yield. The ^{1}H NMR spectrum of **6** exhibited six proton signals in the aromatic region, indicating the formation of a fused and symmetrical molecule.

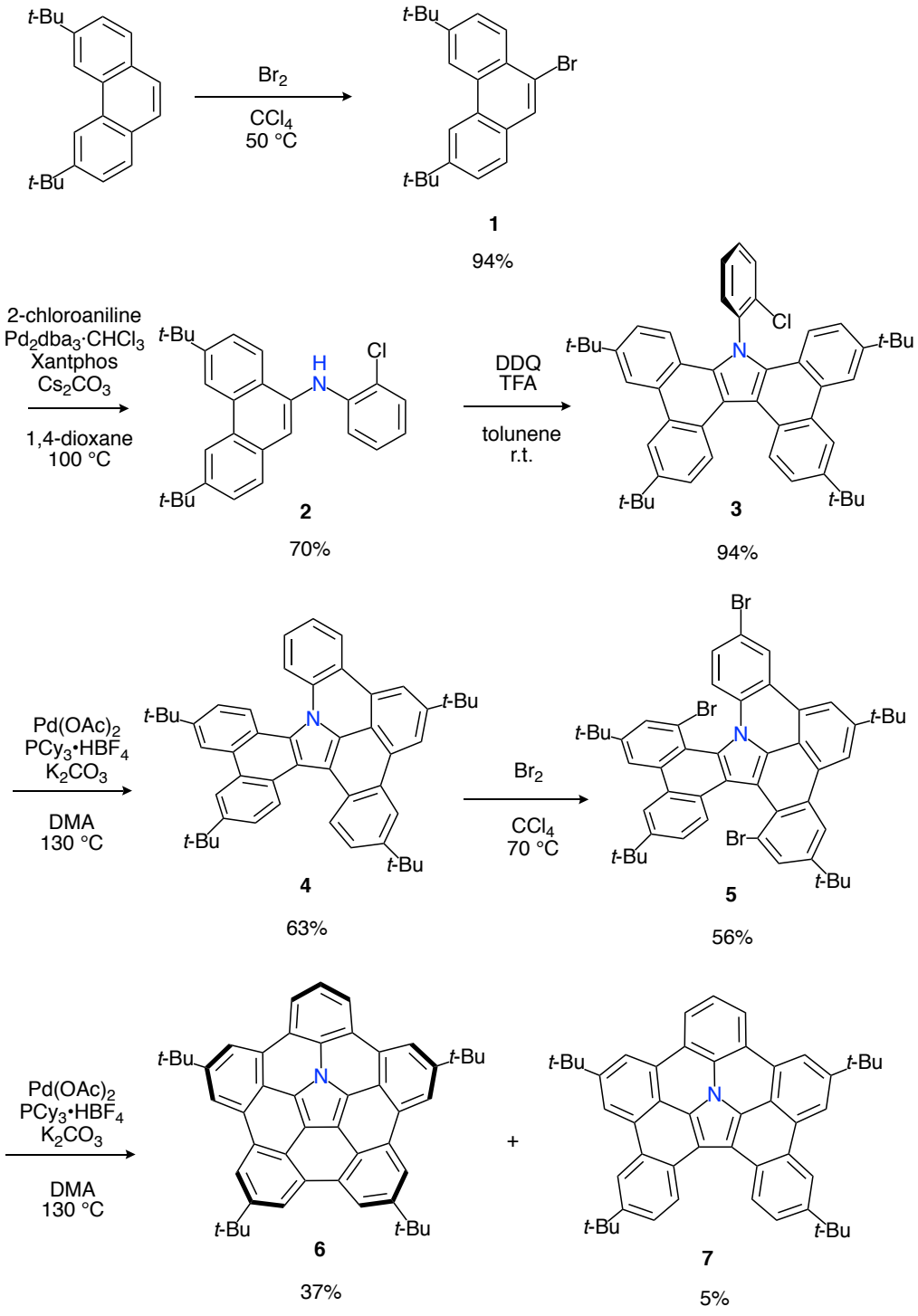

Scheme 2-3. Synthesis of penta-*peri*-pentabenzoazacorannulene **6**.

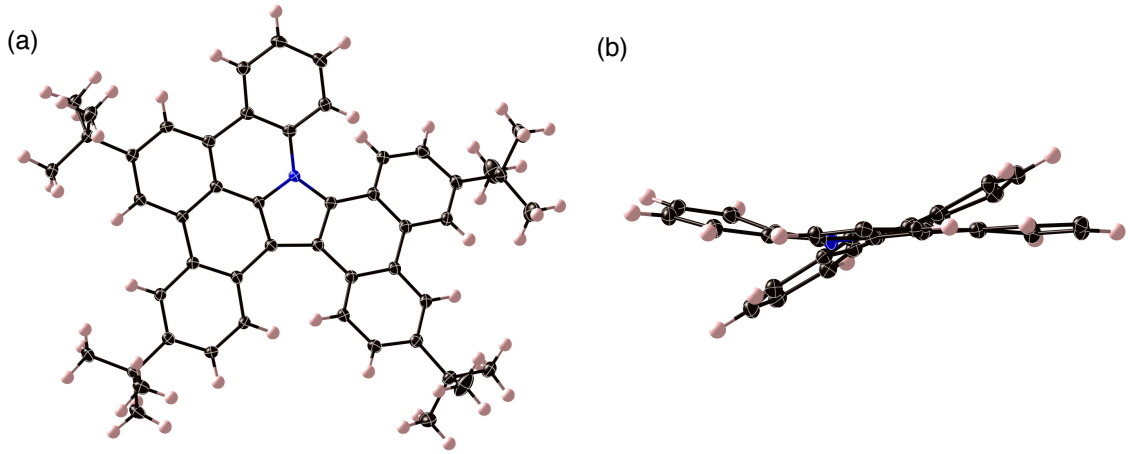

Figure 2-1. X-Ray crystal structure of **4**. (a) Top view and (b) side view. The thermal ellipsoids are scaled at 50% probability level. The *tert*-butyl substituents are omitted for clarity in (b).

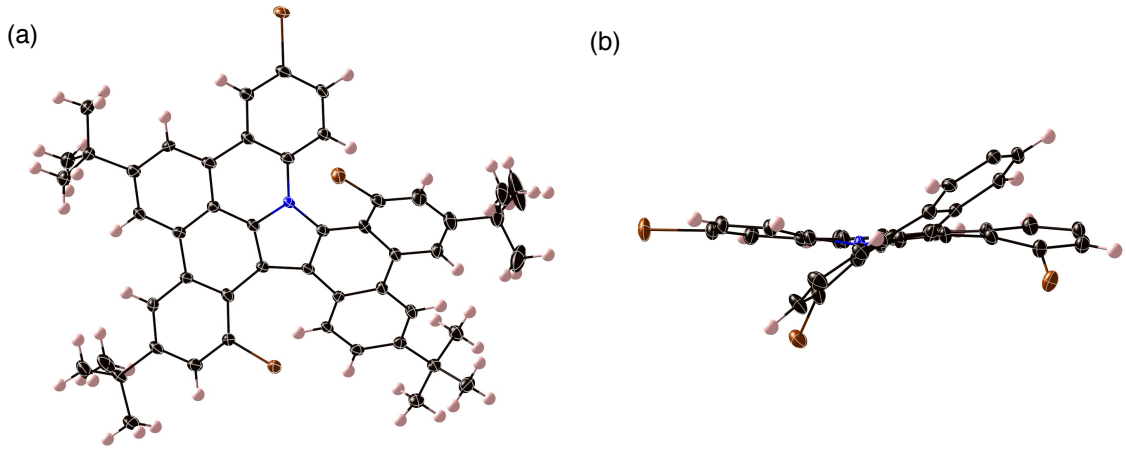

Figure 2-2. X-Ray crystal structure of **5**. (a) Top view and (b) side view. The thermal ellipsoids are scaled at 50% probability level. The *tert*-butyl substituents are omitted for clarity in (b).

2-3. Structural Elucidation

The bowl-shaped structure of **6** was unambiguously elucidated by X-ray diffraction analysis (Figure 2-3). In the crystal, one asymmetric unit contained two independent molecules of **6**. The bowl depth, which is defined as the distance between the mean plane consisted of five carbons at the edge and the centroid of the pyrrole ring,

was 1.65 and 1.70 Å. The curvature of **6** was further evaluated by Haddon's π-orbital axis vector (POAV) angles.[12] As shown in Figure 2-3a, the POAV angles around the central pyrrole rings are in the range of 7.2°–9.2°. These values are comparable with that of corannulene (9.1°). It is noteworthy that the molecules constructed a one-dimensional chain stacking structure in the crystal (Figure 2-3c). Distances between the two closest molecules were 3.25 and 3.41 Å, indicating the existence of a π–π interaction.

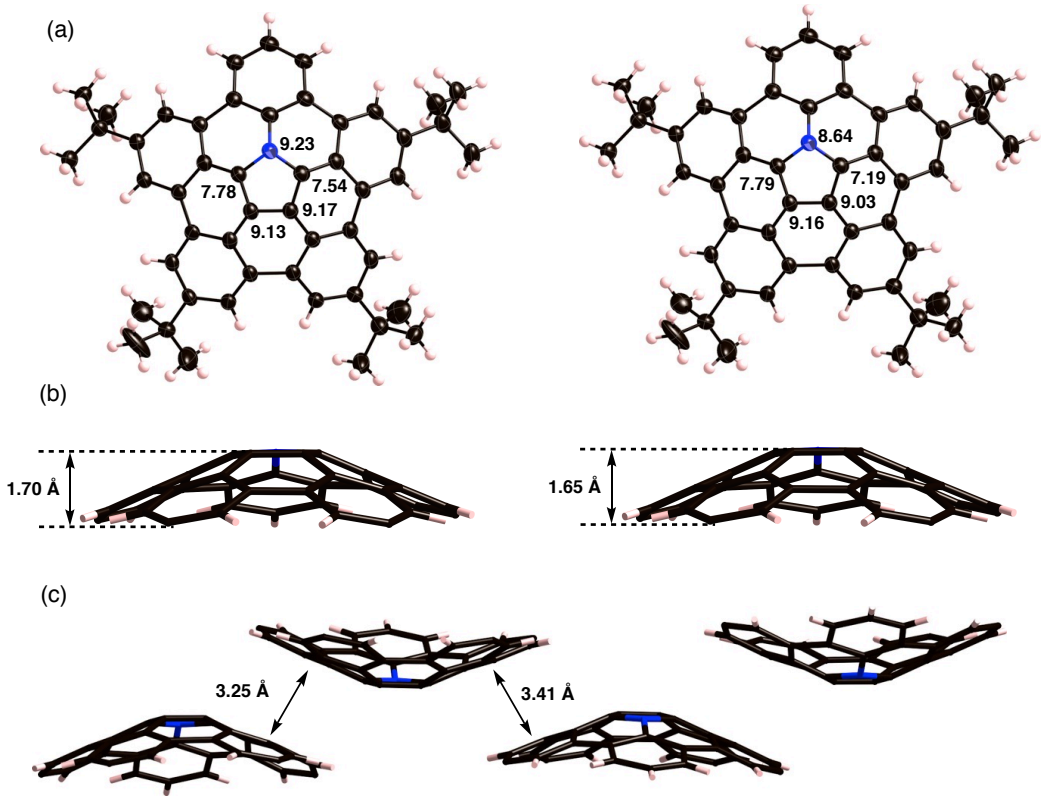

Figure 2-3. Structural features of **6**. (a) Top view and POAV pyramidalization angles, (b) side view, and (c) packing structure. Thermal ellipsoids in (a) are scaled at 50% probability level. The *tert*-butyl groups are omitted for clarity in (b) and (c).

Next, the bowl-to-bowl inversion behavior of the penta-*peri*-pentabenzoazacorannulene was investigated. Because there is no diastereotopic hydrogen atoms, **6** was further functionalized by iridium-catalyzed C–H borylation to provide **8** in 80% yield (Scheme 2-4).[13] The Suzuki–Miyaura cross-coupling reaction of **8** with 2-bromo-1,3,5-triisopropylbenzene furnished the corresponding coupling product **9** in 55% yield.

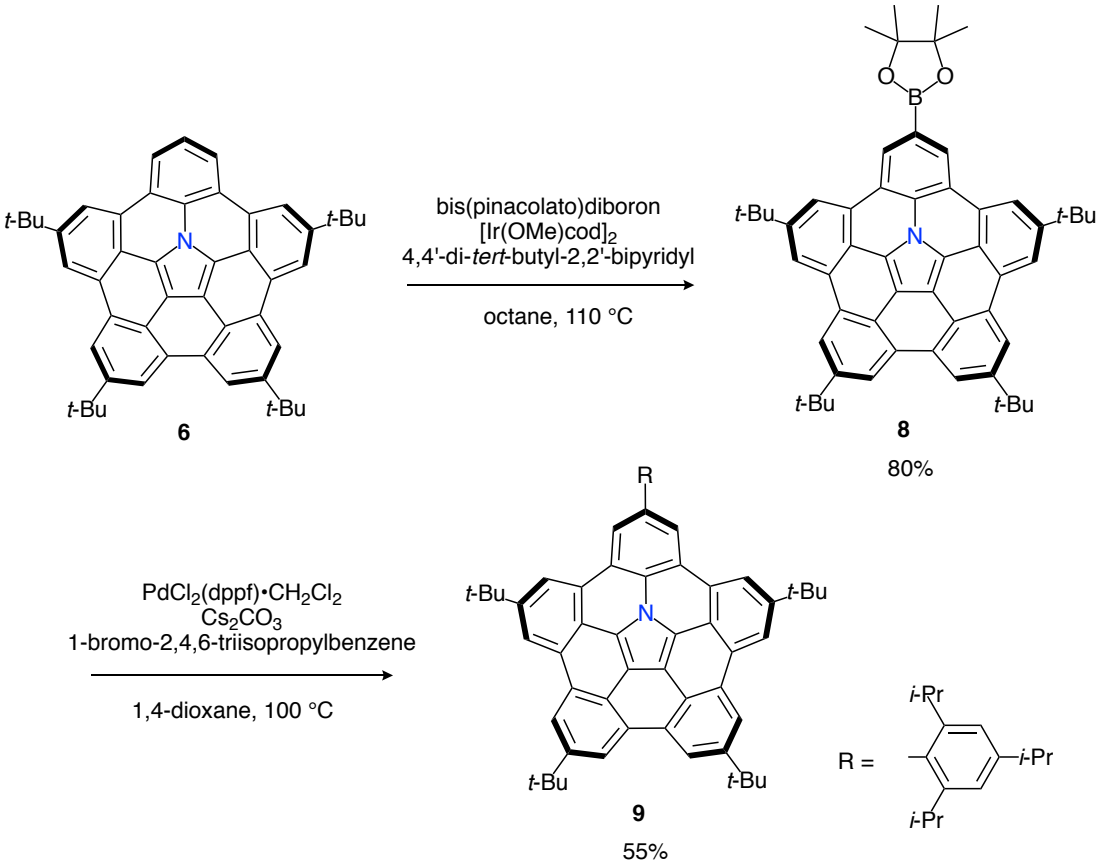

Scheme 2-4. Synthesis of functionalized penta-*peri*-pentabenzoazacorannulene **9**.

The ^{1}H NMR spectrum of **9** in 1,2-dichlorobenzene-d_4 at room temperature exhibited three doublet peaks for methyl protons of isopropyl groups at 1.43, 1.39 and 1.13 ppm. This non-symmetric feature indicates that **9** shows no bowl-to-bowl inversion at room temperature. As the temperature was raised, two proton signals at 1.43 and 1.13 ppm were gradually broadened (Figure 2-4). Even at 170 °C, these signals were not co-

alesced. Accordingly, the bowl-to-bowl inversion energy ($\Delta G^{\ddagger}$) was measured by two-dimensional exchange spectroscopy (2D EXSY) experiments (Figure 2-5).[14] At 393 K, $\Delta G^{\ddagger}$ was determined to be 23.3 kcal mol^{-1} in 1,2-dichlorobenzene-d_4. This value is higher than that of the parent sumanene ($\Delta G^{\ddagger}$ = 19.7–20.4 kcal mol^{-1}).[15] The high bowl-inversion energy of **9** was also supported by theoretical calculations. The inversion barrier of **9** was calculated to be 19.9 kcal mol^{-1} by density functional theory (DFT) calculations at the B3LYP/cc-pVDZ level, which is higher than those of sumanene (18.2 kcal mol^{-1}) and corannulene (9.1 kcal mol^{-1}) calculated at the same level of theory (Table 2-1).[16]

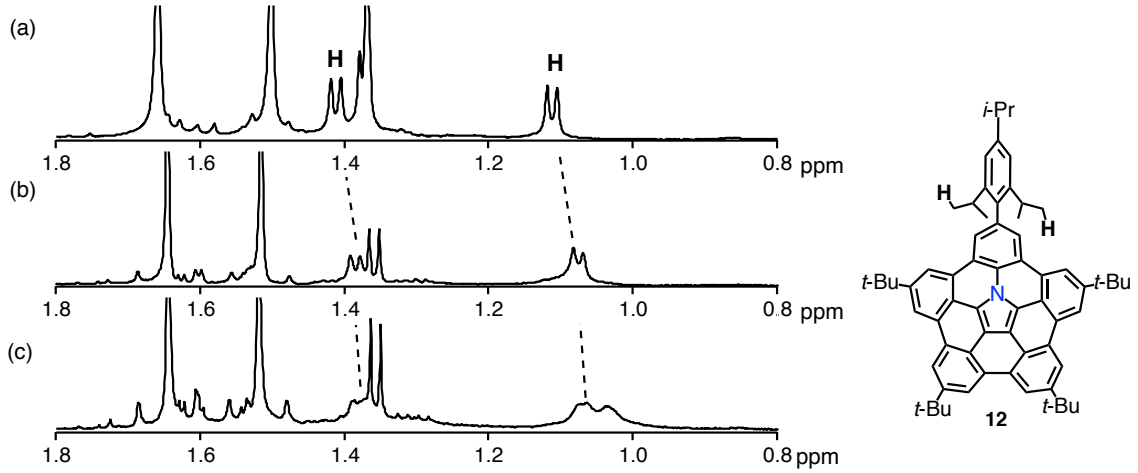

Figure 2-4. VT ^{1}H NMR spectra of **9** in 1,2-dichlorobenzene-d_4. (a) r.t. (b) 130 °C (c) 150 °C.

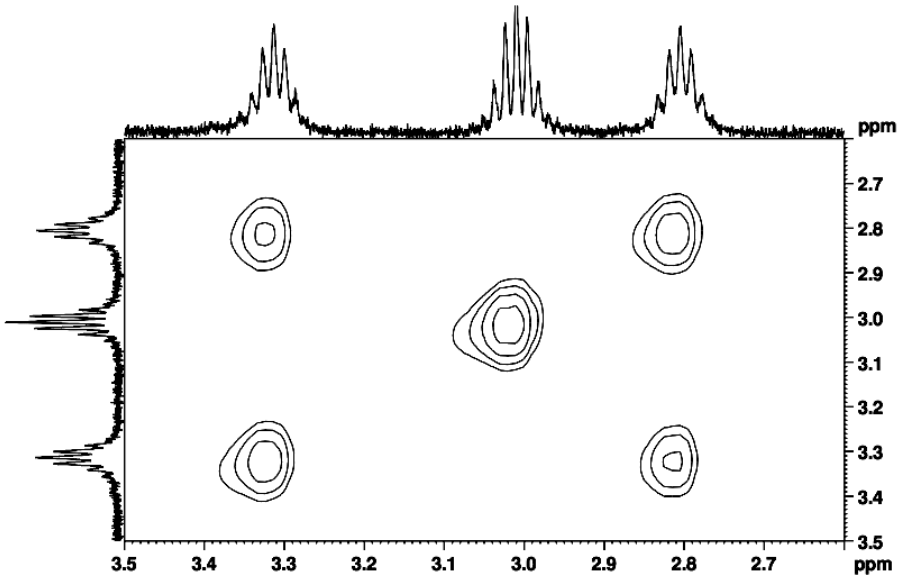

Figure 2-5. 2D EXSY spectrum of **9** in 1,2-dichlorobenzene-d_4 at 120 °C.

Table 2-1. Summary of calculations on the bowl-to-bowl inversion process of **9**.

	ground state	**transition state**
Energy (au)	–2572.302341	–2572.271074
Total Energy (au)	–2572.398423	–2572.366659
E_a (kcal/mol)	0	19.9

2-4. Optical and Electrochemical Properties

Figure 2-6 shows UV-vis absorption and emission spectra of **4**, **6**, and **7** in CH_2Cl_2. The lowest energy bands shifted to the low-energy region as the degree of fusion increased. All compounds exhibited fluorescence in the visible region. The emission quantum yield of **6** was 17%. The Stokes shifts of **4** (2800 cm^{-1}) and **6** (1500 cm^{-1}) were relatively larger than that of **7** (1200 cm^{-1}). This fact reflects the excited state dynamics of **4** and **6**, owing to their distorted characteristics.

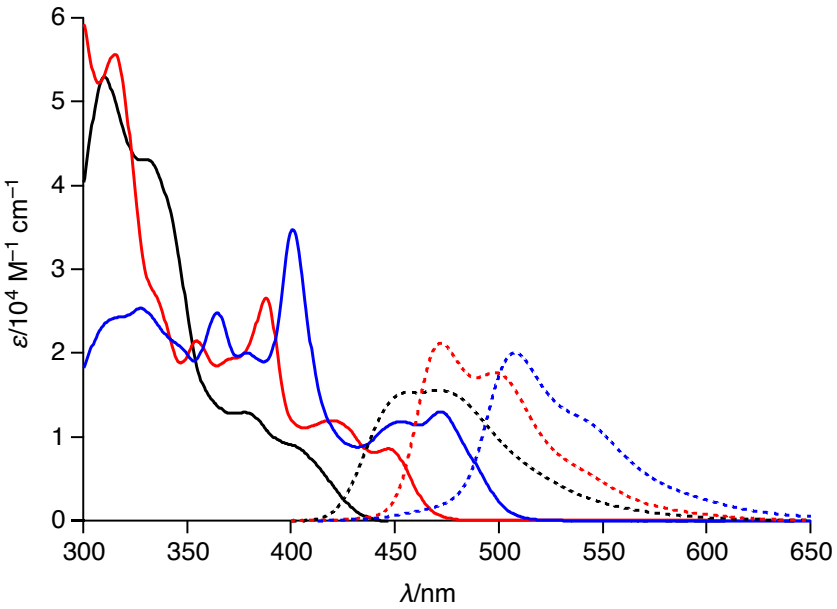

Figure 2-6. UV-vis absorption (solid line) and emission spectra (dashed line) of **4** (black), **6** (blue), and **7** (red) in CH_2Cl_2.

The electronic structures of **3**, **4**, **6,** and **7** were further investigated by an electrochemical analysis (Figure 2-7 and Table 2-2) using cyclic voltammetry. Reversible oxidation waves were observed for all compounds. The first oxidation potentials were lowered in the order of **3** > **4** > **7** > **6**, while the number of fused positions increased in this order.

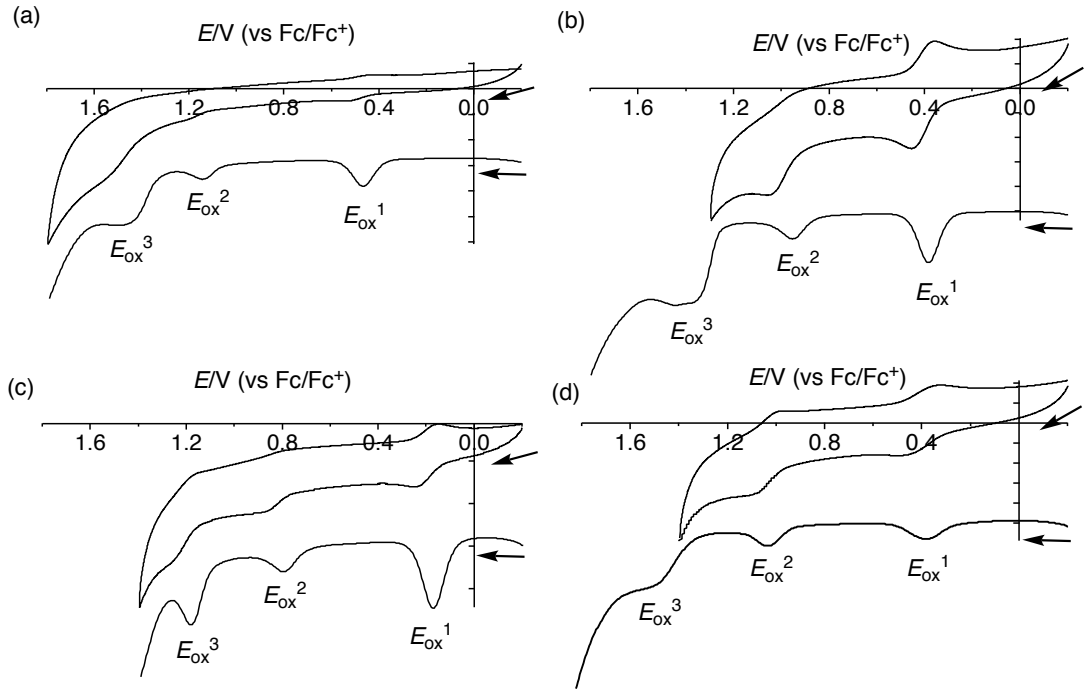

Figure 2-7. Cyclic voltammograms (top) and differential pulse voltammograms (bottom) of (a) **3**, (b) **4**, (c) **6**, and (d) **7**.

Table 2-2. Summary of the oxidation potentials of (a) **3**, (b) **4**, (c) **6**, and (d) **7**.

compound	E_{ox}^{3}	E_{ox}^{2}	E_{ox}^{1}
3	1.50[a]	1.15[a]	0.489
4	—	0.954[a]	0.408
6	1.19[a]	0.80[a]	0.20
7	1.44[a]	1.04	0.398

[a] The values were obtained by DPV measurement.

The author then examined the protonation behavior of **6**. The nitrogen atom of **6** was expected to have higher basicity than that of pyrrole because the central pyrrole ring of **6** is slightly distorted. The addition of TFA to a CH_2Cl_2 solution of **6** induced a dramatic change in its absorption spectrum (Figure 2-8). Interestingly, the same change

was observed on the addition of a one-electron oxidant, tris(4-bromophenyl)aminium hexachloroantimonate (BAHA) (Figure 2-9). The author also monitored the electro-oxidative absorption spectrum of **6** in CH_2Cl_2, which exhibited essentially the same change (Figure 2-10). These facts strongly indicate that the addition of TFA resulted in the generation of the radical cation specie rather than simple protonation. The generation of the radical cation species was also supported by the TD-DFT calculation of $\mathbf{6}^{\bullet+}$ (Figure 2-11).

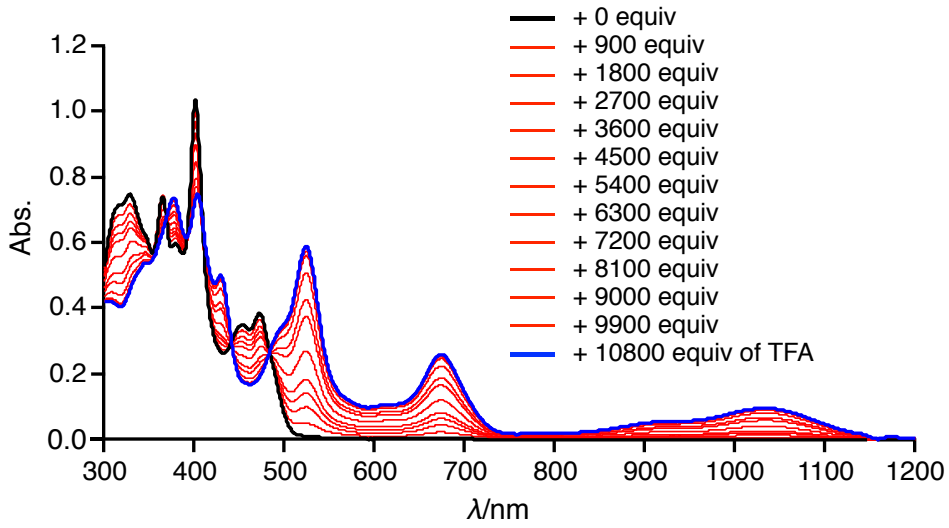

Figure 2-8. Spectral changes in absorption spectra of **6** on the addition of TFA into a CH_2Cl_2 solution of **6**.

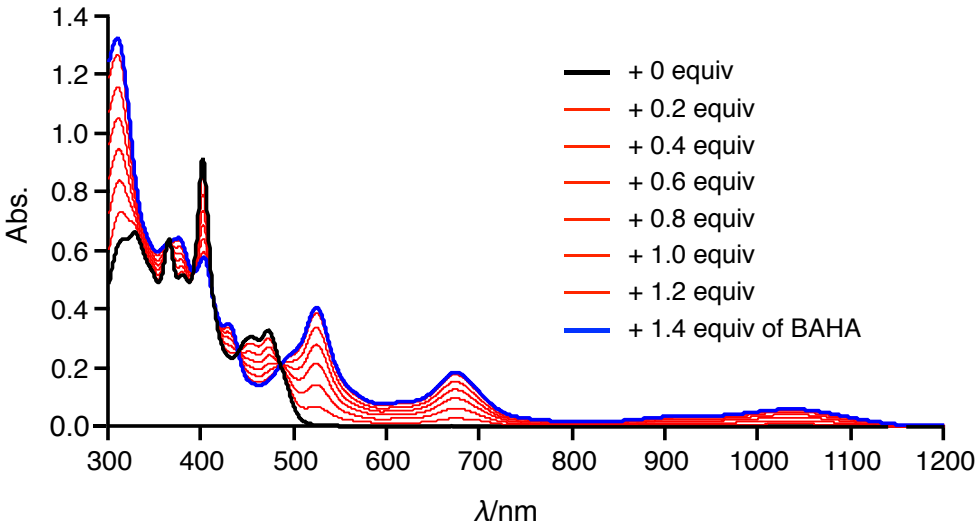

Figure 2-9. Spectral changes in absorption spectra of **6** on the addition of BAHA into a CH_2Cl_2 solution of **6**.

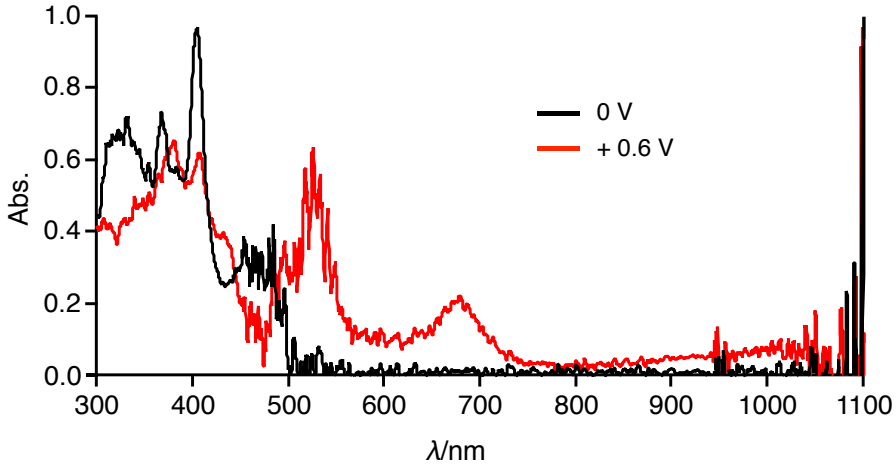

Figure 2-10. Spectroelectrochemical analysis of **6** in CH_2Cl_2.

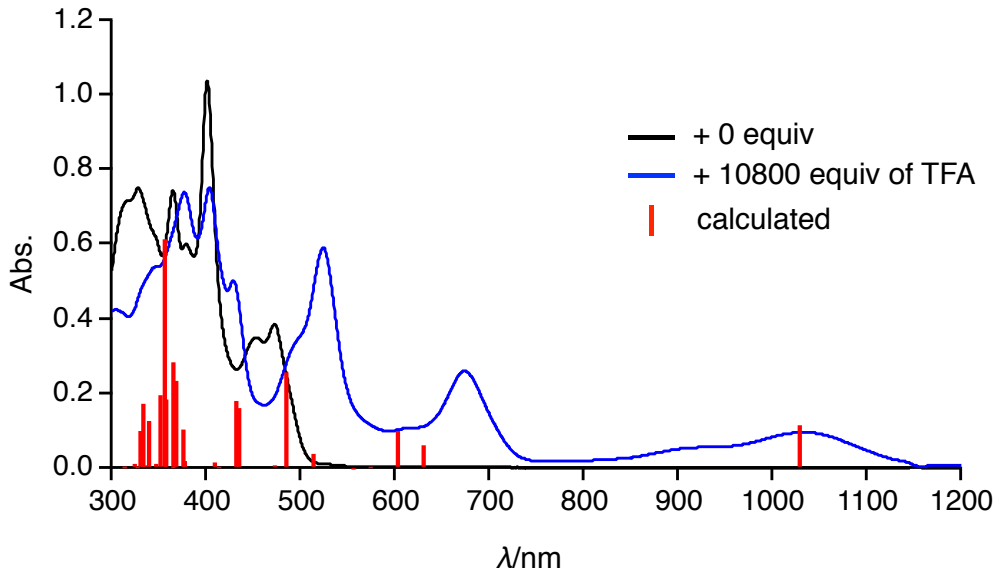

Figure 2-11. Calculated oscillator strengths of $\mathbf{6}^{\bullet+}$ (red line). The spectra of **6** before (black line) and after (blue line) addition of TFA were also displayed.

The formation of the radical cation was also confirmed by electron spin resonance (ESR) measurements (Figure 2-12). The solution of **6** in the presence of TFA exhibited a distinct signal at g = 2.002, as was the case of the oxidation of **6** with BAHA. The conversion of **6** to the radical cation was almost quantitative under air but was substantially lower under argon atmosphere (Figure 2-13). The radical cation generation is likely due to electron transfer between **6** and protonated **6** involving air oxidation.[17]

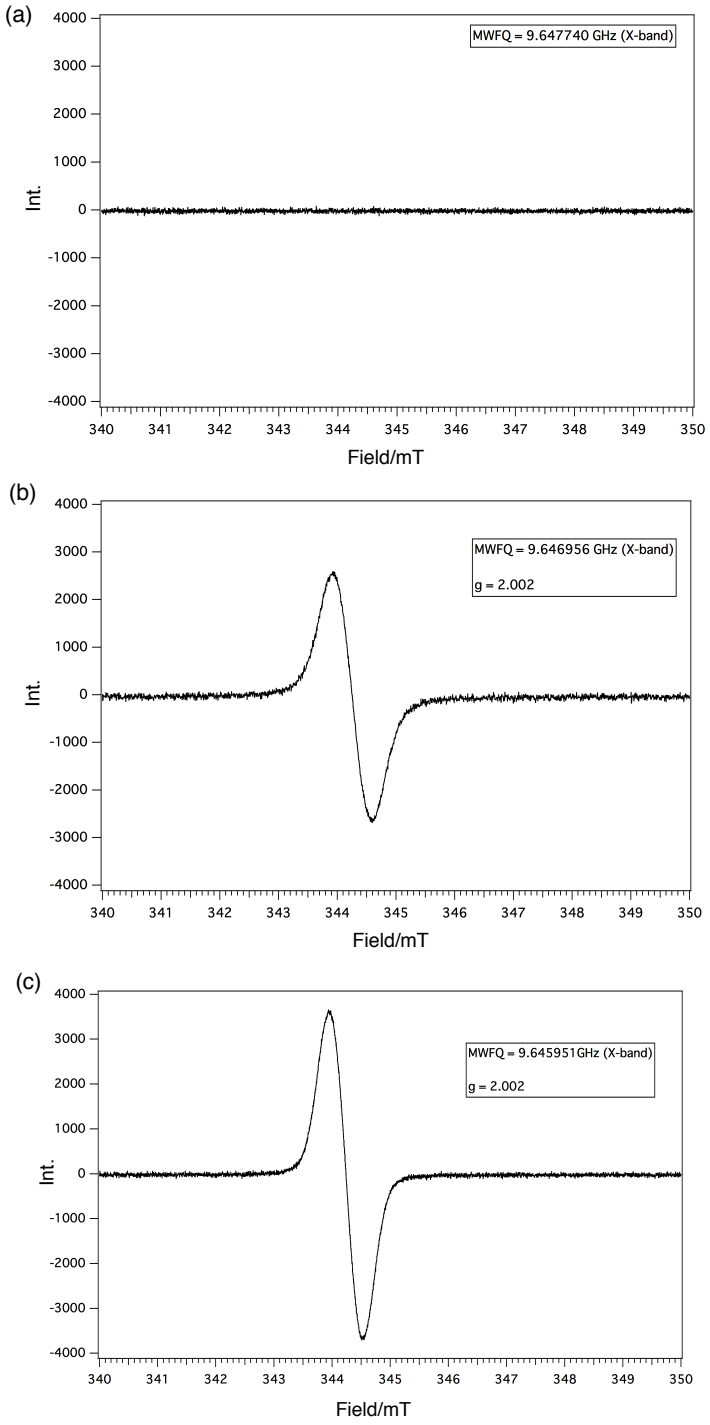

Figure 2-12. ESR spectra of (a) **6** under air, (b) **6** with excess amount (ca. 10800 equiv) of TFA under air, and (c) **6** with 0.8 equiv of BAHA under N_2. All spectra were measured in CH_2Cl_2 solution at room temperature.

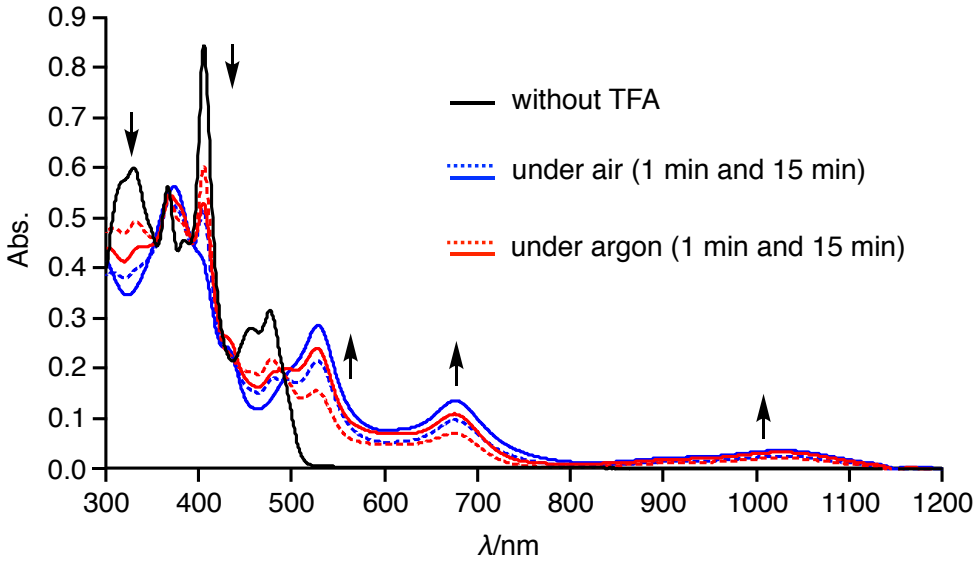

Figure 2-13. UV-vis-NIR absorption spectral changes of **6** in toluene in the presence of TFA (4500 equiv) either under air or argon (dashed line: 1 min, solid line: 15 min).

In the previous experiments, the author added a TFA/CH_2Cl_2 solution to a **6**/CH_2Cl_2 solution. Next, the author conducted the comparison experiment where a **6**/CH_2Cl_2 solution was added to a TFA/CH_2Cl_2 solution. Figure 2-14 shows the result of UV-vis-NIR absorption measurement. The resulting product (described as blue line) exhibited characteristic absorption bands around 500 nm and 600 nm, which is different from the spectrum of $\mathbf{6}^{\bullet+}$ (described as red line). To clarify its detailed structure, the author conducted ^{1}H NMR analysis in $CDCl_3$ (Figure 2-15). The ^{1}H NMR spectrum of **6** exhibited 6 peaks in the aromatic region, while the resulting product showed 12 peaks. These results strongly suggested the formation of protonated **6**. Considering that there were nine singlets, two doublets, and one singlet in Figure 2-15b, the protonation presumably occurred at internal carbon atom of pyrrole ring rather than peripheral one.

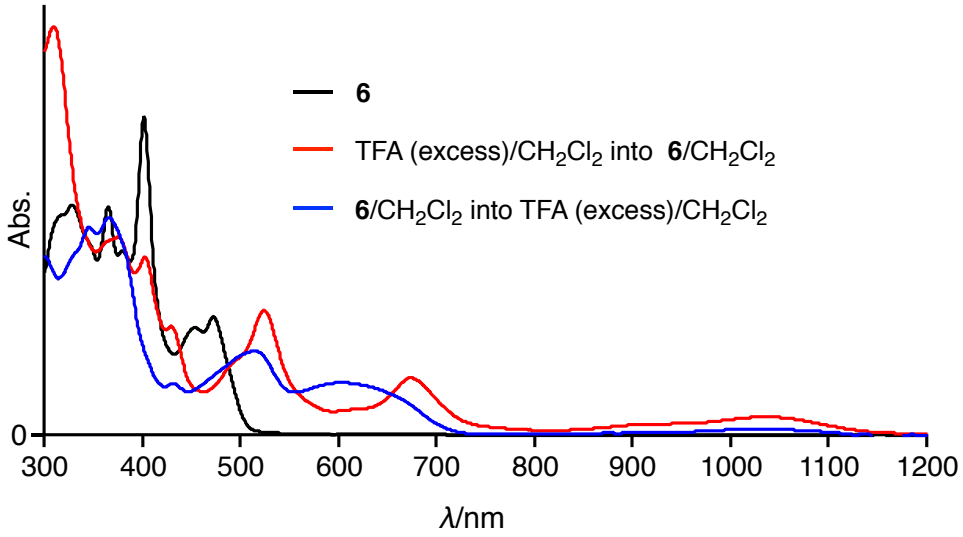

Figure 2-14. UV-vis-NIR absorption spectrum of **6** on the addition of **6** into a CH_2Cl_2 solution of TFA (blue line). The spectra of **6** (black line) and $\mathbf{6}^{\bullet+}$ (red line) were also displayed.

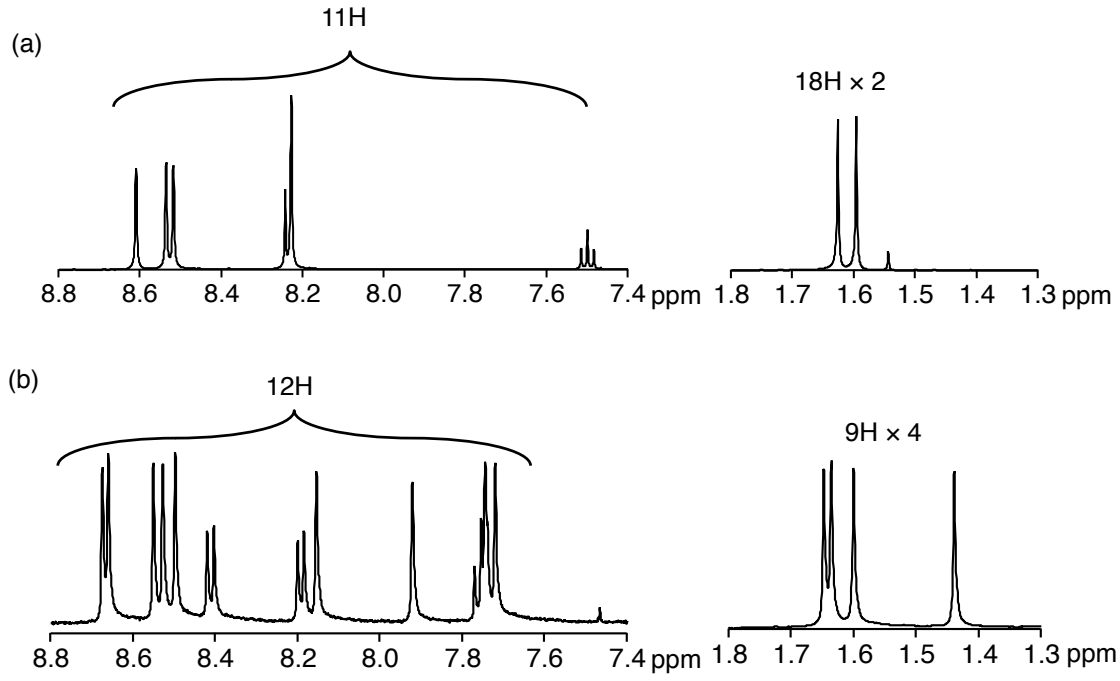

Figure 2-15. ^{1}H NMR spectra of (a) **6** and (b) **6** on the addition of **6** into a CH_2Cl_2 solution of TFA.

2-5. Association Behavior

The effect of nitrogen also appeared in the association behavior of **6** with C_{60}. In the case of hydrocarbon buckybowls, their association constants with C_{60} were too low to be measured.[18] The incorporation of electron-rich nitrogen atom into buckybowls should enable tighter binding with electron-deficient fullerenes. The electrochemical analysis revealed much lower oxidation potential (0.20 V) of **6** when compared with corannulene (1.57 V).[19] The addition of C_{60} into a 1,2-dichlorobenzene solution of **6** induced a change in the UV-vis-NIR absorption and emission spectra (Figure 2-16 and Figure 2-17). In particular, the appearance of broad absorption bands in the NIR region suggests intermolecular charge-transfer interactions between **6** and C_{60}.

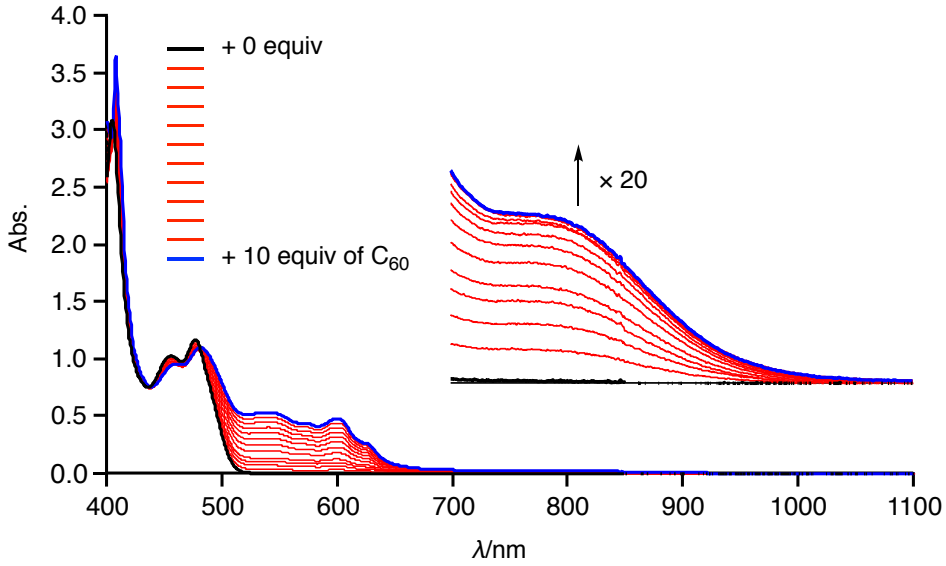

Figure 2-16. UV-vis-NIR absorption spectra on addition of 0–10 equiv of C_{60} into a 1,2-dichlorobenzene solution of **6**.

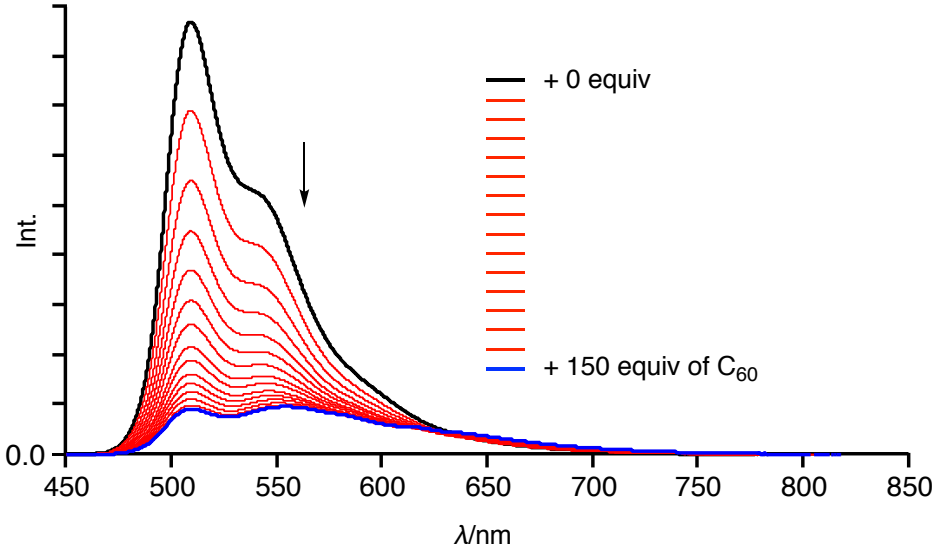

Figure 2-17. Fluorescence spectra on addition of 0–150 equiv of C_{60} into a 1,2-dichlorobenzene solution of **6**.

The association behavior was also monitored by ^{1}H NMR analysis. On the addition of C_{60} into a toluene-d_8 solution of **6**, all aromatic proton signals were upfield shifted (Figure 2-18). This indicates that **6** and C_{60} interacted in a convex–concave manner. This was revealed by the X-ray crystallographic analysis and showed that C_{60} was located above the center of **6** (Figure 2-19). The penetration depth of C_{60} into **6** measured from the centroid of the pyrrole ring to the centroid of C_{60} is 6.82 Å, and that measured from the shortest distance from the concave surface of **6** to a C_{60} surface is 3.29 Å, whereas the depths of C_{60} into the corannulene/C_{60} complex are 6.94 and 3.75 Å. The short distance between **6** and C_{60} indicates the presence of attractive interactions between them. Judging from the relatively long distance (>3.74 Å), the CH–π interaction between *tert*-butyl groups and C_{60} was not essential.

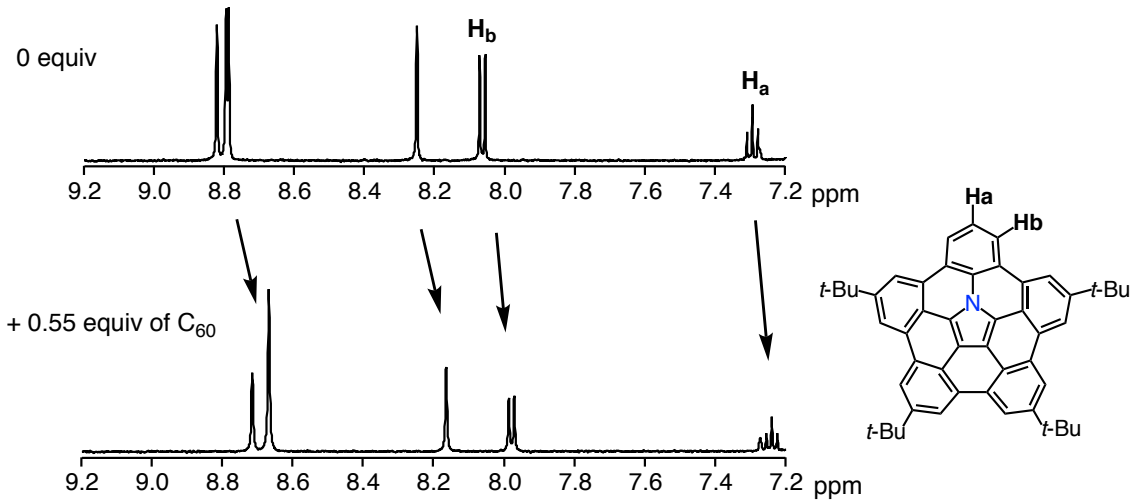

Figure 2-18. ^{1}H NMR spectra before (top) and after (bottom) addition of 0.55 equiv of C_{60} into a toluene-d_8 solution of **6**.

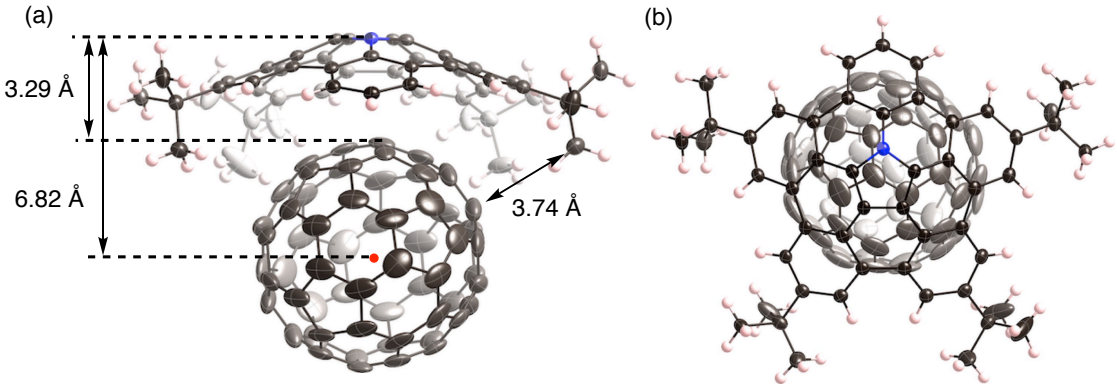

Figure 2-19. X-Ray crystal structure of **6**⊃C_{60}. (a) Side view and (b) top view. Thermal ellipsoids are scaled at 50% probability level.

From Job's plot analysis, **6** interacts with C_{60} in a 1:1 rate in 1,2-dichlorobenzene (Figure 2-20). The binding constant in 1,2-dichlorobenzene was determined to be 3.8×10^3 M^{-1} by titration with absorption and fluorescence spectra (Figure 2-21). This value is approximately three times larger than that of perthiolated corannulene. The existence of intermolecular charge-transfer interactions between **6** and C_{60} was indicated by the quenching behavior of the emission on the addition of C_{60} to a

1,2-dichlorobenzene solution of **6**. The DFT optimization of **6**⊃C_{60} afforded nearly the same structure as the crystal structure (Figure 2-22). The highest occupied molecular orbital (HOMO) was spread over the entire surface of **6**, whereas the lowest unoccupied molecular orbital (LUMO) was delocalized on C_{60}. In addition, oscillator strengths of the absorption of **6**⊃C_{60} were simulated by the time-dependent (TD) DFT method (Figure 2-23). The broad lowest-energy band in the near-infrared region was assigned as the HOMO–LUMO transition. These results supported the conclusion that an intermolecular charge-transfer interaction exists between **6** and C_{60}.

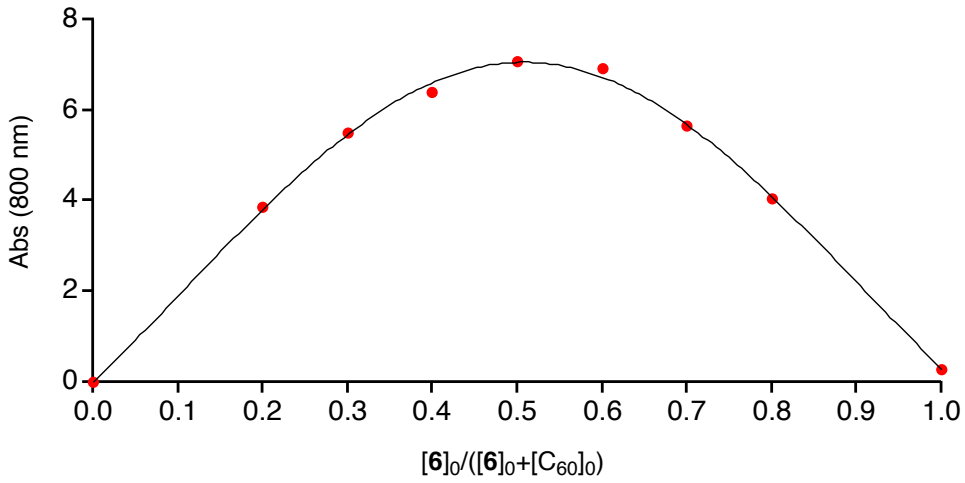

Figure 2-20. Job's plot for complexation of C_{60} and **6** in 1,2-dichlorobenzene.

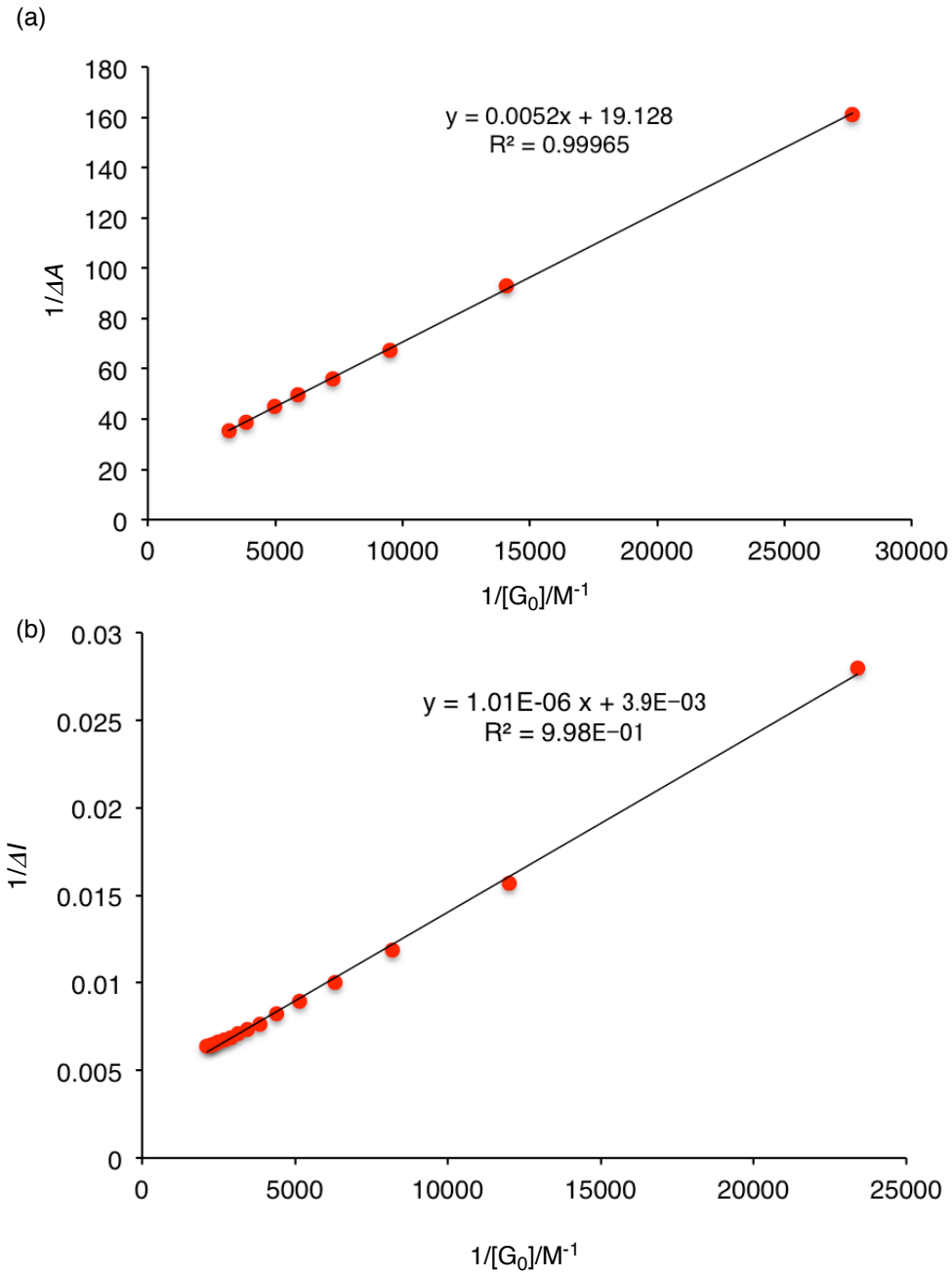

Figure 2-21. Bensi-Hildebrand plot on titration of C_{60} into **6** obtained by (a) UV-vis-NIR absorption spectral analysis and (b) fluorescence spectral analysis. The estimated K_a values by UV-vis-NIR spectral analysis were 3.7×10^3 M^{-1} for first attempt and 3.9×10^3 M^{-1} for second attempt. The estimated K_a values by fluorescence spectral analysis were 3.8×10^3 M^{-1}. The average K_a is 3.8×10^3 M^{-1}.

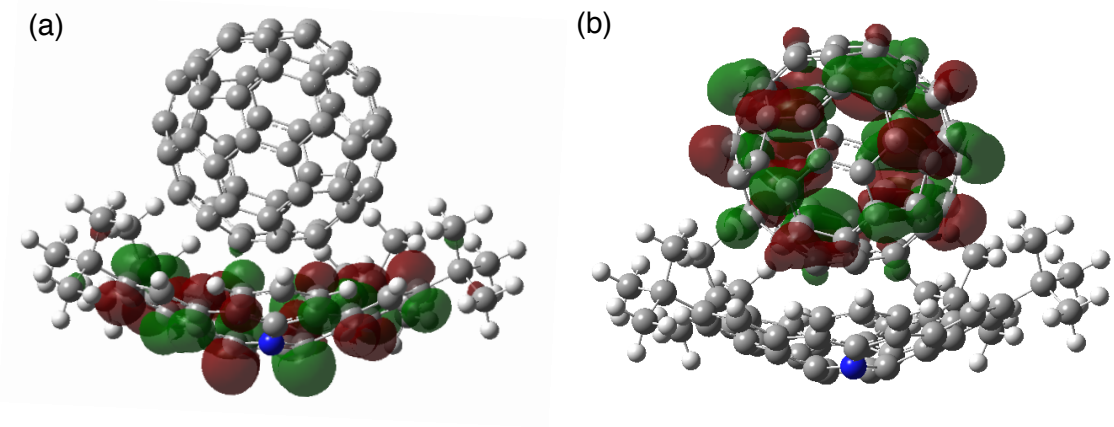

Figure 2-22. (a) HOMO and (b) LUMO of **6**⊃C_{60}.

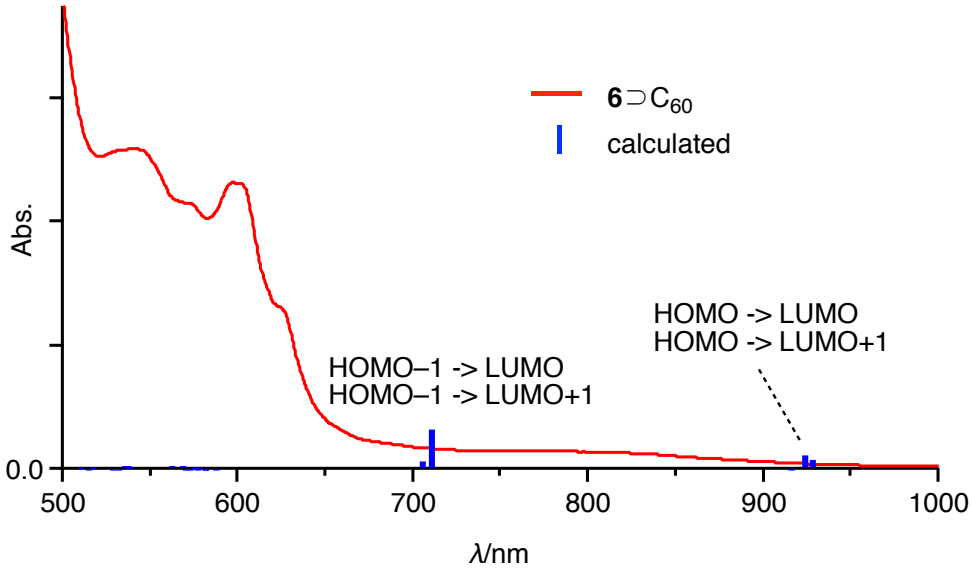

Figure 2-23. Calculated oscillator strengths of **6**⊃C_{60} (blue stick). The spectrum of **6** in the presence of 10 equiv of C_{60} (red line) in 1,2-dichlorobenzene was also displayed for comparison.

Finally, the author investigated the effect of the association with C_{60} of **6** on the charge-carrier mobility of **6** by flash-photolysis time-resolved microwave conductivity (FP-TRMC) measurements (Figure 2-24).[20] The maximum transient conductivity ($\phi\Sigma\mu$) of **6** was measured to be 1.5×10^{-5} cm^2 V^{-1} s^{-1}. For the co-crystal of **6**⊃C_{60}, the

mobility was enhanced to 2.4×10^{-4} cm^2 V^{-1} s^{-1}. The charge-carrier generation efficiency (ϕ) was determined to be 4.4×10^{-3} by the transient absorption spectroscopy measurement. Accordingly, the local charge mobility of **6**⊃C_{60} was 0.17 cm^2 V^{-1} s^{-1}. Such a large mobility of **6**⊃C_{60} should originate from effective charge separation caused by an electronic interaction between **6** and C_{60}. Furthermore, the alignment of **6** and C_{60} in the co-crystal may contribute to mobility enhancement. Both C_{60} and **6** construct one-dimensional chain alignments in the co-crystal (Figure 2-25).

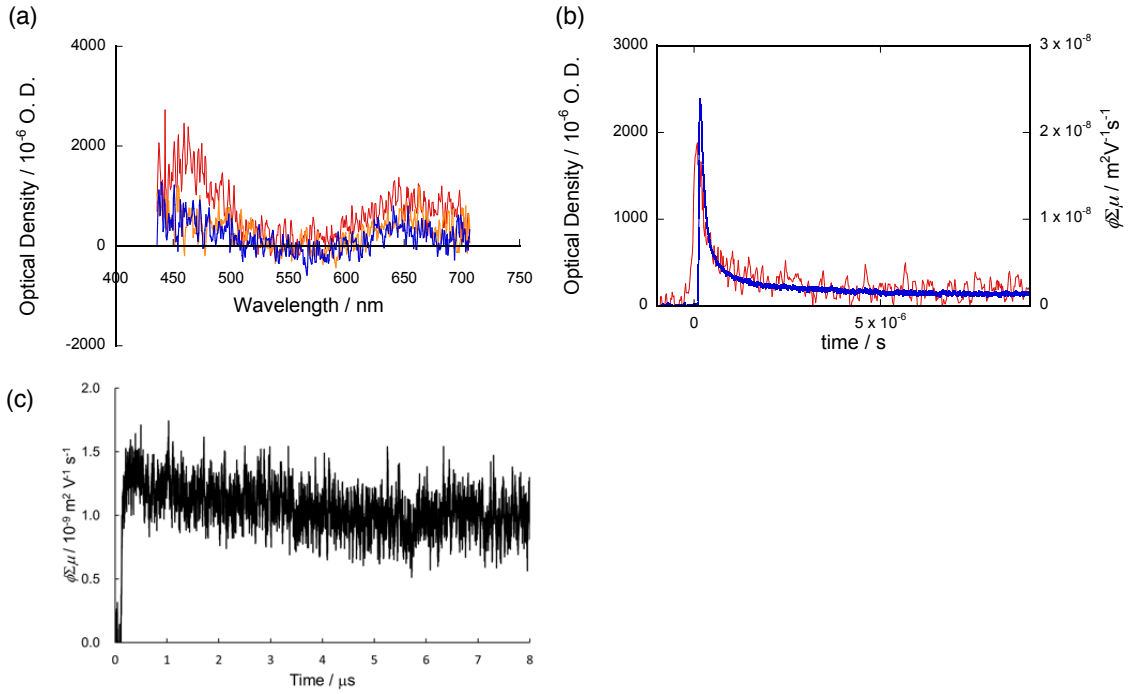

Figure 2-24. (a) Transient absorption spectra of **6**⊃C_{60} on exposure to 355 nm laser pulses at 3.8×10^{16} photons per cm^2. Spectra wire observed immediately after pulse exposure (red), 2 ms (orange) and 7 ms (blue) after pulse exposure. All spectra were recorded at room temperature under air-saturated atmosphere. (b) Kinetic traces of a photoconductivity transient (blue) recorded by FP-TRMC measurements and transient optical absorption at 650 nm for **6**⊃C_{60} on exposure to 355 nm laser pulses at 9.1×10^{15} photons per cm^2 (conductivity) and 3.8×10^{16} photons per cm^2 (optical). (c) Kinetic traces of a photoconductivity transient of **6** recorded by FP-TRMC measurements.

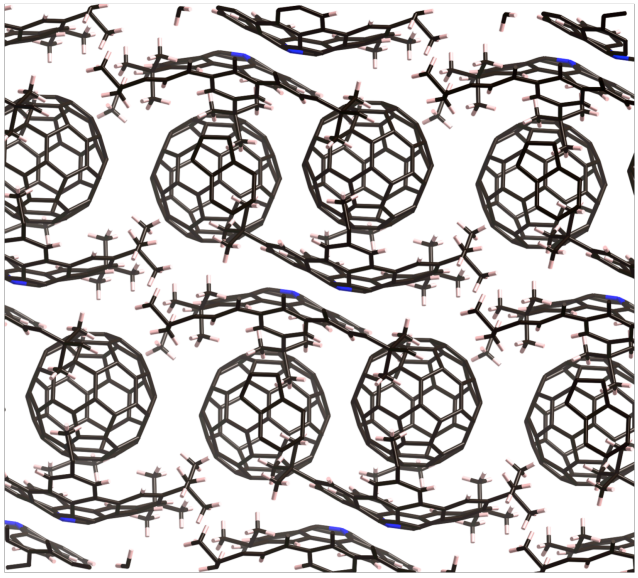

Figure 2-25. Side view of crystal packing of **6**⊃C_{60}.

2-6. Summary

In summary, the author has achieved the synthesis of a nitrogen-embedded bowl-shaped molecule under mild conditions. The total yield of penta-*peri*-pentabenzoazacorannulene **6** was 11% from 9-bromophenanthrene. The author also found that protonation of **6** resulted in efficient generation of radical cation species. The nitrogen-embedded bowl-shaped molecule was electron-rich enough to assemble tightly with C_{60} in solution and solid states. The molecular assembly of **6** with C_{60} exhibited significantly high charge mobility (0.17 $cm^2\ V^{-1}\ s^{-1}$). The nitrogen-embedded bowl-shaped molecule would be a novel molecular entity in the field of curved π-systems as fullerene hosts, anisotropic π-donors and precursors to nitrogen-containing nanocarbon materials.

2-7. Experimental Section

Materials and Characterization

^{1}H NMR (500 MHz) and ^{13}C NMR (126 MHz) spectra were recorded using a Bruker AVANCE III HD spectrometer. Chemical shifts were reported at the delta scale in ppm relative to $CHCl_3$ (d = 7.260 ppm), toluene-d_8 (d = 7.000 ppm), acetone-d_6 (d = 2.05 ppm), and 1,2-dichlorobenzene-d_4 (d = 6.930 ppm) for ^{1}H NMR and $CDCl_3$ (d = 77.0 ppm) for ^{13}C NMR. UV/vis/NIR absorption spectra were recorded using a Shimadzu UV-2550 or JASCO V670 spectrometer. Emission spectra were recorded using a JASCO FP-6500 spectrometer, and absolute fluorescence quantum yields were measured by the photon-counting method using an integration sphere. High-resolution (HR) mass spectra were recorded on a Bruker micro TOF using ESI-TOF or APCI-TOF methods. Unless otherwise noted, materials obtained from commercial suppliers were used without further purification.

Synthesis of 3,6-Di-*tert*-Butyl-9-Bromophenanthrene (1).

3,6-Di-*tert*-butylphenanthrene (0.540 g, 1.86 mmol) was dissolved in CCl_4 (11 ml) in a two-necked flask equipped with a dropping funnel. Br_2 (0.10 ml, 1.95 mmol) and CCl_4 (11 ml) were added into the dropping funnel. The solution was heated to 50 °C and then the bromine solution was added slowly over 1 h. After the addition was completed, the mixture was stirred for additional 30 min. The reaction mixture was cooled to room temperature and then quenched with aqueous $Na_2S_2O_3$. The resulting mixture was extracted with CH_2Cl_2 and the organic layer was washed with aqueous $Na_2S_2O_3$, dried over Na_2SO_4 and concentrated in vacuo. Purification by silica-gel column chromatography (cyclohexane as eluent) afforded **1** (0.645 g, 1.75 mmol) in 94% yield as a white solid. ^{1}H NMR (500 MHz) ($CDCl_3$): δ = 8.70 (d, J = 1.5 Hz, 1H), 8.66 (s, 1H), 8.30 (d, J = 8.5 Hz, 1H), 8.02 (s, 1H), 7.77 (dd, J_1 = 8.5 Hz, J_2 = 1.5 Hz, 1H), 7.74 (d, J = 8.5 Hz, 1H), 7.68 (dd, J_1 = 8.5 Hz, J_2 = 1.5 Hz, 1H), 1.53 (s, 9H), 1.52 (s, 9H) ppm; ^{13}C NMR (126 MHz) ($CDCl_3$): δ = 150.0, 149.6, 131.1, 130.4, 129.5,

129.3, 128.5, 127.8, 127.5, 125.6, 125.4, 120.7, 118.2, 118.1, 35.25, 35.14, 31.42 ppm; HR APCI-MS: m/z = 368.1124, calcd for $(C_{22}H_{25}Br)^+$ = 368.1134 [M^+].

Synthesis of 2

Schlenk tube containing **1** (0.200 g, 0.542 mmol), Cs_2CO_3 (0.265 g, 0.812 mmol), $Pd_2dba_3{\cdot}CHCl_3$ (28.0 mg, 27.1 μmol), and Xantphos (31.3 mg, 54.0 μmol) was flushed with N_2 three times. To the tube, 2-chloroaniline (86 μL, 0.812 mmol) and dry 1,4-dioxane (2.0 mL) were added. The mixture was stirred for 46 h at 100 °C. The resulting mixture was cooled to room temperature, passed through a pad of Celite, and concentrated in vacuo. Purification by silica-gel column chromatography (hexane/CH_2Cl_2) afforded **2** (0.158 g, 0.380 mmol) in 70% yield as a pale yellow solid. ^{1}H NMR (500 MHz) ($CDCl_3$): δ = 8.76 (d, J = 2.0 Hz, 1H), 8.68 (d, J = 1.0 Hz, 1H), 8.04 (d, J = 8.5 Hz, 1H), 7.74 (d, J = 8.5 Hz, 1H), 7.69 (dd, J_1 = 8.5 Hz, J_2 = 2.0 Hz, 1H), 7.66 (dd, J_1 = 8.5 Hz, J_2 = 1.5 Hz, 1H), 7.61 (s, 1H), 7.41 (dd, J_1 = 8.0 Hz, J_2 = 1.5 Hz, 1H), 7.04 (ddd, J_1 = 8.5 Hz, J_2 = 7.0 Hz, J_3 = 1.5 Hz, 1H), 6.88 (dd, J_1 = 8.5 Hz, J_2 = 1.5 Hz, 1H), 6.77 (ddd, J_1 = J_2 = 8.0 Hz, J_3 = 1.5 Hz, 1H), 6.36 (s, 1H), 1.53 (s, 9H), 1.52 (s, 9H), ppm; ^{13}C NMR (126 MHz) ($CDCl_3$): δ = 149.6, 148.6, 142.4, 134.6, 131.4, 130.2, 129.5, 128.5, 127.7, 127.6, 127.1, 125.1, 125.0, 122.8, 120.5, 119.4, 118.9, 118.6, 117.9, 115.6, 35.18, 31.54, 31.48 ppm; HR APCI-MS: m/z = 416.2141, calcd for $(C_{28}H_{31}ClN)^+$ = 416.2140 [$(M + H)^+$].

Synthesis of 3

A flask-containing compound **2** (0.100 g, 0.241 mmol) was flushed with N_2 three times. To the flask, a dry and degassed toluene/TFA (10 mL, 33 μL) solution was added. To the solution, a solution of DDQ (0.109 g, 0.482 mmol) in dry and degassed toluene/TFA (10 mL, 33 μL) was added, and the mixture was stirred for 1 h at room temperature. The reaction mixture was quenched with aqueous $NaHCO_3$ and aqueous $Na_2S_2O_3$ and extracted with CH_2Cl_2. The organic layer was washed with water, dried

over Na_2SO_4, and concentrated in vacuo. Purification by silica-gel column chromatography (hexane/CH_2Cl_2) afforded compound **3** (79.6 mg, 0.113 mmol) in 94% yield as a pale yellow solid. ^{1}H NMR (500 MHz) ($CDCl_3$): δ = 9.00 (d, J = 8.5 Hz, 2H), 8.80 (d, J = 1.5 Hz, 2H), 8.75 (d, J = 1.5 Hz, 2H), 7.85 (dd, J_1 = 8.5 Hz, J_2 = 1.5 Hz, 1H), 7.69–7.77 (m, 4H), 7.62 (ddd, J_1 = J_2 = 7.5 Hz, J_3 = 1.5 Hz, 1H), 7.32 (dd, J_1 = 9.0 Hz, J_2 = 1.5 Hz, 2H), 7.08 (d, J = 9.0 Hz, 2H), 1.58 (s, 18H), 1.48 (s, 18H), ppm; ^{13}C NMR (126 MHz) ($CDCl_3$): δ = 147.3, 146.8, 140.7, 135.7, 132.6, 132.2, 131.3, 131.1, 130.6, 128.9, 127.8, 126.6, 125.8, 124.4, 123.6, 121.7, 120.5, 119.7, 119.4, 116.5, 35.02, 34.91, 31.61, 31.40 ppm; UV/vis (CH_2Cl_2): λ_{max} (ε[M^{-1} cm^{-1}]) = 342 (22000), 359 (23000), 376 (21000) nm; HR APCI-MS: m/z = 702.3872, calcd for $(C_{50}H_{53}ClN)^+$ = 702.3861 [$(M + H)^+$].

Synthesis of 4

A Schlenk tube containing compound **3** (30.1 mg, 42.8 μmol), K_2CO_3 (35.5 mg, 0.257 mmol), $Pd(OAc)_2$ (9.56 mg, 42.6 μmol), and PCy_3·HBF_4 (31.5 mg, 85.5 μmol) was flushed with N_2 three times. To the tube, dry and degassed DMA (1.5 mL) was added. The mixture was stirred for 43 h at 130 °C. The resulting mixture was cooled to room temperature, passed through a pad of Celite, and concentrated in vacuo. Purification by silica-gel column chromatography (hexane/CH_2Cl_2) afforded compound **4** (17.8 mg, 26.8 μmol) in 63% yield as a yellow solid. ^{1}H NMR (500 MHz) ($CDCl_3$): δ = 9.15 (d, J = 9.0 Hz, 1H), 9.13 (d, J = 10 Hz, 1H) 8.92 (d, J = 1.0 Hz, 1H), 8.89 (s, 1H), 8.86 (d, J = 0.5 Hz, 1H), 8.83 (d, J = 0.5 Hz, 1H), 8.61 (dd, J_1 = 8.0 Hz, J_2 = 1.5 Hz, 1H), 8.59 (s, 1H), 8.51 (d, J = 8.5 Hz, 1H), 8.40 (d, J = 8.0 Hz, 1H), 7.88 (d, J = 8.5 Hz, 1H), 7.84 (d, J = 8.5 Hz, 1H), 7.66 (dd, J_1 = 8.5 Hz, J_2 = 1.5 Hz, 1H), 7.50–7.56 (m, 2H), 1.71 (s, 9H), 1.64 (s, 9H), 1.63 (s, 9H), 1.60 (s, 9H), ppm; ^{13}C NMR (126 MHz) ($CDCl_3$): δ = 148.9, 147.7, 147.7, 146.5, 135.2, 132.2, 129.3, 129.1, 129.0, 128.9, 127.5, 127.3, 127.2, 126.9, 126.6, 126.1, 125.4, 124.7, 124.6, 124.2, 124.2, 124.0, 123.4, 123.1, 122.8, 121.9, 120.1, 119.7, 119.6, 119.5, 118.4, 118.1, 116.0, 110.8, 35.84, 35.12, 35.10,

35.01, 32.00, 31.65, 31.64, 31.56 ppm; UV/vis (CH_2Cl_2): λ_{max} (ε[M^{-1} cm^{-1}]) = 310 (53000), 330 (43000), 378 (13000) and 404 (8700) nm; fluorescence (CH_2Cl_2, λ_{ex} = 378 nm): λ_{em} = 456 and 471 nm (Φ_f = 0.18); HR APCI-MS: *m/z* = 666.4088, calcd for $(C_{50}H_{52}N)^+$ = 666.4094 [$(M + H)^+$].

Synthesis of 5

Compound **4** (40.1 mg, 60.3 μmol) was dissolved in CCl_4 (6.0 mL) in a two-necked flask equipped with a dropping funnel. A solution of Br_2 (0.10 mL, 2.0 mmol) in CCl_4 (3.0 mL) was added to the dropping funnel. The mixture was heated to 70 °C, and then, the bromine solution was added slowly over 15 min. After the addition was complete, the mixture was stirred for an additional 12.5 h. The reaction mixture was cooled to room temperature and then quenched with aqueous $Na_2S_2O_3$. The resulting mixture was extracted with CH_2Cl_2, and the organic layer was washed with aqueous $Na_2S_2O_3$, dried over Na_2SO_4, and concentrated in vacuo. Purification by silica-gel column chromatography (hexane only) afforded compound **5** (30.3 mg, 33.6 μmol) in 56% yield as a yellow solid. ^{1}H NMR (500 MHz) ($CDCl_3$): δ = 8.83 (s, 1H), 8.80 (s, 1H), 8.75 (s, 1H), 8.59 (d, *J* = 1.5 Hz, 1H), 8.58 (s, 1H), 8.47 (s, 1H), 8.41 (d, *J* = 8.5 Hz, 1H), 8.05 (s, 1H), 7.96 (d, *J* = 9.0 Hz, 1H), 7.91 (s, 1H), 7.68 (d, J_1 = 7.8 Hz, J_2 = 1.5 Hz, 1H), 7.49 (dd, J_1 = 9.0 Hz, J_2 = 2.0 Hz, 1H), 1.66 (s, 9H), 1.60 (s, 9H), 1.59 (s, 9H), 1.52 (s, 9H) ppm; ^{13}C NMR (126 MHz) ($CDCl_3$): δ = 149.7, 149.0, 147.9, 147.9, 135.7, 132.3, 132.1, 131.0, 130.6, 130.2, 129.9, 129.4, 129.4, 127.8, 127.6, 127.1, 126.8, 125.5, 124.9, 124.6, 124.3, 124.2, 123.4, 121.0, 120.3, 119.9, 119.7, 118.9, 118.8, 118.8, 118.1, 117.4, 117.1, 108.8, 35.91, 35.13, 35.05, 34.99, 31.93, 31.54, 31.51 ppm; HR AP-CI-MS: *m/z* = 900.1403, calcd for $(C_{50}H_{49}Br_3N)^+$ = 900.1410 [$(M + H)^+$].

Synthesis of 6 and 7

A Schlenk tube containing compound **5** (200 mg, 0.222 mmol), K_2CO_3 (246 mg, 1.78 mmol), $Pd(OAc)_2$ (99.5 mg, 0.443 mmol) and $PCy_3{\cdot}HBF_4$ (326 mg, 0.887 mmol) was flushed with N_2 three times. To the tube, dry and degassed DMA (25 ml) was added. The mixture was stirred for 32 h at 130 °C. The resulting mixture was cooled to room temperature and extracted with ethyl acetate. The organic layer was washed with water, dried over Na_2SO_4 and concentrated in vacuo. Purification by silica-gel column chromatography (hexane only) afforded compound **6** (54.1 mg, 81.7 μmol) in 37% yield as a yellow solid and **7** (7.84 mg, 11.8 μmol) in 5% yield as a pale yellow solid. ^{1}H NMR (500 MHz) ($CDCl_3$) of **6**: δ = 8.61 (s, 2H), 8.54 (s, 2H), 8.52 (s, 2H), 8.23–8.24 (m, 4H), 7.50 (t, J = 8.0 Hz, 1H), 1.63 (s, 18H), 1.60 (s, 18H) ppm.; ^{13}C NMR (126 MHz) ($CDCl_3$) of **6**: δ = 148.8, 147.6, 140.1, 135.3, 132.5, 131.1, 130.0, 129.0, 128.6, 127.7, 126.1, 123.4, 123.0, 122.5, 120.5, 120.0, 119.4, 117.9, 35.92, 35.84, 32.30, 32.17 ppm.; UV/vis (CH_2Cl_2): λ_{max} (ε[M^{-1} cm^{-1}]) = 400 (35000), 453 (12000), 472 (13000) nm; fluorescence (CH_2Cl_2, λ_{ex} = 400 nm): λ_{em} = 508 and 542 nm (Φ_f = 0.17); HR APCI–MS: m/z = 662.3748, calcd for $(C_{50}H_{48}N)^+$ = 662.3781 [$(M + H)^+$].
^{1}H NMR (500 MHz) ($CDCl_3$) of **7**: δ = 9.34 (d, J = 8.6 Hz, 2H), 8.95 (d, J = 1.8 Hz, 2H), 8.85 (s, 2H), 8.57 (d, J = 0.85 Hz, 2H), 8.49 (d, J = 7.9 Hz, 2H), 7.97 (d, J_1 = 8.6 Hz, J_2 = 2.0 Hz, 2H), 7.69 (d, J_1 = 7.9 Hz, J_2 = 7.9 Hz, 1H), 1.69 (s, 18H), 1.63 (s, 18H) ppm.; ^{13}C NMR (126 MHz) ($CDCl_3$) of **7**: δ = 149.1, 146.2, 129.5, 129.1, 129.0, 128.5, 126.5, 126.1, 125.0, 125.0, 123.7, 123.5, 121.8, 120.6, 118.5, 118.2, 117.3, 110.7, 35.96, 35.01, 32.11, 31.68 ppm.; UV/vis (CH_2Cl_2): λ_{max} (ε[M^{-1} cm^{-1}]) = 446.5 (8600), 419 (12000), 388 (27000), 354.5 (22000) nm; fluorescence (CH_2Cl_2, λ_{ex} = 380 nm): λ_{em} = 472 and 497 nm (Φ_f = 0.18); HR APCI–MS: m/z = 664.3950, calcd for $(C_{50}H_{50}N)^+$ = 664.3938 [$(M + H)^+$].

Synthesis of 8

A Schlenk tube containing compound **6** (30.5 mg, 46.0 μmol), bis(pinacolato)diboron (117 mg, 0.461 mmol), $[Ir(OMe)(cod)]_2$ (30.5 mg, 46.0 μmol), and 4,4'-di-*tert*-butyl-2,2'-bipyridyl (25.1 mg, 93.4 μmol) was flushed with N_2 three times. To the tube, dry and degassed octane (1.5 mL) was added. The mixture was stirred for 10.5 h at 110 °C. The resulting mixture was cooled to room temperature and concentrated in vacuo. Purification by silica-gel column chromatography afforded compound **8** (29.0 mg, 36.8 μmol) in 80% yield as a yellow solid. ^{1}H NMR (500 MHz) ($CDCl_3$): δ = 8.68 (s, 2H), 8.62 (s, 2H), 8.55 (s, 2H), 8.52 (s, 2H), 8.34 (s, 2H), 1.64 (s, 18H), 1.64 (s, 18H), 1.49 (s, 12H) ppm; ^{13}C NMR (126 MHz) ($CDCl_3$): δ = 148.9, 147.7, 140.0, 137.1, 132.6, 130.9, 130.1, 128.9, 128.5, 127.7, 125.4, 123.0, 120.4, 120.0, 119.4, 118.4, 84.21, 36.01, 35.84, 32.29, 32.24, 24.99 ppm; HR ESI-MS: *m/z* = 787.4571, calcd for $(C_{56}H_{58}BNO_2)^+$ = 787.4564 [$(M)^+$].

Synthesis of 9

A Schlenk tube containing compound **8** (9.48 mg, 12.0 μmol), $PdCl_2$dppf·CH_2Cl_2 (4.97 mg, 6.09 μmol), and Cs_2CO_3 (9.80 mg, 30.1 μmol) was flushed with N_2 three times. To the tube, 2,4,6-triisopropylbromobenzene (56.2 mg, 0.199 mmol) and dry and degassed 1,4-dioxane (1.0 mL) were added. The mixture was stirred for 13 h at 100 °C. The resulting mixture was cooled to room temperature and concentrated in vacuo. Purification by silica-gel column chromatography afforded compound **9** (5.75 mg, 6.66 μmol) in 55% yield as a yellow solid. ^{1}H NMR (500 MHz) (acetone-d_6): δ = 8.85 (s, 2H), 8.79 (s, 2H), 8.79 (s, 2H), 8.65 (d, *J* = 1.0 Hz, 2H), 8.36 (s, 2H), 7.25 (d, *J* = 1.5 Hz, 1H), 7.14 (d, J = 1.5 Hz, 1H), 3.13 (sext, *J* = 7.0 Hz, 1H), 3.01 (sext, *J* = 7.0 Hz, 1H), 2.37 (sext, *J* = 7.0 Hz, 1H), 1.62 (s, 18H), 1.57 (s, 18H), 1.35 (d, *J* = 7.0 Hz, 6H), 1.31 (d, *J* = 7.0 Hz, 6H), 0.88 (d, *J* = 7.0 Hz, 6H) ppm; ^{1}H NMR (500 MHz) (1,2-dichlorobenzene-d_4): δ = 8.75 (s, 2H), 8.74 (s, 2H), 8.72 (s, 2H), 8.25 (s, 2H), 8.21 (s, 2H), 7.35 (s, 1H), 7.28 (s, 1H), 3.35 (sext, *J* = 7.5 Hz, 1H), 3.02 (sext, *J* = 7.0 Hz,

1H), 2.85 (sext, J = 7.0 Hz, 1H), 1.66 (s, 18H), 1.50 (s, 18H), 1.41 (d, J = 7.0 Hz, 6H), 1.37 (d, 6H), 1.11 (d, J = 7.0 Hz, 6H) ppm; ^{13}C NMR (126 MHz) ($CDCl_3$): δ = 148.9, 148.5, 147.6, 147.1, 147.0, 140.4, 137.3, 135.9, 134.3, 132.5, 131.2, 130.1, 129.3, 128.5, 127.9, 125.9, 123.9, 123.3, 121.1, 120.7, 120.5, 119.9, 119.3, 117.9, 35.89, 35.84 34.38, 32.31, 32.10, 30.66, 30.10, 24.36, 24.14, 24.06 ppm; HR ESI-MS: m/z = 863.5438, calcd for $(C_{65}H_{69}N)^+$ = 863.5425 [$(M)^+$].

X-Ray Diffraction Analysis

X-ray data were obtained using a Bruker D8 QUEST X-ray diffractometer with an IμS microfocus X-ray source and a large area (10 cm × 10 cm) CMOS detector (PHOTON 100) for **4** and **5** and using a Rigaku CCD diffractometer (Saturn 724 with MicroMax-007) with Varimax Mo optics using graphite monochromated Mo-Kα radiation (λ = 0.71075 Å) for **6** and **6**$\supset C_{60}$.

Electrochemical Analysis

The cyclic voltammogram and differential-pulse voltammogram of **3**, **4**, **6** and **7** were recorded using an ALS electrochemical analyser 612C. Measurements were performed in freshly distilled CH_2Cl_2 with tetrabutylammonium hexafluorophosphate as the electrolyte. A three-electrode system was used. The system consisted of a platinum working electrode, a platinum wire, and $Ag/AgClO_4$ as the reference electrode. The scan rate was 100 mVs^{-1}. The measurement was performed under nitrogen atmosphere. All potentials are referenced to the potential of ferrocene/ferrocenium cation couple. The electro-oxidative absorption of **6** was recorded under argon atmosphere with a BAS SEC-F spectroelectrochemical flow cell kit equipped with a DH-2000-BAL as the UV-vis-NIR light source and an HR4000CG-UV-NIR spectrometer.

Determination of Binding Constant

The association constant (K_a) of C_{60} with compound **6** was determined by UV-vis absorption and emission spectral analysis. The fitting was performed with the correlation between the change of absorbance or fluorescence intensity (ΔX) at 700 nm and 508 nm and the initial concentration of the guest ($[G]_0$) using the equation as follows:

$$1/\Delta X = 1/(b\Delta\varepsilon[G]_0[H]_0K_a) + 1/(b\Delta\varepsilon[H]_0),$$

where $\Delta\varepsilon$ is the gap of molar coefficients between guest and complex, and $[H]_0$ is the initial concentration of the host. The estimated K_a values by UV/vis spectral analysis were 3.9×10^3 M^{-1} for the first attempt and 3.7×10^3 M^{-1} for the second attempt. The K_a was also estimated by the emission spectral analysis to be 3.8×10^3 M^{-1}. The average K_a is 3.8×10^3 M^{-1}.

ESR Measurement

ESR spectra were recorded at room temperature using a Bruker E500 spectrometer with 2.6ϕ quartz sample tubes. A sample solution of **6** was prepared under air, and the ESR tube was sealed. Other samples were prepared by the addition of the degassed solution of TFA and BAHA in CH_2Cl_2 to the solution of **6**.

Time-Resolved Microwave Conductivity Measurement.[21]

Transient photoconductivity was measured by FP-TRMC. A resonant cavity was used to obtain a high degree of sensitivity in the conductivity measurement. The resonant frequency and microwave power were set at ~9.1 GHz and 3 mW, respectively, such that the electric field of the microwave was sufficiently small not to disturb the motion of charge carriers. The conductivity value is converted to the product of the quantum yield ϕ and the sum of charge-carrier mobilities $\Sigma\mu$ by $\phi\Sigma\mu = \Delta\sigma\,(eI_0F_{light})^{-1}$,

where e, I_0, F_{light}, and $\Delta\sigma$ are the unit charge of a single electron, incident photon density of excitation laser (photons m^{-2}), a correction (or filling) factor (m^{-1}), and a transient photoconductivity, respectively. The sample was set at the highest electric field in a resonant cavity. FP-TRMC experiments were performed at room temperature. The measurements of **6** and **6**⊃C_{60} were performed for crystalline samples covered with a PVA film on a quartz substrate.

Theoretical Calculations.

All calculations were performed using the Gaussian 09 program.[22] The geometry of $\mathbf{6}^{+\bullet}$, in which all *tert*-butyl groups were replaced with hydrogen, was optimized by the DFT method using the B3LYP[23,24] functional and the 6-31G(d) basis set. The geometry of **6**⊃C_{60} was optimized by Zhao's M06-2X functional[25] and the 6-31G(d) basis set. The oscillator strengths of $\mathbf{6}^{\bullet+}$ and **6**⊃C_{60} were calculated by the TD DFT method at the B3LYP/6-31G(d) level. For calculations of the bowl-to-bowl inversion energy, the ground and transition state geometries of **9** were optimized at the B3LYP/cc-pVDZ level. Zero-point energy and thermal energy corrections were conducted for the optimized structures.

Determination of Bowl-to-Bowl Inversion Energy by 2D EXSY Measurement.

The bowl-to-bowl inversion barrier of **9** was measured by 2D EXSY using the signals for methine protons of isopropyl groups at approximately d = 3.3 and 2.8 ppm. 2D EXSY measurements were performed in 1,2-dichlorobenzene-d_4 at 393 K with a phase-sensitive NOESY pulse sequence. The mixing time was increased from 50 to 300 ms. The rate constant (k) was determined using equation as follows:

$$k = (1/\tau_m)\ln((r + 1)/(r - 1)),$$

where τ_m is the mixing time and r is defined by the equation as follows:

$$r = (I_{AA} + I_{BB})/(I_{AB} + I_{BA}),$$

where I_{AB} and I_{BA} are the intensities of the cross peaks between two exchangeable signals A and B, and I_{AA} and I_{BB} are the intensities of the diagonal signals. The free energy ($\Delta G^{\ddagger}$) of the bowl-to-bowl inversion was finally obtained using the Eyring equation.

Crystallographic Data

	4	**5**
empirical formula	$C_{50}H_{51}N$	$C_{55}H_{58}Br_3Cl_5N$
formula weight	665.91	1150.00
habit	prism	prism
T, K	93(2)	93(2)
crystal system	triclinic	triclinic
space group	*P*-1 (2)	*P*-1 (2)
a, Å	9.9215(5)	11.6888(11)
b, Å	11.5220(5)	15.2279(14)
c, Å	17.8122(9)	16.1361(16)
α, deg	104.4750(10)	94.960(3)
β, deg	93.8730(10)	111.005(3)
γ, deg	108.0950(10)	103.447(2)
V, Å^3	1850.60(16)	2561.8(4)
Z	2	2
Dc, g/cm^3	1.195	1.491
F(000)	716	1170
crystal size, mm^3	0.26 x 0.26 x 0.15	0.46 x 0.34 x 0.19
$2\theta_{max}$, °	50.0	50.0
R_1 ($I > 2\sigma(I)$)	0.0433	0.0600
wR_2 (all data)	0.1231	0.1553
GOF	1.017	1.087
obs reflects	6295	8382
total reflects	12793	14718
parameters	472	669
CCDC number	1056760	1056759

	6	**6**⊃C_{60}
empirical formula	$C_{116}H_{114}N_2$	$C_{113.5}H_{51}N$
formula weight	1536.09	1428.55
habit	prism	prism
T, K	103(2)	103(2)
crystal system	triclinic	triclinic
space group	*P*-1 (2)	*P*-1 (2)
a, Å	14.698(2)	13.340(4)
b, Å	17.333(2)	14.585(4)
c, Å	18.574(3)	17.980(5)
α, deg	70.845(5)	98.107(3)
β, deg	87.159(6)	101.423(6)
γ, deg	80.952(6)	97.323(4)
V, Å^3	4414.3(11)	3350.9(15)
Z	2	2
Dc, g/cm^3	1.156	1.416
F(000)	1648	1478
crystal size, mm^3	0.30 x 0.14 x 0.08	0.44 x 0.28 x 0.12
$2\theta_{max}$, °	50.0	50.0
R_1 ($I > 2\sigma(I)$)	0.0728	0.0561
wR_2 (all data)	0.2161	0.1682
GOF	1.064	1.065
obs reflects	15464	11448
total reflects	43659	22169
parameters	1195	1676
CCDC number	1405427	1406873

2-8. References

1. M. A. Petrukhina, L. T. Scott, Fragments of Fullerenes and Carbon Nanotubes: Designed Synthesis, Unusual Reactions, and Coordination Chemistry (Wiley, Hoboken, 2012).

2. (a) W. E. Barth, R. G. Lawton, *J. Am. Chem. Soc.* **1966**, *88*, 380. (b) H. Sakurai, T. Daiko, T. Hiraoka, *Science* **2003**, *301*, 1878.

3. (a) L. T. Scott, M. M. Hashemi, D. T. Meyer, H. B. Warren, *J. Am. Chem. Soc.* **1991**, *113*, 7082. (b) V. M. Tsefrikas, L. T. Scott, *Chem. Rev.* **2006**, *106*, 4868. (c) A. M. Butterfield, B. Gilomen, J. S. Siegel, *Org. Process Res. Dev.* **2012**, *16*, 664. (d) Y. -T. Wu, J. S. Siegel, *Chem. Rev.* **2006**, *106*, 4843.

4. (a) K. Imamura, K. Takimiya, Y. Aso, T. Otsubo, *Chem. Commun.* **1999**, 1859. (b) Q. Tan, S. Higashibayashi, S. Karanjit, H. Sakurai, *Nat. Commun.* **2012**, *3*, 891. (c) S. Furukawa, Y. Suda, J. Kobayashi, T. Kawashima, T. Tada, S. Fujii, M. Kiguchi, M. Saito, *J. Am. Chem. Soc.* **2017**, *139*, 5787. (d) V. M. Tsefrikas, A. K. Greene, L. T. Scott, *Org. Chem. Front.* **2017**, *4*, 688.

5. V. M. Tsefrikas, S. Arns, P. M. Merner, C. C. Warford, B. L. Merner L. T. Scott, G. J. Bodwell, *Org. Lett.* **2006**, *8*, 5195.

6. Z. Ding, T. Sanchez, A. Labouriau, S. Iyer, T. Larson, R. Currier, Y. Zhao, D. Yang, *J. Phys. Chem. B* **2010**, *114*, 10337.

7. (a) M. Akita, S. Hiroto, H. Shinokubo, *Angew. Chem. Int. Ed.* **2012**, *51*, 2894. (b) K. Goto, R. Yamaguchi, S. Hiroto, H. Ueno, T. Kawai, H. Shinokubo, *Angew. Chem. Int. Ed.* **2012**, *51*, 10333. (c) S. Ito, S. Hiroto, S. Lee, M. Son, I. Hisaki, T. Yoshida, D. Kim, N. Kobayashi, H. Shinokubo, *J. Am. Chem. Soc.* **2015**, *137*, 142.

8. X. Gao, S. B. Zhang, Y. Zhao, S. Nagase, *Angew. Chem. Int. Ed.* **2010**, *49*, 6764.

9. S. Ito, Y. Tokimaru, K. Nozaki, *Angew. Chem. Int. Ed.* **2015**, *54*, 7256.

10. Y. Nishihara, M. Suetsugu, D. Saito, M. Kinoshita, M. Iwasaki, *Org. Lett.* **2013**, *15*, 2418.

11. N. Fukui, W. -Y. Cha, S. Lee, S. Tokuji, D. Kim, H. Yorimitsu, A. Osuka, *Angew. Chem. Int. Ed.* **2013**, *52*, 9728.

12. R. C. Haddon, *J. Phys. Chem. A* **2001**, *105*, 4164.

13. (a) I. A. I. Mkhalid, J. H. Barnard, T. B. Marder, J. M. Murphy, J. F. Hartwig, *Chem. Rev.* **2010**, *110*, 890. (b) M. N. Eliseeva, L. T. Scott, *J. Am. Chem. Soc.* **2012**, *134*, 15169.

14. A. Miyawaki, P. Kuad, Y. Takashima, H. Yamaguchi, A. Harada, *J. Am. Chem. Soc.* **2008**, *130*, 17062.

15. T. Amaya, H. Sakane, T. Muneishi, T. Hirao, *Chem. Commun.* **2008**, 765.

16. T. -C. Wu, H. -J. Hsin, M. -Y. Kuo, C. -H. Li, Y. -T. Wu, *J. Am. Chem. Soc.* **2011**, *133*, 16319.

17. R. Rathore, J. K. Kochi, *Acta Chem. Scand.* **1998**, *52*, 114.

18. (a) S. Mizyed, P. E. Georghiou, M. Bancu, B. Cuadra, A. K. Rai, P. Cheng, L. T. Scott, *J. Am. Chem. Soc.* **2001**, *123*, 12770. (b) P. E. Georghiou, A. H. Tran, S. Mizyed, M. Bancu, L. T. Scott, *J. Org. Chem.* **2005**, *70*, 6158. (c) L. N. Dawe, T. A. AlHujran, H. -A. Tran, J. I. Mercer, E. A. Jackson, L. T. Scott, P. E. Georghiou, *Chem. Commun.* **2012**, *48*, 5563. (d) A. S. Filatov, M. V. Ferguson, S. N. Spisak, B. Li, C. F. Campana, M. A. Petrukhina, *Cryst. Growth Des.* **2014**, *14*, 756.

19. T. J. Seiders, K. K. Baldridge, J. S. Siegel, R. Gleiter, *Tetrahedron Lett.* **2000**, *41*, 4519.

20. S. Seki, A. Saeki, T. Sakurai, D. Sakamaki, *Phys. Chem. Chem. Phys.* **2014**, *16*, 11093.

21. A. Saeki, Y. Koizumi, T. Aida, S. Seki, *Acc. Chem. Res.* **2012**, *45*, 1193.

22. Frisch, M. J. *et al. Gaussian 09, Revision D.01* (Gaussian, Inc., Wallingford CT, 2013).

23. A. D. Becke, *Phys. Rev. A* **1988**, *38*, 3098.

24. C. Lee, W. Yang, R. G. Parr, *Phys. Rev. B* **1988**, *37*, 785.

25. Y. Zhao, D. G. Truhlar, *Theor. Chem. Acc.* **2008**, 120, 215.

Chapter 3

Supramolecular Assemblies of Penta-*peri*-Pentabenzoazacorannulene Dimer and C_{60}

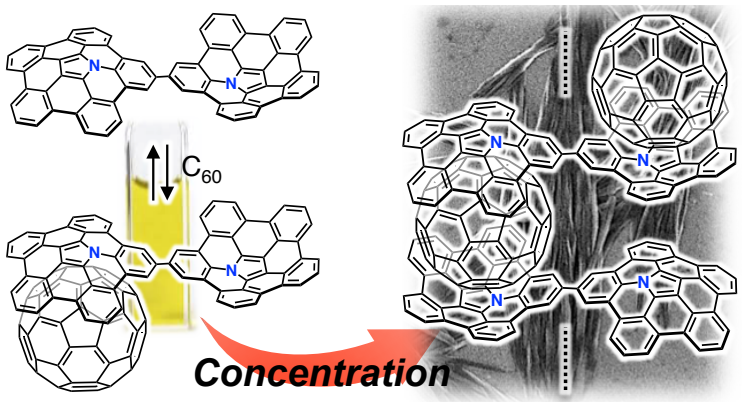

ABSTRACT: A directly connected penta-*peri*-pentabenzoazacorannulene dimer was synthesized via a palladium-catalyzed C–H/C–Br coupling. The electron-donating nature of the pyrrolic nitrogen atoms of the penta-*peri*-pentabenzoazacorannulene enabled a strong complexation with pristine C_{60}. In the presence of two equivalents of C_{60}, the penta-*peri*-pentabenzoazacorannulene dimer formed crystals with a 1:2 stoichiometry. Conversely, in diluted solution, complexes with a 1:1 stoichiometry of the dimer and C_{60} were detected predominantly, and these precipitated upon increasing the concentration of C_{60}. Scanning electron microscopy images of the precipitate showed fiber-like aggregates, indicating the formation of supramolecular assemblies with 1D chain structures. A variable-temperature ^{1}H NMR analysis revealed that the precipitate consists of the dimer and C_{60} in a 1:1 ratio.

Contents

3-1. Introduction

Supramolecular assembly is defined as higher-order aggregates constructed from two or more components, in which the molecules interact by non-covalent interactions such as hydrogen bonding, metal coordination, or hydrophobic interactions.[1] As these interactions are much weaker than covalent bonds, cleavage of the aggregates easily occurs by adjusting the temperature or concentration, which regenerates the corresponding monomers. Due to this flexibility, supramolecular polymers are expected to act as stimulus-responsive materials.[2] Among all the research in this field, supramolecular polymers with fullerenes based on host–guest interactions have been extensively studied in recent years (Figure 3-1).[3–6] Previous studies have often employed molecular tweezers hosts to ensure strong binding with C_{60} derivatives. These strategies require a C_{60} dimer (type a; Figure 3-1) or a functionalized C_{60} bearing a binding site (type b; Figure 3-1). However, supramolecular polymerization with pristine C_{60} remains a challenge because two binding units of the molecular tweezers would be needed to capture one C_{60} molecule.[7] Consequently, stronger yet sterically less-demanding host molecules are required.

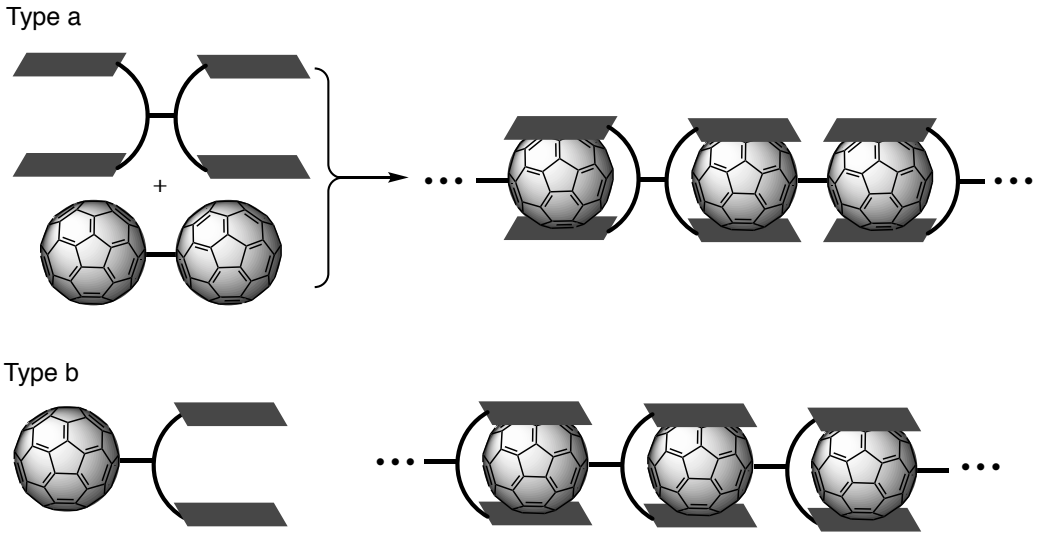

Figure 3-1. Supramolecular polymerization of C_{60} derivatives.

Buckybowls are bowl-shaped π-conjugated molecules, for which sumanenes and corannulenes are representative examples.[8,9] Such curved polycyclic aromatic hydrocarbons have been used for the recognition of fullerenes, given that the concave surface of the former efficiently overlaps with the convex surface of the latter.[10] And it is exactly for this reason that extensive research on assemblies of buckybowls with fullerenes has been carried out.[11] However, due to the poor electron-donating nature of these buckybowls,[12] their binding ability is usually insufficient to construct large supramolecular assemblies. On the other hand, penta-*peri*-pentabenzoazacorannulene **6** (Chart 1) exhibited a large association constant with C_{60} in solution due to the electron-donating nature of the central pyrrolic nitrogen atom. The binding constant of **6** was 3800 M^{-1} in 1,2-dichlorobenzene, which is a top-class value reported for a bowl-shaped molecule. This result suggests that **6** could be used as a new building block for supramolecular assemblies with C_{60}. Herein, the author discloses the synthesis of penta-*peri*-pentabenzoazacorannulene dimer **10** as a host molecule for pristine C_{60}. Owing to its two binding sites, dimer **10** was expected to form higher aggregates with C_{60} by forming a sandwich-type complex (Scheme 3-1).

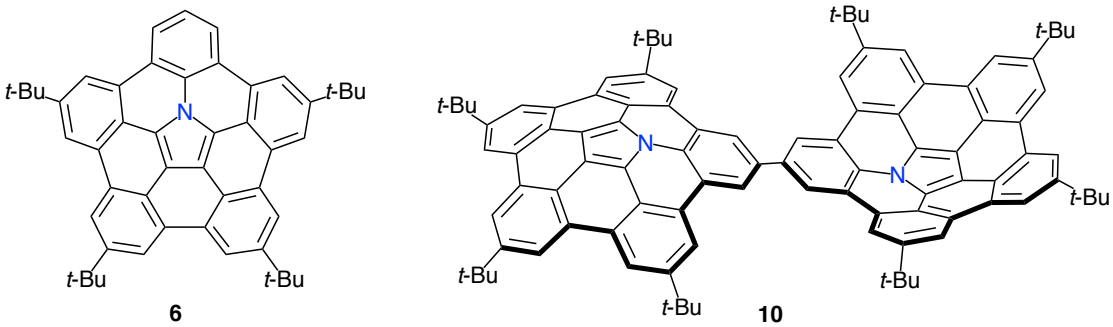

Chart 1. Penta-*peri*-pentabenzoazacorannulene **6** and linked dimer **10**.

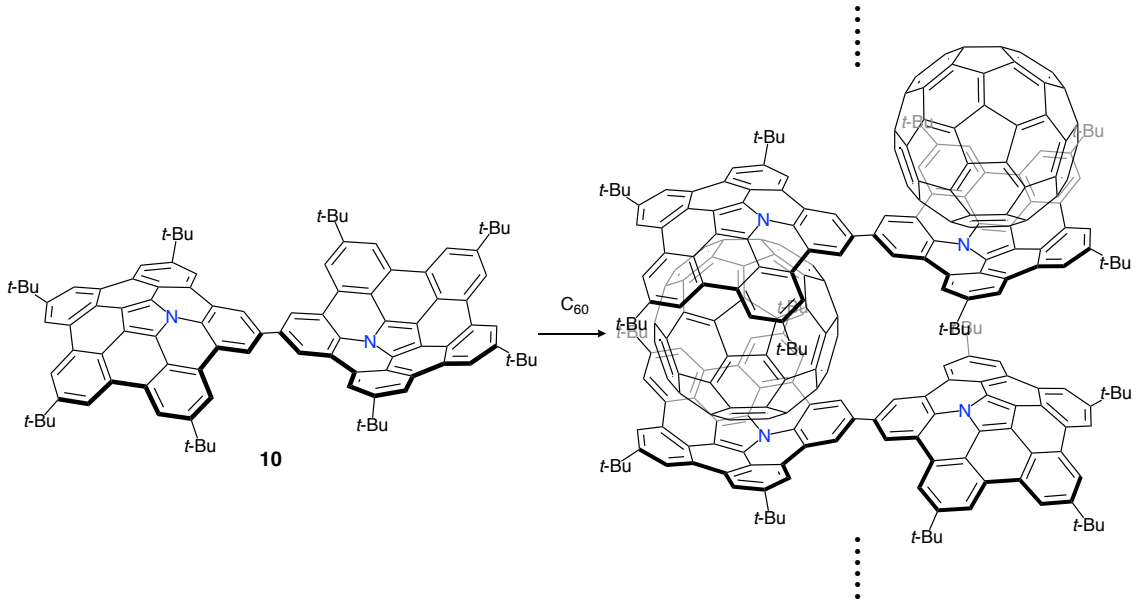

Scheme 3-1. Supramolecular assemblies between **10** and C_{60}.

3-2. Synthesis and Characterization

As shown in Chapter 2, **6** was synthesized via the Pd-mediated C–H/C–Br coupling of tribrominated precursor **5** using an excess of palladium(II) acetate and tricyclohexylphosphonium tetrafluoroborate. Interestingly, the use of catalytic amounts of these reagents provided the linked penta-*peri*-pentabenzoazacorannulene dimer **10** in 31% yield (Scheme 3-2). The structure of **10** was characterized by NMR spectroscopy and mass spectrometry. The parent mass ion peak of **10** was observed at m/z = 1321.7303, which confirms its dimeric structure. The ^{1}H NMR spectrum of **10** exhibited five singlet peaks in the aromatic region, consistent with a symmetric structure for **10**. The downfield shifts of the H_a protons (Scheme 3-2) in **10** compared to those in **6** indicate a deshielding effect by the second penta-*peri*-pentabenzoazacorannulene unit. In addition, the ^{13}C NMR spectrum exhibited 18 peaks assignable to sp^2-carbons, which suggests a conformation with C_{2v} symmetry.

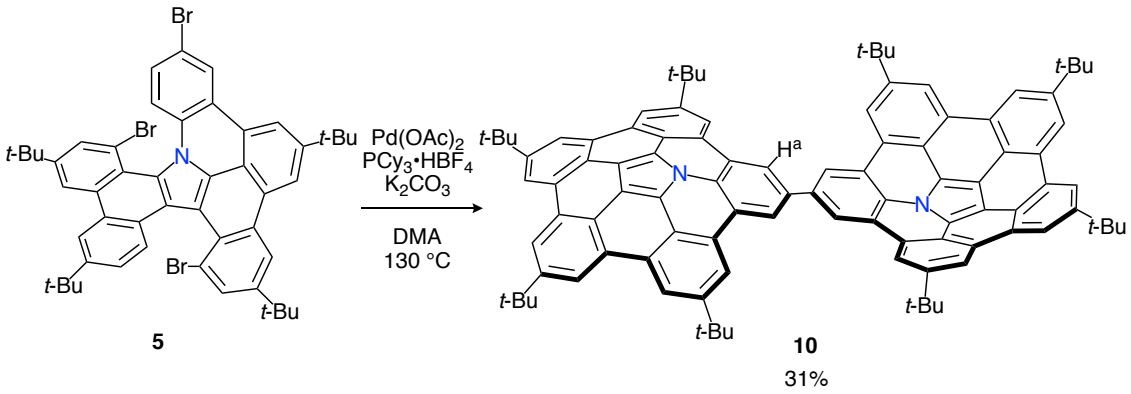

Scheme 3-2. Synthesis of penta-*peri*-pentabenzoazacorannulene dimer **10**.

3-3. Optical and Electrochemical Properties

Figure 3-2 shows the UV-vis absorption and emission spectra of **6** and **10** in CH_2Cl_2. Compared to the spectrum of **6**, the lowest energy band of **10** was red-shifted from 472 nm to 495 nm, which indicates the presence of electronic communication between the two penta-*peri*-pentabenzoazacorannulene units through the covalent bond. The emission band of **10** was observed at 517 nm with a quantum yield of 0.17, which is almost identical to that of **6**. The electrochemical properties of **10** were investigated by cyclic voltammetry (Figure 3-3), where **10** exhibited a lower oxidation potential (0.18 V) than **6** (0.20 V), commensurate with higher electron-donating properties for **10**.

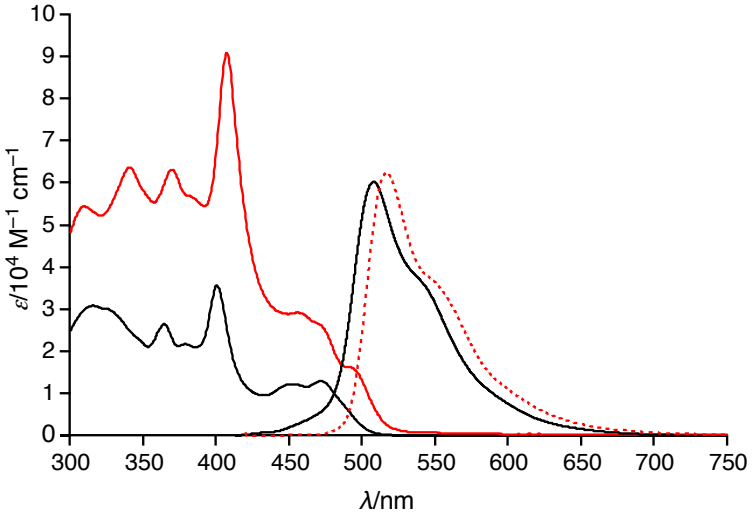

Scheme 3-2. UV-vis absorption (solid line) and emission spectra (dashed line) of **6** (black) and **10** (red) in CH_2Cl_2.

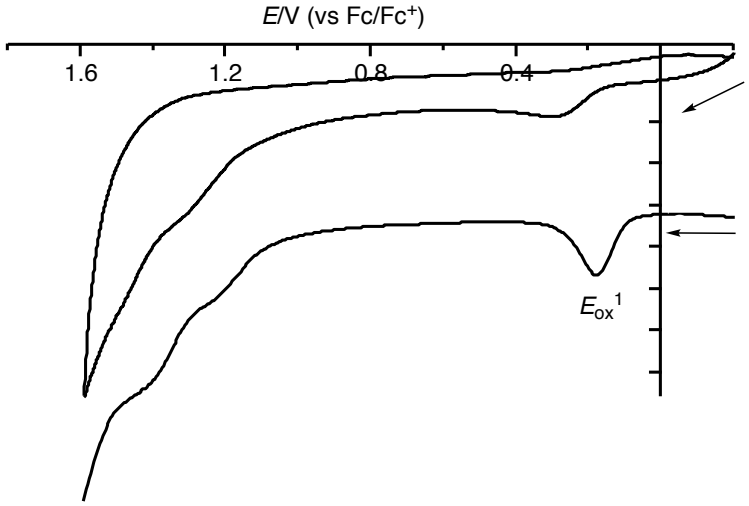

Figure 3-3. Cyclic voltammograms (top) and differential pulse voltammograms (bottom) of **10** in CH_2Cl_2.

3-4. Association Behavior

In order to examine the binding ability of **10** toward C_{60} in solution, the author carried out titration experiments under diluted conditions (c = 1.3 × 10^{-5} M^{-1}) (Figure 3-4). The titration was conducted in 1,2-dichlorobenzene and monitored by UV-vis-NIR absorption spectroscopy. Upon addition of a solution of C_{60} to a solution of **10**, an

absorption band around 800 nm appeared, which is similar to the behavior of **6**. The Job's plot for the absorbance at 800 nm indicated the predominant formation of 1:1 complexes in solution (Figure 3-5). A nonlinear curve fitting based on a 1:1 binding afforded an association constant of 7.8×10^3 M^{-1}, which is higher than that of **6** (K_a = 3.8×10^3 M^{-1}) (Figure 3-6). This result corroborates the superior electron-donating nature of **10** relative to that of **6**. It should also be noted that the binding constant reached 1.0×10^5 M^{-1} in toluene (Figure 3-7, Figure 3-8, and Figure 3-9). Such an enhancement was also observed in the case of **6**, where the binding constant was estimated to be 6.1×10^4 M^{-1} in toluene (Figure 3-10 and Figure 3-11). Such solvent-dependent association constants should probably be attributed to the different solvophobicity of the fullerene in each solvent.[13]

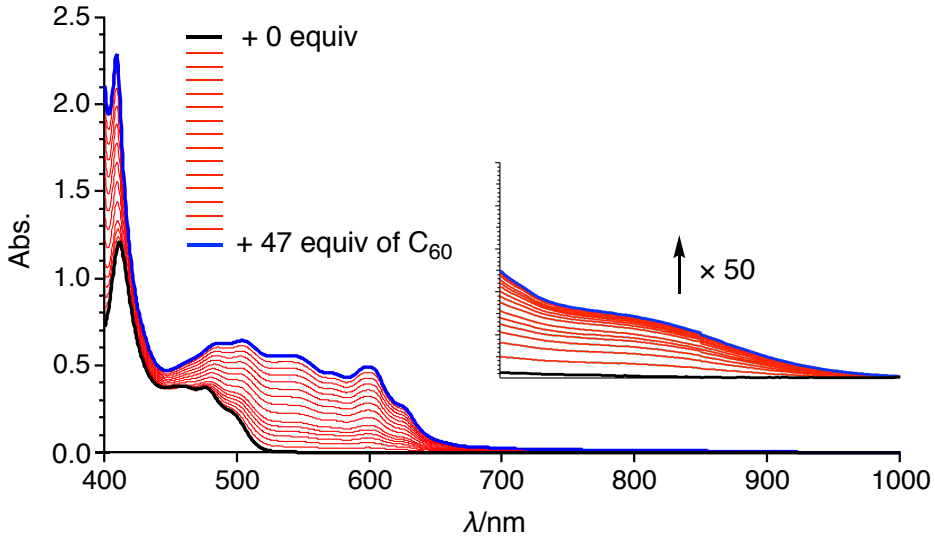

Figure 3-4. UV-vis-NIR absorption spectra of a 1,2-dichlorobenzene solution of **10** upon addition of 0–47 equiv of C_{60}.

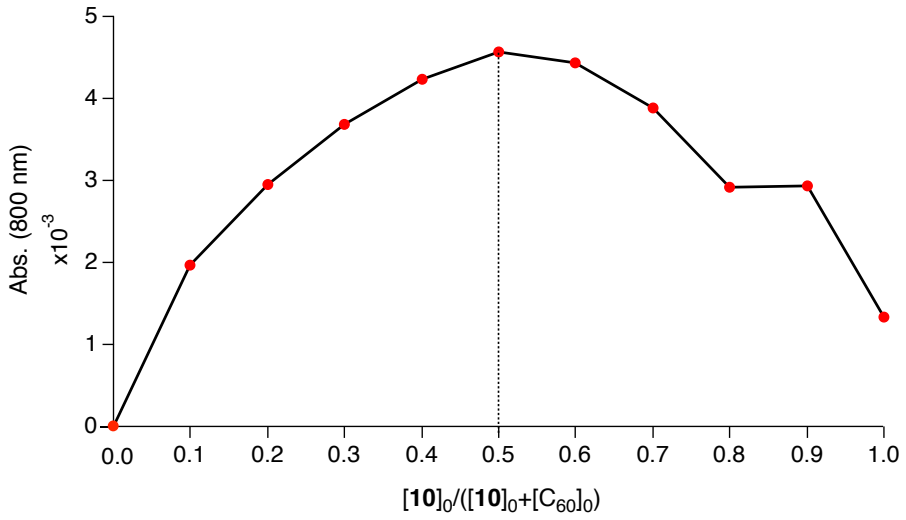

Figure 3-5. Job's plots for the complexation of **10** and C_{60} in 1,2-dichlorobenzene.

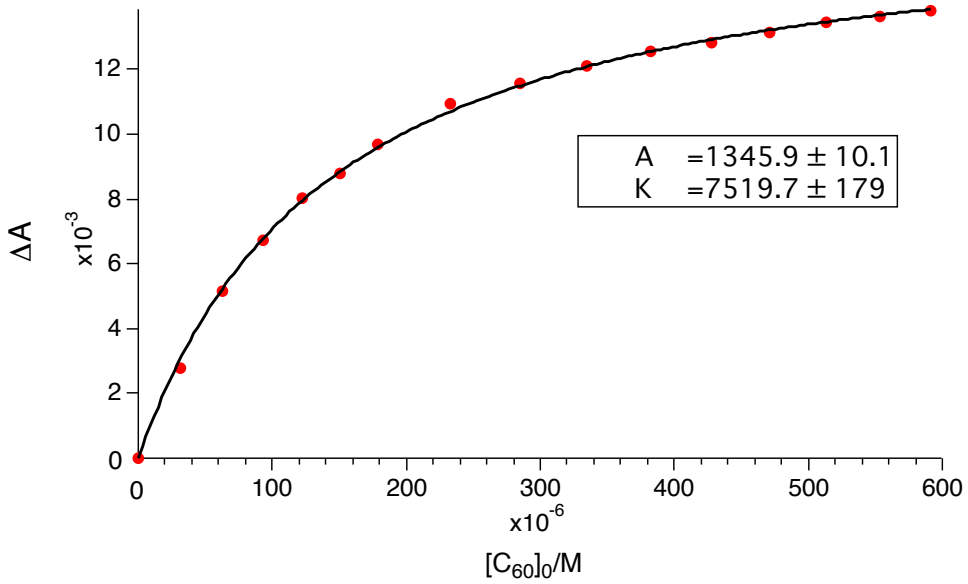

Figure 3-6. Nonlinear curve regression of the titration of **10** with C_{60} in 1,2-dichlorobenzene. The estimated K_a values by UV-vis-NIR spectral analysis were 7.5 × 10^3 M^{-1} for the first attempt and 8.0 × 10^3 M^{-1} for the second attempt. The average K_a is 7.8 × 10^5 M^{-1}.

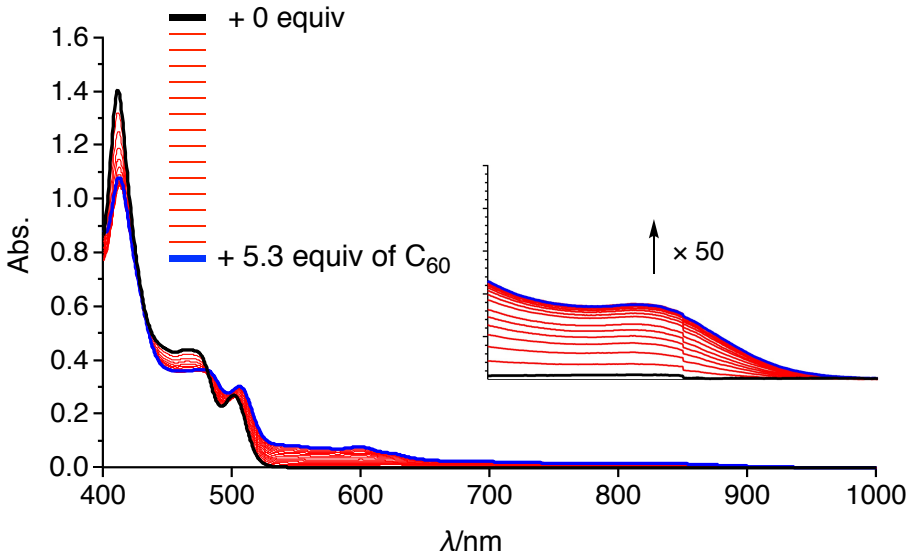

Figure 3-7. UV-vis-NIR absorption spectra on addition of 0–5.3 equiv of C_{60} into a toluene solution of **10** ($c = 1.4 \times 10^{-5}$ M^{-1}).

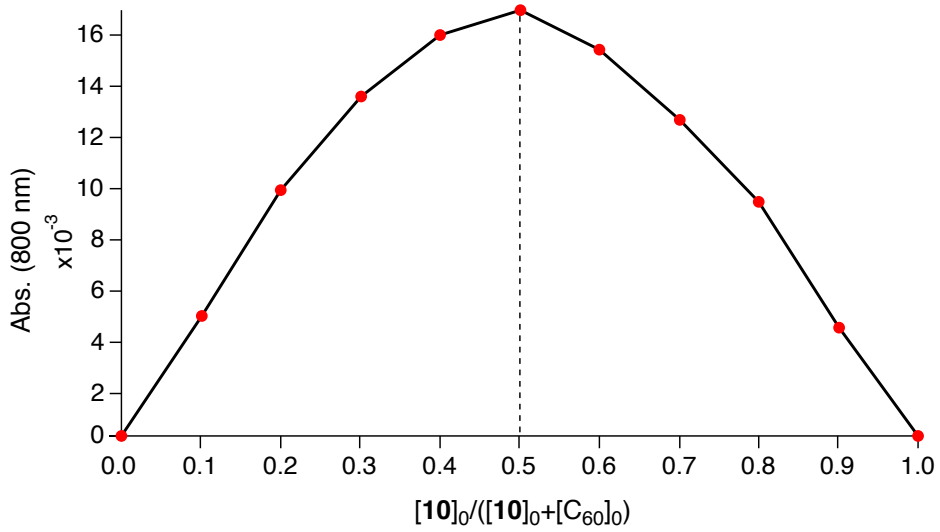

Figure 3-8. Job's plots for the complexation of **10** and C_{60} in toluene.

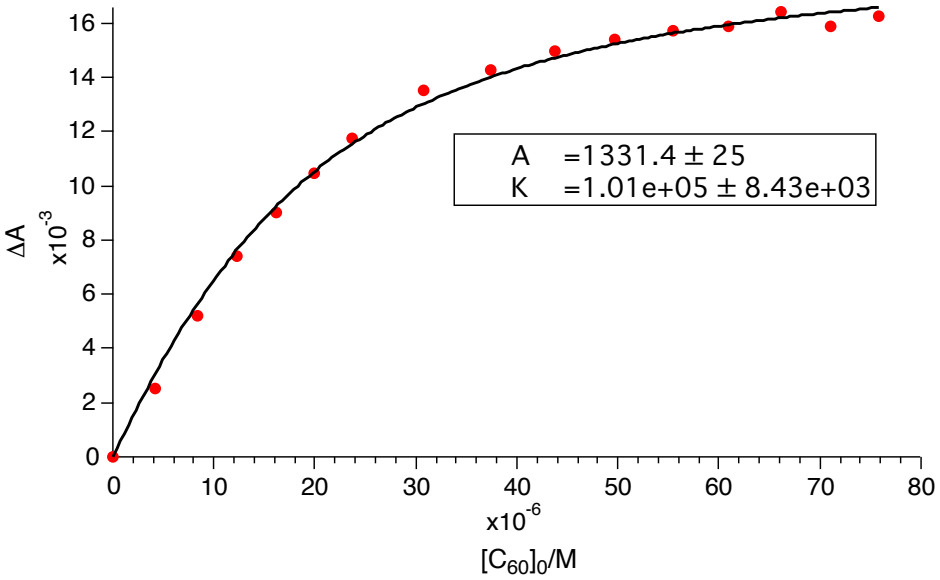

Figure 3-9. Nonlinear curve regression of the titration of **10** with C_{60} in toluene. The estimated K_a values by UV-vis-NIR spectral analysis were 1.0×10^5 M^{-1} for both first and second attempts. The average K_a is 1.0×10^5 M^{-1}.

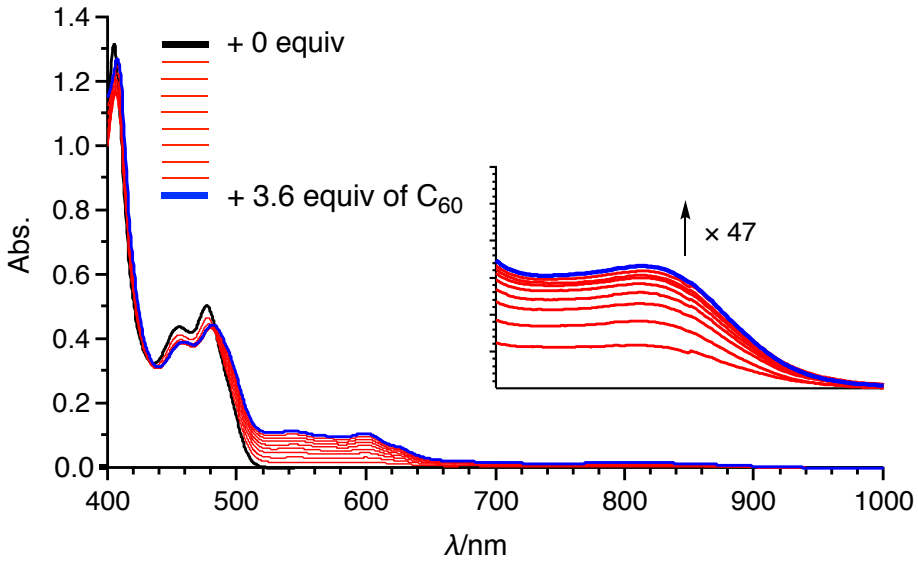

Figure 3-10. UV-vis-NIR absorption spectra on addition of 0–3.6 equiv of C_{60} into a toluene solution of **6** ($c = 3.2 \times 10^{-5}$ M^{-1}).

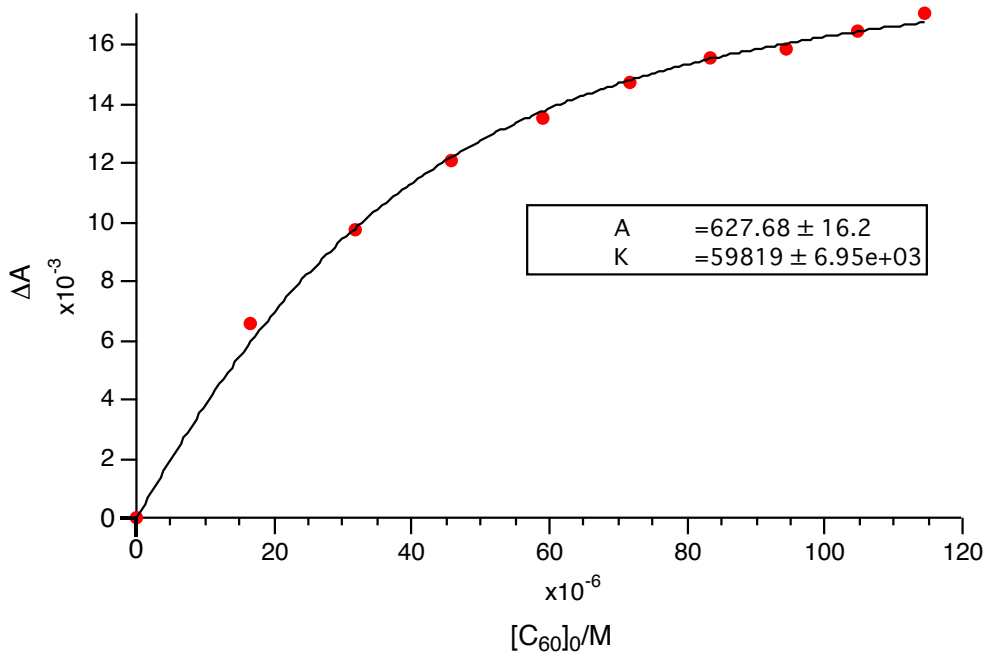

Figure 3-11. Nonlinear curve regression of the titration of **6** with C_{60} in toluene. The estimated K_a values by UV-vis-NIR spectral analysis were 6.0×10^4 M^{-1} for the first attempt and 6.2×10^4 M^{-1} for the second attempt. The average K_a is 6.1×10^4 M^{-1}.

3-5. Structural Elucidation

Fortunately, the author obtained single co-crystals of **10** and C_{60} that were suitable for an X-ray diffraction analysis, which were prepared by vapor diffusion of acetonitrile into a toluene solution of a mixture of **10** and C_{60} (Figure 3-12). In these crystals, the two penta-*peri*-pentabenzoazacorannulene units face in opposite directions, reflected in the tilt angle (50.1°) between the two penta-*peri*-pentabenzoazacorannulene units around the central bond. The C_{60} molecules are coordinated to the penta-*peri*-pentabenzoazacorannulene units in a concave–convex fashion, resulting in a 1:2 ratio in the crystal. Between the centroid of the pyrrole ring to the closest surface of the C_{60} molecules, distances of 3.28 and 3.29 Å were measured. Such short distances indicate the existence of strong electronic interactions between **10** and C_{60} in the solid state. The packing structure is shown in Figure 3-12b. Similar to **6**⊃C_{60}, **10** and the C_{60} molecules present segregate stacking (see Figure 2-25 in Chapter 2). The photo-induced

transient conductivity of **10** and **10**⊃C_{60} was determined by flash-photolysis time-resolved microwave conductivity (FP-TRMC) measurements.[14] The carrier mobility of the **10**⊃C_{60} crystals (2.0×10^{-4} cm^2 V^{-1} S^{-1}) is approximately by one order of magnitude higher than that of **10** (Figure 3-13). The carrier mobility of the **10**⊃C_{60} crystals was similar to that of **6**⊃C_{60}, indicating a similar charge-separation state between C_{60} and the penta-*peri*-pentabenzoazacorannulene unit in the crystal.

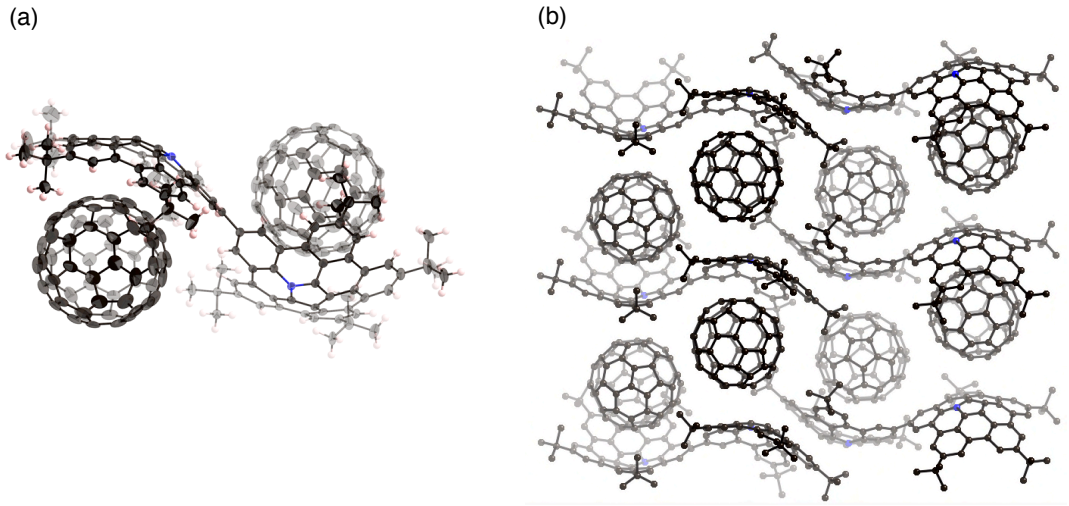

Figure 3-12. Molecular structure of **10**•C_{60} in the crystal. (a) Side view and (b) packing structure. The hydrogen atoms are omitted for clarity in (b). The thermal ellipsoids are scaled at 50% probability level.

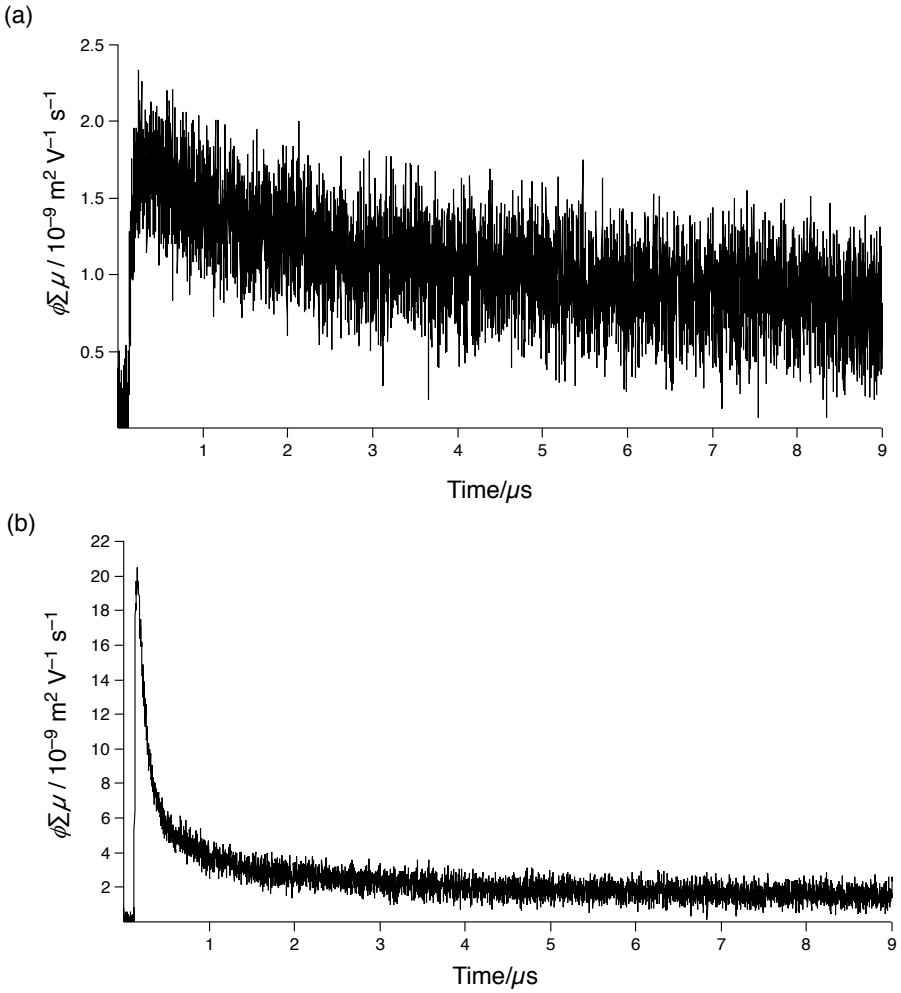

Figure 3-13. Kinetic traces of a photoconductivity transient of (a) **10** and (b) the crystal of **10**•C_{60} by FP-TRMC method.

3-6. Supramolecular Assembly

To uncover the different binding ratios of **10** with C_{60} in solution and the crystalline state, the author carried out titration experiments in toluene at 20 °C, which were monitored by ^{1}H NMR spectroscopy (Figure 3-14). With increasing amount of C_{60}, the spectral shape of the signal peaks became broader and the peak intensities decreased. Notably, a precipitate was formed in the presence of 1.0 equiv or less of C_{60} (Figure 3-15). This phenomenon was not observed in the case of **6**, for which a clear solution was obtained in the presence of C_{60} (Figure 3-16). To clarify this phenomenon, the author performed diffusion-ordered two-dimensional NMR spectroscopy (DOSY)

experiments.[15] The diffusion coefficient (*D*) determined for **10** (6.83×10^{-10} m^2 s^{-1}) decreased by 15% (5.80×10^{-10} m^2 s^{-1}) in the presence of 0.5 equiv of C_{60} (Figure 3-17). In contrast, a reduction of only 2% was observed in the case of **6** (Figure 3-18). This drop in the *D* value of **10** indicates the formation of larger structures.

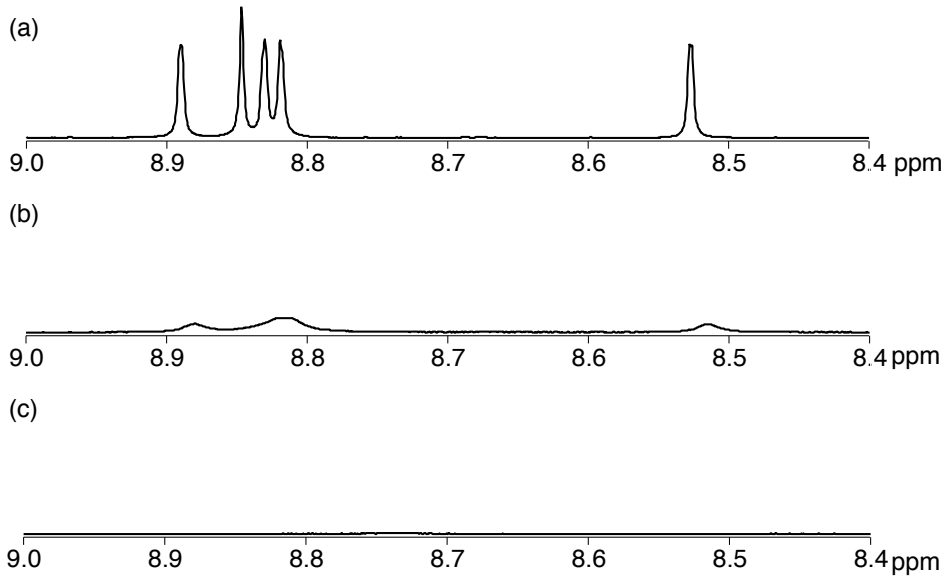

Figure 3-14. ^{1}H NMR spectra of **10** in toluene-d_8 (0.52 mM) in the presence of (a) 0 equiv, (b) 0.5 equiv, and (c) 1.0 equiv of C_{60}.

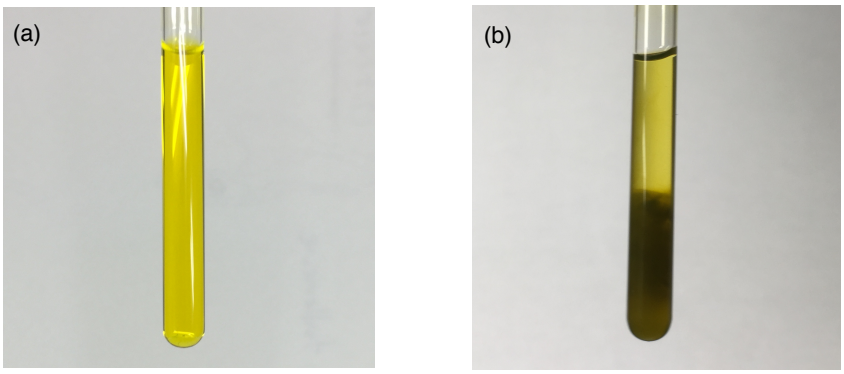

Figure 3-15. Photographs of samples of (a) **10** and (b) **10** + 1 equiv of C_{60} in toluene-d_8.

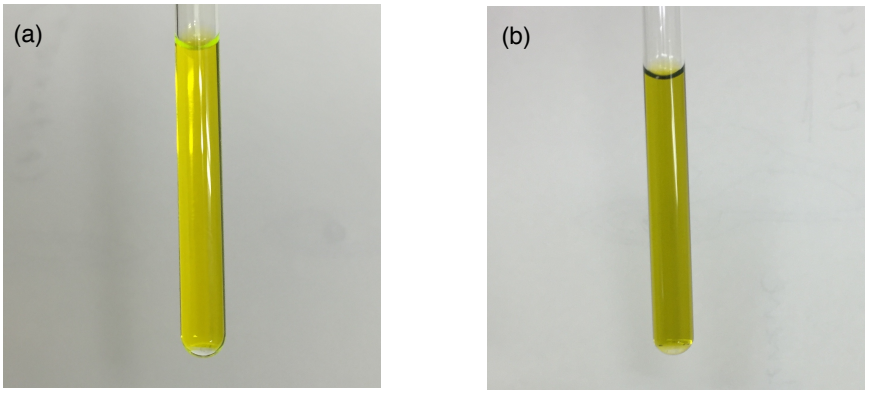

Figure 3-16. Photographs of samples of (a) **6** and (b) **6** + 1 equiv of C_{60} in toluene-d_8.

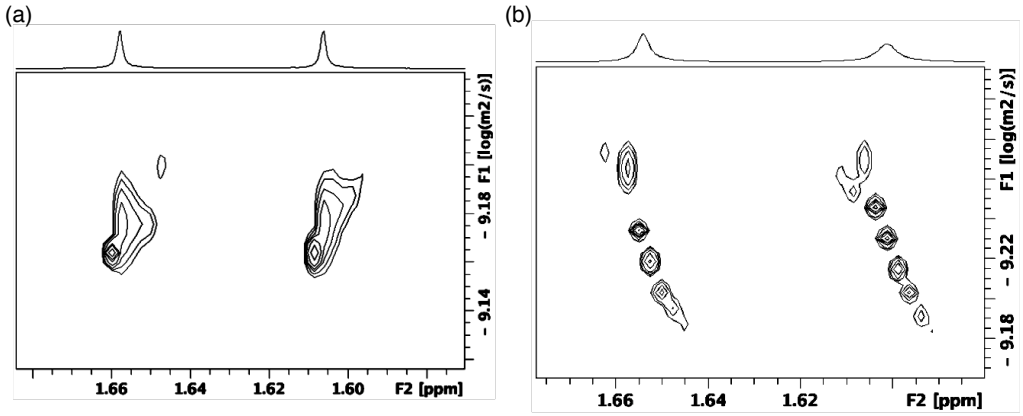

Figure 3-17. DOSY measurements of (a) **10** and (b) **10** + 0.5 equiv of C_{60} in toluene-d_8 (0.8 mM).

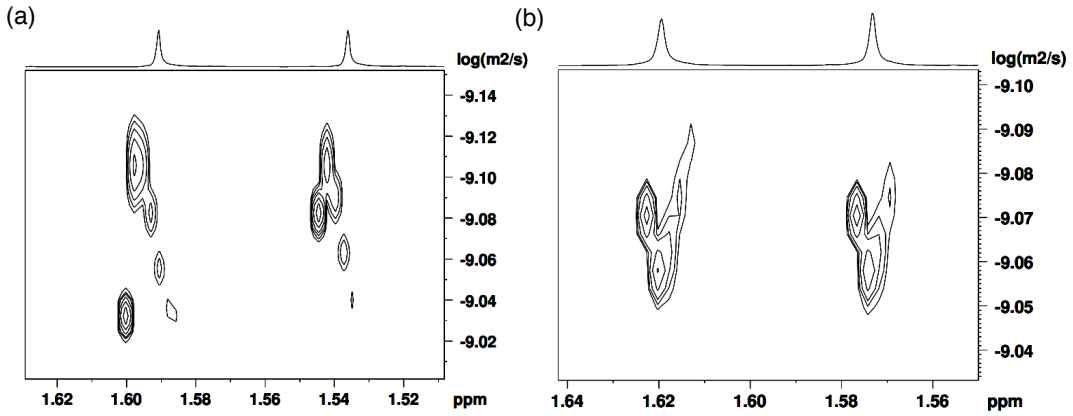

Figure 3-18. DOSY measurements of (a) **6** and (b) **6** + 0.5 equiv of C_{60} (bottom) in toluene-d_8 (0.8 mM). The diffusion coefficient (D) of **6** was 8.74 x 10^{-10} m^2/s, and the value was 8.54 × 10^{-10} m^2/s in the presence of 0.5 equiv of C_{60}.

The macroscopic structure of the precipitate formed in the presence of C_{60} was investigated by scanning electron microscopy (SEM). For that purpose, samples were prepared by dropcasting toluene solutions onto silicon wafers. Figure 3-19 displays the SEM images of **10** and **10** with 1.0 equiv of C_{60}. In the precipitate, fiber-like structures were observed, while a film-like morphology was observed for **10**, similar to the case of **6** with C_{60} (Figure 3-20). These results indicate that **10** and C_{60} assemble into a one-dimensional (1D) supramolecular structure. Based on comparative experiments with **6**, it can be concluded that the dimeric structure plays an important role in the formation of supramolecular assemblies.

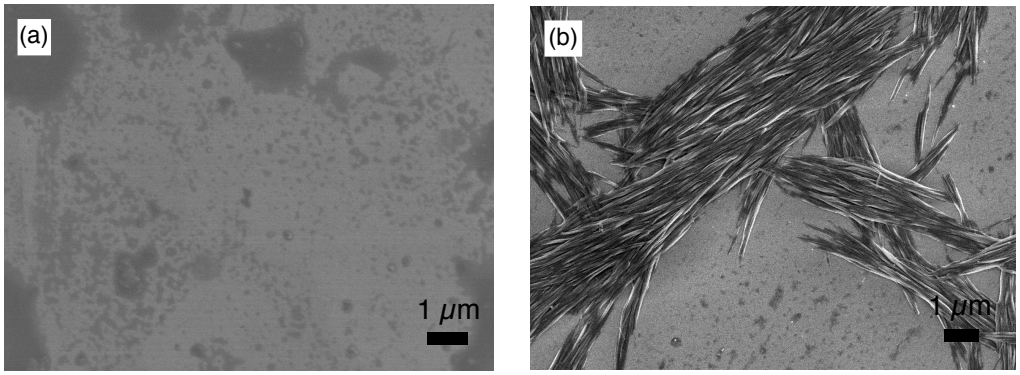

Figure 3-19. SEM images of (a) **10** and (b) **10** with 1.0 equiv of C_{60}.

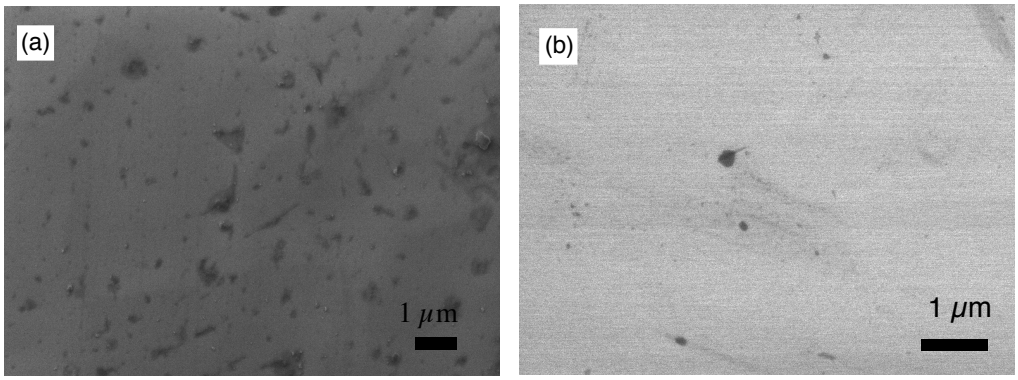

Figure 3-20. SEM images of (a) **6** and (b) **6** with 1.0 equiv of C_{60}.

The stoichiometric ratio between **10** and C_{60} in the precipitate was determined by variable-temperature ^{1}H NMR measurements in toluene-d_8 (Figure 3-21). The author conducted experiments at low temperature to accelerate the assembly process. At –40 °C, the broad spectrum of **10** in the presence of 0.5 equiv of C_{60} became very similar to the spectrum of **10**, which exhibited sharp peaks. Using 1,1,2,2-tetrachloroethane as the internal standard revealed that ~50% the original amount of **10** remained in solution. Consequently, the author concluded that the precipitate consists of **10** and C_{60} in a 1:1 ratio. Notably, peaks in the aromatic region appeared upon addition of 2.0 equiv of C_{60}, and these are completely different from those observed for **10** (see also Figure 3-22).

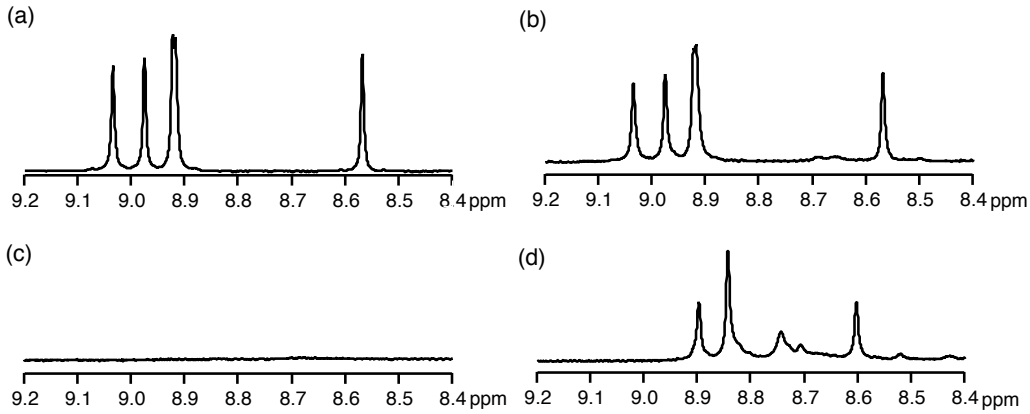

Figure 3-21. ^{1}H NMR spectra of (a) **10** (0.52 mM), (b) **10** + 0.5 equiv of C_{60}, (c) **10** + 1.0 equiv of C_{60}, and (d) **10** + 2.0 equiv of C_{60} at –40 °C in toluene-d_8.

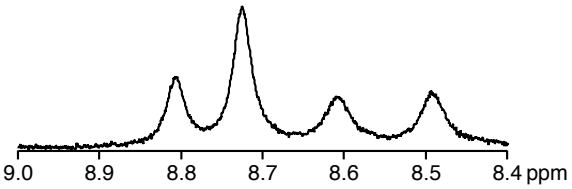

Figure 3-22. The ^{1}H NMR spectra of **10** (0.52 mM) with 2.0 equiv of C_{60} in toluene-d_8 at r.t.

The composition of the fibers was further analyzed by MALDI-TOF mass spectrometry (Figure 3-23). The spectrum exhibited several intense peaks at regular intervals. The gaps between the peaks correspond to the molecular weight of **10** or C_{60}. The largest observable peak was at M_w = 13 kDa, corresponding to a 6:6 complex of **10** and C_{60}. In their entirety, the NMR, SEM, and MS analyses allow the conclusion that the fibers consist of a 1D chain-like assembly of **10** and C_{60} in a 1:1 ratio.

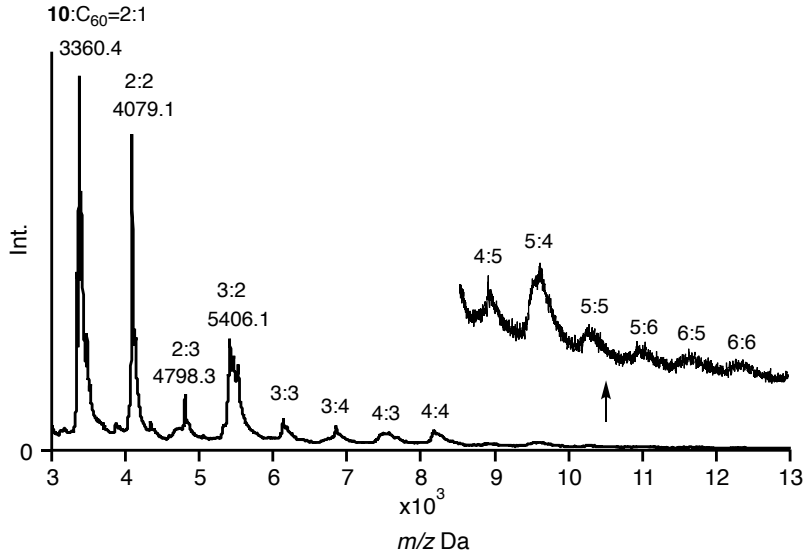

Figure 3-23. MALDI-TOF MS of **10** with 1.0 equiv of C_{60} (Matrix: trans-2-[3-(4-tert-butylphenyl)-2-methyl-2-propenylidene]malononitrile; DCTB).

To elucidate more structural details of the fibers, the author performed a powder X-ray diffraction (XRD) analysis (Figure 3-24 and Table 3-1), which exhibited two broad peaks at 2θ = 2.44° (36.2 Å) and 5.00° (17.7 Å). The spectral pattern of the fibers is thus inconsistent with that of the single crystal of **10**•C_{60}, suggesting the formation of a different packing structure. On the other hand, a powdered sample of **10** showed weak and broad reflections at 2θ = 4.94° (17.9 Å) and 6.18° (14.3 Å), indicating the lack of structural regularity in **10**.

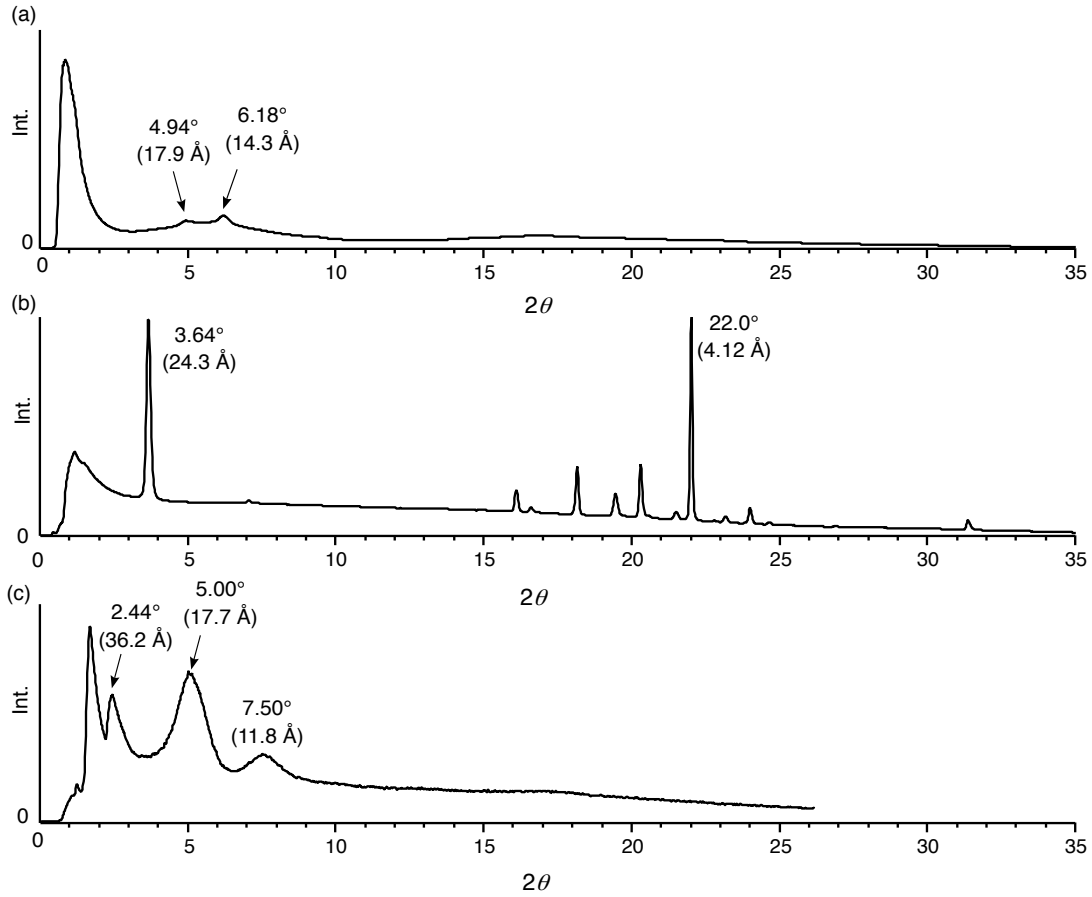

Figure 3-24. The XRD spectra of (a) **10**, (b) **10**•C_{60} crystal, and (c) **10**•C_{60} fiber.

Table 3-1. Peak list details of XRD pattern of **10**, **10**•C_{60} crystal, and **10**•C_{60} fiber

Compound	Angle 2θ (°)	d-value (Å)
10	4.94	17.9
	6.18	14.3
10 + C_{60} crystal	3.64	24.3
	7.04	12.6
	16.08	5.51
	16.58	5.35
	18.14	4.89
	19.44	4.57
	20.3	4.37
	21.5	4.13
	22.0	4.04
	23.16	3.84
	23.98	3.71
	24.64	3.61
	31.36	2.85
10 + C_{60} fiber	2.44	36.2
	5.00	17.7
	7.50	11.8

Figure 3-25 shows the UV-vis-NIR absorption of **10** and its inclusion complexes in the solid state. In contrast to **10**, the **10**•C_{60} crystal exhibits a broad absorption band around 850 nm, which was characterized as a charge transfer (CT) band. The fiber aggregates also exhibit an NIR absorption band, indicating similar

concave-convex binding between **10** and C_{60} in the structure. However, the intensity of this band was higher for the fiber than for the crystal, suggesting different packing structures for these two samples.

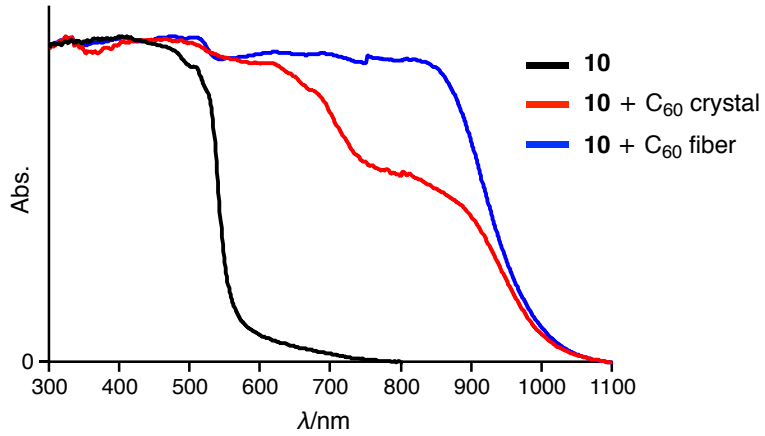

Figure 3-25. Solid-state UV-vis-NIR absorption spectra of **10** (black line), **10** + C_{60} crystal (red line), and **10** + C_{60} fiber (blue line). All spectra were normalized at 300 nm.

Two binding modes are possible for the association of **6** with C_{60}. One is a 1:1 concave–convex complex and the other one involves the formation of a 1:2 sandwich-type complex. The author anticipated that these two binding modes should result in different UV-vis-NIR absorption features in the solid state. Fortunately, by changing the solvents used for recrystallization from methanol/toluene to hexane/chloroform, a 2:1 complex of **6** and C_{60} was obtained. The single-crystal X-ray diffraction analysis of the complex unambiguously revealed a sandwich-type structure, in which two penta-*peri*-pentabenzoazacorannulene molecules cooperatively capture a C_{60} molecule by concave–convex interactions (Figure 3-26). In addition, the author recorded the solid-state UV-vis-NIR absorption spectra of the crystals for both 1:1 and 2:1 binding modes (Figure 3-27). Both 1:1 and 2:1 complexes exhibit CT absorption bands around 850 nm. Notably, the absorption intensity at this wavelength is higher for the 2:1 complex than for the 1:1 complex. The theoretical calculations by the TD-DFT

method at the B3LYP/6-31G(d) level also support these experimental results. The simulated absorption bands assigned to the CT transitions are significantly large in the 2:1 complex as compared to that in the 1:1 complex (Figure 3-28). Such an enhancement of the CT band was also observed in the absorption spectrum of **10** + C_{60}. This spectral similarity strongly indicates a sandwich-type binding mode in the **10**•C_{60} fibers.

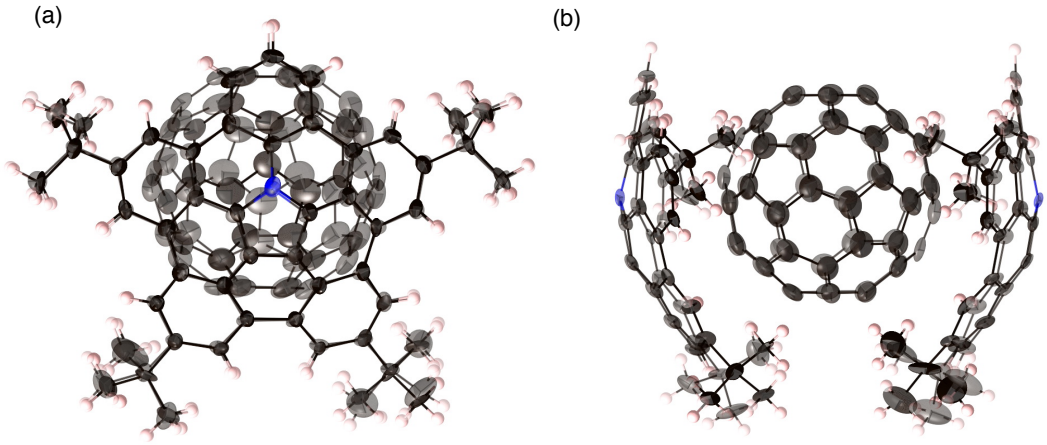

Figure 3-26. Molecular structure of **6**$_2$•C_{60} in the crystal. (a) Top view and (b) side view. The thermal ellipsoids are scaled at 50% probability level.

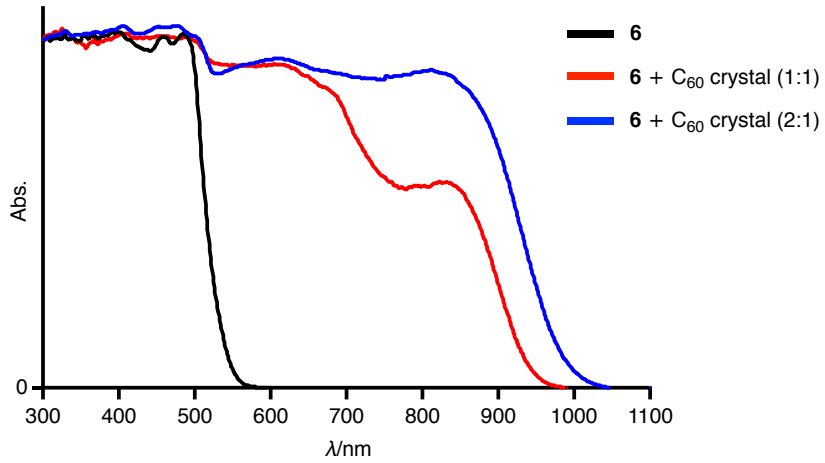

Figure 3-27. Solid state UV-vis-NIR absorption spectra of **6**, **6**•C_{60}, and **6**$_2$•C_{60} All spectra were normalized at 300 nm.

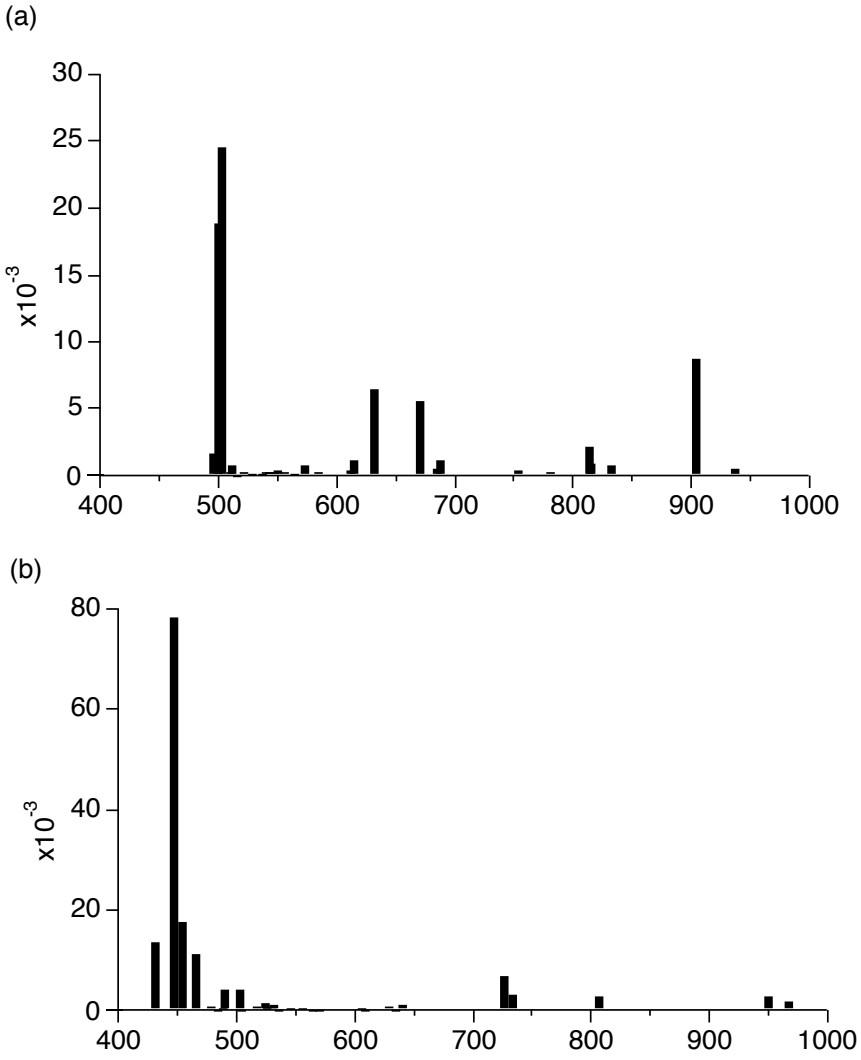

Figure 3-28. The simulated theoretical absorption bands and oscillator strengths of (a) a 2:1 complex between **6** and C_{60} and (b) a 1:1 complex between **6** and C_{60}.

3-7. Plausible Structures and Mechanism of Supramolecular Assembly

Scheme 3-3 illustrates the plausible association mechanism of **10** with C_{60}. In the initial binding step, a 1:1 complex between **10** and C_{60} should be formed. Binding to the second C_{60} molecule would be weaker due to the reduced electron-donating ability of the other penta-*peri*-pentabenzoazacorannulene unit after binding the first electron-deficient C_{60}.[16] Consequently, the 1:1 complex is obtained predominant in dilution. The 1:1 complexes interact with each other under more concentrated

conditions to form fibers by sandwich-type binding, which are insoluble in organic solvents. The author optimized the structure of the 1D chain-like arrangement using PM6 semi-empirical calculations (Figure 3-29). The calculated interplanar spacing (17.8 Å) is in good agreement with the XRD results (17.7 Å). Further addition of C_{60} to the fibers induces cleavage of the polymer chain to form soluble fragments, as detected by ^{1}H NMR spectroscopy.

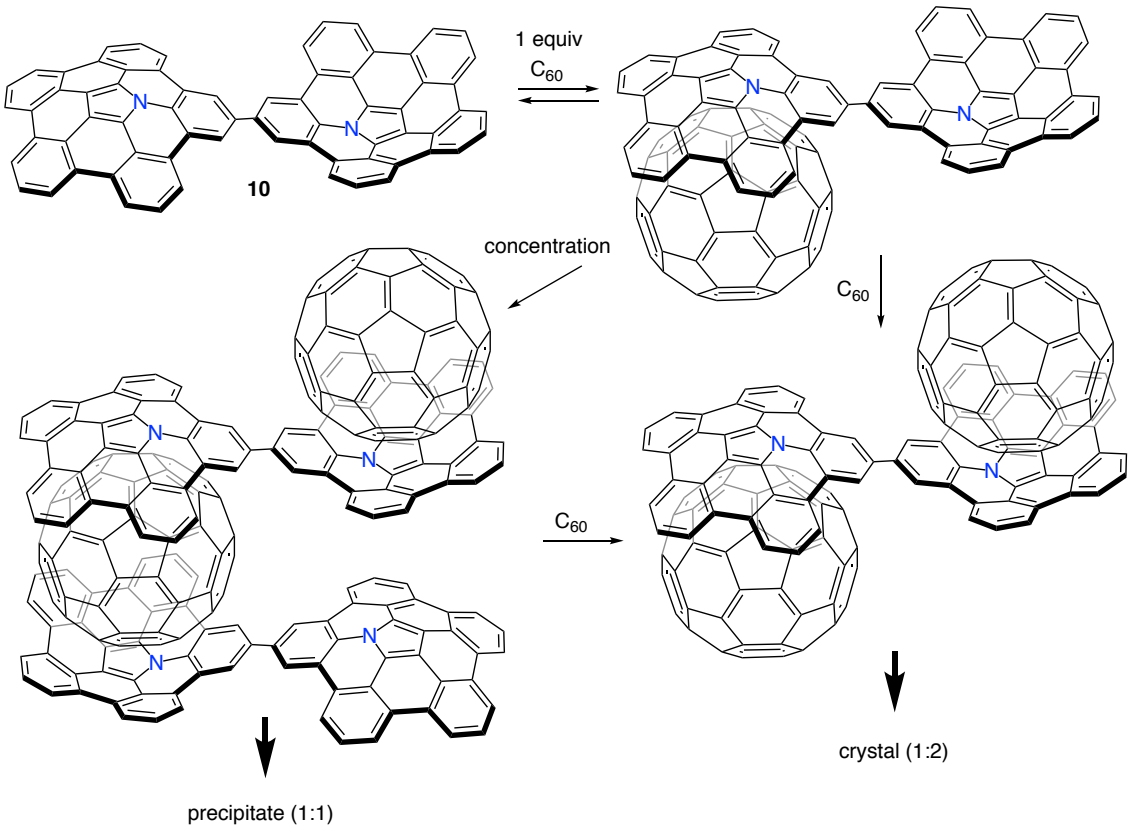

Scheme 3-3. Plausible association mechanism for **10** in the presence of increasing amounts of C_{60} (*tert*-butyl groups are omitted for clarity).

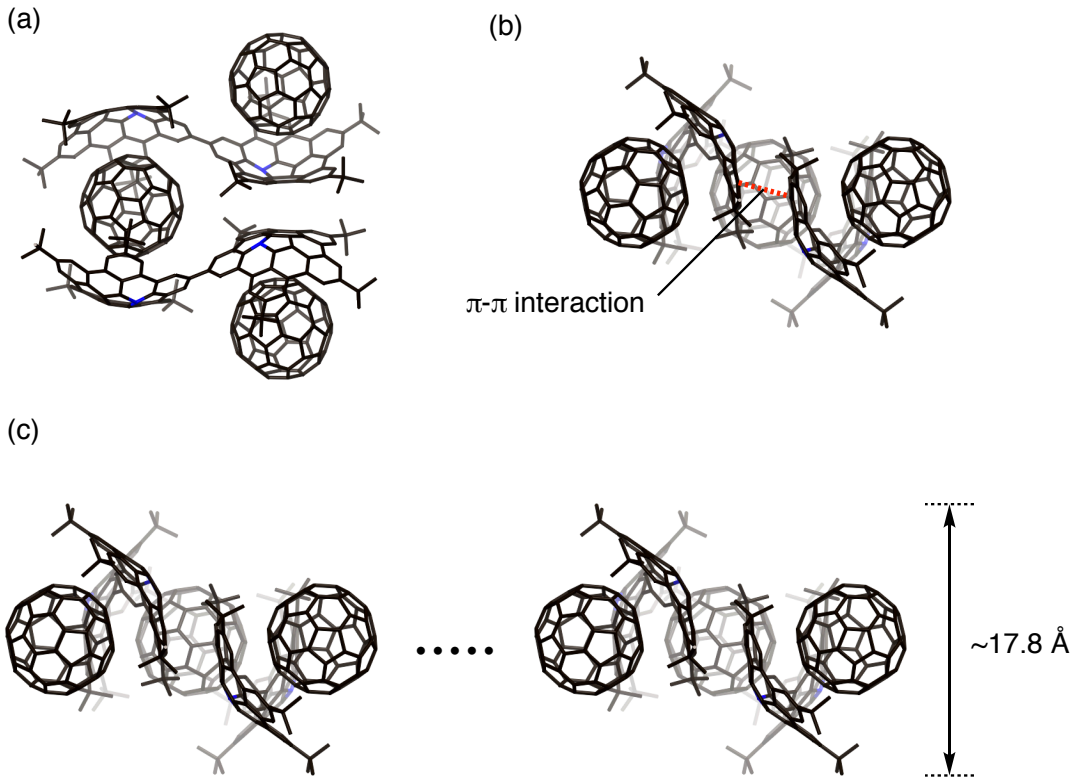

Figure 3-29. The optimized structure of the 1D chain-like supramolecular assembly at the PM6 level.

3-8. Summary

In summary, the author has synthesized a directly linked penta-*peri*-pentabenzoazacorannulene dimer from a tribrominated monomeric precursor. The dimer exhibits strong 1:1 complexation with C_{60} in solution. Segregated stacks of **10** and C_{60} were observed in the crystalline state, suggesting efficient photo-excited charge-carrier mobility. Under concentrated conditions, **10** and C_{60} form 1D chain supramolecular assemblies with a fibrous structure. The present results demonstrate that an electron-donating bowl-shaped π-conjugated molecule can serve as a binding motif for pristine C_{60} for the construction of supramolecular assemblies based on strong donor–acceptor interactions.

3-9. Experimental Section

Materials and Characterization

^{1}H NMR (500 MHz) and ^{13}C NMR (126 MHz) spectra were recorded using a Bruker AVANCE III HD spectrometer. Chemical shifts were reported at the delta scale in ppm relative to $CHCl_3$ (d = 7.260 ppm), toluene-d_8 (d = 7.000 ppm) for ^{1}H NMR and $CDCl_3$ (d = 77.0 ppm) for ^{13}C NMR. UV/vis/NIR absorption spectra were recorded using a Shimadzu UV-2550 or JASCO V670 spectrometer. Emission spectra were recorded using a JASCO FP-6500 spectrometer, and absolute fluorescence quantum yields were measured by the photon-counting method using an integration sphere. High-resolution (HR) mass spectrum was recorded on a Bruker micro TOF using APCI-TOF method. Unless otherwise noted, materials obtained from commercial suppliers were used without further purification.

Synthesis of Penta-*peri*-Pentabenzoazacorannulene Dimer (10).

A Schlenk tube containing compound **5** (50.0 mg, 55.4 μmol), K_2CO_3 (61.2 mg, 0.443 mmol), $Pd(OAc)_2$ (2.45 mg, 10.9 μmol) and $PCy_3{\cdot}HBF_4$ (8.14 mg, 22.1 μmol) were flushed with N_2 three times. To the tube, dry and degassed DMA (6.25 ml) was added. The mixture was stirred for 29 h at 130 °C. The resulting mixture was cooled to room temperature and extracted with ethyl acetate. The organic layer was washed with water, dried over Na_2SO_4 and concentrated in vacuo. Purification by silica-gel column chromatography (hexane/CH_2Cl_2 = 85:15 v/v%) afforded compound **10** (11.2 mg, 8.50 μmol) in 31% yield as a yellow solid. ^{1}H NMR (500 MHz) ($CDCl_3$): δ = 8.68 (s, 2H), 8.62 (s, 2H), 8.58 (s, 2H), 8.56 (s, 2H), 8.42 (s, 2H), 1.65 (s, 18H), 1.64 (s, 18H) ppm.; ^{13}C NMR (126 MHz) ($CDCl_3$): δ = 148.96, 147.81, 140.20, 137.66, 134.66, 132.60, 131.30, 130,17, 129.39, 128.61, 127.66, 126.47, 123.28, 122.10, 120.86, 120.15, 119.44, 118.04, 36.02, 35.88, 32.32, 32.20 ppm.; UV/vis (CH_2Cl_2): λ_{max} (ε[M^{-1} cm^{-1}]) = 407 (91000), 456 (29000), 470 (26000), 494 (17000) nm; fluorescence (CH_2Cl_2,

λ_{ex} = 400 nm): λ_{em} = 519 and 551 nm (Φ_f = 0.17); High-resolution APCI–MS: *m/z* = 1321.7303, calcd for $(C_{100}H_{93}N_2)^+$ = 1321.7339 [$(M + H)^+$].

X-Ray Diffraction Analysis

X-Ray data were obtained using a Bruker D8 QUEST X-ray diffractometer with an IμS microfocus X-ray source and a large area (10 cm × 10 cm) CMOS detector (PHOTON 100) for **6_2•**C_{60} and using a Rigaku CCD diffractometer (Saturn 724 with MicroMax-007) with Varimax Mo optics using graphite monochromated Mo-Kα radiation (λ = 0.71075 Å) for **10**⊃C_{60}.

Electrochemical Analysis

The cyclic voltammogram and differential-pulse voltammogram of **10** were recorded using an ALS electrochemical analyser 612C. Measurements were performed in freshly distilled CH_2Cl_2 with tetrabutylammonium hexafluorophosphate as the electrolyte. A three-electrode system was used. The system consisted of a platinum working electrode, a platinum wire, and $Ag/AgClO_4$ as the reference electrode. The scan rate was 100 mVs^{-1}. The measurement was performed under nitrogen atmosphere. All potentials are referenced to the potential of ferrocene/ferrocenium cation couple.

Determination of Binding Constant

The binding constants (K_a) of C_{60} with compound **6** or **10** were determined by UV-vis absorption spectra. The titrations were performed by the addition of a C_{60} solution into the host solution. After the every addition, the mixture was stirred over 10 min to achieve the equilibrium state. The fitting was performed with the correlation between the change of absorbance (ΔA_{obs}) at 800 nm and the initial concentration of the guest $[G]_0$ using the equation as follows (1:1 binding model)[17]:

$$\Delta A_{obs} = \varepsilon_{\Delta HG}*\{([G]_0+[H]_0+1/K_a)/2-(([G]_0+[H]_0+1/K_a)^2-4*[G]_0*[H]_0)^{0.5}\}$$

K_a and $\varepsilon\Delta_{HG}$ were optimized as parameters in the nonlinear curve fitting using Igor Pro 6.37 (Wavemetrics, Inc.).

Parameters and Variables:

$\Delta A_{obs} = A_{exp} - A_0$

ε_{HG}= molar extinction coefficient for the 1:1 complex

$[G]_0$ = the initial concentration of the guest

$[H]_0$ = the initial concentration of the host

Time-Resolved Microwave Conductivity Measurement.

Transient photoconductivity was measured by FP-TRMC. A resonant cavity was used to obtain a high degree of sensitivity in the conductivity measurement. The resonant frequency and microwave power were set at ~9.1 GHz and 3 mW, respectively, such that the electric field of the microwave was sufficiently small not to disturb the motion of charge carriers. The conductivity value is converted to the product of the quantum yield ϕ and the sum of charge-carrier mobilities $\Sigma\mu$ by $\phi\Sigma\mu = \Delta\sigma\,(eI_0F_{light})^{-1}$, where e, I_0, F_{light}, and $\Delta\sigma$ are the unit charge of a single electron, incident photon density of excitation laser (photons m^{-2}), a correction (or filling) factor (m^{-1}), and a transient photoconductivity, respectively. The sample was set at the highest electric field in a resonant cavity. FP-TRMC experiments were performed at room temperature. The measurements of **10** and **10**$\supset C_{60}$ were performed for crystalline samples covered with a PVA film on a quartz substrate.

DOSY Measurement

The diffusion coefficients (D) of **6**, **6** + C_{60}, **10**, and **10** + C_{60} were determined by ^{1}H NMR measurement at the concentrations of 0.8 mM. The mixture of host and C_{60} were dissolved in toluene-d_8, and then stirred over 10 min to achieve the equilibrium state. All experiments were conducted at 20 °C.

SEM Measurement

Field emission scanning electron microscopy (FE-SEM) samples were prepared by drop-cast of toluene solution of **6**, **6** + C_{60}, **10**, and **10** + C_{60} on silicon wafer. The images were recorded on a JEOL JSM-7500F microscope with the accelerating voltages of 1 kV for **6**, **10**, and 2 kV for **6** + C_{60}, **10** + C_{60}.

XRD Measurement

The measurements of **10** and **10**•C_{60} crystal were performed for powder and crystalline samples respectively. The sample of **10**•C_{60} fiber was prepared by drop-cast of toluene solution of the mixture of **10** and 1 equiv of C_{60} on silicon wafer. X-Ray diffraction data of **10**, **10** + C_{60} crystal and **10** + C_{60} fiber were taken on a X-ray diffractometer Rigaku FR-E equipped with two-dimensional detector Rigaku R-axis IV using CuKα radiation (λ = 1.5418 Å)

Theoretical Calculations

All calculations were performed using the Gaussian 09 program. The simulated absorption spectra of 1:1 and 2:1 complexes between **6** and C_{60} were obtained by the TD-DFT method at the B3LYP functional and the 6-31G(d) basis set using X-ray crystal structures without any structural optimization. The estimated structure of the 1D chain-like supramolecular assembly was calculated by PM6 semi-empirical calculations.

Crystallographic Data

	10•$(C_{60})_2$	**6$_2$**•C_{60}
empirical formula	$C_{247.73}H_{123.18}N_2$	$C_{320}H_{188}N_4$
formula weight	3127.42	4088.73
habit	prism	prism
T, K	93(2)	113(2)
crystal system	monoclinic	monoclinic
space group	$P2_1/c$	$P2_1$
a, Å	13.1579(2)	17.0175(8)
b, Å	37.8588(7)	28.9186(13)
c, Å	30.9277(5)	22.7929(10)
α, deg	90	90
β, deg	96.192(2)	100.4840(10)
γ, deg	90	90
V, Å^3	15316.5(4)	11029.6(9)
Z	4	2
Dc, g/cm^3	1.356	1.231
F(000)	6494	4272
crystal size, mm^3	0.70 x 0.074 x 0.066	0.40 x 0.20 x 0.16
$2\theta_{max}$, °	50.0	50.0
R_1 ($I > 2\sigma(I)$)	0.1090	0.0969
wR_2 (all data)	0.3338	0.2627
GOF	1.085	1.077
obs reflects	26953	34976
total reflects	130177	75648
parameters	3503	4135
CCDC number	1579079	1579080

3-10. References

1. (a) L. Brunsveld, B. J. B. Folmer, E. W. Meijer, R. P. Sijbesma, *Chem. Rev.* **2001**, *101*, 4071. (b) T. F. A. De Greef, M. M. J. Smulders, M. Wolffs, A. P. H. J. Schenning, R. P. Sijbesma, E. W. Meijer, *Chem. Rev.* **2009**, *109*, 5687. (c) L. Yang, X. Tan, Z. Wang, X. Zhang, *Chem. Rev.* **2015**, *115*, 7196.

2. (a) X. Yan, F. Wang, B. Zheng, F. Huang, *Chem. Soc. Rev.* **2012**, *41*, 6042. (b) X. Ma, H. Tian, *Acc. Chem. Res.* **2014**, *47*, 1971.

3. F. Giacalone, N. Martín, *Chem. Rev.* **2006**, *106*, 5136.

4. N. Martín, J. -F. Nierengarten Eds., in Supramolecular Chemistry of Fullerenes and Carbon Nanotubes, Wiley-VCH, Weinheim, 2012

5. (a) G. Fernández, E. M. Pérez, L. Sánchez, N. Martín, *Angew. Chem. Int. Ed.* **2008**, *47*, 1094. (b) G. Fernández, E. M. Pérez, L. Sánchez, N. Martín, *J. Am. Chem. Soc.* **2008**, *130*, 2410.

6. (a) T. Hirao, M. Tosaka, S. Yamago, T. Haino, *Chem. Eur. J.* **2014**, *20*, 16138. (b) T. Haino, Y. Matsumoto, Y. Fukazawa, *J. Am. Chem. Soc.* **2005**, *127*, 8936. (c) H. Isla, E. M. Pérez, N. Martín, *Angew. Chem. Int. Ed.* **2014**, *53*, 5629.

7. (a) Y. Liu, H. Wang, P. Liang, H. -Y. Zhang, *Angew. Chem. Int. Ed.* **2004**, *43*, 2690. (b) Y. Liu, Y. -W. Yang, Y. Chen, H. -X. Zou, *Macromolecules* **2005**, *38*, 5838. (c) M. Shirakawa, N. Fujita, S. Shinkai, *J. Am. Chem. Soc.* **2003**, *125*, 9902. (d) M. Fathalla, S. -C. Li, U. Diebold, A. Alb, J. Jayawickramarajah, *Chem. Commun.* **2009**, 4209.

8. M. A. Petrukhina and L. T. Scott Eds., in Fragments of Fullerenes and Carbon Nanotubes: Designed Synthesis, Unusual Reactions, and Coordination Chemistry, Wiley, Hoboken, 2012.

9. (a) Y. -T. Wu, J. S. Siegel, *Chem. Rev.* **2006**, *106*, 4843. (b) H. Sakurai, T. Daiko, T. Hirao, *Science* **2003**, *301*, 1878. (c) W. E. Barth, R. G. Lawton, *J. Am. Chem. Soc.* **1966**, *88*, 380.

10. T. Kawase, H. Kurata, *Chem. Rev.* **2006**, *106*, 5250.

11. (a) L. N. Dawe, T. A. AlHujran, H. -A. Tran, J. I. Mercer, E. A. Jackson, L. T. Scott,

P. E. Georghiou, *Chem. Commun.* **2012**, *48*, 5563. (b) A. S. Filatov, M. V. Ferguson, S. N. Spisak, B. Li, C. F. Campana, M. A. Petrukhina, *Cryst. Growth Des.* **2014**, *14*, 756. (c) S. Mizyed, P. E. Georghiou, M. Bancu, B. Cuadra, A. K. Rai, P. Cheng, L. T. Scott, *J. Am. Chem. Soc.* **2001**, *123*, 12770. (d) A. Sygula, F. R. Fronczek, R. Sygula, P. W. Rabideau, M. M. Olmstead, *J. Am. Chem. Soc.* **2007**, *129*, 3842. (e) M. Yanney, F. R. Fronczek, A. Sygula, *Angew. Chem. Int. Ed.* **2015**, *54*, 11153. (f) C. M. Álvarez, L. A. García-Escudero, R. García-Rodríguez, J. M. Martín-Álvarez, D. Miguel, V. M. Rayón, *Dalton Trans.* **2014**, *43*, 15693. (g) P. L. A. Kuragama, F. R. Fronczek, A. Sygula, *Org. Lett.* **2015**, *17*, 5292.

12. (a) J. Janata, J. Gendell, C. -Y. Ling, W. E. Barth, L. Backes, H. B. Mark, R. G. Lawton, *J. Am. Chem. Soc.* **1967**, *89*, 3056. (b) T. J. Seiders, K. K. Baldridge, J. S. Siegel, R. Gleiter, *Tetrahedron Lett.* **2000**, *41*, 4519. (c) P. Zanello, S. Fedi, F. F. de Biani, G. Giorgi, T. Amaya, H. Sakane, T. Hirao, *Dalton Trans.* **2009**, 9192.

13. V. H. Le, M. Yanney, M. McGuire, A. Sygula, E. A. Lewis, *J. Phys. Chem. B* **2014**, *118*, 11956.

14. S. Seki, A. Saeki, T. Sakurai, D. Sakamaki, *Phys. Chem. Chem. Phys.* **2014**, *16*, 11093.

15. C. S. Johnson Jr, *Prog. Nucl. Magn. Reson. Spectrosc.* **1999**, *34*, 203.

16. A negative allosteric effect of C_{60} has been reported; see: (a) K. Miki, T. Matsushita, Y. Inoue, Y. Senda, T. Kowada, K. Ohe, *Chem. Commun.* **2013**, *49*, 9092. (b) H. Sato, K. Tashiro, H. Shinmori, A. Osuka, Y. Murata, K. Komatsu, T. Aida, *J. Am. Chem. Soc.* **2005**, *127*, 13086. (c) L. Moreira, J. Calbo, J. Aragó, B. M. Illescas, I. Nierengarten, B. Delavaux-Nicot, E. Ortí, N. Martín, J. -F. Nierengarten, *J. Am. Chem. Soc.* **2016**, *138*, 15359.

17. P. Thordarson, *Chem. Soc. Rev.* **2011**, *40*, 1305.

Chapter 4

Reversible σ-Bond Dimerization of Bowl-Shaped Radical Cation

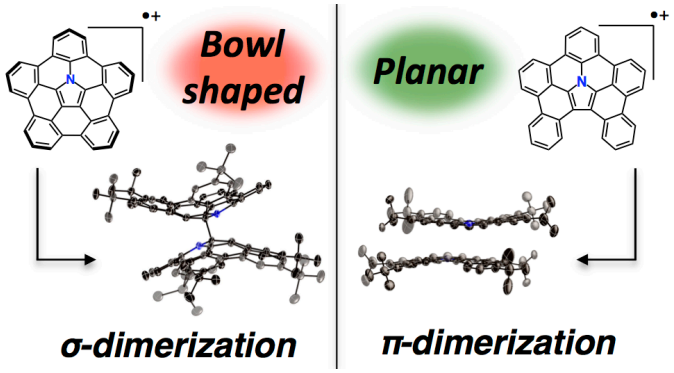

ABSTRACT: Reversible σ-bond formation between two organic radicals has been widely investigated. However, formation of σ-dimers from delocalized π-radical cations has been limited. The author found the reversible σ-dimerization behavior of a bowl-shaped π-radical cation, which was generated from a nitrogen-embedded penta-*peri*-pentabenzoazacorannulene, both in crystalline and solution states. A single crystal X-ray diffraction analysis elucidated the detailed structure of the σ-dimer in the crystalline state. In the solution state, the monomeric radical cation predominantly existed at room temperature, while dimerization of the radical cation occurred through carbon–carbon σ-bond formation as the temperature decreased. The ^{1}H NMR and optical spectroscopic measurements supported the formation of the σ-dimer at low temperatures. Comparative studies with a similar planar π-conjugated system suggested that the curved structure of the bowl-shaped π-radical cation facilitated the σ-dimerization at the internal sp^{2} carbon atom. This trend was also observed in the nucleophilic addition reaction of methanol to the π-radical cations. The methoxylation reaction proceeded only for the curved π-radical cation but not for the planar π-radical cation. Theoretical calculations indicated a large relief of the structural strain at the α-carbon in the course of the dimerization or nucleophilic addition reactions accelerated the bond formation at the internal carbon atom of the curved radical cation.

Contents

4-1. Introduction

Reversible σ-bond formation and dissociation processes of organic radicals has attracted much attention in the fields of polymeric soft matter, self-healing, and mechanochromic materials.[1–3] Among these researches, the reversible σ-dimerization with radical cations has been limited due to the coulombic repulsion between two positively charged species or the instability of monomeric radical cations. Furthermore, most of delocalized π-conjugated radical cations usually form π-dimers both in the solution and solid state.

A σ-bonded dicationic dimer is suggested as a key intermediate in oxidative C–C bond-forming reactions such as electrochemical polymerization of thiophenes or pyrroles.[4] However, the direct observation of these dicationic species have remained challenging because of their short lifetimes. To date, several research groups have succeeded in observing the σ-dimeric dications.[5] For example, Effenberger and co-workers have reported the oxidative dimerization reactions of amino-substituted benzene derivatives and elucidated the structure of σ-bonded dicationic dimer by a single crystal X-ray diffraction analysis.[5b–e] In 1999, Merz and co-workers have revealed that the interconversion between the σ-dicationic species consists of two bipyrroles and its corresponding monomer proceeds reversibly in solution depending on temperatures.[5g] Power and co-workers have demonstrated the σ-dimerization of persistent organic radical cations in the crystalline state.[5m] However, their low solubility hampered detailed studies in the solution state.

Most of reactions of π-conjugated molecules occur at peripheral positions rather than at internal atoms. For instance, all the reversible σ-dimerization reactions of organic radical cations occurred at their peripheral carbon atoms. On the other hand, in the case of nanocarbon materials such as fullerene, carbon nanotube, and graphene, reactions can proceed at the internal sp^2 carbon atoms on the surface.[6,7] Recently, such a specific reactivity has been also reported for bowl-shaped π-conjugated molecules.[8] While the reactions of corannulene usually proceed at the peripheral sp^2 carbon atoms,

the addition of dihalocarbene to corannulene occurs at its internal sp^2 carbon atom.[8a] Petrukhina and co-workers have also succeeded in the isolation and characterization of an inner-substituted corannulene arenium cations.[8b] In 2008, Scott and Bronstein suggested that a relief of the geometric strain in the course of the addition reaction at internal sp^2 carbons is larger in bowl-shaped molecules than that in planar π-systems by theoretical calculations.[8h] However, there is no report that experimentally demonstrates the effect of the curved π-structure on their specific reactivity at the internal position through the comparative study with its planar analogue.

The author revealed that oxidation of penta-*peri*-pentabenzoazacorannulene **6** with tris(4-bromophenyl)aminium hexachloroantimonate (BAHA) successfully affords the radical cation $\mathbf{6}^{\bullet+}SbCl_6^-$ due to its electron-rich nature (see Chapter 2). The persistent nature of this radical cation enables the further investigation into its chemical properties. Herein, the author discloses a reversible σ-bond formation behavior of $\mathbf{6}^{\bullet+}$ at its internal sp^2 carbon atom upon crystallization or lowering temperature in solution (Scheme 4-1). The author also experimentally demonstrated the importance of the curved structure for σ-dimerization through comparison with an analogous planar radical cation $\mathbf{7}^{\bullet+}SbCl_6^-$, which underwent selective π-dimerization.

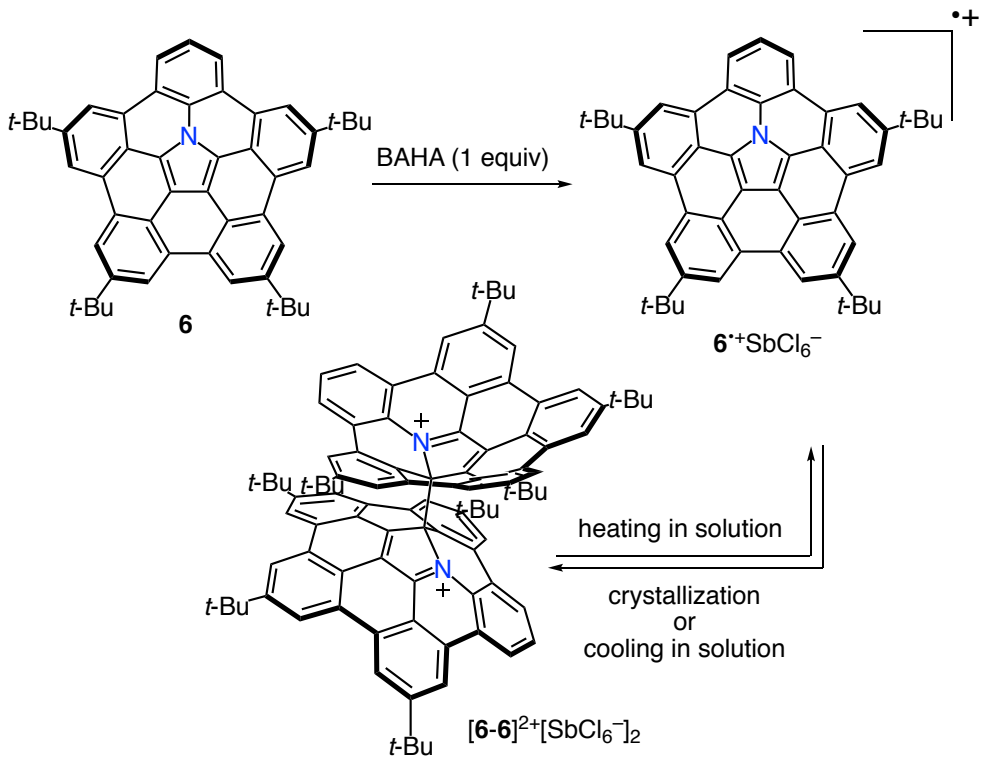

Scheme 4-1. Dimerization and dissociation behavior between $\mathbf{6}^{\bullet+}SbCl_6^-$ and $[\mathbf{6}\text{-}\mathbf{6}]^{2+}[SbCl_6^-]_2$.

4-2. σ-Dimerization of a Bowl-Shaped Radical Cation

To characterize the detailed structure of $\mathbf{6}^{\bullet+}$, the author attempted to get its single crystal by a vapor diffusion of hexane into a chlorobenzene/diethyl ether solution of $\mathbf{6}^{\bullet+}SbCl_6^-$. Contrary to expectation, the author obtained the crystal of σ-dimer $[\mathbf{6}\text{-}\mathbf{6}]^{2+}[SbCl_6^-]_2$, where two penta-*peri*-pentabenzoazacorannulene units were connected by a covalent carbon–carbon bond at the internal α-carbons of the central pyrrole ring (Figure 4-1). The sum of the angles around the α-carbons (326°/327°) clearly indicates their sp^3 configuration. In addition, the existence of two counter anions in a unit cell indicated the dicationic state of this dimer. The length of the central bridging bond (1.64 Å) is close to those of previously reported σ-dimeric dications, but apparently longer than the standard $C(sp^3)$–$C(sp^3)$ single bond.[5c,m] There are two possible diastereomers for $[\mathbf{6}\text{-}\mathbf{6}]^{2+}$, one of which is *meso*-dimer and the other is *chiral*-dimer. The calculated

energies of *meso*- and *chiral*-dimers are almost identical (Figure 4-2 and Table 4-1). However, only the *meso*-dimer was observed in crystal. As revealed in Chapter 2, $\mathbf{6}^{\bullet+}SbCl_6^-$ exists as the monomer in the solution state at room temperature. Consequently, the dimerization behavior of $\mathbf{6}^{\bullet+}$ was induced by crystallization. Dissolving of the crystal of σ-dimer $[\mathbf{6}\text{-}\mathbf{6}]^{2+}[SbCl_6^-]_2$ in CH_2Cl_2 reproduced the monomeric radical cation.

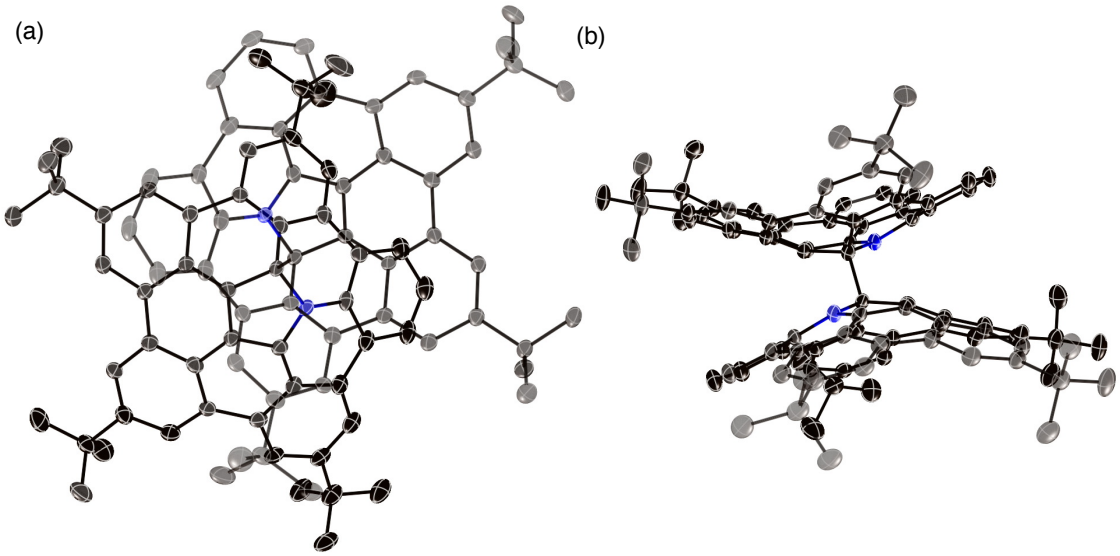

Figure 4-1. X-Ray crystal structure of $[\mathbf{6}\text{-}\mathbf{6}]^{2+}[SbCl_6^-]_2$. (a) Top view and (b) side view. The thermal ellipsoids are scaled at 50% probability level. The hydrogen atoms, solvent molecules and $[SbCl_6]^-$ ions are omitted for clarity.

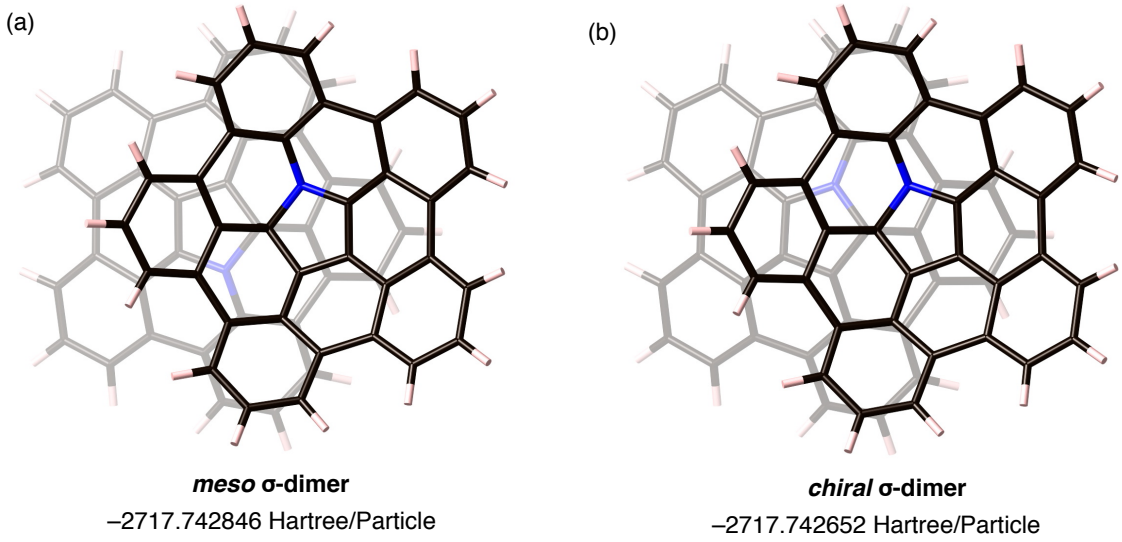

Figure 4-2. The sum of the electronic and zero-point energies of *meso* and *chiral* σ-dimer.

Table 4-1. Summary of the electronic and zero-point energies of each σ-dimer

Units (Hartree/Particle)

Compound	ZPE^a	$E_0{}^b$
Meso σ-dimer	0.764763	–2717.742846
Chiral σ-dimer	0.764729	–2717.742652

[a] Zero-point correction. [b] Sum of electronic and zero-point energies.

The σ-dimerization reaction was also observed in the solution state by lowering the temperature. Figure 4-3 shows variable-temperature (VT) ^{1}H NMR spectra of **6**$^{\bullet+}$$SbCl_6^-$ in $CDCl_3$. No signal was observed at 25 °C, suggesting the predominant existence of a paramagnetic species at room temperature. The broad peaks gradually appeared in the aromatic region as the temperature decreased. These peaks finally became sharp at –55 °C, indicating the formation of a diamagnetic species. Judging from ^{1}H–^{1}H COSY NMR measurement and their relative integral values estimated by comparison with those of tris(4-bromophenyl)amine, there were eight singlets, two

doublets, and one triplet (Figure 4-4 and Figure 4-5). These signals were assigned as peripheral protons of penta-*peri*-pentabenzoazacorannulene with a lower symmetry.

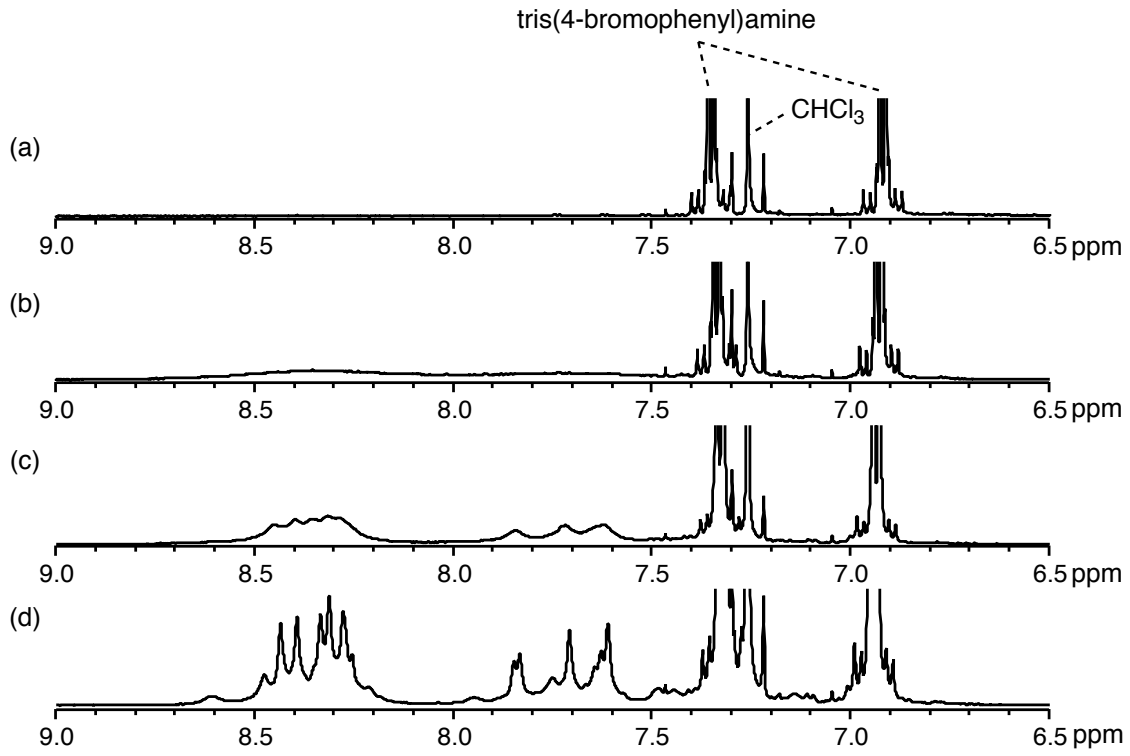

Figure 4-3. VT ^{1}H NMR spectra of **6**$^{\bullet+}$$SbCl_6^-$ in $CDCl_3$. (a) 25 °C, (b) –20 °C, (c) –40 °C, and (d) –55 °C.

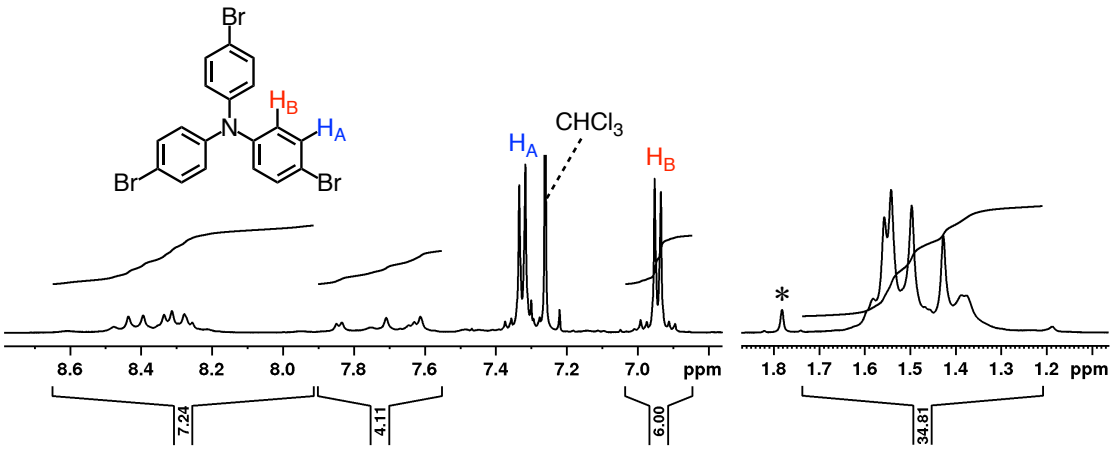

Figure 4-4. ^{1}H NMR spectra of **6**$^{\bullet+}$$SbCl_6^-$ at –55 °C in $CDCl_3$.

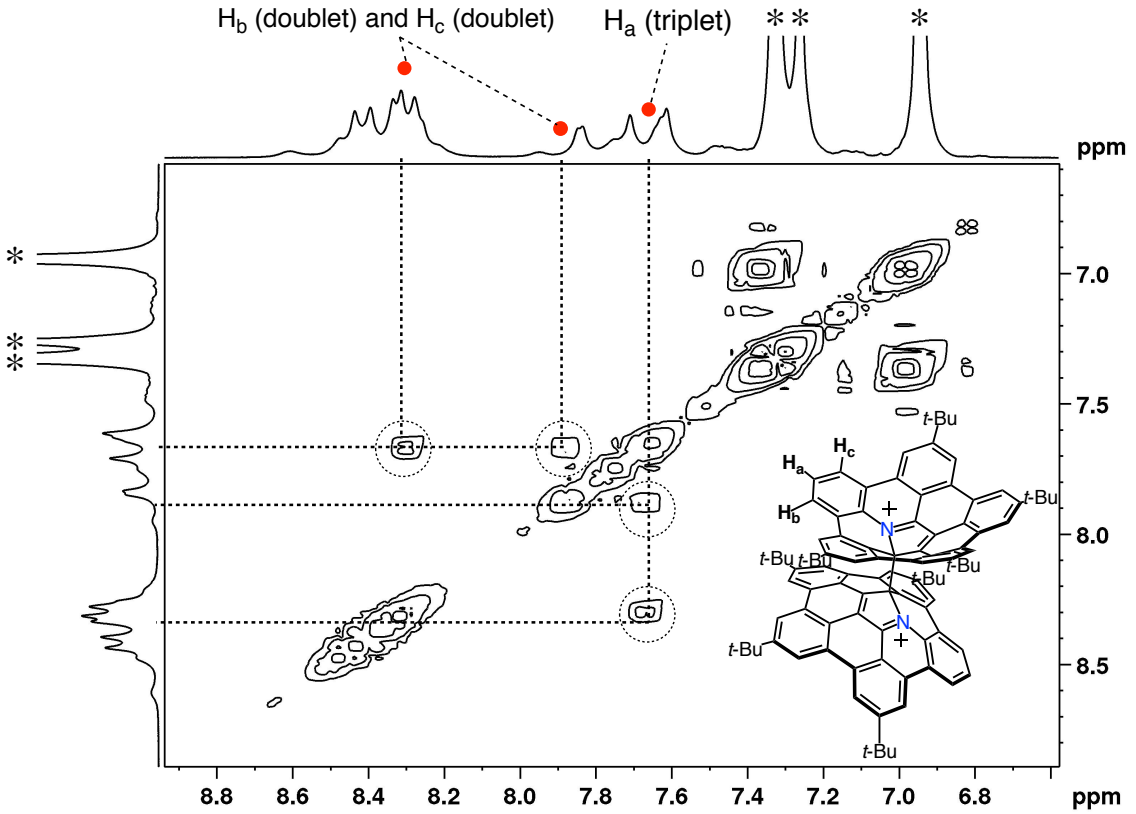

Figure 4-5. ^{1}H–^{1}H COSY NMR spectrum of **6**$^{\bullet+}$$SbCl_6^-$ in $CDCl_3$ at –55 °C.

The author also measured VT UV-vis-NIR absorption spectra of **6**$^{\bullet+}$$SbCl_6^-$ in CH_2Cl_2 (Figure 4-6). At room temperature, the characteristic broad band in the near-infrared (NIR) region due to the monomeric radical cation was observed. On the other hands, this NIR absorption band was diminished at lower temperatures, while the new absorption bands around 580 nm and 720 nm were generated with isosbestic points. The disappearance of NIR absorption band suggests the formation of σ-dimer.[5g,i] In addition, the simulated absorption spectrum of the σ-dimer [**6**-**6**]$^{2+}$ calculated by the time-dependent (TD) DFT method are in good agreement with the experimental spectra (Figure 4-7). These spectroscopic analysis indicated the formation of σ-dimer [**6**-**6**]$^{2+}$ even in the solution state as in the case of the crystalline state. According to the optical experiments, the thermodynamic parameters of this dimerization process were determined to be ΔH = –11.1 kcal mol^{-1} and ΔS = –25.6 cal K^{-1} mol^{-1} by a van't Hoff

plot (Figure 4-8 and Figure 4-9).

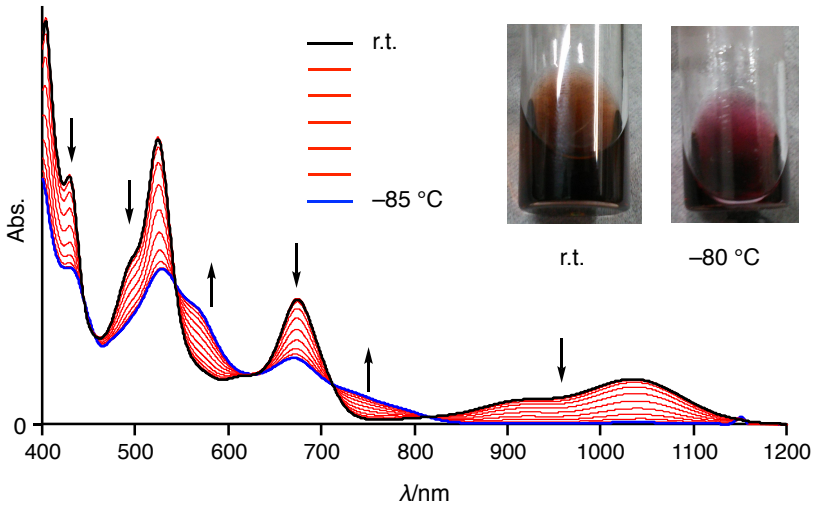

Figure 4-6. VT UV/vis/NIR absorption spectra of $\mathbf{6}^{\bullet+}SbCl_6^-$ in CH_2Cl_2. The inset shows the changes of the solution color.

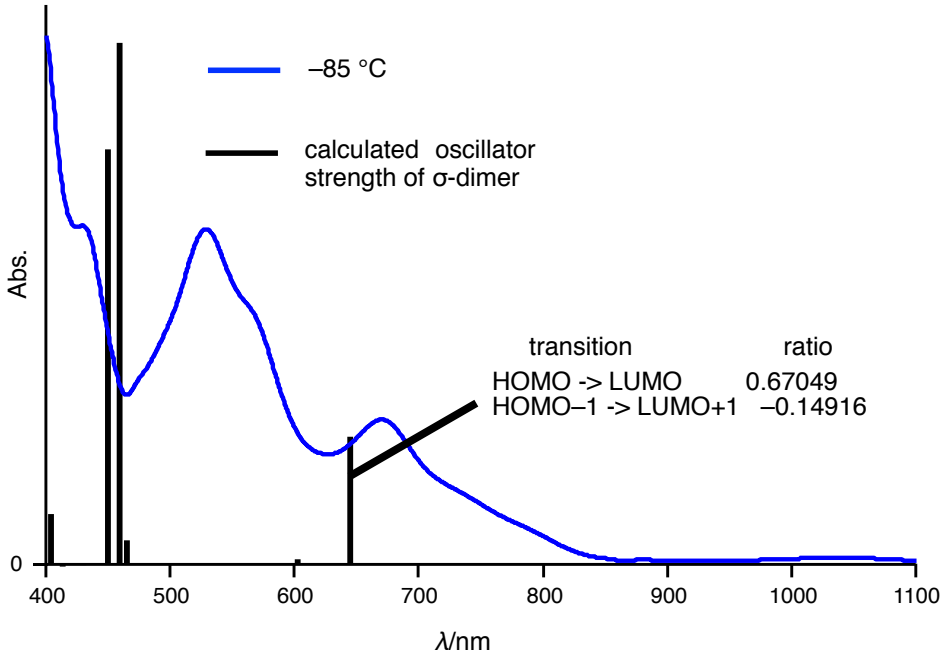

Figure 4-7. Calculated absorption spectrum of the σ-dimer. The experimental absorption spectrum of $\mathbf{6}^{\bullet+}$ in CH_2Cl_2 at –85 °C was also displayed for comparison (blue line).

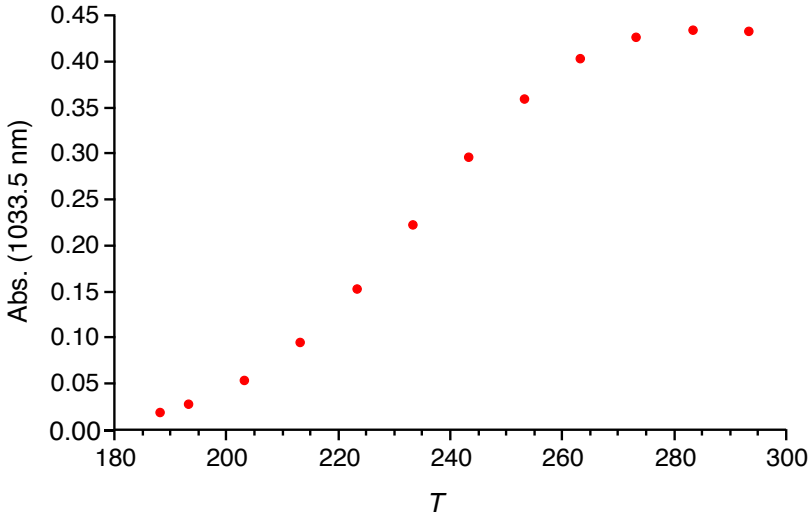

Figure 4-8. The temperature-dependent absorbance (at 1033.5 nm) of $\mathbf{6}^{\bullet+}$ in CH_2Cl_2.

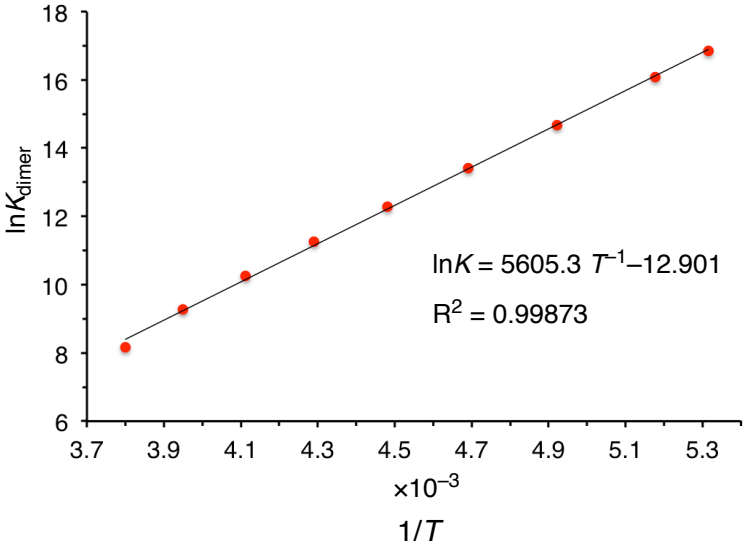

Figure 4-9. van't Hoff plot using UV/vis/NIR absorption measurement.

The author also performed VT-ESR measurement in CH_2Cl_2 (Figure 4-10). The signal derived from $\mathbf{6}^{\bullet+}$ completely disappeared at –85 °C. From these experiments, the thermodynamic parameters were estimated to be ΔH = –11.8 kcal mol^{-1} and ΔS = –23.9 cal K^{-1} mol^{-1}, which are almost consistent with those evaluated by optical measurements (Figure 4-11 and Figure 4-12). The ΔH value in this system is larger than

that of previously reported σ-dimeric dications.[5i–k] In addition, the dimerization reaction of alkylated C_{60} radicals shows much smaller ΔH value (up to –35.5 kcal mol^{-1}).[9] The relatively large ΔH value of $\mathbf{6}^{\bullet+}$ is consistent with its reversible σ-dimerization and dissociation behavior in solution around room temperature.

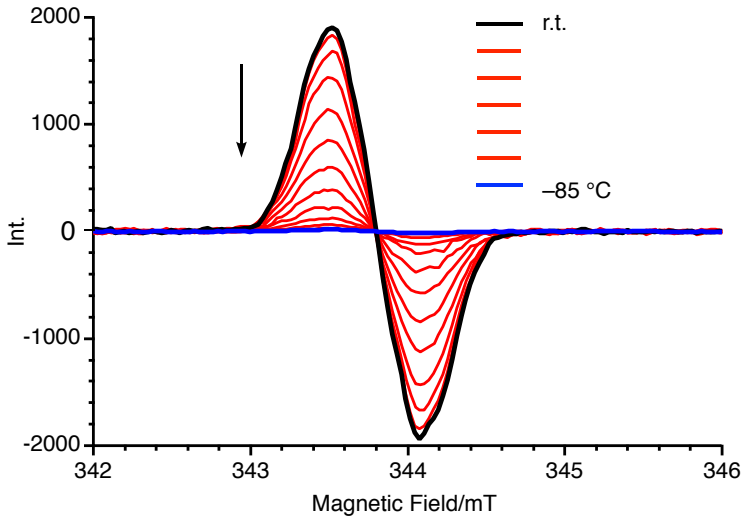

Figure 4-10. VT ESR spectra of $\mathbf{6}^{\bullet+}SbCl_6^-$ in CH_2Cl_2.

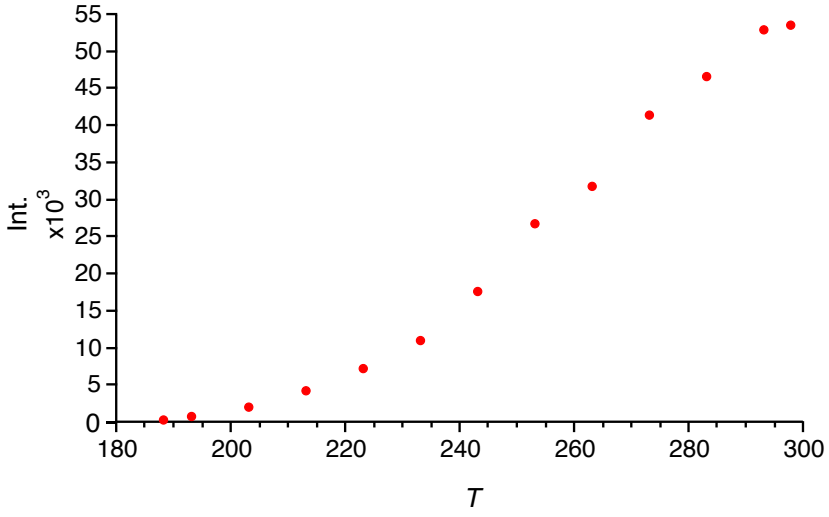

Figure 4-11. The temperature-dependent integration of the ESR signal of $\mathbf{6}^{\bullet+}$ in CH_2Cl_2.

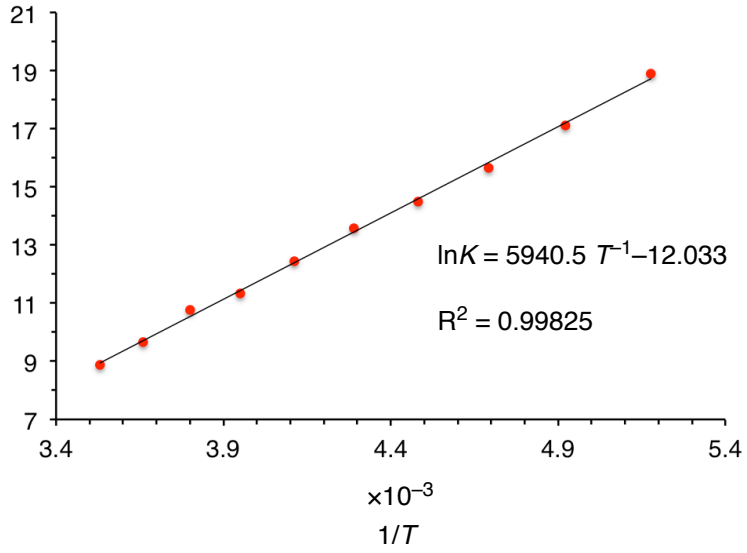

Figure 4-12. van't Hoff plot using ESR measurement.

4-3. π-Dimerization of an Analogous Planar Radical Cation

Contrary to the present bowl-shaped π-radical cation **6**$^{\bullet+}$, delocalized π-radical cations often forms their π-dimers in the solution state.[10] The author speculated that the bowl-shaped structure of **6**$^{\bullet+}$ would contribute to the σ-bond formation at the internal position. To elucidate the effect of the bowl shape on σ-dimerization, the author conduced comparison experiment with analogous planar molecule **7** (see Scheme 2-3 in Chapter 2). Compound **7** has the one carbon–carbon bond deficient structure of **6**. The structure of **7** was unambiguously elucidated by a single crystal X-ray diffraction analysis. In the crystal, there are four independent molecules, which arranged to form 1D columnar π-stack (Figure 4-13). The deviations from the mean plane consisting of core 35 atoms are 0.077 Å, 0.125 Å, 0.135 Å, and 0.154 Å, corroborating its highly planar structure.

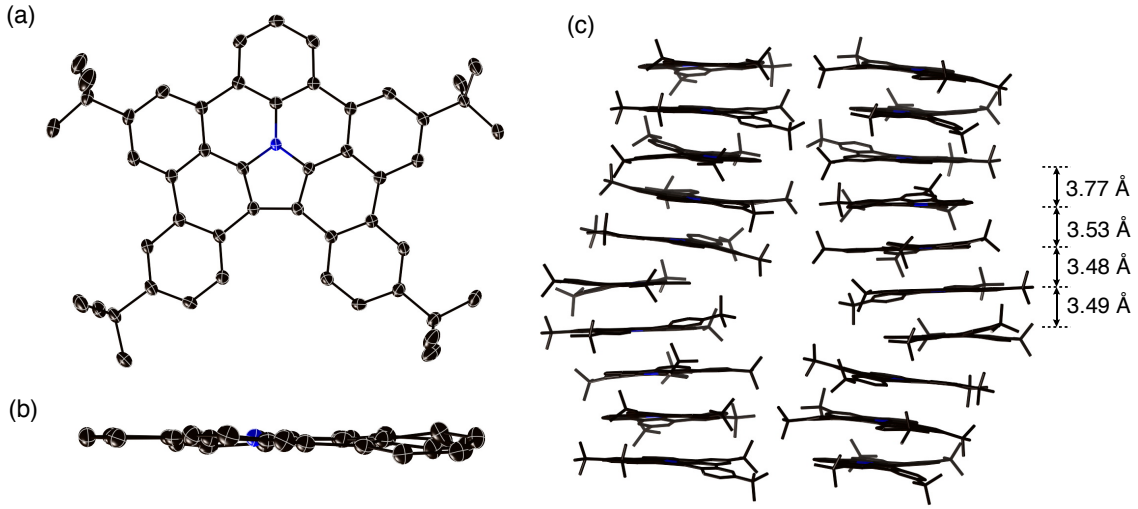

Figure 4-13. X-Ray crystal structure of **7**. (a) Top view, (b) side view, and (c) packing structure. The thermal ellipsoids are scaled at 50% probability level. The hydrogen atoms and solvent molecules are omitted for clarity.

The oxidation of **7** with 1 equiv of BAHA resulted in disappearance of its NMR proton signals and generation of NIR bands in the UV/vis/NIR absorption spectrum (Figure 4-14 and Figure 4-15). The formation of a paramagnetic specie was confirmed by ESR measurement in the CH_2Cl_2 solution, showing a distinct peak at g = 2.003 (Figure 4-16). The simulated UV-vis-NIR absorption spectrum of $\mathbf{7}^{\bullet+}$ by the TD-DFT method at the B3LYP/6-31G(d) level was consistent with the experimental result, supporting the formation of $\mathbf{7}^{\bullet+}$ (Figure 4-17).

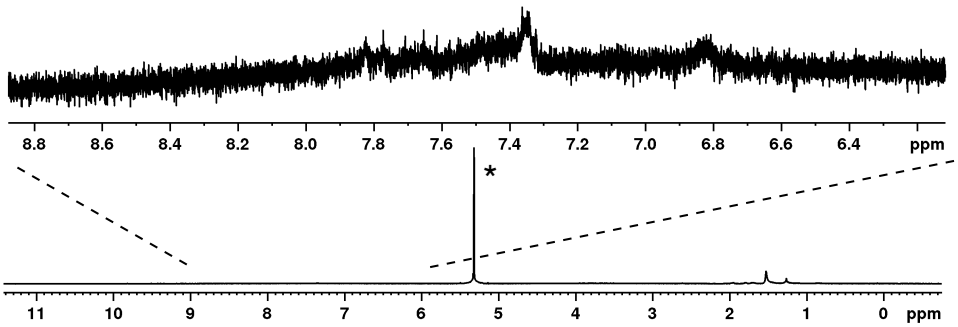

Figure 4-14. ^{1}H NMR spectrum of **7** with 1.0 equiv of BAHA in CD_2Cl_2.

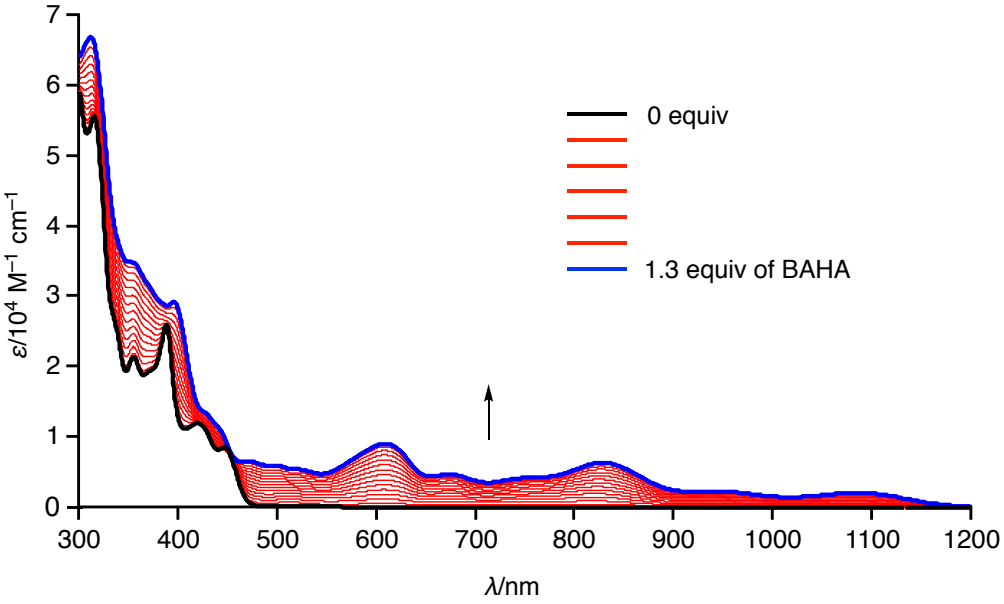

Figure 4-15. UV/vis/NIR absorption spectral changes of **7** with 1.0 equiv of BAHA in CH_2Cl_2.

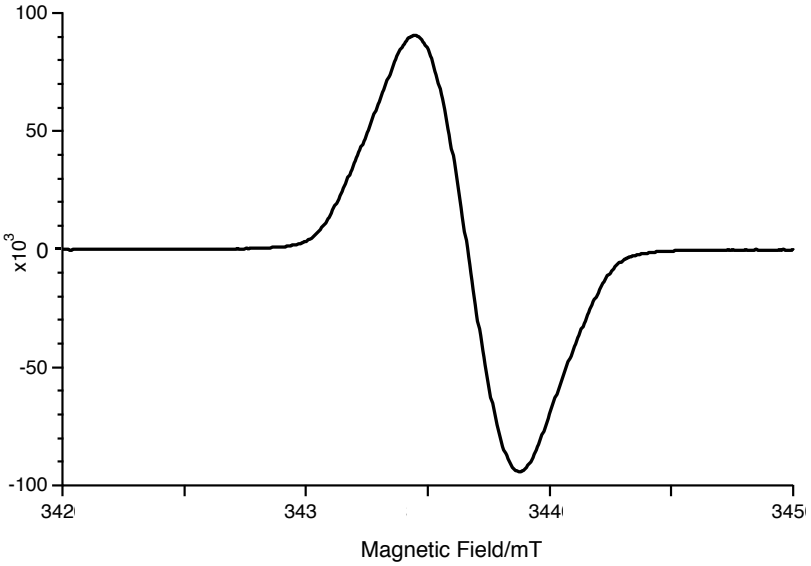

Figure 4-16. ESR spectrum of $\mathbf{7}^{\bullet+}SbCl_6^-$ in CH_2Cl_2.

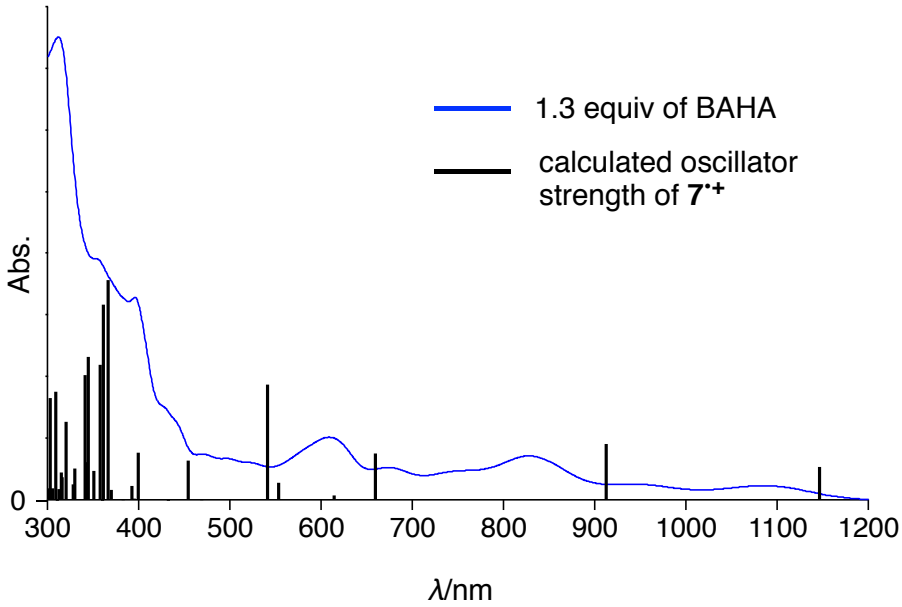

Figure 4-17. Calculated absorption spectrum of $\mathbf{7}^{\bullet+}$. The experimental absorption spectrum of **7** with 1.3 equiv of BAHA in CH_2Cl_2 was also displayed for comparison (blue line).

Fortunately, the author obtained the X-ray crystal structure of $\mathbf{7}^{\bullet+}$, which revealed that the radical cation molecule remained nearly planar (Figure 4-18). The mean plane deviation became 0.131 Å, which is almost identical to the averaged value (0.123 Å) of **7**. Furthermore, the two molecules of $\mathbf{7}^{\bullet+}$ were stacked in a face-to-face manner in the crystalline state. The presence of 2 equiv of a counter anion $SbCl_6^-$ in one unit cell confirms the dicationic character of this dimer. The closest interplanar distance was 3.144 Å between the two α-carbons of central pyrrole rings, which is a typical value for π-dimers.[10a–d,11] The shorter distance than the sum of van der Waals radii of a C(sp^2) atom (3.40 Å) indicates the presence of strong attractive interactions between these two paramagnetic species.[12]

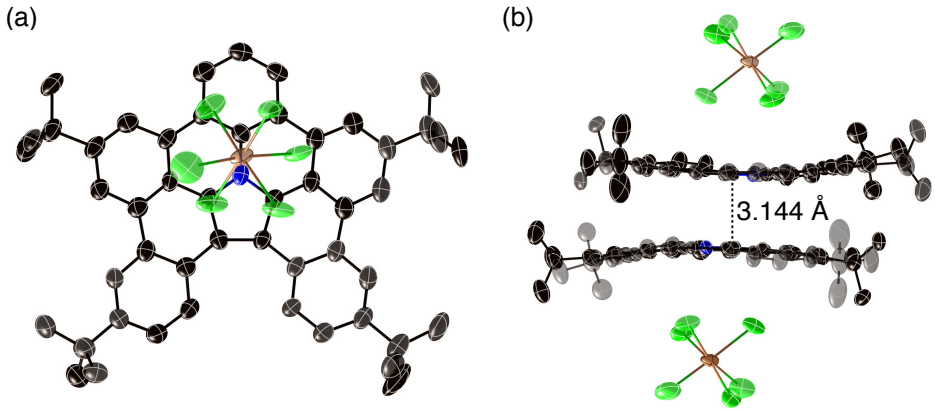

Figure 4-18. X-Ray crystal structure of $[\mathbf{7}\text{-}\mathbf{7}]^{2+}[SbCl_6]^-_2$. (a) Top view and (b) packing structure. The thermal ellipsoids are scaled at 50% probability level. The hydrogen atoms and solvent molecules are omitted for clarity.

The dimerization behavior of $\mathbf{7}^{\bullet+}$ in solution was investigated. In VT ^{1}H NMR measurement, two broad peaks appeared in the aromatic region at –80 °C, indicating the existence of a diamagnetic species (Figure 4-19). These changes were also monitored by VT ESR spectroscopy. A single peak at g = 2.003 due to $\mathbf{7}^{\bullet+}$ was gradually weakened at low temperatures (Figure 4-20). Different from $\mathbf{6}^{\bullet+}$, the signal was still observed even at –85 °C. The structure of the resulting product was finally determined by VT UV-vis-NIR absorption measurement of $\mathbf{7}^{\bullet+}$ (Figure 4-21). The absorption bands in the UV/visible region remained almost unchanged at low temperature. On the other hand, new absorption band around 1300 nm was appeared. According to the reported π-dimerization reactions, the generation of the NIR absorption band at low temperatures strongly suggests the formation of a π-dimer. TD-DFT calculations of π-dimer $[\mathbf{7}\text{-}\mathbf{7}]^{2+}$ also supported these spectral changes (Figure 4-22). The new absorption band around 1300 nm was mostly attributed to the transition from HOMO–1 to LUMO of the π-dimer. In HOMO–1, there is the bonding interaction between two units of $\mathbf{7}^{\bullet+}$ (Figure 4-23). Consequently, the generation of this band suggests the existence of the π-dimer. The thermodynamic parameters were also determined to be ΔH = –5.8 kcal mol^{-1} and ΔS = 2.7 cal K^{-1} mol^{-1} by ESR measurement (Figure 4-24 and Figure 4-25). The ΔH

value is larger than that of the σ-dimerization process of $\mathbf{6}^{\bullet+}$.

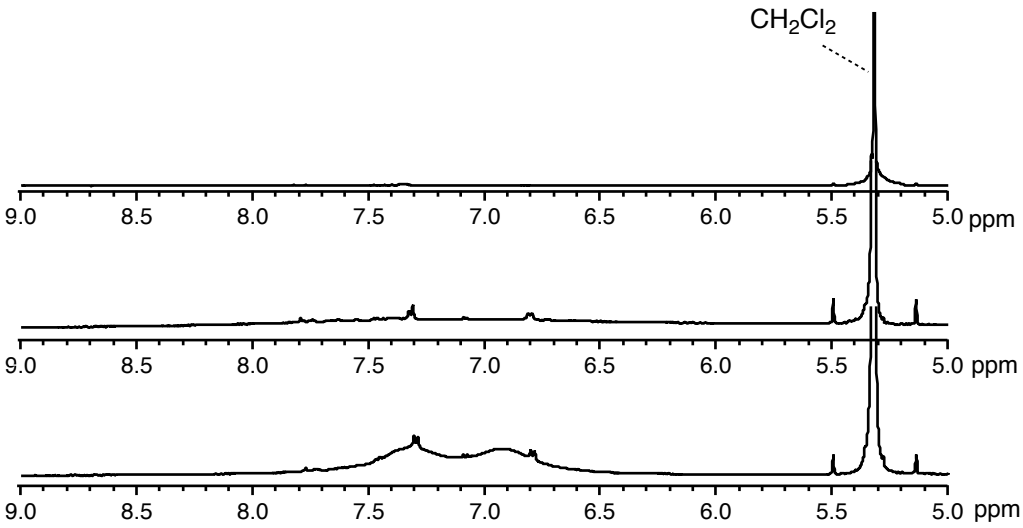

Figure 4-19. VT ^{1}H NMR spectra of $\mathbf{7}^{\bullet+}SbCl_6^-$ in $CDCl_3$. (a) 25 °C, (b) –40 °C, and (c) –80 °C.

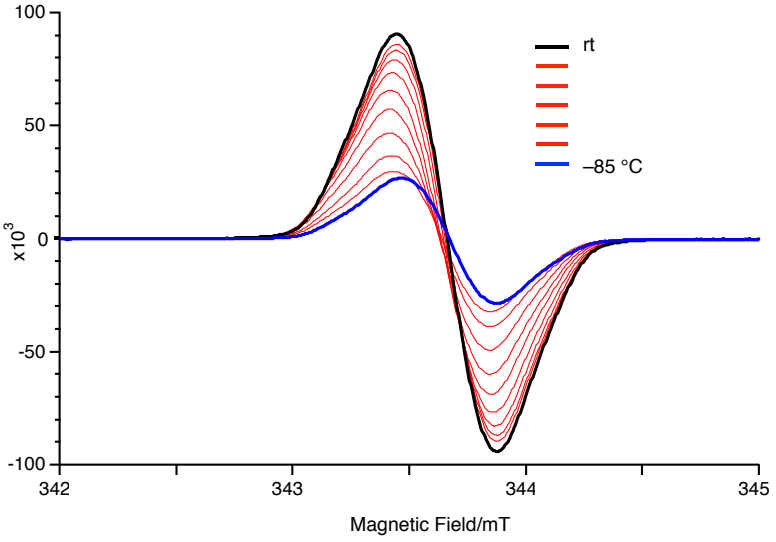

Figure 4-20. VT ESR spectra of $\mathbf{7}^{\bullet+}SbCl_6^-$ in CH_2Cl_2.

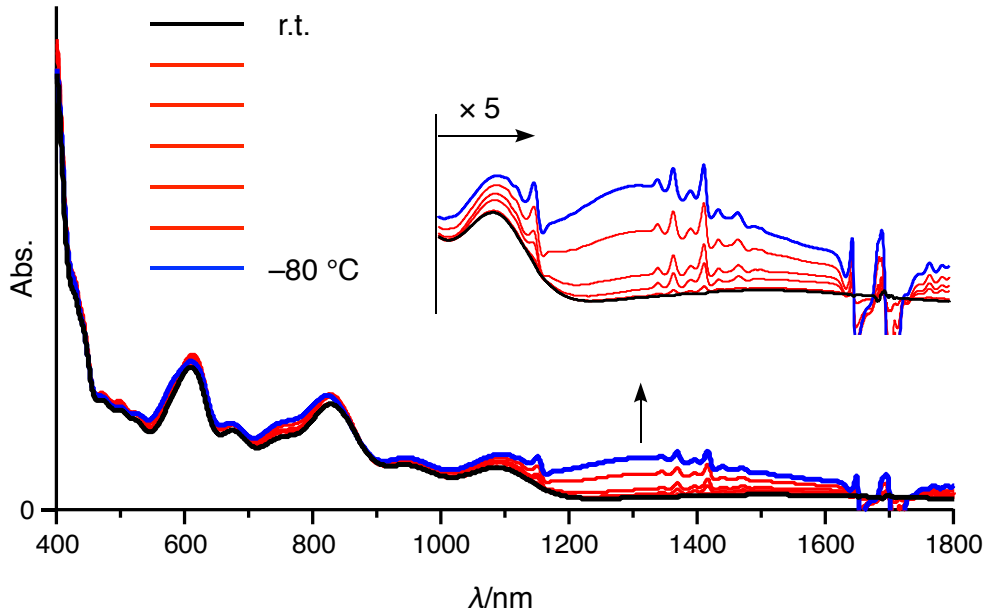

Figure 4-21. VT UV/vis/NIR absorption spectra of $\mathbf{7}^{\bullet+}SbCl_6^-$ in CH_2Cl_2.

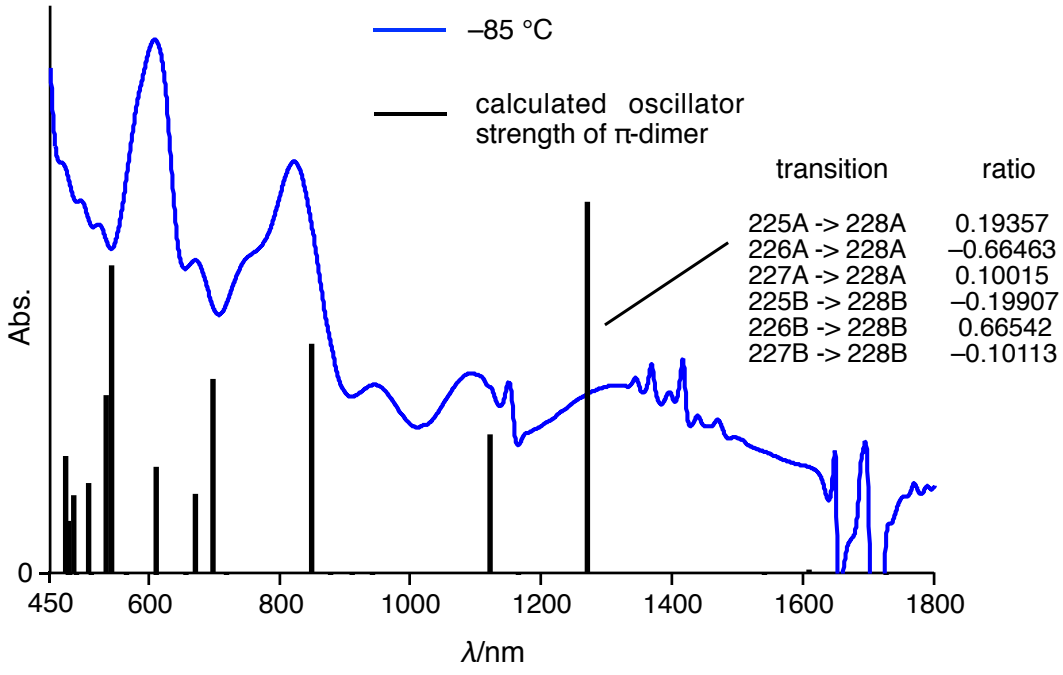

Figure 4-22. Calculated absorption spectrum of the π-dimer. The experimental absorption spectrum of $\mathbf{7}^{\bullet+}$ at –85 °C in CH_2Cl_2 was also displayed for comparison (blue line).

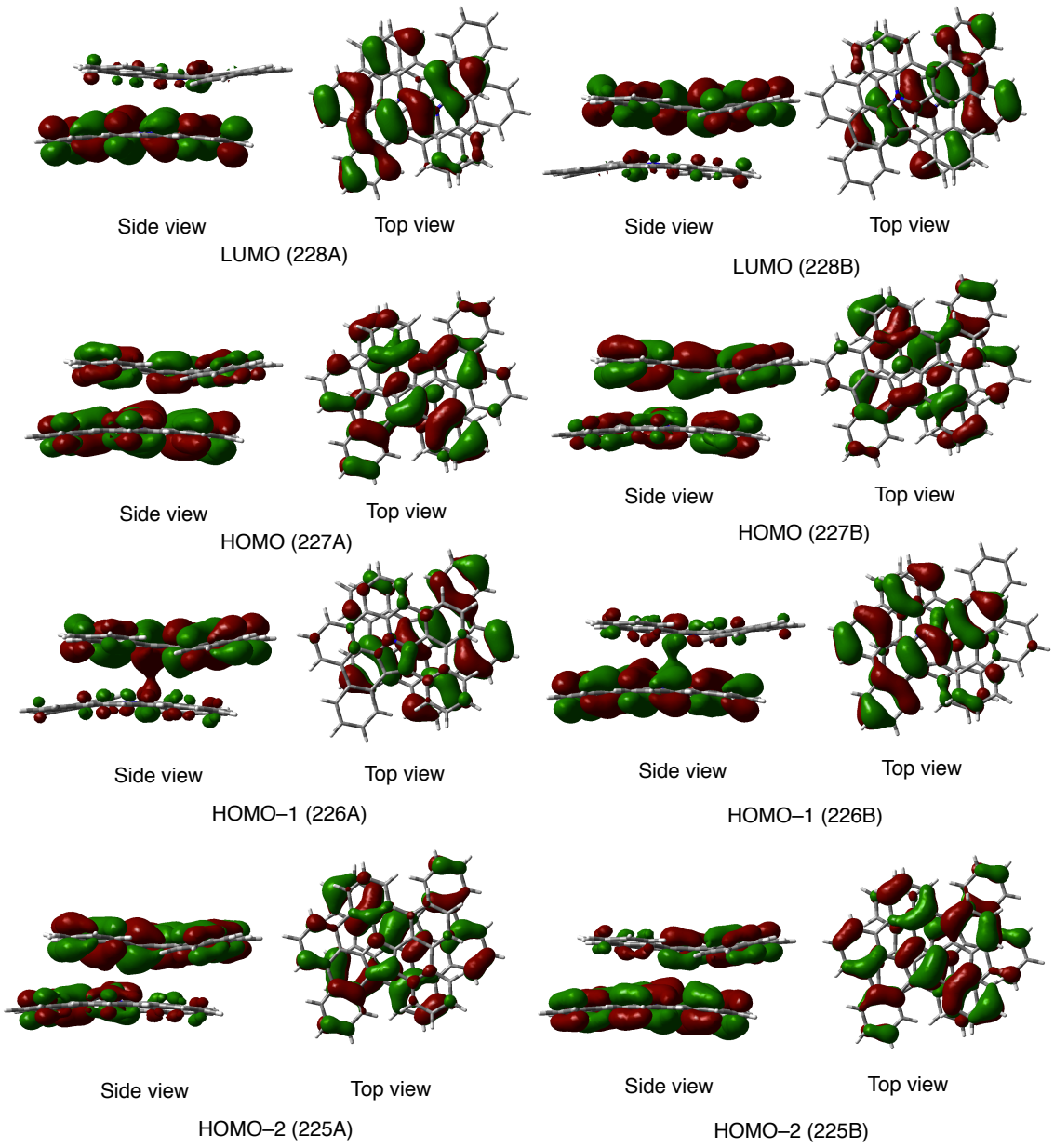

Figure 4-23. Calculated MOs of the π-dimer $[\mathbf{7}\text{-}\mathbf{7}]^{2+}$ by the DFT method at the UM06/6-31G(d) level (singlet only).

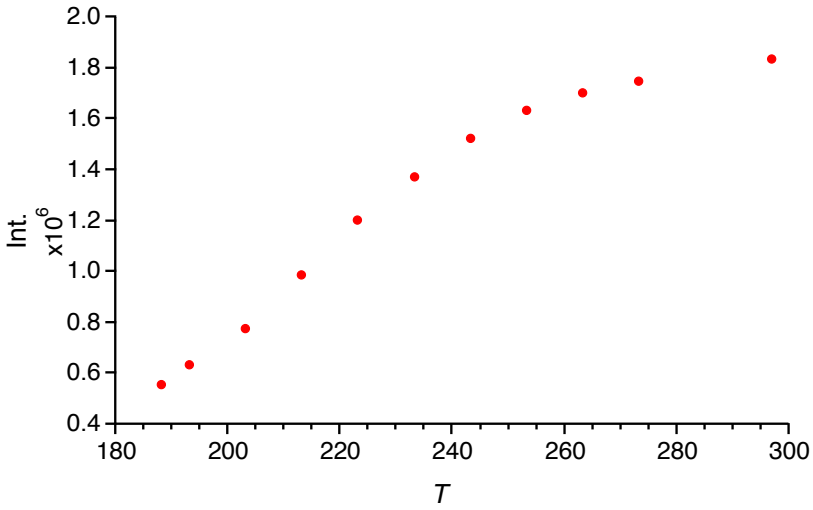

Figure 4-24. The temperature-dependent integration of the ESR signal of $\mathbf{7}^{\bullet+}$ in CH_2Cl_2.

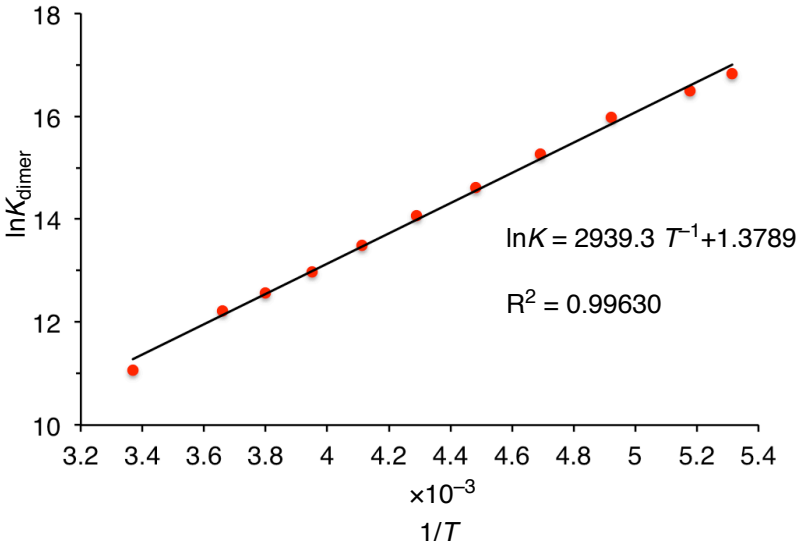

Figure 4-25. van't Hoff plot using ESR measurement.

4-4. Nucleophilic Addition to a Bowl-Shaped Radical Cation

The specific reactivity at the internal carbon atom of $\mathbf{6}^{\bullet+}$ was also demonstrated by the reaction with nucleophiles. In the presence of an excess amount of methanol, $\mathbf{6}^{\bullet+}$ was converted to methoxylated product $\mathbf{6{\bullet}OMe}^{+}$ in 99% yield, whereas no reaction occurred in the case of $\mathbf{7}^{\bullet+}$. In the ^{1}H NMR spectrum of $\mathbf{6{\bullet}OMe}^{+}$ in $CDCl_3$, eight singlets, two doublets and one triplet were observed in the aromatic region, which

accorded with its less symmetric structure.

The X-ray crystal structure of **6•OMe**$^+$ revealed that the methoxy group was selectively introduced at the α-carbon of central pyrrole ring (Figure 4-26). The length of C1–O1 bond (1.417(3) Å) is consistent with a standard C–O single bond (1.43 Å). The C2–C3 bond length (1.359(4) Å) suggests its double bond character. In addition, the N1–C4 bond (1.337(3) Å) is longer than C–N double bonds but shorter than C–N single bonds. Accordingly, **6•OMe**$^+$ has large contribution of the resonance structures depicted in Figure 4-26c.

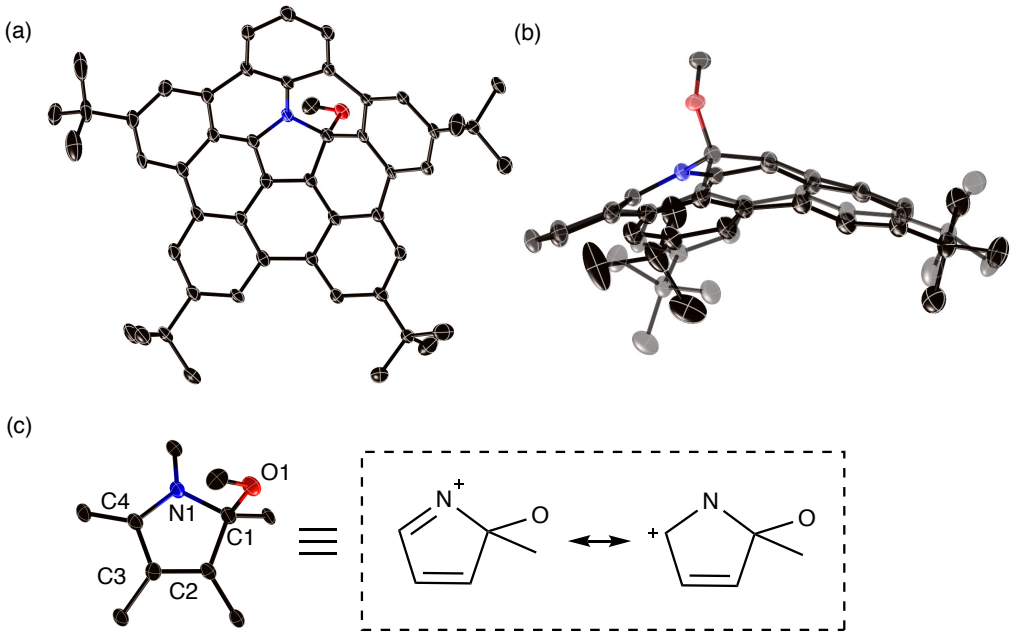

Figure 4-26. X-Ray crystal structure of [**6•OMe**]$^+$[$SbCl_6$]$^-$. (a) Top view and (b) side view. The thermal ellipsoids are scaled at 50% probability level. The hydrogen atoms, [$SbCl_6$]$^-$ ion and solvent molecules are omitted for clarity. Selected bond lengths [Å]: N1–C1 1.487(3), C1–C2 1.499(4), C2–C3 1.359(4), C3–C4 1.412(4), C4–N1 1.337(3), C1–O1 1.417(3).

Interestingly, only one equiv of BAHA was required to complete the production of **6•OMe**$^+$ from **6**. This addition reaction should be initiated by the nucleophilic attack of methanol to the α-carbon of the central pyrrole ring (Scheme 4-2).[13] Subsequent deprotonation would result in the formation of neutral radical **6•OMe**$^\bullet$. Considering that the hexachloroantimonate ion can serve as an oxidant, **6•OMe**$^\bullet$ could be oxidized to afford **6•OMe**$^+$.[14] The change of the oxidizing reagent from BAHA to $AgPF_6$, where hexafluorophosphate ion has no oxidizing ability, resulted in decrease of the yield to 63%.

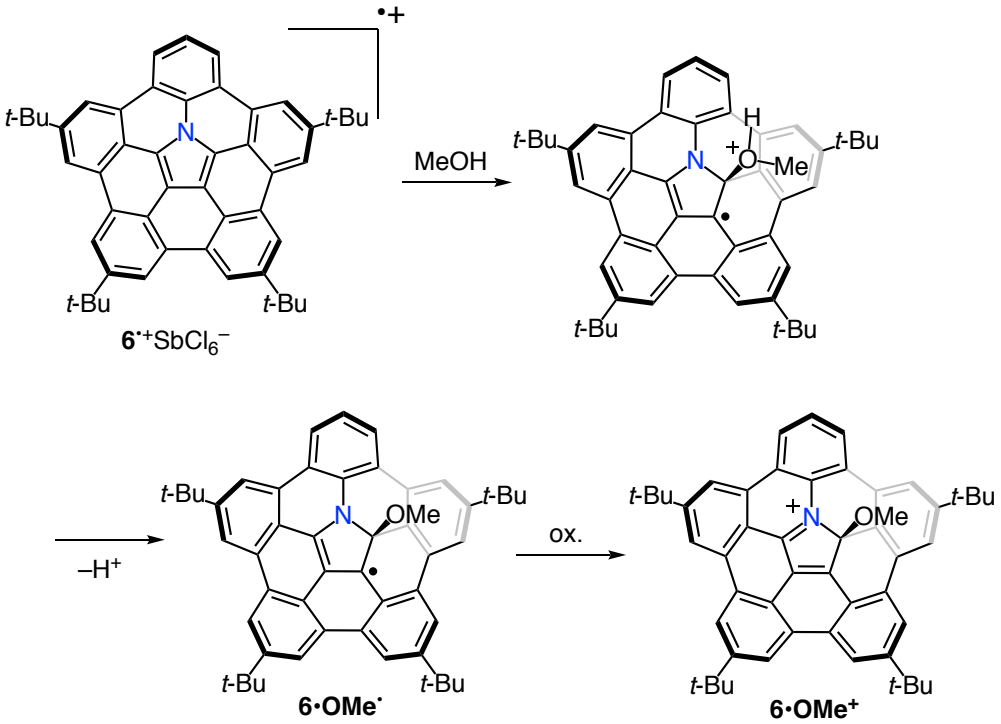

Scheme 4-2. A proposed reaction mechanism for methoxylation of **6**$^{\bullet+}$$SbCl_6^-$.

Figure 4-27 shows the UV-vis absorption spectrum of **6•OMe**$^+$ in CH_2Cl_2, which exhibited two characteristic absorption bands in the visible region. The spectral similarity between **6•OMe**$^+$ and σ-dimer [**6**-**6**]$^{2+}$ suggests the resemblance of electronic structures between these two cationic species.

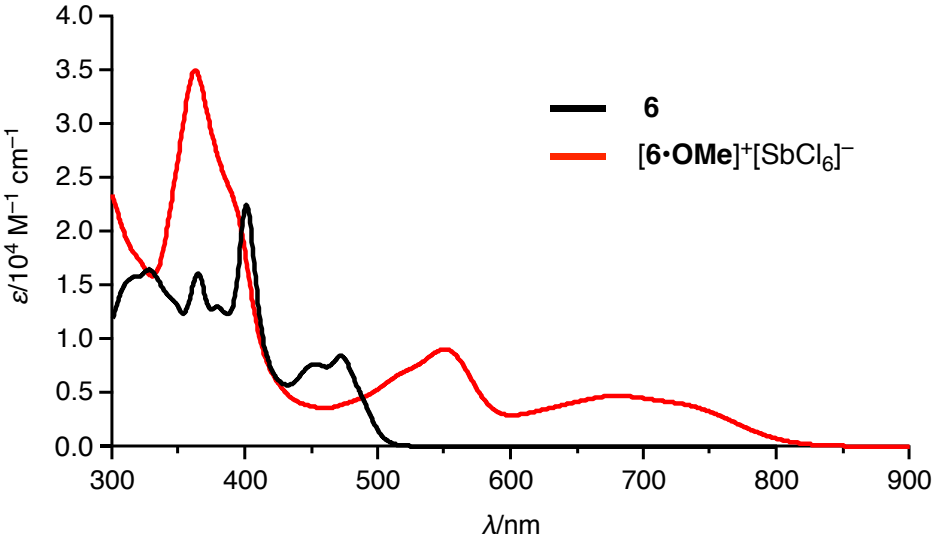

Figure 4-27. UV/vis absorption spectra of **6** and [**6•OMe**]$^{+}$[$SbCl_6$]$^{-}$ in CH_2Cl_2.

4-5. Origin of The Different Reactivity of a Bowl-Shaped Radical Cation

For bowl-shaped π-conjugated molecules such as corannulene and sumanene, the pyramidalization strain mainly concentrates on internal sp^2 carbon atoms rather than the peripheral region.[15,16] Consequently, the major driving force of the chemical reaction at its internal positions should be a large relief of the strain. The author calculated the electronic and geometric structures of **6**$^{\bullet+}$ and **7**$^{\bullet+}$ by the DFT method at the B3LYP/6-31G(d) level (Figure 4-28). For both radical cations, the spin density mostly exists at the α-carbon of the central pyrrole ring. The spin density at this position is almost the same between these two radical cations, indicating that the electronic factor is not crucial for their different reactivities. The author also estimated the π-orbital axis vector (POAV) angles, which can evaluate the degree of curvature.[17] As expected, **6**$^{\bullet+}$ has relatively large POAV angle at its internal α-carbons ($\theta_{\sigma\pi}$ = 6.6°). On the other hand, **7**$^{\bullet+}$ has planer structure, which results in significantly smaller POAV angle ($\theta_{\sigma\pi}$ = 0.5°). In the σ-dimer [**6**-**6**]$^{2+}$ or methoxylated product **6•OMe**$^{+}$, the POAV angles of newly formed sp^3 carbons are close to the ideal sp^3 geometry ($\theta_{\sigma\pi}$ = 20.0° and 21.5° respectively) (Figure 4-29). That means the geometric strains at these positions are successfully relieved. On the other hand, the POAV angles in the other sp^2 carbons in

the central pyrrole ring slightly decreased. Thus, dimerization and methoxylation lead to an additional relief of pyramidalization strain at the remaining sp^2 carbons.

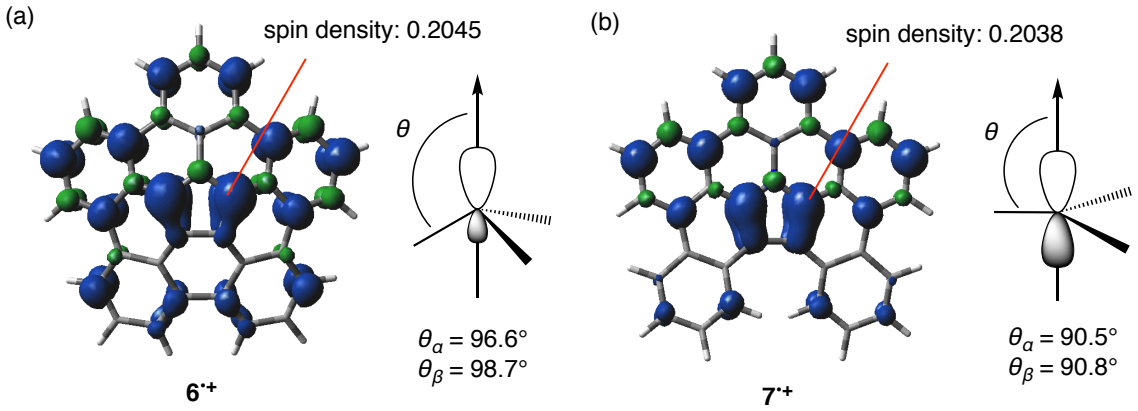

Figure 4-28. Calculated POAV angles and spin density distributions of (a) **6**$^{\bullet+}$ and (b) **7**$^{\bullet+}$ at the B3LYP/6-31G(d) level. *tert*-Butyl substituents were replaced with hydrogen atoms.

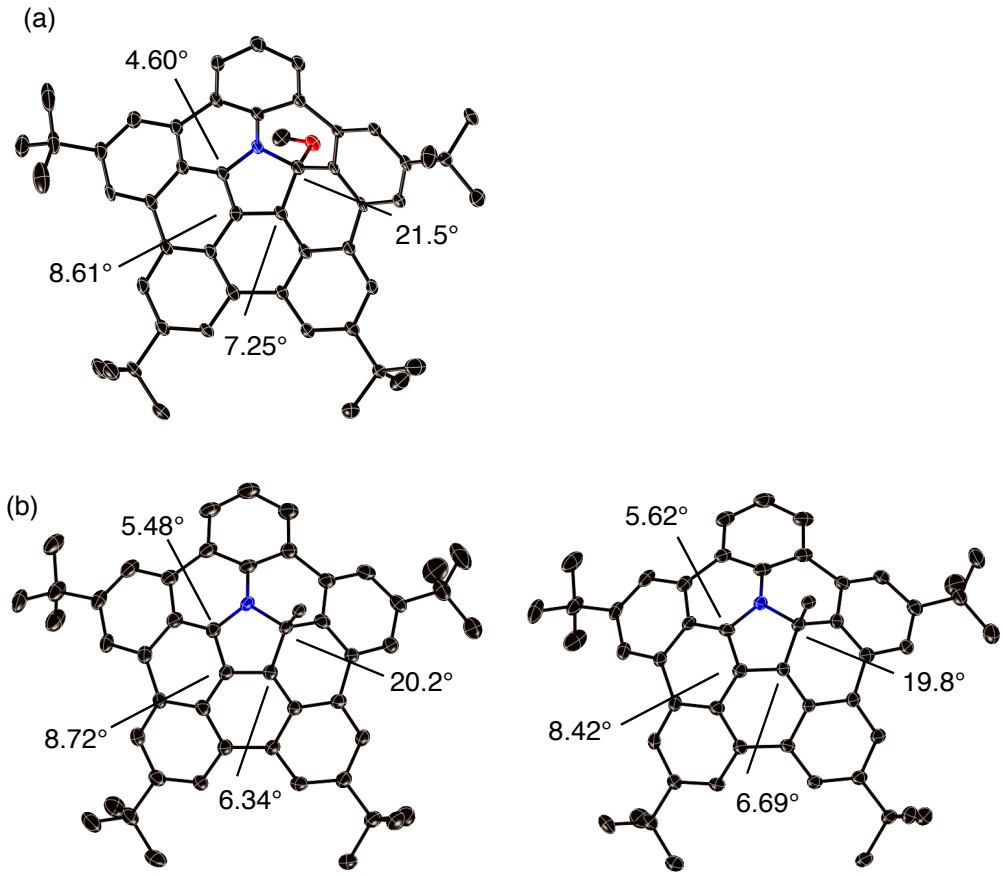

Figure 4-29. The POAV angles of (a) [**6•OMe**]$^{+}$[$SbCl_6$]$^{-}$ and (b) σ-dimer [**6**-**6**]$^{2+}$[$SbCl_6^{-}$]$_2$.

Finally, the author conducted the DFT calculations against the homodesmotic reaction as shown in Scheme 4-3 to estimate the relative energy balance in the course of methoxylation. Consequently, the addition reaction of **6**$^{\bullet+}$ was energetically more favorable than **7**$^{\bullet+}$ by 15.2 kcal mol^{-1} (Table 4-2). These results clearly indicate a relief of the strain is larger in **6**$^{\bullet+}$ than **7**$^{\bullet+}$, which should accelerate the bond formation of **6**$^{\bullet+}$ at its internal position. In contrast, the addition reaction against **7**$^{\bullet+}$ would rather increase the geometric strain at newly formed sp^3 carbon as well as the neighboring atoms.

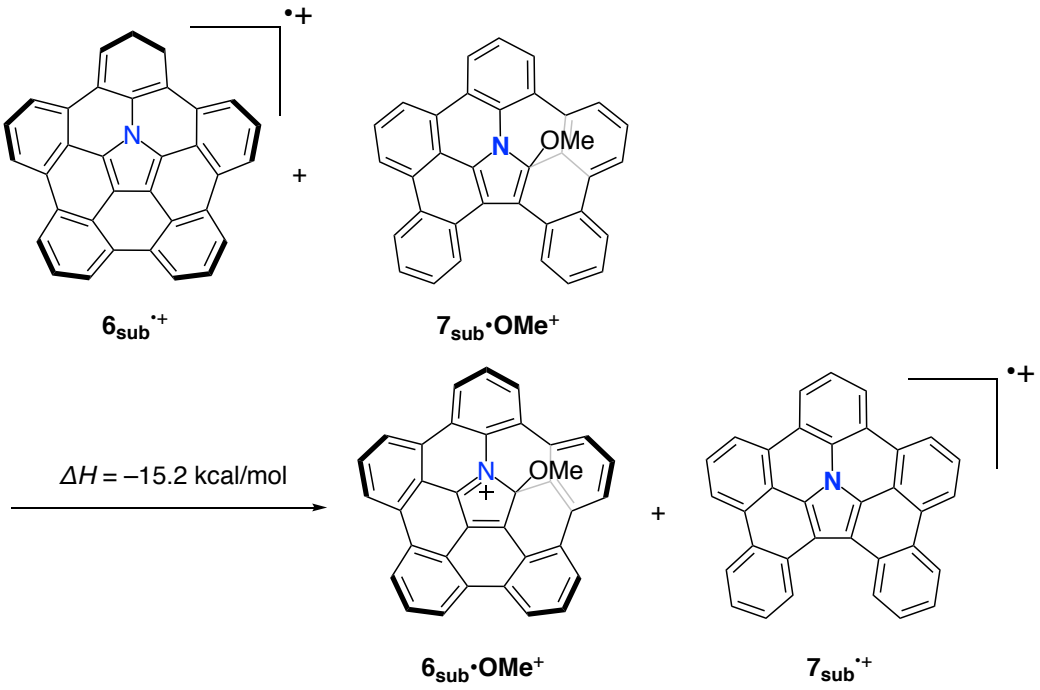

Scheme 4-3. Homodesmotic reaction energy at the B3LYP/6-31G(d) level. *tert*-Butyl substituents were replaced with hydrogen atoms.

Table 4-2. Summary of the electronic and zero-point energies of each σ-dimer

Units (Hartree/Particle)

compound	*ZPE*[a]	E_0[b]	*E*[c]	*H*[d]
$\mathbf{6}_{sub}^{\bullet+}$	0.381175	–1358.876301	–1358.855741	–1358.854797
$\mathbf{7}_{sub}^{\bullet+}$	0.403035	–1360.090036	–1360.068036	–1360.067092
$\mathbf{6}_{sub}$•$\mathbf{OMe}^{+}$	0.425836	–1473.950661	–1473.927210	–1473.926266
$\mathbf{7}_{sub}$•$\mathbf{OMe}^{+}$	0.448146	–1475.139999	–1475.115251	–1475.114307

[a] Zero-point correction. [b] Sum of electronic and zero-point energies. [c] Sum of electronic and thermal energies. [d] Sum of electronic and thermal enthalpies.

4-6. Summary

In summary, the author has investigated the unique dimerization behavior of the radical cation with a bowl-shaped structure. In the crystalline state, $\mathbf{6}^{\bullet+}$ formed the σ-dimeric dication, where the bond formation occurred between internal α-carbon atoms of the central pyrrole ring. Different from many other organic radical cations, $\mathbf{6}^{\bullet+}$ exhibited the reversible σ-dimerization behavior in the solution state depending on temperatures. The formation of the σ-dimer was dominant at low temperatures, suggesting that the dimer is thermodynamically more stable than the monomer. In sharp contrast, planar radical cation $\mathbf{7}^{\bullet+}$ furnished a π-dimer selectively both in the crystalline and solution states. The different reactivities between $\mathbf{6}^{\bullet+}$ and $\mathbf{7}^{\bullet+}$ were also observed in the nucleophilic addition reaction with methanol. Bowl-shaped radical cation $\mathbf{6}^{\bullet+}$ reacted with methanol to form the α-methoxylated product, while no change was observed in the case of planar radical cation $\mathbf{7}^{\bullet+}$. The bowl-shaped structure is advantageous for the bond formation at its internal curved surface due to a large relief of pyramidalization strain. On the other hand, the addition reaction to internal sp^2 carbon of the planar π-system is energetically unfavorable because the conversion of a trigonal planar sp^2 carbon to a tetrahedral sp^3 configuration increases the geometric strain. Theoretical calculations also supported these hypotheses. These researches offer a new insight into the molecular design for advanced material utilizing the reversible σ-dimerization behavior of organic radical cations.

4-7. Experimental Section

Materials and Characterization

^{1}H NMR (500 MHz) and ^{13}C NMR (126 MHz) spectra were recorded using a Bruker AVANCE III HD spectrometer. Chemical shifts were reported at the delta scale in ppm relative to $CHCl_3$ (d = 7.260 ppm) and CH_2Cl_2 (d = 5.320 ppm) for ^{1}H NMR and $CDCl_3$ (d = 77.0 ppm) for ^{13}C NMR. UV/vis/NIR absorption spectra were recorded using a Shimadzu UV-2550 or JASCO V670 spectrometer. High-resolution (HR) mass spectrum was recorded on a Bruker micro TOF using ESI-TOF method. Unless otherwise noted, materials obtained from commercial suppliers were used without further purification.

Synthesis of $[\mathbf{6{\bullet}OMe}]^{+}[SbCl_6]^{-}$

In a glovebox, the mixture of **6** (4.00 mg, 6.04 μmol) and tris(4-bromophenyl)ammoniumyl hexachloroantimonate (9.87 mg, 12.1 mmol) was dissolved in CH_2Cl_2 (3 mL), toluene (2 mL) and diethyl ether (1 mL). To the mixture, methanol (0.10 mL) was added. The resulting solution was used for recrystallization (hexane was used as poor solvent), affording $[\mathbf{6{\bullet}OMe}]^{+}[SbCl_6]^{-}$ (5.75 mg, 5.60 μmol) in 93% yield as a purple solid. ^{1}H NMR (500 MHz) ($CDCl_3$): δ = 8.42 (s, 2H), 8.35 (d, J = 9.3 Hz, 1H), 8.34 (s, 1H), 8.31 (s, 1H), 8.27 (s, 1H), 8.13 (d, J = 7.7 Hz, 1H), 7.96 (s, 1H), 7.74 (s, 1H), 7.73 (s, 1H), 7.71 (s, 1H), 7.65 (t, J_1 = 7.9 Hz, J_2 = 7.9 Hz, 1H), 4.00 (s, 3H), 1.61 (s, 9H), 1.58 (s, 9H), 1.55 (s, 9H), 1.41 (s, 9H) ppm.; ^{13}C NMR (126 MHz) ($CDCl_3$): δ = 167.6, 158.5, 155.7, 155.0, 154.7, 151.9, 139.4, 138.8, 135.9, 135.3, 134.4, 132.9, 132.5, 132.5, 129.8, 128.9, 127.2, 126.8, 126.5, 126.2, 126.1, 125.3, 125.0, 124.4, 124.0, 123.7, 123.1, 122.4, 122.2, 121.0, 120.9, 119.7, 117.2, 88.18, 53.55, 37.80, 36.56, 36.36, 35.67, 31.53, 31.23, 31.22, 31.18 ppm.; UV/vis (CH_2Cl_2): λ_{max} (ε[M^{-1} cm^{-1}]) = 679.5 (4700), 550 (9100), 362 (35000) nm; High-resolution ESI–MS: m/z = 692.3881, calcd for $(C_{51}H_{50}NO)^{+}$ = 692.3887 [M^{+}].

X-Ray Diffraction Analysis

X-Ray data were obtained using a Bruker D8 QUEST X-ray diffractometer with an IμS microfocus X-ray source and a large area (10 cm × 10 cm) CMOS detector (PHOTON 100) for [**6•OMe**]$^{+}$[$SbCl_6$]$^{-}$ and using a Rigaku CCD diffractometer (Saturn 724 with MicroMax-007) with Varimax Mo optics using graphite monochromated Mo-Kα radiation (λ = 0.71075 Å) for [**6**-**6**]$^{2+}$[$SbCl_6^{-}$]$_2$, **7**, and [**7**-**7**]$^{2+}$[$SbCl_6$]$^{-}_2$.

Theoretical Calculations

The simulated absorption spectrum of the σ-dimer [**6**-**6**]$^{2+}$ was obtained by the TD-DFT method at the camB3LYP/6-31G(d) level (spin restricted). The geometry of the X-ray crystal structure of [**6**-**6**]$^{2+}$[$SbCl_6^{-}$]$_2$ was used for the calculation without any structural optimization. The geometry of **7**$^{\bullet+}$ was optimized by the DFT method at the B3LYP/6-31G(d) level. The simulated absorption spectrum of **7**$^{\bullet+}$ was obtained by the TD-DFT method at the B3LYP/6-31G(d) level. The simulated absorption spectrum of the π-dimer [**7**-**7**]$^{2+}$ was obtained by the TD-DFT method at the UM06/6-31G(d) level (singlet only). The geometry of the X-ray crystal structure of [**7**-**7**]$^{2+}$[$SbCl_6^{-}$]$_2$ was used for the calculation without any structural optimization. The molecular geometries of all **6**$_{sub}^{\bullet+}$, **7**$_{sub}^{\bullet+}$, **6**$_{sub}$**•OMe**$^{+}$, and **7**$_{sub}$**•OMe**$^{+}$ were fully optimized by DFT method at the B3LYP/6-31G(d) level. All *tert*-butyl substituents were replaced with hydrogen atoms.

Crystallographic Data

	$[\mathbf{6}\text{-}\mathbf{6}]^{2+}[SbCl_6^-]_2$	**7**
empirical formula	$C_{106}H_{99}Cl_{13}N_2Sb_2$	$C_{199.77}H_{195.32}N_4$
formula weight	2105.22	2652.15
habit	prism	block
T, K	93(2)	93(2)
crystal system	triclinic	monoclinic
space group	*P*-1 (2)	$P2_1/n$
a, Å	17.484(8)	21.4102(5)
b, Å	18.351(8)	30.3917(5)
c, Å	18.671(9)	25.3832(5)
α, deg	110.418(4)	90
β, deg	104.903(2)	108.985(3)
γ, deg	108.5972(16)	90
V, Å^3	4842(4)	15618.2(6)
Z	2	4
Dc, g/cm^3	1.444	1.128
F(000)	2144	5688
crystal size, mm^3	0.36 x 0.13 x 0.04	0.11 x 0.066 x 0.065
$2\theta_{max}$, °	55.0	55.0
R_1 ($I > 2\sigma(I)$)	0.0687	0.0607
wR_2 (all data)	0.2367	0.1795
GOF	1.089	1.033
obs reflects	21568	35380
total reflects	48579	125174
parameters	1169	1978
CCDC number	1815258	1815712

	[**7**-**7**]$^{2+}$[$SbCl_6^-$]$_2$	[**6**•**OMe**]$^+$[$SbCl_6$]$^-$
empirical formula	$C_{51.83}H_{52.66}Cl_{9.72}NSb_{0.98}$	$C_{128.76}H_{137.19}Cl_{14.90}N_2O_{2.73}Sb_2$
formula weight	1153.46	2528.09
habit	fiber	block
T, K	93(2)	113(2)
crystal system	monoclinic	monoclinic
space group	$P2_1/c$	$C2/c$
a, Å	11.5521(6)	32.3774(8)
b, Å	24.1457(9)	12.2907(3)
c, Å	19.7738(10)	29.9008(7)
α, deg	90	90
β, deg	106.010(5)	90.309(2)
γ, deg	90	90
V, Å^3	5301.6(5)	11220
Z	4	4
Dc, g/cm^3	1.445	1.411
F(000)	2343	5204
crystal size, mm^3	0.25 x 0.010 x 0.010	0.32 x 0.21 x 0.12
$2\theta_{max}$, °	50.0	50.0
R_1 ($I > 2\sigma(I)$)	0.0945	0.0541
wR_2 (all data)	0.2635	0.1430
GOF	1.083	1.081
obs reflects	9329	10424
total reflects	44754	72103
parameters	655	836
CCDC number	1815259	1815260

4-8. References

1. J. L. Zafra, L. Qiu, N. Yanai, T. Mori, M. Nakano, M. P. Alvarez, J. T. López Navarrete, C. J. Gómez-García, M. Kertesz, K. Takimiya, J. Casado, *Angew. Chem. Int. Ed.* **2016**, *55*, 14563.

2. (a) K. Imato, A. Takahara, H. Otsuka, *Macromolecules* **2015**, *48*, 5632. (b) K. Imato, M. Nishihara, T. Kanehara, Y. Amamoto, A. Takahara, H. Otsuka, *Angew. Chem. Int. Ed.* **2012**, *51*, 1138.

3. (a) Y. Wang, X. Tan, Y. -M. Zhang, S. Zhu, I. Zhang, B. Yu, K. Wang, B. Yang, M. Li, B. Zou, S. X. -A. Zhang, *J. Am. Chem. Soc.* **2015**, *137*, 931. (b) A. Ruiz de Luzuriaga, J. M. Matxain, F. Ruipérez, R. Martin, J. M. Asua, G. Cabañero, I. Odriozola, *J. Mater. Chem. C* **2016**, *4*, 6220. (c) K. Imato, J. C. Natterodt, J. Sapkota, R. Goseki, C. Weder, A. Takahara, H. Otsuka, *Polym. Chem.* **2017**, *8*, 2115.

4. (a) J. Heinze, B. A. Frontana-Uribe, S. Ludwigs, *Chem. Rev.* **2010**, *110*, 4724. (b) E. T. Seo, R. F. Nelson, J. M. Fritsch, L. S. Marcoux, D. W. Leedy, R. N. Adams, *J. Am. Chem. Soc.* **1966**, *88*, 3498. (c) S. C. Creason, J. Wheeler, R. F. Nelson, *J. Org. Chem.* **1972**, *37*, 4440.

5. (a) T. Nishinaga, K. Komatsu, *Org. Biomol. Chem.* **2005**, *3*, 561. (b) F. Effenberger, W. D. Stohrer, A. Steinbach, *Angew. Chem. Int. Ed. Engl.* **1969**, *8*, 280. (c) F. Effenberger, K. -E. Mack, R. Niess, F. Reisinger, A. Steinbach, W. -D. Stohrer, J. J. Stezowski, I. Rommel, A. Maier, *J. Org. Chem.* **1988**, *53*, 4379. (d) F. Effenberger, *Acc. Chem. Res.* **1989**, *22*, 27. (e) F. Effenberger, W. -D. Stohrer, K. -E. Mack, F. Reisinger, W. Seufert, H. E. A. Kramer, R. Föll, E. Vogelmann, *J. Am. Chem. Soc.* **1990**, *112*, 4849. (f) J. Heinze, C. Willmann, P. Bäuerle, *Angew. Chem. Int. Ed.* **2001**, *40*, 2861. (g) A. Merz, J. Kronberger, L. Dunsch, A. Neudeck, A. Petr, L. Parkanyi, *Angew. Chem. Int. Ed.* **1999**, *38*, 1442. (h) J. Taquet, O. Siri, J. -P Collin, A. Messaoudi, P. Braunstein, *New J. Chem.* **2005**, *29*, 188. (i) A. Smie, J. Heinze, *Angew. Chem. Int. Ed.* **1997**, *36*, 363. (j) P. Tschuncky, J. Heinze, A. Smie, G. Engelmann, G. Koßmehl, *J. Electroanal. Chem.* **1997**, *433*, 223. (k) J. Heinze, P. Tschuncky, A. Smie, *J. Solid State Electrochem.*

1998, *2*, 102. (l) J. Heinze, H. John, M. Dietrich, P. Tschuncky, *Synth. Met.* **2001**, *119*, 49. (m) X. Chen, X. Wang, Z. Zhou, Y. Li, Y. Sui, J. Ma, X. Wang, P. P. Power,. *Chem., Int. Ed.* **2013**, *52*, 589.

6. A. Hirsch, M. Brettreich, *Fullerenes: Chemistry and Reactions* (Wiley-VCH, Weinheim, 2005).

7. (a) J. M. Hawkins, A. Meyer, *Science* **1993**, *260*, 1918. (b) A. L. Balch, V. J. Catalano, J. W. Lee, M. M. Olmstead, S. R. Parkin, *J. Am. Chem. Soc.* **1991**, *113*, 8953. (c) A. L. Balch, J. W. Lee, M. M. Olmstead, *Angew. Chem. Int. Ed. Engl.* **1992**, *31*, 1356. (d) J. M. Hawkins, A. Meyer, M. A. Solow, *J. Am. Chem. Soc.* **1993**, *115*, 7499. (e) N. Karousis, N. Tagmatarchis, *Chem. Rev.* **2010**, *110*, 5366. (f) J. Park, M. Yan, *Acc. Chem. Res.* **2013**, *46*, 181.

8. (a) D. V. Preda, L. T. Scott, *Tetrahedron Lett.* **2000**, *41*, 9633. (b) A. V. Zabula, S. N. Spisak, A. S. Filatov, A. Y. Rogachev, M. A. Petrukhina, *Angew. Chem. Int. Ed.* **2011**, *50*, 2971. (c) N. Ngamsomprasert, J. -S. Dang, S. Higashibayashi, Y. Yakiyama, H. Sakurai, *Chem. Commun.* **2017**, *53*, 697. (d) L. T. Scott, *Chem. Soc. Rev.* **2015**, *44*, 6464. (e) C. Dubceac, A. V. Zabula, A. S. Filatov, F. Rossi, P. Zanello, M. A. Petrukhina, *J. Phys. Org. Chem.* **2012**, *25*, 553. (f) C. Dubceac, A. S. Filatov, A. V. Zabula, M. A. Petrukhina, *Cryst. Growth Des.* **2015**, *15*, 778. (g) M. Yanney, F. R. Fronczek, A. Sygula, *Org. Lett.* **2012**, *14*, 4942. (h) H. E. Bronstein, L. T. Scott, *J. Org. Chem.* **2008**, *73*, 88. (i) H. Y. Cho, R. B. M. Ansems, L. T. Scott, *Beilstein J. Org. Chem.* **2014**, *10*, 956.

9. (a) J. R. Morton, K. F. Preston, P. J. Krusic, E. Wasserman, *J. Chem. Soc. Perkin Trans. 2* **1992**, 1425. (b) J. R. Morton, K. F. Preston, P. J. Krusic, S. A. Hill, E. Wasserman, *J. Am. Chem. Soc.* **1992**, *114*, 5454. (c) Y. Lee, T. Kitagawa, K. Komatsu, *J. Org. Chem.* **2004**, *69*, 263.

10. (a) T. Nishinaga, K. Komatsu, *Org. Biomol. Chem.* **2005**, *3*, 561. (b) D. Yamazaki, T. Nishinaga, N. Tanino, K. Komatsu, *J. Am. Chem. Soc.* **2006**, *128*, 14470. (c) W. W. Porter, III, T. P. Vaid, *J. Org. Chem.* **2005**, *70*, 5028. (d) J. -M. Lü, S. V. Rosokha, J. K.

Kochi, *J. Am. Chem. Soc.* **2003**, *125*, 12161. (e) D. D. Graf, R. G. Duan, J. P. Campbell, L. L. Miller, K. R. Mann, *J. Am. Chem. Soc.* **1997**, *119*, 5888. (f) A. Y. Ziganshina, Y. H. Ko, W. S. Jeon, K. Kim, *Chem. Commun.* **2004**, 806. (g) L. L. Miller, K. R. Mann, *Acc. Chem. Res.* **1996**, *29*, 417. (h) T. Nishinaga, Y. Sotome, *J. Org. Chem.* **2017**, *82*, 7245. (f) C. B. Nielsen, A. Angerhofer, K. A. Abboud, J. R. Reynolds, *J. Am. Chem. Soc.* **2008**, *130*, 9734. (i) N. S. Rizalman, C. C. Ferrón, W. Niu, A. L. Wallace, M. He, R. Balster, J. Lampkin, V. Hernández, J. T. López Navarrete, M. C. Ruiz Delgado, F. Hartl, *RSC Adv.* **2013**, *3*, 25644.

11. (a) C. Femoni, M. C. Iapalucci, G. Longoni, C. Tiozzo, J. Wolowska, S. Zacchini, E. Zazzaroni, *Chem. Eur. J.* **2007**, *13*, 6544. (b) K. Goto, T. Kubo, K. Yamamoto, K. Nakasuji, K. Sato, D. Shiomi, T. Takui, M. Kubota, T. Kobayashi, K. Yakusi, J. Ouyang, *J. Am. Chem. Soc.* **1999**, *121*, 1619. (c) A. Merz, J. Kronberger, L. Dunsch, A. Neudeck, A. Petr, L. Parkanyi, *Angew. Chem. Int. Ed.* **1999**, *38*, 1442.

12. (a) K. E. Preuss, *Polyhedron* **2014**, *79*, 1. (b) F. Mota, J. S. Miller, J. J. Novoa, *J. Am. Chem. Soc.* **2009**, *131*, 7699. (c) Z. -h. Cui, H. Lischka, H. Z. Beneberu, M. Kertesz, *J. Am. Chem. Soc.* **2014**, *136*, 5539.

13. C. Adams, N. Jacobsen, J. H. P. Utley, *J. Chem. Soc. Perkin Trans. 2* **1978**, 1071.

14. (a) N. G. Connelly, W. E. Geiger, *Chem. Rev.* **1996**, *96*, 877. (b) G. W. Cowell, A. Ledwith, A. C. White, H. J. Woods, *J. Chem. Soc. B* **1970**, 227.

15. M. A. Petrukhina and L. T. Scott, *Fragments of Fullerenes and Carbon Nanotubes: Designed Synthesis, Unusual Reactions, and Coordination Chemistry* (Wiley, Hoboken, 2012).

16. (a) T. -C. Wu, H. -J. Hsin, M. -Y. Kuo, C. -H. Li, Y. -T. Wu, *J. Am. Chem. Soc.* **2011**, *133*, 16319. (b) T. Amaya, T. Nakata, T. Hirao, *J. Am. Chem. Soc.* **2009**, *131*, 10810. (c) Y. Okuda, N. Fukui, J. Kim, T. Kim, H. -W. Jiang, G. Copley, M. Kitano, D. Kim, A. Osuka, *Angew. Chem. Int. Ed.* **2017**, *56*, 12317.

17. (a) R. C. Haddon, *J. Am. Chem. Soc.* **1987**, *109*, 1676. (b) R. C. Haddon, *Science* **1993**, *261*, 1545. (c) R. C. Haddon, L. T. Scott, *Pure Appl. Chem.* **1986**, *58*, 137.

Appendix 1

Oxidation of 2-Amino-Substituted BODIPYs Providing Pyrazine-Fused BODIPY Trimers

ABSTRACT: Oxidation of 2-amino-substituted BODIPYs afforded BODIPY trimers in a one-step operation. The trimer consists of a pyrazine-fused BODIPY dimer to which one BODIPY unit is connected through an NH linkage. Effective expansion of π-conjugation over the fused dimer was observed in optical and electrochemical measurements.

Contents

5-1. Introduction

BODIPYs, 4,4-difluoro-4-bora-3*a*,4*a*-diaza-*s*-indacenes, have been some of the most attractive functional dyes in materials science.[1] They exhibit high thermal and photochemical stability as well as strong absorption and emission in the visible region due to their rigid frameworks and betaine-like electronic structures. These characteristics are now applied to fluorescent probes for bioimaging,[2] photodynamic therapy[3] and organic emissive materials such as OLEDs.[4] Many chemists have recently focused on the synthesis of BODIPY oligomers to achieve NIR absorption and emission properties through expansion of π-conjugation.[5] In particular, BODIPY oligomers with fused structures have attained fascinating features (Scheme 5-1). Yamaguchi, Wakamiya, and co-worker have demonstrated potential application of an α,β-benzene-fused BODIPY dimer to stable NIR dyes owing to the lowered HOMO energy by the fused structure (Scheme 5-1a).[6a] Uno, Nagata, and co-workers have also reported β,β'-benzene-fused BODIPY oligomers as NIR-selective light-absorbing materials (Scheme 5-1b).[6b]

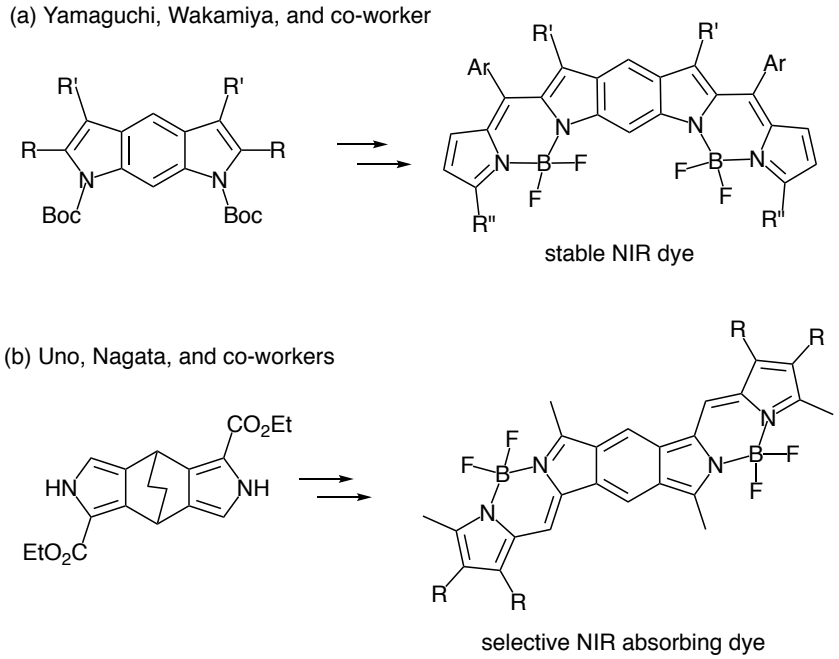

Scheme 5-1. Examples of fused BODIPY dimers.

Oxidation of amino-substituted π-conjugated molecules has been a useful tool for construction of fused systems. For example, aniline is oxidized to well-known black pigments, which are a mixture of oligomeric materials containing C–N double bonds and fused structures. Shinokubo and co-workers have recently developed oxidative coupling of amino-substituted functional π-systems such as porphyrins and anthracenes, providing pyrazine and pyrrole-fused dimers in high yields with excellent regioselectivity.[7] These dimers exhibited absorption in longer wavelength region compared with their corresponding monomers due to the fused structure. Thus, the author tried the oxidation reaction of 2-amino BODIPYs to achieve NIR absorption dye, which resulted in the formation of BODIPY trimers with a pyrazine-fused BODIPY dimer structure.

5-2. Synthesis and Characterizations

2-Amino-8-mesityl BODIPY **13a** was prepared from 2-bromo BODIPY **11a** (Scheme 5-2). Palladium-catalyzed imination of **11a** with benzophenone imine provided imino BODIPY **12a** in 69% yield, which afforded a purple-colored solution containing **13a** and benzophenone after hydrolysis of **12a** with aqueous HCl. Because decomposition of amino BODIPY **13a** occurred during concentration of its solution, the author subjected the crude product **13a** to the oxidation reaction without complete evaporation of solvents. Oxidation of **13a** with DDQ afforded a blue compound **14a** in 34% yield in two steps, which was stable in air. Its parent mass ion peaks were observed at m/z = 968.4118, suggesting its trimeric structure.

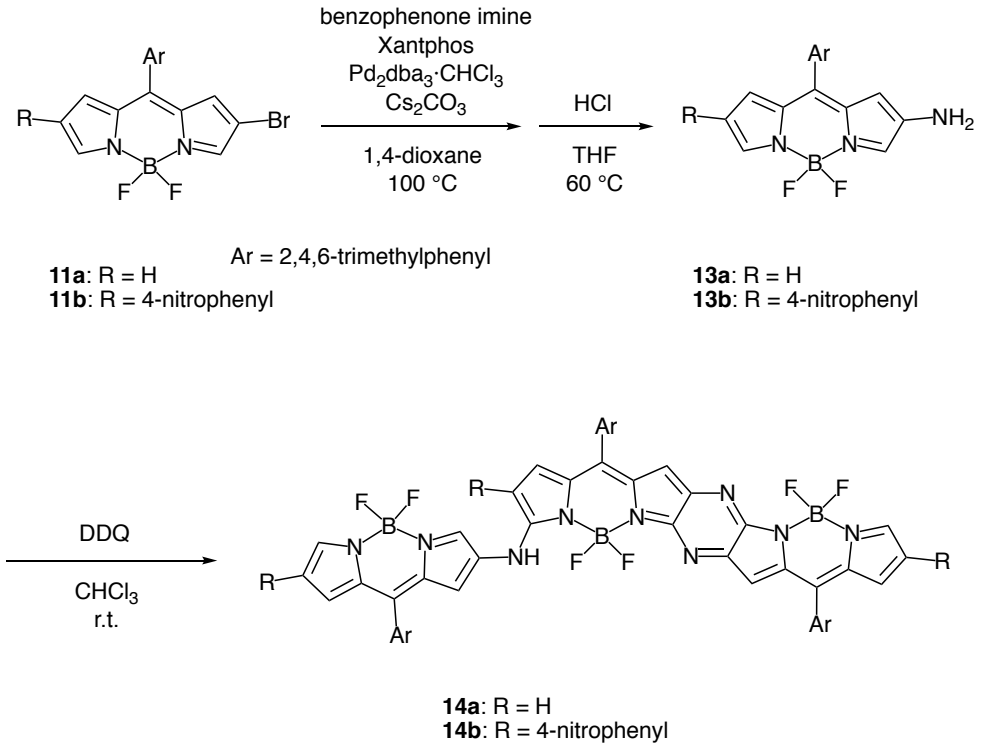

Scheme 5-2. Synthesis of BODIPY trimers.

The structure of **14a** was unambiguously elucidated by X-ray diffraction analysis. Figure 5-1 shows the crystal structure of **14a**, which contains three BODIPY skeletons. Two of the BODIPY units constitute a pyrazine-fused BODIPY dimer, to which one BODIPY unit is connected through an NH linkage. The BODIPY dimer part is completely planar and the mean plane deviation from the plane consisting of 18 carbon and six nitrogen atoms in the dimer is 0.107 Å. The planar geometry suggests effective π-extension among the dimer units. On the other hand, the flanking BODIPY moiety is tilted to 44.5° from the dimer plane, indicating a small π-conjugation with the dimer moiety. The bond length of C(1)–N(9) is 1.33 Å which is shorter than that of a standard C_{sp3}–N bond (1.47 Å), while C(20)–N(9) is standard (1.42 Å). These data indicate that the lone pair on the N(9) atom mainly participates in π-conjugation with the fused BODIPY dimer.

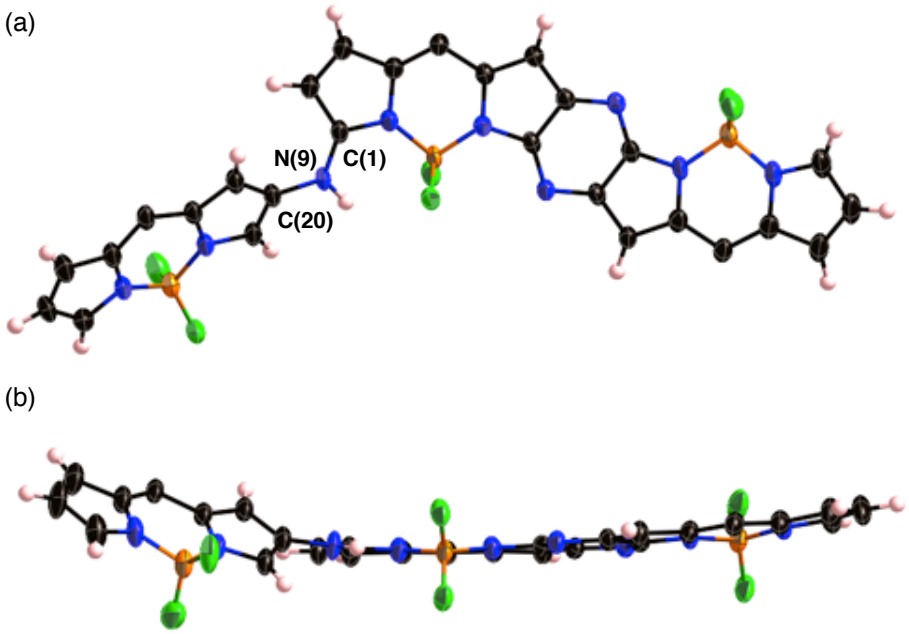

Figure 5-1. X-Ray crystal structure of **14a**. (a) Top view and (b) side view. The thermal ellipsoids are scaled at a 50% probability level. Mesityl groups are omitted for clarity.

To stabilize amino-substituted BODIPY **13a**, the author introduced electron-withdrawing groups. As expected, nitrophenyl-substituted BODIPY **13b** could be purified as a stable compound. Oxidation of **13b** with DDQ in chloroform exclusively afforded the pyrazine-fused trimer **14b** in 59% yield. In this reaction, no other oligomers were observed. The structure of **14b** was also confirmed by X-ray diffraction analysis (Figure 5-2). Two nitrophenyl groups at the terminal positions are placed almost in the same plane with the adjacent BODIPY core, indicating effective π-conjugation. The hanging BODIPY monomer unit is displaced from the plane of the dimeric unit at an angle of 21.5°. The dihedral angle between the dimer plane and the flanking BODIPY unit is 54.8°, which is larger than that of **14a**. These displacements are caused by steric repulsion between the nitrophenyl substituent and the BODIPY monomer unit.

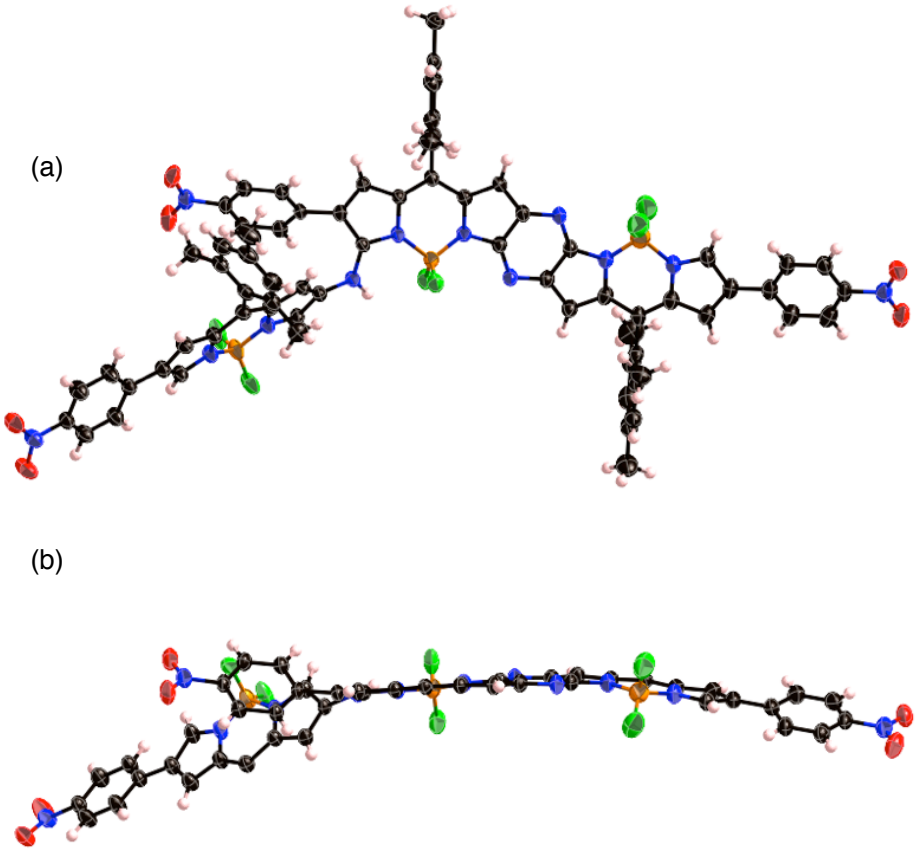

Figure 5-2. X-Ray crystal structure of **14b**. (a) Top view and (b) side view. The thermal ellipsoids are scaled at a 50% probability level. Mesityl groups are omitted for clarity in (b).

5-3. Optical and Electrochemical Properties

Figure 5-3 shows the UV-vis-NIR absorption spectra of **14a** and **14b** in CH_2Cl_2 along with the spectra of the corresponding monomers, 8-mesityl BODIPY **15a** and 2-(4-nitrophenyl)-8-mesityl BODIPY **15b**. As compared to the monomers **15a** and **15b**, the absorption spectra of trimers **14a** and **14b** are significantly intensified. The lowest energy absorption bands of **15a** and **15b** are red-shifted to 701 and 761 nm, respectively. The absorption maximum of trimer **14b** is longer than that of **14a** because of extended π-conjugation by the nitrophenyl groups. Interestingly, a new absorption band of **14a** appeared at around 850 nm in polar solvents such as acetone and acetonitrile (Figure 5-4). Further investigation was conducted by theoretical calculations.

The frontier orbitals of **14a**, **14b** were calculated by the DFT method at the B3LYP/6-31G(d) level (Figure 5-5 and Figure 5-6). While the HOMO is delocalized over the fused BODIPY dimer unit, the LUMO+1 is located at the monomeric BODIPY moiety. Time-dependent (TD) DFT calculations of **14a** revealed that the lowest energy absorption band consists of three transitions (Figure 5-7). All of the transitions occur from HOMO to LUMO+1. These results indicate that intramolecular charge transfer interactions between the pyrazine-fused BODIPY dimer and amino BODIPY units resulted in the broad and red-shifted absorption band. In the fluorescence spectra, **14a** and **14b** show weak emissions in the near infrared region (Φ_F < 0.01, Figure 5-8). The addition of various acids in the solution of **14a** to prevent CT interactions did not enhance its fluorescence intensity. Therefore, the low fluorescence quantum yields are probably due to the non-radiative decay by rotation of the amino BODIPY substituent.

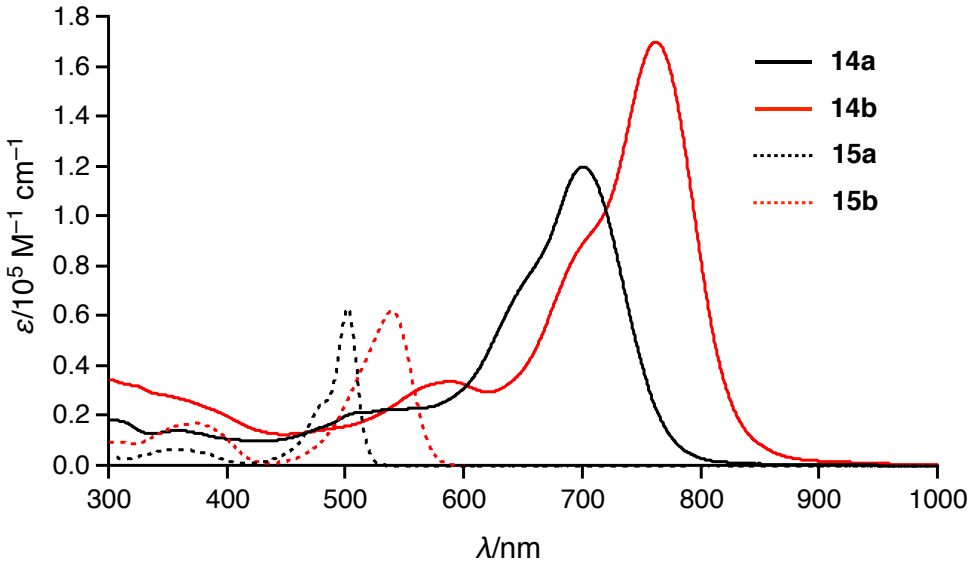

Figure 5-3. UV-vis-NIR absorption spectra of **14a** (black, solid line), **14b** (red, solid line), **15a** (black, dashed line), and **15b** (red, dashed line) in CH_2Cl_2.

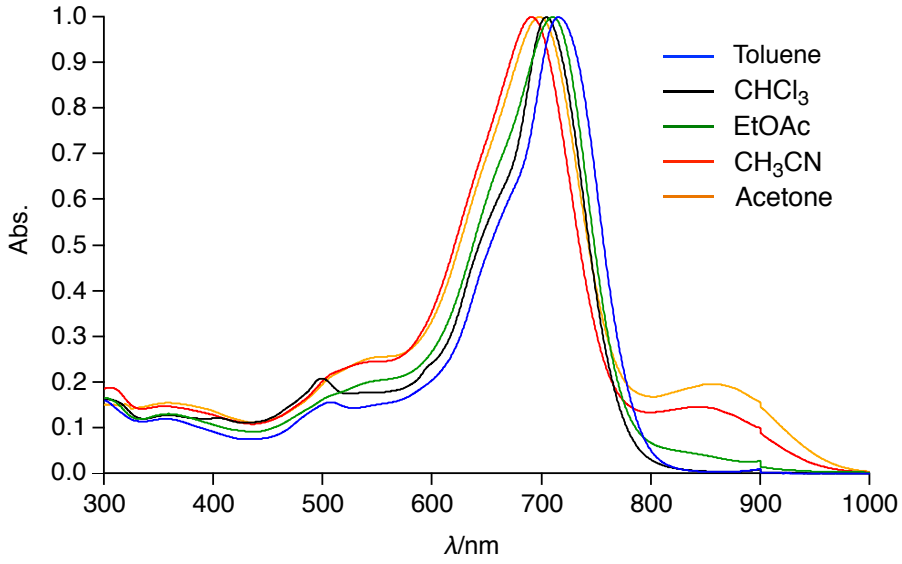

Figure 5-4. UV-vis-NIR absorption spectra of **14a** in various solvents.

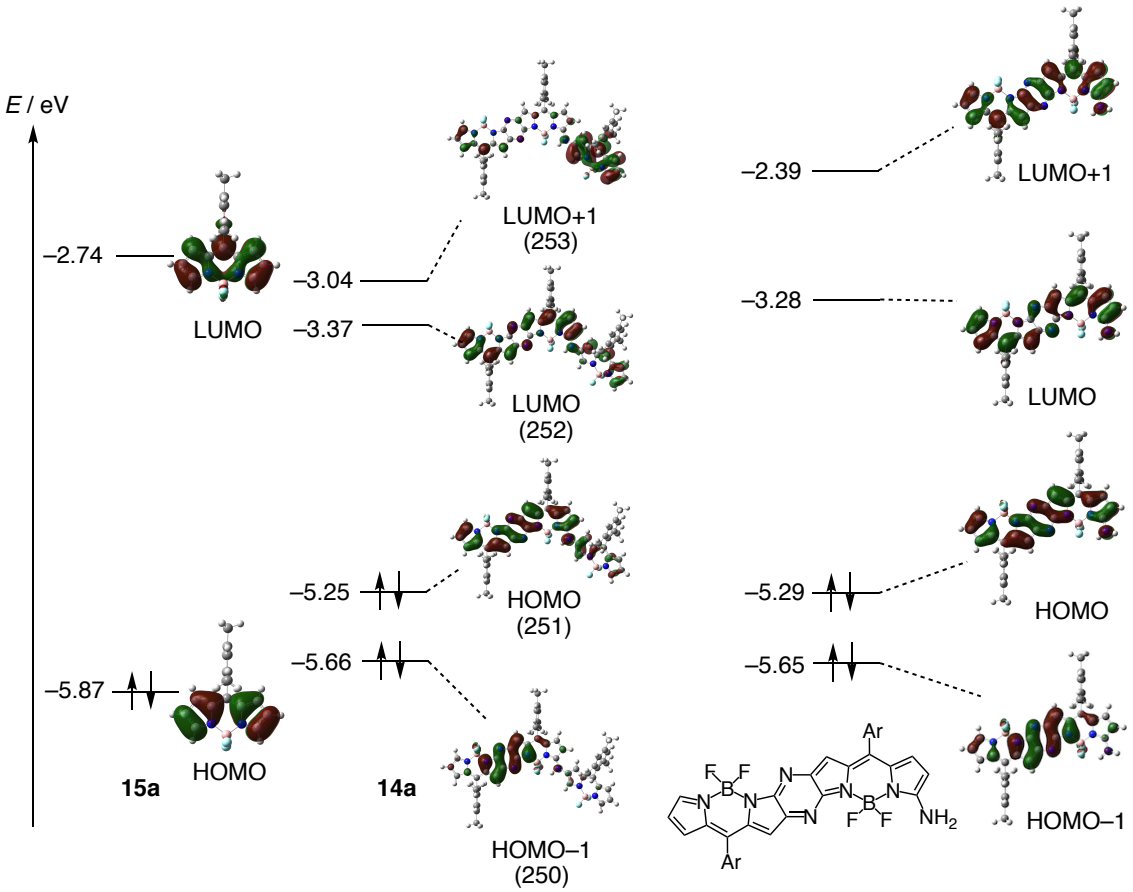

Figure 5-5. Molecular orbitals of **14a**, **15a**, and the pyrazine-fused dimer.

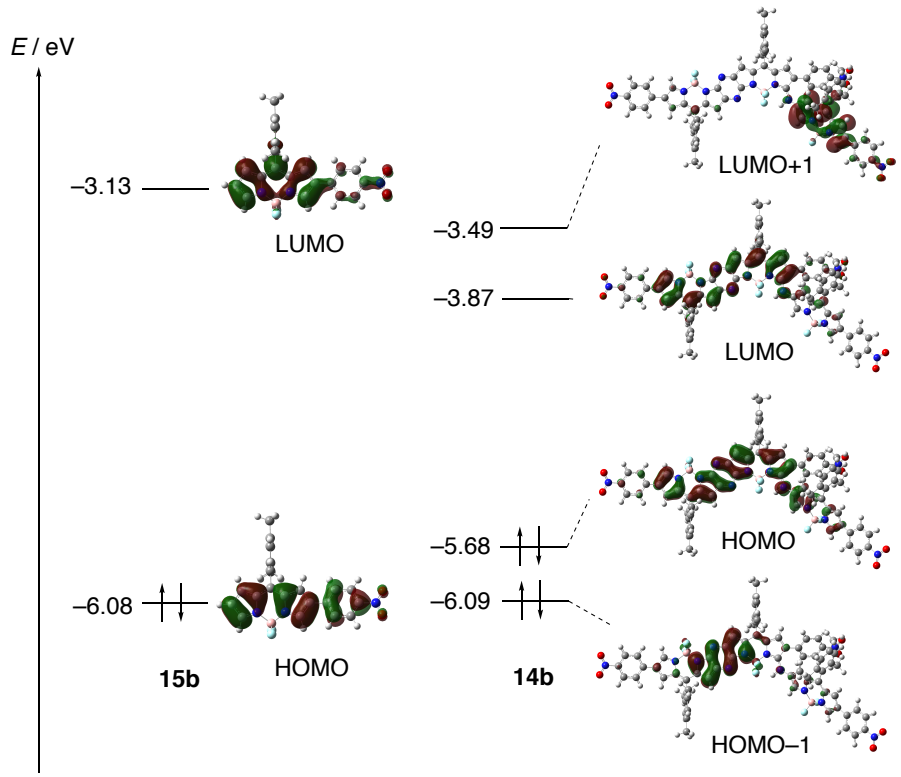

Figure 5-6. Molecular orbitals of **14b** and **15b**.

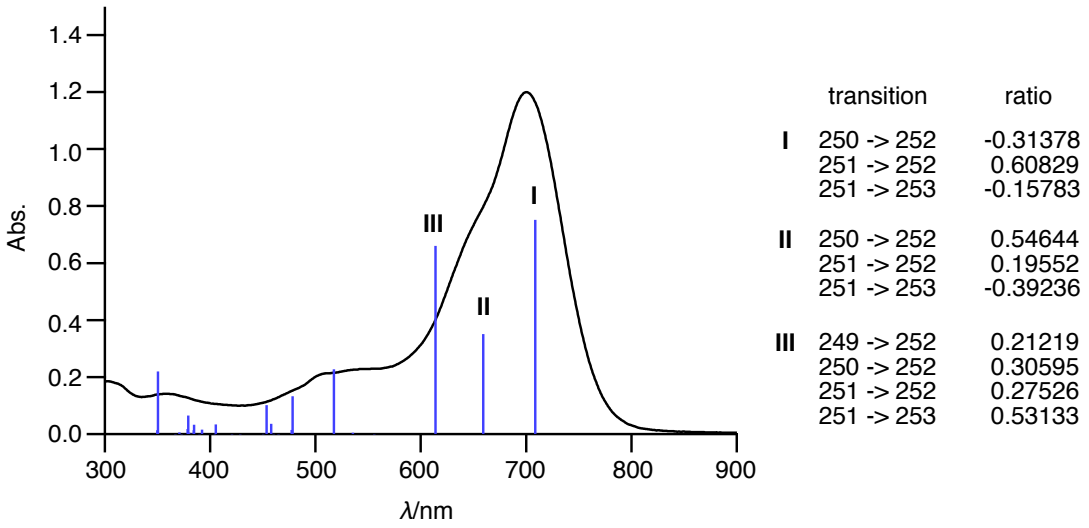

Figure 5-7. Calculated absorption spectrum of **14a** (blue line) by the DFT method using the B3LYP functional and the 6-31G(d) basis set. The spectra of **14a** in CH_2Cl_2 (black line) were also displayed.

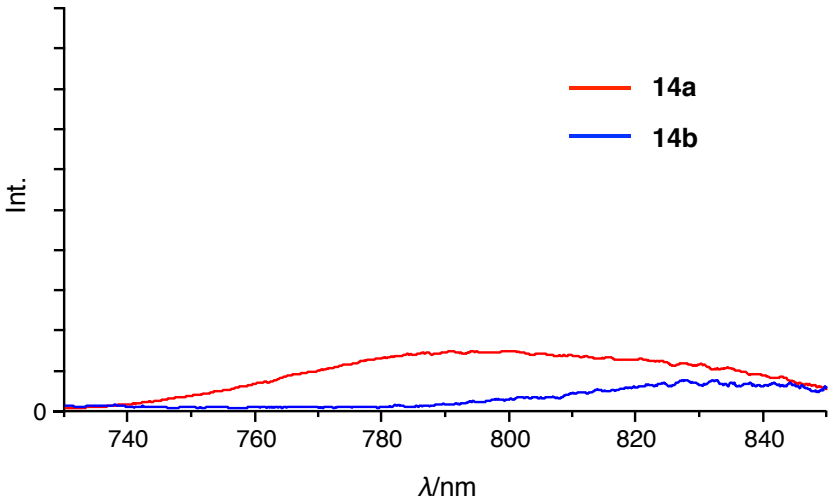

Figure 5-8. Emission spectra of **14a** and **14b** in CH_2Cl_2.

Electrochemical properties of **14a** and **14b** and the corresponding monomers **15a** and **15b**[5c] were investigated by cyclic voltammetry (Figure 5-9). The results are summarized in Table 5-1. Both **14a** and **14b** exhibited clear and reversible reduction waves and irreversible oxidation waves. As compared to the corresponding monomers **15a** and **15b**, the gap between the first oxidation and first reduction potentials (ΔE) becomes narrower in trimers **14a** and **14b**. Because the value of the third reduction potential of **14** is almost identical to the first reduction potential of monomer **15**, the third reduction can be considered to occur on the amino BODIPY unit. Accordingly, both the first and second reductions proceed at the fused dimer unit. The theoretical calculations also support this assignment: the calculated energy levels of HOMO, HOMO–1 and LUMO of the corresponding pyrazine-fused BODIPY dimer unit are almost comparable with those of **14a** (Figure 5-5). The split of the reduction waves indicates the strong electronic interaction between two BODIPY moieties in the fused dimer. The remarkable decrease of the first reduction potential in trimers suggests that fusion with the pyrazine ring at 2,3-positions is effective to lower the LUMO level. Such a compound with a low LUMO level is a promising candidate for effective electron-accepting molecules applied for solar cells and n-type conducting materials.

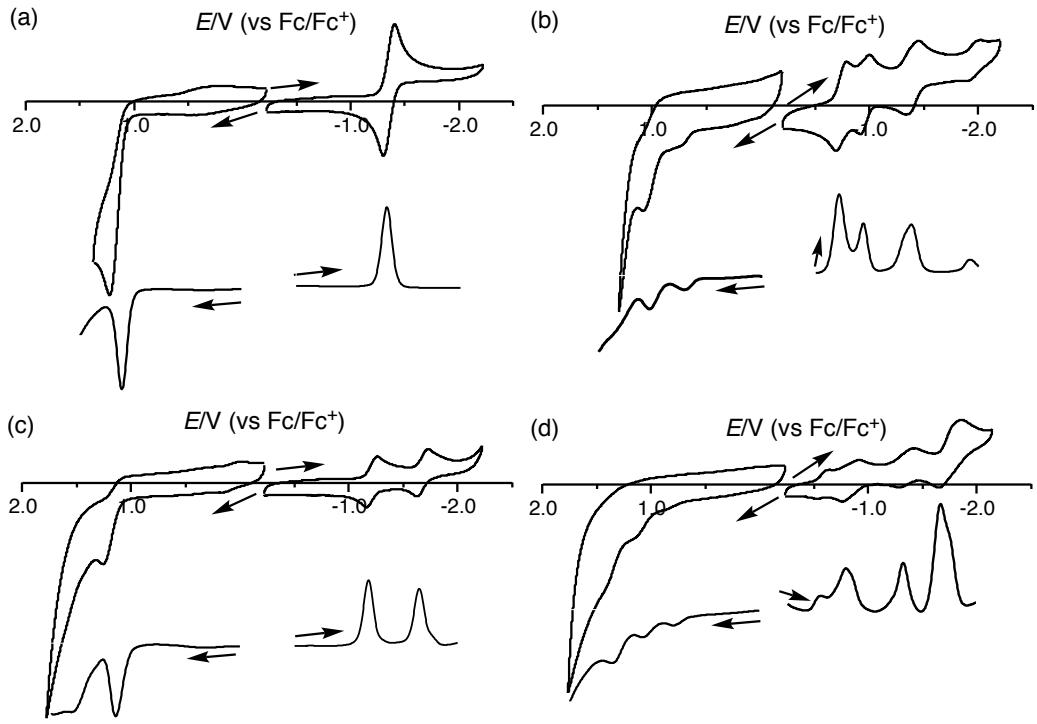

Figure 5-9. Cyclic voltammograms of (a) **15a**, (b) **14a**, (c) **15b**, and (d) **14b**.

Table 5-1. Summary of electrochemical data.

compound	E_{ox}^{2}	E_{ox}^{1}	E_{red}^{1}	E_{red}^{2}	E_{red}^{3}	E_{red}^{4}	ΔE^{a}
15a	—	1.12[b]	–1.35	—	—	—	2.47
14a	1.04[b]	0.716[b]	–0.735	–0.950	–1.39	–1.92	1.45
15b	—	1.15[b]	–1.21	–1.67	—	—	2.36
14b	1.08[b]	0.796[b]	–0.556	–0.817	–1.33	–1.73	1.35

[a] $\Delta E = (E_{ox}^{1} - E_{red}^{1})$ [b] Irreversible wave. The values were obtained by DPV measurement.

5-4. Summary

In conclusion, the author has achieved one-pot synthesis of pyrazine-fused BODIPY trimers through oxidation of 2-aminosubstituted BODIPYs. The reaction proceeded with excellent regioselectivity due to high electrophilicity at 3,5-positions. BODIPY trimers **14** exhibit bathochromic shifted strong absorption bands, indicating effective expansion of π-conjugation. Theoretical calculations revealed the presence of intramolecular charge transfer interactions between the BODIPY dimer and monomer units. This protocol would be applicable to efficient access to NIR dyes not only with BODIPYs but also with other functional π-systems.

5-5. Experimental Section

Materials and Characterization

^{1}H NMR (500 MHz) and ^{13}C NMR (126 MHz) spectra were recorded using a Varian INOVA-500 spectrometer. Chemical shifts were reported at the delta scale in ppm relative to $CHCl_3$ (δ = 7.260 ppm) and CH_2Cl_2 (δ = 5.320 ppm) for ^{1}H NMR, $CDCl_3$ (δ = 77.0 ppm) for ^{13}C NMR. UV/vis/NIR absorption spectra were recorded using a Shimadzu UV-2550 or JASCO V670 spectrometer. Emission spectra were recorded using a JASCO FP-6500 spectrometer, and absolute fluorescence quantum yields were measured by the photon-counting method using an integration sphere. High-resolution (HR) mass spectrum were recorded on a Bruker micro TOF using APCI-TOF method. Unless otherwise noted, materials obtained from commercial suppliers were used without further purification.

Synthesis of 12a

A Schlenk tube containing compound **11a** (101 mg, 0.258 mmol), Cs_2CO_3 (167 mg, 0.512 mmol), Xantphos (15.4 mg, 26.6 μmol), and $Pd_2dba_3{\cdot}CHCl_3$ (13.7 mg, 13.2 μmol) was flushed with N_2 three times. To the Schlenk, dry 1,4-dioxane (3 mL) and benzophenone imine (64.6 μL, 0.385 mmol) were added. The mixture was stirred for 3 h at 100 °C. After the reaction, the resulting mixture was cooled down to room temperature, passed through a short pad of Celite, and concentrated in vacuo. Purification by silica-gel column chromatography (hexane/CH_2Cl_2) afforded compound **12a** (87.6 mg, 0.179 mmol) in 69% yield as a purple solid. ^{1}H NMR ($CDCl_3$): δ = 7.80 (s, 1H), 7.71–7.74 (m, 2H), 7.52 (s, 1H), 7.42–7.45 (m, 1H), 7.35–7.38 (m, 5H), 7.13–7.14 (m, 2H), 6.86 (s, 2H), 6.57 (d, J = 4.5 Hz, 1H), 6.40 (dd, J_1 = 3.8 Hz, J_2 = 1.8 Hz, 1H), 5.60 (s, 1H), 2.34 (s, 3H), 1.96 (s, 6H) ppm; ^{13}C NMR ($CDCl_3$): δ = 168.4, 146.6, 143.6, 143.2, 142.2, 139.0, 138.5, 137.1, 136.1, 135.1, 134.2, 130.9, 129.4, 129.0, 128.9, 128.8, 128.2, 128.1, 127.9, 120.5, 117.8, 21.09, 19.86 ppm; HR APCI-MS: m/z = 490.2257, calcd for $(C_{31}H_{27}BF_2N_3)^+$ = 490.2266 [$(M + H)^+$].

Synthesis of 12b

A Schlenk tube containing compound **11b** (50.7 mg, 99.4 μmol), Cs_2CO_3 (66.3 mg, 0.203 mmol), Xantphos (23.2 mg, 40.1 μmol), $Pd_2dba_3{\cdot}CHCl_3$ (20.7 mg, 20.0 μmol) was flushed with N_2 three times. To the Schlenk, dry 1,4-dioxane (3 mL) and benzophenone imine (24.7 μL, 0.147 mmol) were added. The mixture was stirred for 2 h at 100 °C. After the reaction, the resulting mixture was cooled down to room temperature and passed through a short pad of Celite, and concentrated in vacuo. Purification by silica-gel column chromatography (hexane/CH_2Cl_2) afforded compound **12b** (33.0 mg, 54.1 μmol) in 54% yield as a purple solid. ^{1}H NMR ($CDCl_3$): δ = 8.17–8.19 (m, 2H), 8.15 (s, 1H), 7.72–7.74 (m, 2H), 7.65 (s, 1H), 7.57–7.59 (m, 2H), 7.45–7.48 (m, 1H), 7.37–7.40 (m, 5H), 7.14–7.16 (m, 2H), 6.92 (s, 2H), 6.78 (s, 1H), 5.68 (s, 1H), 2.37 (s, 3H), 2.00 (s, 6H) ppm; ^{13}C NMR ($CDCl_3$): δ = 169.6, 146.6, 146.3, 145.2, 145.1, 144.9, 139.6, 139.2, 139.0, 138.7, 136.8, 136.1, 135.5, 135.5, 131.2, 130.2, 129.2, 129.1, 129.0, 128.9, 128.3, 128.1, 125.4, 124.3, 123.0, 120.9, 21.14, 19.92 ppm; HR APCI-MS: m/z = 611.2407, calcd for $(C_{37}H_{30}BF_2N_4O_2)^+$ = 611.2431 [$(M + H)^+$].

Synthesis of 13b

Compound **12b** (20.2 mg, 33.1 μmol) in THF (2.69 mL) was added 1 M HCl (0.587 mL) and the mixture was stirred for 1 h at 60 °C. After the reaction, the resulting mixture was cooled down to room temperature, and then aqueous $NaHCO_3$ was added into reaction mixture. The resulting solution was extracted with CH_2Cl_2 and the organic layer was washed with water, dried over with Na_2SO_4, and concentrated in vacuo. Purification by silica-gel column chromatography (hexane/CH_2Cl_2) afforded compound **13b** (13.5 mg, 30.2 μmol) in 91% yield as a dark blue solid. ^{1}H NMR ($CDCl_3$): δ = 8.16–8.18 (m, 2H), 8.05 (s, 1H), 7.80 (s, 1H), 7.57–7.58 (m, 2H), 6.98 (s, 2H), 6.67 (s, 1H), 5.85 (s, 1H), 3.63 (s, 2H), 2.38 (s, 3H), 2.15 (s, 6H) ppm; ^{13}C NMR ($CDCl_3$): δ = 146.0, 143.0, 142.7, 141.9, 140.3, 138.9, 136.9, 136.4, 136.4, 135.0, 129.6, 128.9, 128.3,

125.2, 124.3, 121.0, 108.8, 21.16, 19.99 ppm; HR APCI-MS: m/z = 447.1788, calcd for $(C_{24}H_{22}BF_2N_4O_2)^+$ = 447.1803 [$(M + H)^+$].

Synthesis of 14a

Compound **12a** (30.2 mg, 61.7 μmol), THF (5.0 mL), and 1M HCl (1.1 mL) were added into a 30 mL round-bottomed flask, and the mixture was stirred for 1 h at 60 °C. After the reaction, the resulting solution was cooled down to room temperature, and then aqueous $NaHCO_3$ was added. The resulting mixture was extracted with $CHCl_3$ and then the organic extract was washed with water, dried over with Na_2SO_4, and evaporated the solvent to ca. 40 mL of the total volume. The solution was diluted with $CHCl_3$ (40 mL) and degassed by bubbling with N_2 for 45 minutes. To the resulting solution was added DDQ (29.3 mg, 129 μmol). The reaction mixture was stirred for 30 min at room temperature. After the reaction, the resulting mixture was concentrated in vacuo. Purification by silica-gel column chromatography (hexane/EtOAc) afforded compound **14a** (6.69 mg, 6.92 μmol) in 34% yield (2 steps) as a blue solid. ^{1}H NMR ($CDCl_3$): δ = 8.29 (s, 1H), 8.08 (s, 1H), 7.85 (s, 1H), 7.04 (s, 1H), 6.98 (s, 2H), 6.97 (s, 2H), 6.97 (s, 2H), 6.89 (d, J = 4.5 Hz, 1H), 6.87 (d, J = 5.2 Hz, 1H), 6.83 (d, J = 4.1 Hz, 1H), 6.68 (dd, J = 0.8, 4.3 Hz, 1H), 6.57–6.59 (m, 3H), 6.52 (s, 1H), 2.39 (s, 3H), 2.37 (s, 3H), 2.36 (s, 3H), 2.12 (s, 6H), 2.10 (s, 6H), 2.09 (s, 6H) ppm; ^{13}C NMR ($CDCl_3$): δ = 161.0, 151.6, 151.3, 149.4, 148.6, 147.7, 145.5, 143.8, 140.4, 139.8, 139.6, 139.3, 139.0, 138.5, 137.3, 137.0, 136.6, 136.3, 136.1, 135.4, 133.3, 132.9, 132.8, 131.1, 129.1, 128.7, 128.5, 128.4, 128.2, 123.0, 120.7, 119.9, 119.2, 118.0, 109.5, 21.17, 21.13, 20.13, 20.06, 20.05 ppm; UV/vis (CH_2Cl_2): λ_{max} (ε [M^{-1} cm^{-1}]) = 359 (14000), 507 (21000), 700 (120000) nm; HR APCI-MS: m/z = 968.4118, calcd for $(C_{54}H_{47}B_3F_6N_9)^+$ = 968.4156 [$(M + H)^+$].

Synthesis of 14b

A Schlenk tube containing compound **13b** (4.93 mg, 11.0 μmol) and DDQ (5.15 mg, 22.7 μmol) was flushed with N_2 three times. To the Schlenk, dry $CHCl_3$ (3.66 mL) was added. The mixture was stirred for 4 h at room temperature. After the reaction, the resulting mixture was passed through short pad of Celite, and concentrated in vacuo. Purification by silica-gel column chromatography (hexane/CH_2Cl_2) afforded compound **14b** (2.91 mg, 2.19 μmol) in 59% yield as a black solid. ^{1}H NMR ($CDCl_3$): δ = 8.68 (s, 1H), 8.54 (s, 1H), 8.28 (s, 1H), 8.23 (d, J = 9.0 Hz, 2H), 8.18 (d, J = 9.0 Hz, 2H), 7.99 (d, J = 8.7 Hz, 2H) 7.73 (d, J = 9.0 Hz, 2H), 7.61 (d, J = 9.0 Hz, 2H), 7.32 (s, 1H), 7.27 (d, J = 8.8 Hz, 2H), 7.16 (s, 1H), 7.06 (s, 3H), 7.04 (s, 2H), 6.96 (s, 3H), 6.93 (s, 1H), 6.58 (s, 1H), 6.43 (s, 1H), 2.39 (s, 3H), 2.37 (s, 3H), 2.36 (s, 3H), 2.17 (s, 6H), 2.17 (s, 6H), 2.02 (s, 6H) ppm; ^{13}C NMR ($CDCl_3$): δ = 157.9, 152.4, 150.0, 149.0, 148.6, 148.4, 147.8, 147.4, 147.0, 146.2, 144.8, 144.3, 140.8, 140.5, 139.9, 139.8, 139.5, 139.0, 138.8, 138.1, 137.7, 137.2, 137.0, 136.9, 136.6, 135.8, 135.6, 135.4, 133.5, 133.0, 133.0, 132.1, 128.9, 128.8, 128.6, 128.5, 128.2, 127.9, 126.5, 126.4, 126.3, 126.0, 124.5, 124.4, 123.5, 121.3, 120.2, 110.6, 21.18, 21.15, 20.23, 19.88 ppm; UV/vis (CH_2Cl_2): λ_{max} (ε [M^{-1} cm^{-1}]) = 587 (34000), 762 (170000) nm; HR APCI-MS: m/z = 1353.4495, calcd for $(C_{72}H_{55}B_3F_6N_{12}O_6Na)^+$ = 1353.4473 [$(M + Na)^+$].

X-Ray Diffraction Analysis

X-Ray data were obtained using a Rigaku CCD diffractometer (Saturn 724 with MicroMax-007) with Varimax Mo optics using graphite monochromated Mo-Kα radiation (λ = 0.71075 Å) for **14a** and using a Bruker SMART APEX X-ray diffractometer equipped with a large area CCD detector for **14b**.

Electrochemical Analysis

The cyclic voltammogram and differential-pulse voltammogram of **14a**, **14b**, **15a**, and **15b** were recorded using an ALS electrochemical analyser 612C.

Measurements were performed in freshly distilled CH_2Cl_2 with tetrabutylammonium hexafluorophosphate as the electrolyte. A three-electrode system was used. The system consisted of a glassy carbon working electrode, a platinum wire, and $Ag/AgClO_4$ as the reference electrode. The scan rate was 100 mVs^{-1}. The measurement was performed under nitrogen atmosphere. All potentials are referenced to the potential of ferrocene/ferrocenium cation couple.

Theoretical Calculations.

All calculations were performed using the Gaussian 09 program. The molecular orbitals of **14a**, **14b**, **15a**, **15b**, and the pyrazine-fused dimer were calculated by single point calculation at the B3LYP functional and the 6-31G(d) basis set using the geometry optimized at the B3LYP/6-31G(d) level. The simulated absorption spectrum of **14a** was obtained by the TD-DFT method at the B3LYP/6-31G(d) level.

Crystallographic data

	14a	**14b**
empirical formula	$C_{58}H_{50}B_3Cl_{12}F_6N_9$	$C_{80.12}H_{67.72}B_3Cl_{1.09}F_6N_{15.52}O_{6.25}$
formula weight	1444.90	1533.00
habit	prism	prism
T, K	103(2)	90(2)
crystal system	monoclinic	triclinic
space group	$P2_1/n$	*P*-1 (2)
a, Å	15.068(5)	14.6707(6)
b, Å	14.208(5)	17.1450(7)
c, Å	30.518(10)	18.0545(10)
α, deg	90.00	118.3350(17)
β, deg	99.173(4)	96.657(3)
γ, deg	90.00	90.695(2)
V, Å^3	6450(4)	3958.5(3)
Z	4	2
Dc, g/cm^3	1.488	1.286
F(000)	2936	1589
crystal size, mm^3	0.2 x 0.2 x 0.2	0.19 x 0.17 x 0.16
$2\theta_{max}$, °	50.0	50.0
R_1 ($I > 2\sigma(I)$)	0.0938	0.0871
wR_2 (all data)	0.2931	0.2809
GOF	1.050	1.026
obs reflects	11168	13197
total reflects	26983	24961
parameters	913	1082
CCDC number	971649	971650

5-6. References

1. (a) S. Chibani, B. L. Guennic, A. Charaf-Eddin, A. D. Laurent, D. Jacquemin, *Chem. Sci*. **2013**, *4*, 1950. (b) G. Ulrich, R. Ziessel, A. Harriman, *Angew. Chem. Int. Ed*. **2008**, *47*, 1184. (c) A. Loudet, K. Burgess, *Chem. Rev*. **2007**, *107*, 4891.

2. (a) Y. Urano, D. Asanuma, Y. Hama, Y. Koyama, T. Barrett, M. Kamiya, T. Nagano, T. Watanabe, A. Hasegawa, P. L. Choyke, H. Kobayashi, *Nat. Med*. **2009**, *15*, 104. (b) J. Han, A. Loudet, R. Barhoumi, R. C. Burghardt, K. Burgess, *J. Am. Chem. Soc*. **2009**, *131*, 1642.

3. (a) T. Myochin, K. Hanaoka, T. Komatsu, T. Terai, T. Nagano, *J. Am. Chem. Soc*. **2012**, *134*, 13730. (b) T. Yogo, Y. Urano, Y. Ishitsuka, F. Maniwa, T. Nagano, *J. Am. Chem. Soc*. **2005**, *127*, 12162.

4. L. Bonardi, H. Kanaan, F. Camerel, P. Jolinat, P. Retailleau, R. Ziessel, *Adv. Funct. Mater*. **2008**, *18*, 401.

5. (a) M. Bröring, R. Krüger, S. Link, C. Kleeberg, S. Köhler, X. Xie, B. Ventura, L. Flamigni, *Chem. Eur. J*. **2008**, *14*, 2976. (b) S. Rihn, M. Erdem, A. D. Nicola, P. Retailleau, R. Ziessel, *Org. Lett*. **2011**, *13*, 1916. (c) Y. Hayashi, S. Yamaguchi, W. Y. Cha, D. Kim, H. Shinokubo, *Org. Lett*. **2011**, *13*, 2992. (d) A. Poirel, A. De Nicola, P. Retailleau, R. Ziessel, *J. Org. Chem*. **2012**, *77*, 7512.

6. (a) A. Wakamiya, T. Murakami, S. Yamaguchi, *Chem. Sci*. **2013**, *4*, 1002. (b) M. Nakamura, H. Tahara, K. Takahashi, T. Nagata, H. Uoyama, D. Kuzuhara, S. Mori, T. Okujima, H. Yamada, H. Uno, *Org. Biomol. Chem*. **2012**, *10*, 6840.

7. (a) K. Goto, R. Yamaguchi, S. Hiroto, H. Ueno, T. Kawai, H. Shinokubo, *Angew. Chem. Int. Ed*. **2012**, *51*, 10333. (b) M. Akita, S. Hiroto, H. Shinokubo, *Angew. Chem. Int. Ed*. **2012**, *51*, 2894. (c) S. Ito, S. Hiroto, S. Lee, M. Son, I. Hisaki, T. Yoshida, D. Kim, N. Kobayashi, H. Shinokubo, *J. Am. Chem. Soc*. **2015**, *137*, 142.

Appendix 2

Synthesis of Diazo-Bridged BODIPY Dimer and Tetramer by Oxidative Coupling of *β*-Amino-Substituted BODIPYs

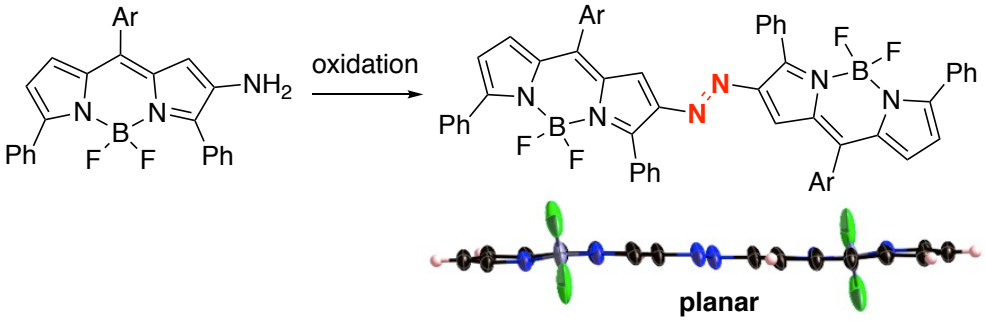

ABSTRACT: A diazo-bridged BODIPY dimer and tetramer were prepared by the oxidative coupling reaction of *β*-amino-substituted BODIPYs. The structure of the dimer was elucidated by X-ray diffraction analysis, showing its coplanar orientation of two BODIPY units. Effective extension of π-conjugation was confirmed by optical and electrochemical investigations.

Contents

6-1. Introduction

BODIPY, 4,4-difluoro-4-bora-3*a*,4*a*-diaza-*s*-indacene, has been one of the most important functional dyes in a wide area of material science due to its high thermal and photochemical stability as well as strong absorption and emission in the visible region.[1] A number of BODIPY-based molecules have been extensively explored for bioimaging probes,[2] photodynamic therapy,[3] and light emitting devices.[4] Recently, BODIPY oligomers with covalent linkages have attracted much interest for their NIR light absorbing property.[5] Although a number of BODIPY oligomers have been reported, there is no example of diazo-bridged ones.

Diazo-bridged π-conjugated materials represented by azobenzene are photoactive materials, exhibiting photochromic behavior through *cis-trans* isomerization.[6] The diazo linkage also enables effective π-conjugation due to its less sterically demanding nature in comparison to ethylene and imino linkages.[7] In addition, the electron-withdrawing feature of diazo groups effectively stabilizes π-conjugated systems to prevent decomposition by air oxidation. Here, the author describes the synthesis of a diazo-bridged BODIPY dimer and tetramer as novel covalently linked BODIPYs through oxidative dimerization of amino-substituted BODIPYs.

6-2. Synthesis and Characterizations

3,5-Diphenyl-2-amino BODIPY **21** was prepared as a starting substrate from 2-phenylpyrrole in six steps (Scheme 6-1). The reaction between 2-phenylpyrrole and mesitaldehyde in the presence of TFA afforded dipyrromethane **16**. The oxidation of **16** with DDQ provided dipyrrin **17** quantitatively. The complexation of **17** with $BF_3{\cdot}OEt_2$ successfully proceeded, resulting in BODIPY **18** in 85% yield. 2-Bromo BODIPY **19** was obtained in 94% yield by treatment of **18** with 1.1 equiv of NBS. The palladium-catalyzed cross-coupling reaction of **19** with benzophenone imine followed by acidic hydrolysis furnished **21** in good yield. Compound **21** was stable enough for handling under air and concentrated conditions. This is in sharp contrast to 2-amino

BODIPYs without α-substituents, which decomposed during concentration by rotary evaporator (see APPENDIX 1).

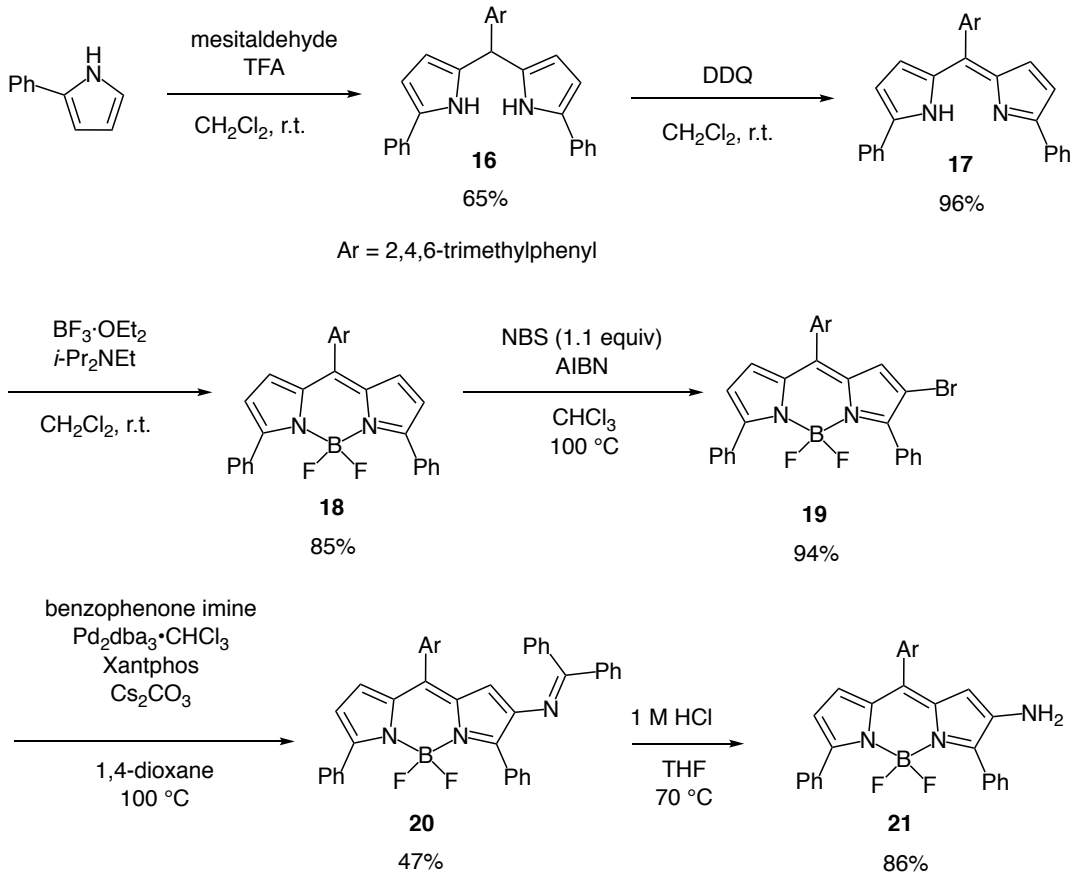

Scheme 6-1. Synthesis of 2-amino substituted BODIPY **21**.

Next, the author attempted oxidative coupling of **21** with several oxidizing reagents (Scheme 6-2).[8] A copper-mediated oxidative coupling resulted in the formation of a complex mixture. On the other hand, oxidation of **21** with DDQ in chloroform provided a diazo-linked BODIPY dimer **22** in 8% yield (Table 6-1). In this reaction, the formation of DDQ adducts was also observed as side products. Accordingly, the author further optimized the reaction conditions with other oxidants. Oxidation of **21** with *p*-chloranil improved the yield to 12%. However, a large amount of the starting material remained unreacted. The use of MnO_2 as the oxidant furnished **22** in 17% yield. *t*-BuOCl, recently reported by Minakata and co-workers[9a], provided **22** in 33%, but

inseparable chlorinated byproducts were formed. Oxidation with bis(trifluoroacetoxy)iodobenzene (PIFA) afforded the desired product **22** in 34% yield without formation of chlorinated byproducts.[9b,c] In this case, the starting material **21** was completely consumed.

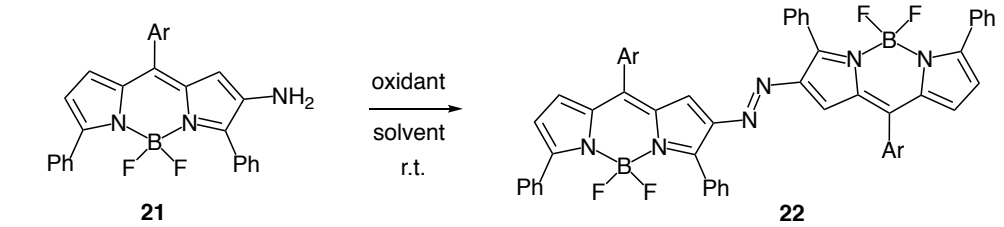

21 **22**

Ar = 2,4,6-trimethylphenyl

Scheme 6-2. Oxidative dimerization of **21**.

Table 6-1. Summary of Scheme 6-2.

Entry	Oxidant (equiv)	Time (h)	Solvent	Yield (%)
1	DDQ (2.1)	1	$CHCl_3$	8
2	*p*-chloranil (2.1)	23[a]	$CHCl_3$	12
3	MnO_2 (26)	24	$CHCl_3$	17
4	*t*-BuOCl (2.0) + NaI (2.0)	13	DME	33
5	$PhI(OCOCF_3)_2$ (2.1)	2	$CHCl_3$	34

[a] The reaction was conducted at r.t. for 17 h and at 60 °C for an additional 6 h.

The product **22** was assigned by spectroscopic methods. The parent mass ion peak observed at m/z = 951.4119 (calcd for $(C_{60}H_{49}B_2F_4N_6)^+$ = 951.4154 $[(M + H)^+]$) indicated its dimeric structure. In its ^1H NMR spectrum, peaks for pyrrole protons of **22** were shifted in the lower field as compared to **21** and the broad NH_2 signal of **21** disappeared after oxidation. This spectral change indicates conversion of the electron-donating NH_2 group to the electron-withdrawing diazo linkage. Finally, the structure of **22** was unambiguously elucidated by X-ray diffraction analysis. Figure 6-1

displays the X-ray crystal structure of **22**, revealing its highly planar structure including the diazo linkage. The deviation from the mean plane which consisted of the two BODIPY cores and the diazo moiety is 0.088 Å, and the dihedral angle between the BODIPY unit and the diazo linkage is only 1.1°. The length of the C(2)−N(3) bond is 1.40 Å, which is shorter than the standard $C_{sp}{}^2$–$N_{sp}{}^2$ single bond length. These structural features indicate the presence of effective conjugation between two BODIPY cores through the diazo linkage.

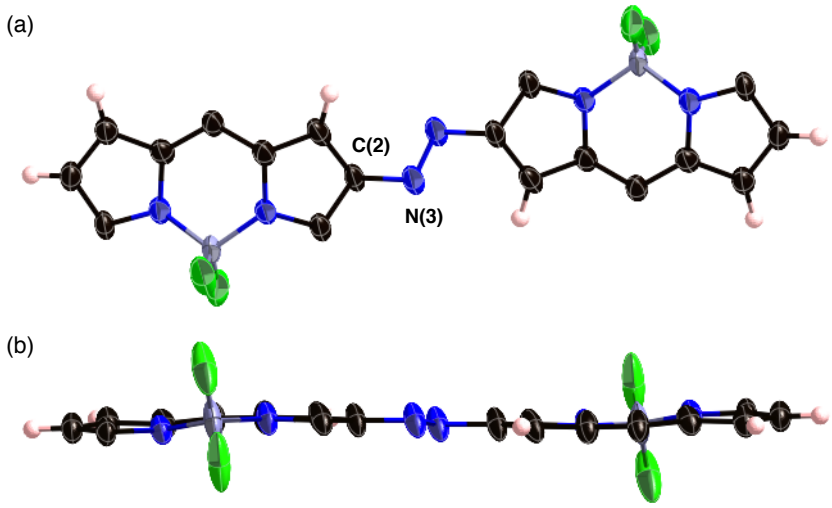

Figure 6-1. X-Ray crystal structure of **22**. (a) Top view and (b) side view. The thermal ellipsoids are scaled at 50% probability level. The mesityl and phenyl groups are omitted for clarity.

The author then attempted to obtain higher oligomers (Scheme 6-3). Bromination of **22** with NBS proceeded regioselectively. Amino-substituted BODIPY dimer **23** was prepared in a similar manner as **21**. Oxidation of **23** with MnO_2 furnished tetramer **24** in 4% yield. The yield was improved to 24% with PIFA as an oxidant. The formation of **24** was confirmed by mass and NMR spectroscopic analyses. The high-resolution (HR) mass spectrum of **24** exhibits the parent mass ion peak at m/z = 1927.8142, indicating its tetrameric structure. The ^{1}H NMR spectrum of **24** showed a C_2 symmetric feature. Singlet signals for pyrrole protons of **23** at 6.51, 6.36, and 5.87 ppm

were shifted further downfield to 6.58, 6.57, and 6.52 ppm in **24**, suggesting the formation of a new diazo group. Although the yield of the oxidative coupling reaction was not high, tetramer **24** was stable under the aerobic conditions, demonstrating the prospective utility of the diazo linkage to obtain stable and highly conjugated BODIPY oligomers.

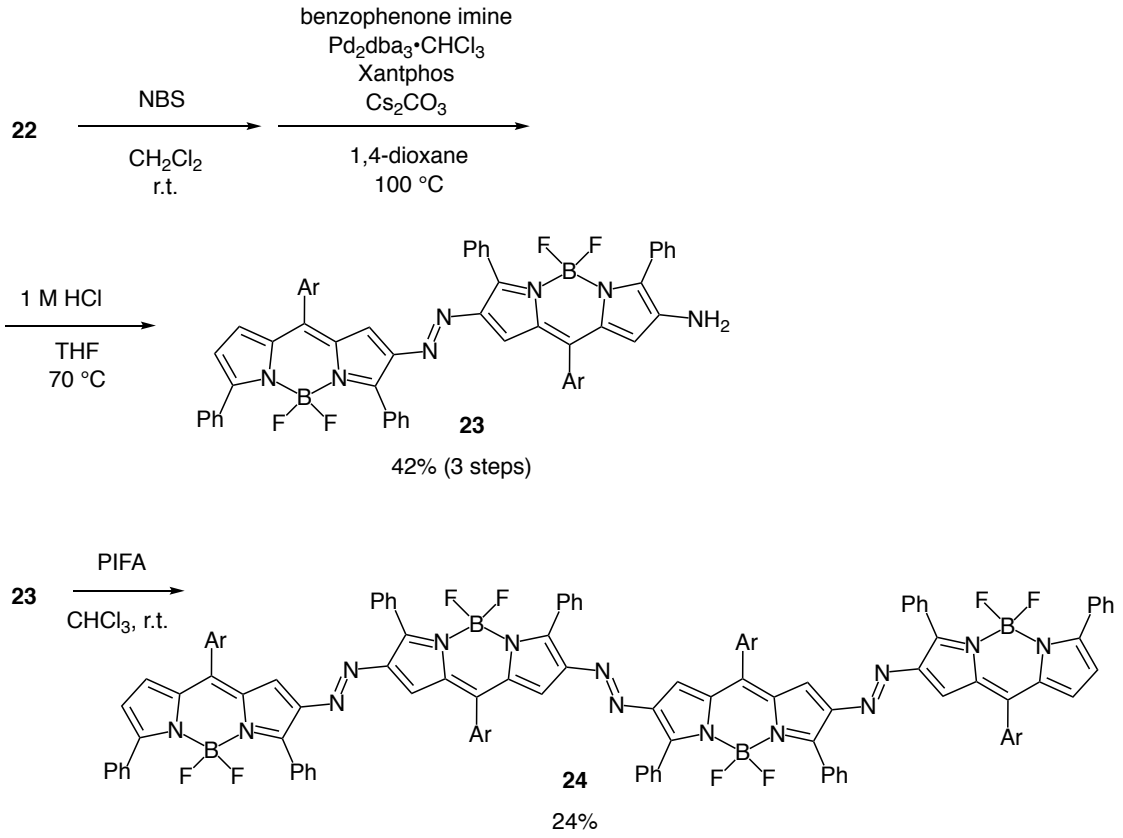

Scheme 6-3. Synthesis of diazo-linked BODIPY tetramer **24**.

6-3. Optical and Electrochemical Properties

Figure 6-2 shows the UV/vis absorption spectra of **18**, **22**, and **24** in CH_2Cl_2. The lowest energy bands were substantially shifted to the low energy region in the order of **24** > **22** > **18**, indicating effective expansion of π-conjugation upon oligomerization. The splitting absorption band at 690 nm for **22** also indicates strong π-conjugation, showing an anisotropic transition over the BODIPY plane.[10] Tetramer **24** exhibited an

intense absorption band in the near-infrared region at 802 nm. The intense emission was observed for **18** with a fluorescence quantum yield of 0.88, while dimer **22** exhibited weak and red-shifted emission ($\Phi_f = 0.02$) at 743 nm (Figure 6-3).

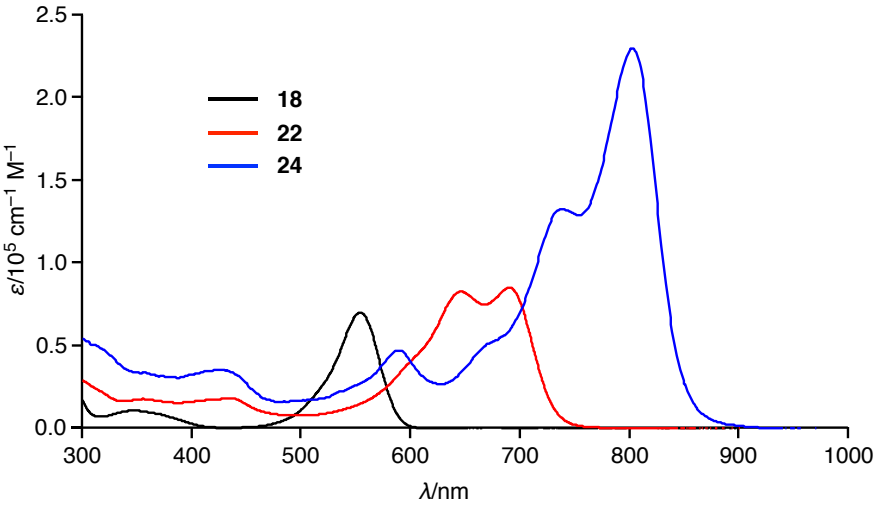

Figure 6-2. UV-vis-NIR absorption spectra of **18** (black), **22** (red), and **24** (blue) in CH_2Cl_2.

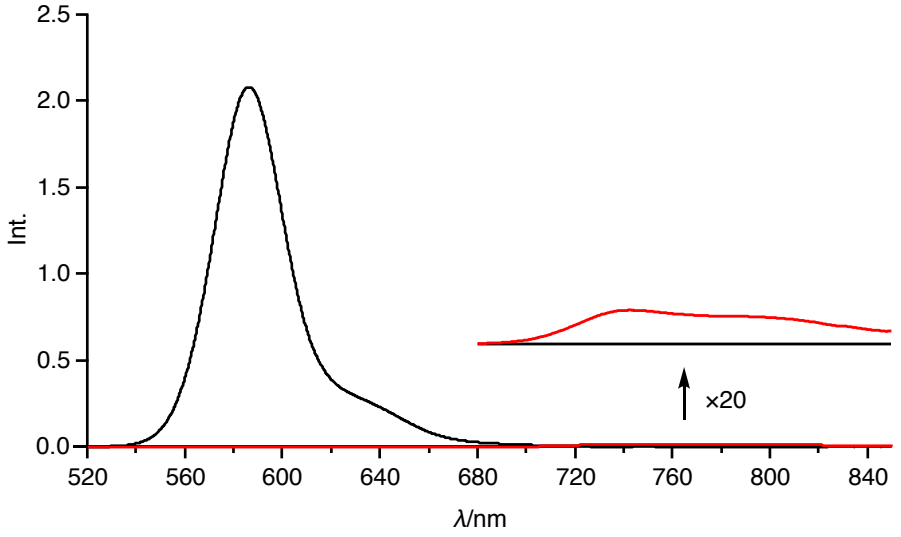

Figure 6-3. Emission spectra of **18** (black) and **22** (red) in CH_2Cl_2.

To investigate the electronic structure of oligomers **22** and **24**, electrochemical analysis was performed by cyclic voltammetry (Figures 6-4 and Table 6-2). Dimer **22** exhibited three reversible oxidation waves at 0.708, 0.818, and 1.19 V and two reversible reduction waves at −1.15 and −1.33 V. In the case of tetramer **24**, two reversible reduction waves at −0.985 and −1.19 V and irreversible oxidation waves were observed. The gaps between the first oxidation and first reduction potentials decrease in the order **18** > **22** > **24**. This tendency is consistent with the result by optical analysis. Furthermore, both oxidation and reduction potentials in **22** and **24** are split, indicating the effective electronic communication between two BODIPY units. Interestingly, significant changes were observed for reduction potentials of **18**, **22**, and **24**, while their first oxidation potentials remained almost unchanged. This is probably due to the electron-withdrawing feature of the diazo groups, which only affect the energy level of LUMOs. These results demonstrate that the connection of the BODIPY units with the diazo linkage is beneficial to obtain air-stable BODIPY-based oligomers and polymers.[11]

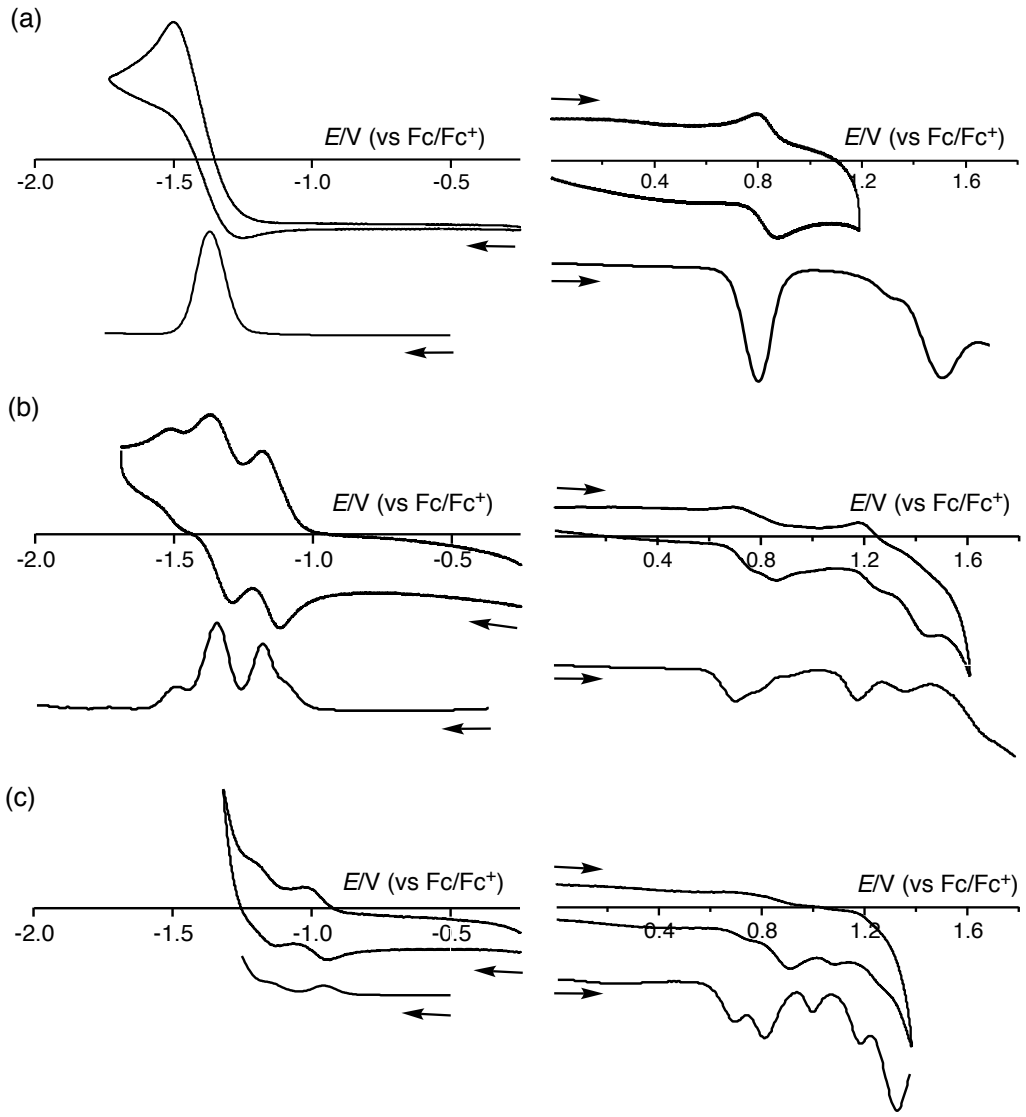

Figure 6-4. Cyclic voltammograms of (a) **18**, (b) **22**, and (d) **24**.

Table 6-2. Summary of cyclic voltammetry for compound **18**, **22**, and **24**.

compound	E_{red}^{3}	E_{red}^{2}	E_{red}^{1}	E_{ox}^{1}	E_{ox}^{2}	E_{ox}^{3}	E_{ox}^{4}
18	—	—	–1.36[a]	0.835	—	—	—
22	1.46[a]	1.33	–1.15	0.708[a]	0.818	1.19[a]	1.38[a]
24	—	1.19	–0.985	0.695[a]	0.809[a]	0.997[a]	1.19[a]

[a] The values were obtained by DPV measurement.

6-4. Summary

In conclusion, the author synthesized diazo-bridged BODIPY dimer **22** and tetramer **24** by oxidative coupling of 2-amino-substituted BODIPYs. The structure of **22** was unveiled by X-ray diffraction analysis, showing its highly planar conformation. Optical and electrochemical studies indicate the presence of effective elongation of π-conjugation through the diazo bridge. These diazo-linked BODIPY oligomers have potential as a novel near-IR light absorbing dye.

6-5. Experimental Section

Materials and Characterization

^{1}H NMR (500 MHz) and ^{13}C NMR (126 MHz) spectra were recorded using a Varian INOVA-500 spectrometer or a Bruker AVANCE III HD spectrometer. Chemical shifts were reported at the delta scale in ppm relative to $CHCl_3$ (δ = 7.260 ppm) and CH_2Cl_2 (δ = 5.320 ppm) for ^{1}H NMR and $CDCl_3$ (δ = 77.0 ppm) for ^{13}C NMR. UV/vis/NIR absorption spectra were recorded using a Shimadzu UV-2550 or JASCO V670 spectrometer. Emission spectra were recorded using a JASCO FP-6500 spectrometer, and absolute fluorescence quantum yields were measured by the photon-counting method using an integration sphere. HR mass spectra were recorded using a Bruker microTOF by positive mode ESI-TOF or APCI-TOF methods. Unless otherwise noted, materials obtained from commercial suppliers were used without further purification.

Synthesis of 16

2-Phenylpyrrole (201 mg, 1.40 mmol), mesitaldehyde (92.3 μL, 0.635 mmol), and CH_2Cl_2 (5.0 mL) were added in a 50 mL two-necked flask. Trifluoroacetic acid (TFA, 10.5 μL) was added under N_2 atmosphere, and then the mixture was stirred for 3 h at room temperature. The resulting mixture was quenched with saturated $NaHCO_3$ (aq.). The resulting solution was extracted with CH_2Cl_2 and the organic layer was

washed with water, dried over Na_2SO_4, and then concentrated in vacuo. Purification by silica-gel column chromatography (hexane/EtOAc followed by hexane/CH_2Cl_2) afforded **16** (172 mg, 0.413 mmol) in 65% yield as a pale orange solid. ^{1}H NMR ($CDCl_3$): δ = 8.19 (s, 2H), 7.39 (dd, J_1 = 8.4 Hz, J_2 = 1.1 Hz, 4H), 7.32–7.35 (m, 4H), 7.16–7.19 (m, 2H), 6.92 (s, 2H), 6.49–6.50 (m, 2H), 6.07–6.09 (m, 2H), 6.01 (s, 1H), 2.32 (s, 3H), 2.18 (s, 6H) ppm; ^{13}C NMR ($CDCl_3$): δ = 137.5, 136.8, 133.8, 132.7, 132.4, 130.9, 130.5, 128.8, 125.9, 123.4, 108.7, 106.3, 38.69, 20.80, 20.74 ppm; HR APCI-MS: m/z = 417.2319, calcd for $(C_{30}H_{29}N_2)^+$ = 417.2325 [$(M + H)^+$].

Synthesis of 17

To a solution of **16** (102 mg, 0.245 mmol) in CH_2Cl_2 (8 mL), DDQ (56.0 mg, 0.247 mmol) was added, and the mixture was stirred for 2 h at room temperature. The resulting mixture was concentrated in vacuo. Purification by silica-gel column chromatography (hexane/CH_2Cl_2) afforded **17** (97.3 mg, 0.235 mmol) in 96% yield as an orange solid. ^{1}H NMR ($CDCl_3$): δ = 13.6 (br, 1H), 7.93–7.95 (m, 4H), 7.50 (t, J = 7.5 Hz, 4H), 7.38–7.41 (m, 2H), 6.95 (s, 2H), 6.78 (d, J = 4.2 Hz, 2H), 6.48 (d, J = 4.2 Hz, 2H), 2.38 (s, 3H), 2.17 (s, 6H) ppm; ^{13}C NMR ($CDCl_3$): δ = 153.8, 141.8, 138.5, 137.4, 136.9, 133.2, 133.2, 128.9, 128.7, 128.4, 127.8, 126.1, 115.6, 21.14, 20.06 ppm; HR APCI-MS: m/z = 415.2172, calcd for $(C_{30}H_{27}N_2)^+$ = 415.2169 [$(M + H)^+$].

Synthesis of 18

In a 200 mL three-necked flask, **17** (805 mg, 1.94 mmol) was dissolved in dry CH_2Cl_2 (65 mL). To the solution, *i*-Pr_2NEt (3.36 mL, 19.3 mmol) and $BF_3{\cdot}Et_2O$ (7.14 mL, 57.9 mmol) were added dropwise under N_2 atmosphere at 0 °C. The mixture was stirred for 6 h at room temperature and then quenched with water. The resulting mixture was extracted with CH_2Cl_2 and the organic layer was washed with water, dried over Na_2SO_4, and concentrated in vacuo. Purification by silica-gel column chromatography (hexane/CH_2Cl_2) afforded **18** (759 mg, 1.64 mmol) in 85% yield as an orange solid. ^{1}H

NMR ($CDCl_3$): δ = 7.89 (dd, J_1 = 8.0 Hz, J_2 = 1.5 Hz, 4H), 7.39–7.45 (m, 6H), 6.99 (s, 2H), 6.66 (d, J = 4.5 Hz, 2H), 6.56 (d, J = 4.0 Hz, 2H), 2.39 (s, 3H), 2.21 (s, 6H) ppm; ^{13}C NMR ($CDCl_3$): δ = 158.7, 143.9, 138.5, 136.8, 136.5, 132.6, 130.3, 129.4, 129.4, 129.4, 128.2, 128.1, 120.8, 21.15, 20.12 ppm; UV/vis (CH_2Cl_2): λ_{max} (ε [M^{-1} cm^{-1}]) = 346 (11000), 554 (70000) nm; HR APCI-MS: m/z = 462.2070, calcd for $(C_{30}H_{25}BF_2N_2)^+$ = 462.2079 [M^+].

Synthesis of 19

A flask containing **18** (900 mg, 1.95 mmol), NBS (383 mg, 2.15 mmol), and AIBN (34.1 mg, 0.208 mmol) was flushed with N_2 three times, and then degassed $CHCl_3$ (195 mL) was added into the flask. The mixture was stirred for 25 h at 100 °C. The resulting mixture was cooled to room temperature, and then the reaction was quenched with acetone. The mixture was extracted with $CHCl_3$ and then the organic layer was washed with water, dried over Na_2SO_4, and concentrated in vacuo. Purification by silica-gel column chromatography (hexane/CH_2Cl_2) afforded **19** (994 mg, 1.84 mmol) in 94% yield as a brown solid. ^1H NMR ($CDCl_3$): δ = 7.86–7.88 (m, 2H), 7.69–7.71 (m, 2H), 7.40–7.47 (m, 6H), 7.01 (s, 2H), 6.75 (d, J = 4.0 Hz, 1H), 6.70 (s, 1H), 6.62 (d, J = 4.5 Hz, 1H), 2.40 (s, 3H), 2.23 (s, 6H) ppm; ^{13}C NMR ($CDCl_3$): δ = 161.1 153.9, 144.0, 138.9, 137.2, 136.7, 133.8, 131.9, 131.2, 130.5, 130.4, 130.0, 129.7, 129.4, 128.4, 128.3, 128.2, 127.7, 122.0, 108.0, 107.9, 21.14, 20.14 ppm; HR APCI-MS: m/z = 540.1175, calcd for $(C_{30}H_{24}BF_2N_2Br)^+$ = 540.1184 [M^+].

Synthesis of 20

A Schlenk tube containing **19** (1.00 g, 1.85 mmol), Cs_2CO_3 (1.21 g, 3.73 mmol), $Pd_2dba_3{\cdot}CHCl_3$ (38.9 mg, 37.6 μmol), Xantphos (43.1 mg, 74.5 μmol) was flushed with N_2 three times. To the Schlenk tube, benzophenone imine (0.466 mL, 2.78 mmol) and dry 1,4-dioxane (13 mL) was added. The mixture was stirred for 15 h at 100 °C. The resulting mixture was cooled to room temperature, passed through a pad of Celite, and concentrated in vacuo. Purification by silica-gel column chromatography

(hexane/CH_2Cl_2) afforded **20** (558 mg, 0.870 mmol) in 47% yield as a purple solid. ^{1}H NMR (CD_2Cl_2): δ = 7.76–7.78 (m, 2H), 7.72–7.74 (m, 2H), 7.58–7.60 (m, 2H), 7.36–7.43 (m, 7H), 7.26–7.33 (m, 5H), 6.99–7.01 (m, 2H), 6.89 (s, 2H), 6.55 (d, J = 4.3 Hz, 1H), 6.51 (d, J = 4.0 Hz, 1H), 5.29 (s, 1H), 2.35 (s, 3H), 1.98 (s, 6H) ppm; ^{13}C NMR ($CDCl_3$): δ = 168.2 157.9, 154.4, 142.8, 142.7, 139.0, 138.2, 136.9, 136.6, 136.3, 134.0, 132.8, 130.8, 130.6, 130.1, 129.3, 129.2, 129.2, 129.1, 129.0, 128.6, 128.3, 128.1, 128.1, 128.0, 127.8, 127.5, 120.1, 120.0, 118.0, 21.13, 19.98 ppm; HR APCI-MS: m/z = 642.2919, calcd for $(C_{43}H_{35}BF_2N_3)^+$ = 642.2894 [$(M + H)^+$].

Synthesis of 21

To a 50 mL flask, **20** (100 mg, 0.156 mmol), THF (12.8 mL), and 1M HCl (2.78 mL) were added, and then the mixture was stirred for 1 h at 70 °C. The resulting mixture was cooled to room temperature, and then aqueous $NaHCO_3$ solution was added. The resulting mixture was extracted with CH_2Cl_2 and the organic layer was washed with water, dried over Na_2SO_4, and concentrated in vacuo. Purification by silica-gel column chromatography (hexane/CH_2Cl_2) afforded **21** (64.2 mg, 0.134 mmol) in 86% yield as a dark blue solid. ^{1}H NMR ($CDCl_3$): δ = 7.81 (dd, J_1 = 8.3 Hz, J_2 = 1.3 Hz, 2H), 7.74 (d, J = 7.0 Hz, 2H), 7.42–7.50 (m, 3H), 7.31–7.38 (m, 3H), 6.97 (s, 2H), 6.45 (d, J = 4.0 Hz, 1H), 6.42 (d, J = 4.0 Hz, 1H), 5.86 (s, 1H), 3.36 (s, 2H), 2.38 (s, 3H), 2.23 (s, 6H) ppm; ^{13}C NMR ($CDCl_3$): δ = 155.4 150.6, 140.4, 140.3, 138.2, 136.8, 135.8, 134.4, 133.2, 130.7, 130.0, 129.7, 129.6, 129.1, 128.7, 128.5, 128.0, 128.0, 126.4, 118.4, 108.4, 21.13, 20.12 ppm; HR APCI-MS: m/z = 477.2166, calcd for $(C_{30}H_{26}BF_2N_3)^+$ = 477.2188 [M^+].

Synthesis of 22

To a solution of **21** (9.77 mg, 20.4 μmol) in dry $CHCl_3$ (3.3 mL) was added dropwise a solution of PIFA (17.8 mg, 41.5 μmol) in dry $CHCl_3$ (3.3 mL) at room temperature over 5 min. The mixture was stirred at room temperature for another 2 h.

The resulting mixture was concentrated in vacuo. Purification by silica-gel column chromatography (hexane/CH_2Cl_2) afforded **22** (3.26 mg, 3.43 μmol) in 34% yield as a brown solid. ^{1}H NMR ($CDCl_3$): δ = 7.88–7.90 (m, 4H), 7.74–7.76 (m, 4H), 7.43–7.41 (m, 6H), 7.39–7.36 (m, 2H), 7.34–7.30 (m, 4H), 6.96 (s, 4H), 6.76 (d, J = 4.5 Hz, 2H), 6.64 (d, J = 4.5 Hz, 2H), 6.54 (s, 2H), 2.39 (s, 6H), 2.17 (s, 12H) ppm; ^{13}C NMR ($CDCl_3$): δ = 161.8 155.5, 148.0, 145.6, 138.7, 138.3, 136.6, 133.8, 131.9, 131.2, 130.2, 130.1, 129.8, 129.5, 129.2, 128.3, 128.1, 127.3, 122.6, 113.4, 113.3, 21.13, 20.17 ppm; UV/vis (CH_2Cl_2): λ_{max} (ε [M^{-1} cm^{-1}]) = 355 (18000), 435 (18000), 646 (83000), 690 (85000) nm; HR APCI-MS: m/z = 951.4119, calcd for $(C_{60}H_{49}B_2F_4N_6)^+$ = 951.4154 [$(M + H)^+$].

Synthesis of 23

To a solution of **22** (684 mg, 0.720 mmol) in dry CH_2Cl_2 (84 mL) was added dropwise a solution of NBS (128 mg, 0.719 mmol) in dry CH_2Cl_2 (66 mL) at 0 °C over 1.5 h. The mixture was stirred at room temperature for 83 h. The resulting mixture was cooled to room temperature, and then the reaction was quenched with acetone. The mixture was extracted with CH_2Cl_2 and then the organic layer was washed with water, dried over Na_2SO_4, and concentrated in vacuo. The residue was then passed through a short plug of silica. (CH_2Cl_2/hexane). The residue was transferred to a Schlenk tube. To the tube were added Cs_2CO_3 (1.29 g, 3.95 mmol), Pd_2dba_3·$CHCl_3$ (149 mg, 0.144 mmol), and Xantphos (167 mg, 0.289 mmol), and the tube was flushed with N_2 three times. Benzophenone imine (0.604 mL, 3.60 mmol) and dry 1,4-dioxane (24 mL) was added, and then the mixture was stirred for 21 h at 100 °C. The resulting mixture was cooled to room temperature, then passed through a pad of Celite, and concentrated in vacuo. The residue was then passed through a short plug of silica. (CH_2Cl_2/hexane). The crude product was dissolved in THF (80 mL) and 1 M HCl (17.3 mL) was added. The solution was stirred for 1.5 h at 70 °C. The resulting mixture was cooled to room temperature, and then aqueous $NaHCO_3$ solution was added. The resulting mixture was extracted

with CH_2Cl_2 and the organic layer was washed with water, then dried over Na_2SO_4, and concentrated in vacuo. Purification by silica-gel column chromatography (hexane/CH_2Cl_2) afforded **23** (289 mg, 0.299 mmol) in 42% yield (in there steps) as a purple solid. ^{1}H NMR (CD_2Cl_2): δ = 7.84–7.82 (m, 2H), 7.70–7.67 (m, 4H), 7.62–7.60 (m, 2H), 7.50–7.49 (m, 3H), 7.44–7.42 (m, 3H), 7.40–7.38 (m, 1H), 7.35–7.31 (m, 3H), 7.29–7.26 (m, 2H), 6.97 (s, 2H), 6.96 (s, 2H), 6.74 (d, J = 5.0 Hz, 1H), 6.65 (d, J = 4.0 Hz, 1H), 6.46 (s, 1H), 6.28 (s, 1H), 5.85 (s, 1H), 3.62 (br, 2H), 2.37 (s, 3H), 2.36 (s, 3H), 2.15 (s, 6H), 2.13 (s, 6H) ppm; ^{1}H NMR ($CDCl_3$): δ = 7.89–7.87 (m, 2H), 7.76–7.72 (m, 4H), 7.69–7.67 (m, 2H), 7.51–7.46 (m, 3H), 7.43–7.41 (m, 3H), 7.37–7.34 (m, 1H), 6.95 (s, 2H), 6.94 (s, 2H), 6.72 (d, J = 4.3 Hz, 1H), 6.61 (d, J = 4.4 Hz, 1H), 6.51 (s, 1H), 6.36 (s, 1H), 5.87 (s, 1H), 3.51 (br, 2H), 2.37 (s, 6H), 2.17 (s, 6H), 2.16 (s, 6H) ppm, Several aryl proton peaks were overlapped with the signal of $CHCl_3$.; ^{13}C NMR ($CDCl_3$): δ = 161.1, 155.5, 154.9, 152.9, 148.3, 146.6, 145.3, 141.8, 140.8, 138.6, 138.4, 138.0, 136.7, 136.7, 136.6, 133.9, 133.6, 132.1, 131.3, 131.3, 130.7, 130.7, 130.3, 130.3, 130.2, 129.9, 129.5, 129.2, 129.2, 128.7, 128.3, 128.1, 128.1, 127.2, 127.2, 122.1, 113.7, 110.5, 107.4, 21.13, 20.17 ppm; HR APCI-MS: m/z = 966.4285, calcd for $(C_{60}H_{50}B_2F_4N_7)^+$ = 966.4263 [$(M + H)^+$].

Synthesis of 24

To a solution of **23** (30.1 mg, 31.6 μmol) in dry $CHCl_3$ (1.6 mL) was added dropwise a solution of PIFA (27.6 mg, 64.2 μmol) in dry $CHCl_3$ (0.9 mL) at room temperature over 1 min. The mixture was stirred at room temperature for another 15 h. The resulting mixture was concentrated in vacuo. Purification by silica-gel column chromatography (hexane/CH_2Cl_2) afforded **24** (7.21 mg, 3.74 μmol) in 24% yield as a black solid. ^{1}H NMR ($CDCl_3$): δ = 7.90–7.88 (m, 4H), 7.74–7.70 (m, 12H), 7.43 (t, 6H), 7.39–7.36 (m, 6H), 7.33–7.29 (m, 12H), 6.95 (s, 4H), 6.93 (s, 4H), 6.77 (d, J = 4.5 Hz, 2H), 6.66 (d, J = 4.5 Hz, 2H), 6.58 (s, 2H), 6.57 (s, 2H), 6.52 (s, 2H), 2.38 (s, 12H), 2.16 (s, 12H), 2.11 (s, 12H) ppm; ^{13}C NMR ($CDCl_3$): δ = 162.4 158.6, 158.1, 155.7,

149.1, 148.7, 147.8, 147.7, 145.7, 138.9, 138.8, 138.6, 136.6, 136.5, 135.5, 135.2, 133.9, 131.7, 131.6, 131.2, 131.2, 130.3, 130.1, 129.8, 129.7, 129.7, 129.7, 129.7, 129.6, 129.6, 129.4, 129.3, 128.4, 128.2, 127.4, 127.3, 123.0, 114.9, 114.5, 113.1, 21.13, 20.21, 20.17 ppm; UV/vis (CH_2Cl_2): λ_{max} (ε [M^{-1} cm^{-1}]) = 421 (35000), 589 (47000), 739 (130000), 802 (230000) nm; HR APCI-MS: *m/z* = 1927.8142, calcd for $(C_{120}H_{95}B_4F_8N_{14})^+$ = 1927.8156 [$(M + H)^+$].

X-Ray Diffraction Analysis

X-Ray data were obtained using a Rigaku CCD diffractometer (Saturn 724 with MicroMax-007) with Varimax Mo optics using graphite monochromated Mo-Kα radiation (λ = 0.71075 Å) for **22**.

Electrochemical Analysis

The cyclic voltammogram and differential-pulse voltammogram of **18**, **22**, and **24** were recorded using an ALS electrochemical analyser 612C. Measurements were performed in freshly distilled CH_2Cl_2 with tetrabutylammonium hexafluorophosphate as the electrolyte. A three-electrode system was used. The system consisted of a glassy carbon working electrode, a platinum wire, and $Ag/AgClO_4$ as the reference electrode. The scan rate was 100 mVs^{-1}. The measurement was performed under nitrogen atmosphere. All potentials are referenced to the potential of ferrocene/ferrocenium cation couple.

References

(1) (a) Y. Ni, J. Wu, *Org. Biomol. Chem.* **2014**, *12*, 3774. (b) H. Lu, J. Mack, Y. Yang, Z. Shen, *Chem. Soc. Rev.* **2014**, *43*, 4778. (c) G. Ulrich, R. Ziessel, A. Harriman, *Angew. Chem. Int. Ed.* **2008**, *47*, 1184. (d) A. Loudet, K. Burgess, *Chem. Rev.* **2007**, *107*, 4891.

(2) (a) Y. Urano, D. Asanuma, Y. Hama, Y. Koyama, T. Barrett, M. Kamiya, T. Nagano, T. Watanabe, A. Hasegawa, P. L. Choyke, H. Kobayashi, *Nat. Med.* **2009**, *15*, 104. (b) J. Han, A. Loudet, R. Barhoumi, R. C. Burghardt, K. Burgess, *J. Am. Chem. Soc.* **2009**, *131*, 1642.

(3) (a) T. Myochin, K. Hanaoka, T. Komatsu, T. Terai, T. Nagano, *J. Am. Chem. Soc.* **2012**, *134*, 13730. (b) T. Yogo, Y. Urano, Y. Ishitsuka, F. Maniwa, T. Nagano, *J. Am. Chem. Soc.* **2005**, *127*, 12162.

(4) L. Bonardi, H. Kanaan, F. Camerel, P. Jolinat, P. Retailleau, R. Ziessel, *Adv. Funct. Mater.* **2008**, *18*, 401.

(5) For recent examples, see: (a) J. Ahrens, B. Haberlag, A. Scheja, M. Tamm, M. Bröring, *Chem. Eur. J.* **2014**, *20*, 2901 and references are therein. (b) A. Wakamiya, T. Murakami, S. Yamaguchi, *Chem. Sci.* **2013**, *4*, 1002. (c) M. Nakamura, H. Tahara, K. Takahashi, T. Nagata, H. Uoyama, D. Kuzuhara, S. Mori, T. Okujima, H. Yamada, H. Uno, *Org. Biomol. Chem.* **2012**, *10*, 6840. (d) Y. Hayashi, S. Yamaguchi, W. Y. Cha, D. Kim, H. Shinokubo, *Org. Lett.* **2011**, *13*, 2992. (e) A. Poirel, A. De Nicola, P. Retailleau, R. Ziessel, *J. Org. Chem.* **2012**, *77*, 7512. (f) W. Pang, X. -F. Zhang, J. Zhou, C. Yu, E. Hao, L. Jiao, *Chem. Commun.* **2012**, *48*, 5437. (g) M. T. Whited, N. M. Patel, S. T. Roberts, K. Allen, P. I. Djurovich, S. E. Bradforth, M. E. Thompson, *Chem. Commun.* **2012**, *48*, 284. (h) N. Sakamoto, C. Ikeda, M. Yamamura, T. Nabeshima, *Chem. Commun.* **2012**, *48*, 4818. (i) Y. Cakmak, S. Kolemen, S. Duman, Y. Dede, Y. Dolen, B. Kilic, Z. Kostereli, L. T. Yildirim, A. L. Dogan, D. Guc, E. U. Akkaya, *Angew. Chem. Int. Ed.* **2011**, *50*, 11937.

(6) (a) E. Merino, M. Ribagorda, *Beilstein J. Org. Chem.* **2012**, *8*, 1071. (b) J. García-Amorós, D. Velasco, *Beilstein J. Org. Chem.* **2012**, *8*, 1003. (c) H. M. D.

Bandara, S. C. Burdette, *Chem. Soc. Rev.* **2012**, *41*, 1809.

(7) (a) T. E. O. Screen, I. M. Blake, L. H. Rees, W. Clegg, S. J. Borwick, H. L. Anderson, *J. Chem. Soc., Perkin Trans. 1* **2002**, 320. (b) L. J. Esdaile, P. Jensen, J. C. McMurtrie, D. P. Arnold, *Angew. Chem. Int. Ed.* **2007**, *46*, 2090.

(8) (a) S. Farhadi, P. Zaringhadam, R. Z. Sahamieh, *Acta Chim. Slov.* **2007**, *54*, 647. (b) K. Orito, T. Hatakeyama, M. Takeo, S. Uchiito, M. Tokuda, H. Suginome, *Tetrahedron* **1998**, *54*, 8403. (c) H. Firouzabadi, Z. Mostafavipoor, *Bull. Chem. Soc. Jpn.* **1983**, *56*, 914. (d) B. Ortiz, P. Villanueva, F. Walls, *J. Org. Chem.* **1972**, *37*, 2748. (e) K. Kinoshita, *Bull. Chem. Soc. Jpn.* **1959**, *32*, 780. (f) E. Baer, A. L. Tosoni, *J. Am. Chem. Soc.* **1956**, *78*, 2857.

(9) (a) Y. Takeda, S. Okumura, S. Minakata, *Angew. Chem. Int. Ed.* **2012**, *51*, 7804. (b) H. Ma, W. Li, J. Wang, G. Xiao, Y. Gong, C. Qi, Y. Feng, X. Li, Z. Bao, W. Cao, Q. Sun, C. Veaceslav, F. Wang, Z. Lei, *Tetrahedron* **2012**, *68*, 8358. (c) K. Monir, M. Ghosh, S. Mishra, A. Majee, A. Hajra, *Eur. J. Org. Chem.* **2014**, 1096.

(10) S. Chibani, B. L. Guennic, A. Charaf-Eddin, A. D. Laurent, D. Jacquemin, *Chem. Sci.* **2013**, *4*, 1950.

(11) (a) A. Nagai, J. Miyake, K. Kokado, Y. Nagata, Y. Chujo, *J. Am. Chem. Soc.* **2008**, *130*, 15276. (b) A. B. Nepomnyashchii, M. Bröring, J. Ahrens, A. J. Bard, *J. Am. Chem. Soc.* **2011**, *133*, 8633. (c) Y. Cakmak, E. U. Akkaya, *Org. Lett.* **2009**, *11*, 85.

Summary of This Thesis

The synthesis and properties as well as the applications of nitrogen-embedded bowl-shaped molecules, that is, penta-*peri*-pentabenzoazacorannulenes has been described in this thesis. A penta-*peri*-pentabenzoazacorannulene has nitrogen atom in its central position. The introduction of electron-rich amine-type nitrogen atom drastically enhanced its electron-donating character.

The synthesis of penta-*peri*-pentabenzoazacorannulene was discussed in Chapter 2. The consecutive fusion reactions of the *N*-aryl-tetrabenzocarbazole successfully afforded penta-*peri*-pentabenzoazacorannulene. Different from conventional bowl-shaped molecules consisting of only carbon atoms, the penta-*peri*-pentabenzoazacorannulene can strongly associate with C_{60}. The electron-rich nature of the penta-*peri*-pentabenzoazacorannulene also enabled the formation of its radical cation species in the presence of acid through intermolecular electron transfer.

In Chapter 3, the author described the formation of supramolecular assemblies consisting of a directly connected penta-*peri*-pentabenzoazacorannulene dimer and C_{60}. The dimer and C_{60} formed 1:2 complex in the crystal state, while only 1:1 complex was detected in the solution state. At higher concentration, the dimer and C_{60} formed 1D chain supramolecular assemblies with sandwich structure.

Chapter 4 disclosed the reactivities of a bowl-shaped molecule. The radical cation of penta-*peri*-pentabenzoazacorannulene formed σ-dimer in the crystal state. The σ-dimer was also confirmed in the solution state upon lowering temperature. On the other hand, an analogous planar molecule formed π-dimer in the crystal state or solution state at low temperatures. Therefore, the bowl-shaped structures should play an important role on the bond formation at internal carbon atoms.

The author also found the oxidation of amino-substituted BODIPY is useful for the synthesis of near-infrared (NIR) absorbing dyes. The oxidation of 2-amino-substituted BODIPYs afforded pyrazine-fused BODIPY trimers or diazo-bridged BODIPY dimer. The resulting products have strong absorption at NIR

region. These oxidation reactions should be useful for the creation of other functional π-systems.

List of Publications

1. "Oxidation of 2-amino-substituted BODIPYs providing pyrazine-fused BODIPY trimers"
   Hiroki Yokoi, Naruhiko Wachi, Satoru Hiroto, Hiroshi Shinokubo
   Chem. Commun. **2014**, *50*, 2715–2717.
2. "Synthesis of Diazo-Bridged BODIPY Dimer and Tetramer by Oxidative Coupling of β-Amino-Substituted BODIPYs"
   Hiroki Yokoi, Satoru Hiroto, Hiroshi Shinokubo
   Org. Lett. **2014**, *16*, 3004–3007.
3. "Nitrogen-embedded buckybowl and its assembly with C_{60}"
   Hiroki Yokoi, Yuya Hiraoka, Satoru Hiroto, Daisuke Sakamaki, Shu Seki, Hiroshi Shinokubo
   Nat. Commun. **2015**, *6*, 8215.
4. Supramolecular assemblies of a nitrogen-embedded buckybowl dimer with C_{60}
   Hiroki Yokoi, Satoru Hiroto, Daisuke Sakamaki, Shu Seki, Hiroshi Shinokubo
   Chem. Sci. **2018**, in press.

Acknowledgement

The author would like to express his sincerest gratitude for Prof. Dr. Hiroshi Shinokubo for his supervision, precious advices, and encouragement throughout his study. The author would like to show my greatest appreciation to Assistant Prof. Dr. Satoru Hiroto for his suggestions and encouragement from the beginning of the research. The author desires to express his appreciation to Associate Prof. Dr. Yoshihiro Miyake for his helpful discussion and suggestion of the study. The author also wishes to show acknowledgement to Prof. Dr. Ji-Young Shin for valuable advices.

The author is deeply grateful to Prof. Dr. Takashi Ooi and Prof. Dr. Kenichiro Itami for their helpful suggestions and discussion on his dissertation committee.

The author feels grateful to Prof. Dr. Takahiro Seki and Assistant Prof. Dr. Mituo Hara at Department of Molecular & Macromolecular Cheimstry, Nagoya University for the XRD measurement.

The author gratefully acknowledges to Assistant Prof. Dr. Ichiro Hisaki at Department of Material and Life Science, Osaka University for the synchrotron X-ray diffraction analysis (Spring-8).

The author is obliged to Prof. Dr. Taishi Takenobu and Assistant Prof. Dr. Hisaaki Tanaka at Department of Applied Physics, Nagoya University for the ESR measurement.

The author wishes to express his sincere appreciation to Prof. Dr. Shu Seki, Assistant Prof. Dr. Tsuneaki Sakurai, and Assistant Prof. Dr. Daisuke Sakamaki at Department of Molecular Engineering, Kyoto University for the TRMC measurement.

The author would like to express the deepest appreciation to all members of Shinokubo group for their enthusiasm and consideration:

Dr. Ryuichi Yamaguchi	Dr. Satoru Ito	Mr. Yutaro Koyama
Mr. Takeshi Kondo	Dr. Kazuma Oda	Dr. Ayaka Yamaji
Mr. Kiyohiko Goto	Ms. Ami Shigeno	Mr. Takaki Fukuoka
Mr. Naruhiko Wachi	Mr. Hiromitsu Kido	Ms. Hiroko Tanaka
Mr. Yuma Serizawa	Mr. Takuya Yoshida	Mr. Yuya Hiraoka
Mr. Ryo Nozawa	Mr. Hiroto Omori	Mr. Takashi Matsuno
Mr. Takuto Kamatsuka	Mr. Keitaro Yamamoto	Mr. Shohei Kato
Mr. Hiroyuki Kawashima	Mr. Hideo Tsuboi	Ms. Ayako Ushiyama
Mr. Yuki Ando	Mr. Yusuke Morita	Mr. Tsubasa Yonezawa
Mr. Yuya Nagata	Ms. Juri Nagasaki	Mr. Masayuki Ueda
Mr. Tsubasa Nishimura	Mr. Shuhei Akahori	Ms. Shiori Itabuchi
Mr. Tatsuya Ochiai	Mr. Motoki Takeda	Mr. Tomohiro Nagai
Ms. Takumi Nakazato	Mr. Kazuhiro Kubokoya	Mr. Yuma Shiratani
Mr. Daisuke Yamashita	Mr. Yasutaka Nakamura	Mr. Syuto Yokoyama
Ms. Sakiho Hayakawa	Ms. Asahi Takiguchi	Mr. Hiroyasu Murase
Ms. Haruka Takekoshi	Mr. Yuki Tanaka	Mr. Tomoya Yokota
Ms. Siham Asyiqin Shafie	Ms. Wen Xi Chia	Ms. Hanako Tsuji
Mr. Nathan Hikaru Faialaga	Ms. Siyu Liu	Ms. Ayako Kimata

Last but not least, the author deeply indebted to his father, Mr. Shigeyoshi Yokoi, his mother, Mrs. Nobumi Yokoi, his brother, Mr. Ryosuke Yokoi, his sister, Ms. Rika Yokoi, Ms. Misato Yokoi, his grandfathers, Mr. Takenori Aoki, his grandmother Mrs. Suzuko Yokoi, Mrs. Yasuko Aoki for their hearty encouragement and continuous assistant.

Hiroki Yokoi

Department of Applied Chemistry
Graduate School of Engineering
Nagoya University
February 2018